# The Relationship of Large-Scale Atmospheric Circulation Patterns to Tornadoes and the Impacts of Climate Change

This thesis is submitted to the Department of Geography and the College of Arts and Sciences at Kent State University in partial fulfillment of the requirements for the degree of

Master of Arts

By
Cameron C. Lee
August, 2010

Thesis written by

Cameron C. Lee

B.S., Kent State University, 2003
M.A., Kent State University, 2010

Approved by

Dr. Scott Sheridan____________________, Advisor

Dr. Tom Schmidlin____________________, Chair, Department of Geography

Dr. Timothy Moerland________________, Dean, College of Arts and Sciences

**TABLE OF CONTENTS**

## LIST OF FIGURES

**LIST OF TABLES**

## ACKNOWLEDGEMENTS

Through long hours, long weekends, an engagement, a house, a puppy, wedding planning, home improvement projects galore, and a few bouts of frustration, I first want to thank my wife Amanda for supporting me (and us) over the past two years while I attended grad school. Between staying late at McGilvrey Hall, attending far away meetings and field trips, and hovering over the computer in the wee hours of the morning while I completed this thesis, I don't know if I ever got a chance to stop and say thank you. Thank you. I could not have done any of this without you. Only a few more years now while I pursue a PhD!

Although they are over 2000 miles away, my family is always at the back of my mind. I want to thank my mom, my dad, and my brother for all that they have done for me through the years. Mom and Dad, you were, and continue to be great parents. Thank you for being so supportive of my decision to pursue a graduate degree. Grandear and Scotty, thank you for your support and encouragement as I went back to school.

I want to thank my advisor, Scott Sheridan, for introducing me to the world of synoptic climatology, teaching me the methods, showing me the tools, including me in some of his research, and remaining patient while I learned on the go. This thesis might have taken another two years without your constant advice and our hour-long meetings that ended up lasting two hours… twice a week.

I also want to thank the other two members of my thesis committee, Tom Schmidlin and Walker Ashley, for their helpful comments and quick responses – especially as I prepared to defend. Thank you for your valuable input on the various questions that I had, and the numerous (and probably confusing) presentations I sent via e-mail.

Lastly, I want to thank the rest of the Kent State Geography Department, both the faculty and the graduate student body, for making McGilvrey Hall such a collegial and fun environment to work and socialize in. Best of luck to everyone in all of your future endeavors.

# CHAPTER 1

# INTRODUCTION

The over 1000 tornadoes (Hyndman and Hyndman, 2009) that occur annually in the United States (US) are among the leaders of all weather-related natural hazards in terms of annual deaths and damages in the US (Changnon, 2003; Brooks and Doswell, 2001, 2002). The Intergovernmental Panel on Climate Change (IPCC) has concluded that some of the main atmospheric ingredients that go into creating tornadic environments will likely increase over the next century. However, due to the limitations of modern global climate models (GCMs), the direct investigation into the impacts of climate change on tornadoes remains largely under-explored (Diffenbaugh et al., 2008).

The recent research that has been undertaken on this topic favors an ingredients-based method that aims to project future tornadoes using GCM output data to create approximations of convective available potential energy (CAPE), moisture, and deep layer wind shear – in effect accounting for three of the four major ingredients in creating severe environments (Brooks et al., 2003a; Trapp et al., 2007). While the fourth ingredient (storm initiation) is already recognized as a shortcoming of this method (Trapp et al., 2009), these investigations also seem to neglect the large-scale processes of atmospheric circulation and the interaction of air masses that both play a vital role in steering weather systems into ideal locations for tornado development.

Within the discipline of climatology, there is an entire sub-field that focuses on directly relating atmospheric circulation to surface events – synoptic climatology (Yarnal, 1993). Synoptic methods utilize a holistic approach to the climate system, often taking the large-scale and long-term statistics of the atmosphere into consideration to create daily classifications of atmospheric circulation or weather types. These classifications are then associated to a variety of smaller-scale surface events for analysis purposes. Because of their ability to relate large-scale processes to local-scale events, synoptic methods are becoming a popular tool for use with GCM output data in analyzing the potential impacts of climate change (Sheridan and Lee, 2010).

This thesis utilizes synoptic climatological methods to provide a supplement to the ingredients-based research method outlined above. First, this thesis presents a synoptic climatology of tornadoes in the United States that uses historic data to relate large-scale atmospheric circulation patterns to tornadic activity. Secondly, using atmospheric temperature and geopotential height output data from two GCMs, this synoptic climatology is then utilized in order to infer possible changes in the frequency and seasonality of tornadoes under a range of future scenarios.

This research project was undertaken under the guidance of two overarching research questions:

- Which large-scale atmospheric circulation patterns are favorable for the development of tornadoes?
- How will future climate change affect the frequency of the atmospheric circulation patterns that are associated with tornadic weather?

The four hypotheses that follow were developed to help analyze the two over-arching research questions posed in the previous paragraph:

- Certain continental-scale atmospheric circulation patterns are associated with tornadic weather more than others.
- Different continental-scale atmospheric circulation patterns are favorable for tornadic weather in different regions of the US.
- Different combinations of continental-scale atmospheric circulation patterns at different levels of the atmosphere are favorable for tornadic weather.
- Future climate change will impact the frequency and seasonality of the different atmospheric circulation patterns that are favorable for tornadic weather.

Broadly, this thesis research was completed with three main steps: the synoptic map classification, the tornado association, and the future frequency comparison. The first two steps of the research were completed to establish an association between tornadoes and large scale atmospheric circulation patterns; in effect, helping to answer the first research question and evaluate the first three hypotheses. The third step was then completed in order to evaluate the fourth hypothesis and answer the second research question. Through these means, this study infers the likely change in future tornadic activity due to a changing climate.

# CHAPTER 2

# BACKGROUND

## *2.1 – Tornadoes and Tornado Ingredients*

On average, tornadoes account for over 50 deaths per year (Brooks and Doswell, 2002; Ashley, 2007) in the United States. After adjustments for inflation, US tornadoes caused nearly $450 million (in 1997 US dollars; Changnon, 2003) of damage per year from 1950-1997 – with some single tornado events coming with a price tag in excess of $1 billion (Brooks and Doswell, 2001). Additionally, behind only hurricanes and floods, severe storms and tornadoes together are the third most costly of all weather-related natural hazards in the US; accounting for over $2 billion of damage per year – or about 20% of all the losses among major weather-related disasters (Changnon, 2003).

Due to the flat topography of the Great Plains in the US, large air masses of differing thermodynamic composition often collide throughout the spring and summer months, triggering severe thunderstorms and creating an environment favorable for tornado activity in and around the region (Hyndman and Hyndman, 2009). Although 'Tornado

Alley' (Brooks et al., 2003b) is the area of the majority of US tornadoes, they are found throughout the US, most often east of the Rocky Mountains. Generally, tornadoes occur more often in the late winter and early spring in the Southeastern US, and can be induced by landfalling hurricanes and tropical storms in the Gulf Coast states during the late summer and early fall (especially in Florida; Aguado and Burt, 2001). The peak tornado season in the Southern Plains (and the southern portion of Tornado Alley), however, shifts more into April and May, before the prime tornado season begins in May and June in the Northern Plains (and the northern part of Tornado Alley) when the warmer weather moves northward and conditions become more favorable. Overall, tornadoes can happen throughout the entire calendar year in the US, but the vast majority are confined to a seven-month period from February to August (ibid.).

While the general geography of tornadoes is not believed to have changed dramatically over the past 60 years, the frequency and seasonality of tornadoes over this period has been shown to exhibit what some researchers have termed "secular" trends (Brooks et al., 2003b; Doswell, 2007). These trends will be discussed in section 2.2 below.

The intensity of tornadoes plays an important role in the selection of the tornado data for this research. Since the 1970s, tornado intensity has been measured by the Fujita Scale (Fujita, 1971; Aguado and Burt, 2001) or the F-scale for short – which has since been updated to the Enhanced Fujita Scale, or the EF-scale for short (Figure 1). This scale gives a rating of (E)F0 to (E)F5 (weakest to strongest, respectively) for all reported tornadoes. Nearly 85% of tornadoes in the US are classified as weak (F0 or F1), cause little damage, and account for a very small faction of annual US tornado deaths (Hyndman and Hyndman, 2009). While roughly 15% of US tornadoes are classified as strong (F2 or F3) and only 1% are given a violent classification (F4 or F5; ibid.), together F2 and stronger (F2+) tornadoes account for over 98% of the tornado-related deaths (Ashley, 2007).

| (Enhanced) Fujita Scale Intensity | Wind Speed (in m.p.h.) | Damage Caused |
|---|---|---|
| F0<br>EF0 | 45 – 78<br>65 – 85 | **Light damage:**<br>some signs and chimneys show light damage, broken tree limbs |
| F1<br>EF1 | 79 – 117<br>86 – 109 | **Moderate damage:**<br>shingles peeled off roofs, mobile homes toppled, vehicles blown off roads |
| F2<br>EF2 | 118 – 161<br>110 – 137 | **Considerable damage:**<br>whole rooftops blown off, mobile homes obliterated, big trees uprooted and snapped |
| F3<br>EF3 | 162 – 209<br>138 – 167 | **Severe damage:**<br>some walls and roofs blown out of single-family houses, whole forests uprooted, cars lifted and thrown, trains toppled |
| F4<br>EF4 | 210 – 261<br>168 – 189 | **Devastating damage:**<br>Most free-standing houses obliterated, large and heavy objects become missiles |
| F5<br>EF5 | 262 – 317<br>200 – 234 | **Incredible damage:**<br>Free standing houses are lifted and carried before destruction, cars become missiles and are thrown 100s of yerds, trees are debarked |

**Figure 1** – Fujita scale intensities, wind speeds and damage (adapted from Hyndman and Hyndman, 2009)

Fundamental concepts in meteorology tell us that severe storms, tornadoes, and weather in general are all very dependent on the wind patterns aloft – zonal flow generally leads to calmer weather and straighter isotherms across the latitudes; while meridional flow, on the other hand, favors more unsettling weather. Sharp temperature and humidity contrasts at the surface tend to coincide with jet streaks aloft (Moran et al., 1997; Aguado and Burt, 2001), while tornadoes can be strongly associated with jet streaks  as well (Rose et al., 2004; Whitney, Jr., 1977). Frontal boundaries often provide the lifting parameter necessary for the initiation of severe weather. Large-scale circulation patterns at different levels of the atmosphere are strongly related to the position and the movement of these air masses and fronts (Moran et al., 1997; Aguado and Burt, 2001).

Severe weather, and tornadoes in specific, need many ingredients in order to form. Instability is one of four key variables in determining a severe weather environment. Most often, instability is measured by calculating the convective available potential energy (Brooks et al., 2003a), but can also be measured by other instability indices, including the Lifted Index (LI), the Total-Totals (TT), the Severe Weather Threat Index (SWEAT Index), and others (Schultz, 1989; Davis and Walsh, 2008).

Another primary component of severe storms is vertical wind shear – defined as the change in wind speed and/or direction with height. Most often, the shear is measured by calculating the change in wind speed and direction between the surface and 1-6 kilometers above ground level (Brooks et al., 2003a; Craven and Brooks, 2004).

A third key ingredient, moisture, is also vitally important to the development of severe weather – it is normally measured by the low-level atmospheric water vapor (Trapp et al., 2009), or can be accounted for in the calculation of CAPE (Brooks et al., 2003a). Greater amounts of low-level moisture and higher dew point temperatures lead to steeper lapse rates, creating a more unstable atmosphere, and in turn enhancing the development of storm clouds (Moran et al., 1997).

A fourth key ingredient in developing severe environments is a triggering lifting mechanism, which contributes to the original initiation of storms. As mentioned before, often a migrating frontal boundary or a mid-latitude cyclone acts as this mechanism (Wilson and Roberts, 2006). Although numerous studies have been done that highlight the important role surface air mass boundaries have on tornadogenesis (Brazzell, Kellenbenz, and Bramer, 1998; Maddox, 1983; Maddox, Hoxit, and Chappell, 1980; Markowski, Rasmussen, and Straka, 1998), this fourth ingredient remains unaccounted for in the research thus far on climate change impacts on tornado frequency.

*2.2 – Tornadoes – Data Quality Issues*

Before the widespread usage of Doppler radar in meteorology, many weak tornadoes could go unreported if little damage and/or no deaths resulted. On the other hand, stronger tornadoes (at least F1 or stronger) caused the majority of tornado deaths and a lot more damage, and thus received some attention from news outlets and their numbers are thought to have more stability (Verbout et al., 2006). Doswell (2007) went into considerable detail outlining some of the data quality questions with tornado data that arise from this discrepancy between reported tornadoes and actual tornadoes. 'Secular tends,' or non-meteorological factors, were found to be the most likely cause of inaccurate trends in tornado data archived in the Storm Prediction Center (SPC) database (Brooks et al., 2003b). Most notably, simple line graphs appeared to show a significant increase of total US tornadoes since 1950 because of this inaccuracy in reporting. It was also noted in this research that there appears to be a slight decrease in the occurrence of F2+ tornadoes since the 1970s. This issue is likely due to the involvement of structural engineers being included in determining F-Scale ratings for damages to buildings (Doswell, 2007 and references therein) – although the *decrease* in F2+ tornadoes is not as steep as the *increase* in both F0 and F1 tornadoes since 1970.

Doswell (2007) outlined a number of options that could help mitigate this issue as much as possible – each of which, however, ushered in the possibility of having too few data to be able to test certain conclusions robustly. Furthermore, when some of these options were combined, this sample size issue was enhanced even further. The research noted that the further back into the data set that one went from 1970, the greater the problems of secular trends manifest. Thus, one possible remedy for mitigation of the secular trends was to use only tornado data collected since 1970. Using tornado days instead of total tornadoes was another possible solution. This method required setting a threshold to count a tornado day as a day that had anywhere from at least one to at least 30 tornadoes – the greater the threshold, however, the smaller the sample size of tornado days became. Another method to help with this issue was to use strings of consecutive days on which a tornado occurred (or a threshold for a tornado day was met) as a way of eliminating secular trends. These secular trends could potentially be problematic when considering the impacts of climate change on tornadoes (Doswell, 2007). The steps taken to help mitigate the issue of secular trends in the tornado data used in this research are discussed in section 3.1.2 below.

## *2.3 – Climate Change*

The leading international and interdisciplinary body on climate change – the Intergovernmental Panel on Climate Change (IPCC) – has concluded that it is very likely that anthropogenically-induced climate change due to increasing levels of greenhouse gas emissions will warm global temperatures by anywhere from 1.1°C to 6.4°C by the 2090s (IPCC, 2007a). The best estimate under a 'business as usual' scenario of future emissions has global temperatures rising 4.0°C by the 2090s (ibid.). This finding has led to countless studies on both the impacts of climate change and the mitigation of its causes and effects. Researchers contributing to IPCC reports have concluded that natural hazards such as heavy precipitation events, extreme droughts, heat waves, and tropical cyclones all will likely increase in frequency and/or intensity due to this warming (IPCC, 2007a). Much of the research that goes into the IPCC reports is based off of the output of global climate models (analogous to general circulation models – or GCMs).

Coupled atmospheric and oceanic global climate models, or AOGCMs (again, referred to as GCMs in this study) are continually being improved to take an increasing number of different factors into consideration when trying to project future climates under different scenarios (IPCC, 2007b). Due to their ability to reproduce observed climates of the past, scientists have used GCMs to project the impacts of climate change on fields such as agriculture, human health, water resources, and a number of other critical areas (IPCC, 2007b). In their fourth and most recent assessment report (AR4; IPCC, 2007b), the IPCC went into considerable detail outlining the variables that GCMs have shown a marked improvement in projecting since their third assessment report six years before. Among such variables, are large-scale distributions of temperature and pressure, general atmospheric circulation, wind patterns, and storm tracks – to the point of being able to accurately forecast the weather on much shorter time scales (IPCC, 2007b).

One of the major limitations of all GCMs, however, lies in their very coarse spatial resolution. While drastic improvements in resolution have also taken place over recent years, a single value for a variable within a space as large as a 1° x 1° latitude and longitude box, is still far from satisfactory for accurately projecting small-scale process, such as those necessary for resolving individual severe storms. Thus, if a researcher wishes to examine local-scale changes in future climates, some type of "downscaling" estimate must be made from GCM output (Wilby et al., 2004).

One of the more common types of downscaling is termed 'statistical downscaling.' Statistical downscaling involves creating equations that represent statistical relationships between atmospheric variables resolved at a large spatial resolution (predictors) and the local surface event (or variable) of interest (predictands; Wilby et al., 2004). Once this relationship has been established (based off of historical climate data), then GCM output data can be put into the equation in order to assess the local scale impacts of climate change on the predictand.

GCMs are normally run under the guidance of different emissions scenarios in order to provide a range of possible future climates. Future emissions scenarios are created by the Special Reports on Emissions Scenarios (SRES) for use with most of the research undertaken in the IPCC's Fourth Assessment Report. Among these scenarios are the A1FI, the A2 and the B1 scenarios used in this study (Figure 2). The A1FI scenario is in a family with two other A1 scenarios that outline a global future with increasing economic growth and a worldwide population that continues to increase until around 2050 before declination (IPCC, 2007a). The A1FI scenario however is often regarded as the 'business as usual' scenario due to its storyline's continued reliance on fossil-fuels to encourage technological growth (ibid.). The SRES B1 scenario is characterized by the introduction of many clean and efficient energy technologies (ibid.) and could be considered the most environmentally friendly of the scenarios considered in this research, while the A2 scenario would represent an intermediate scenario between the previous two.

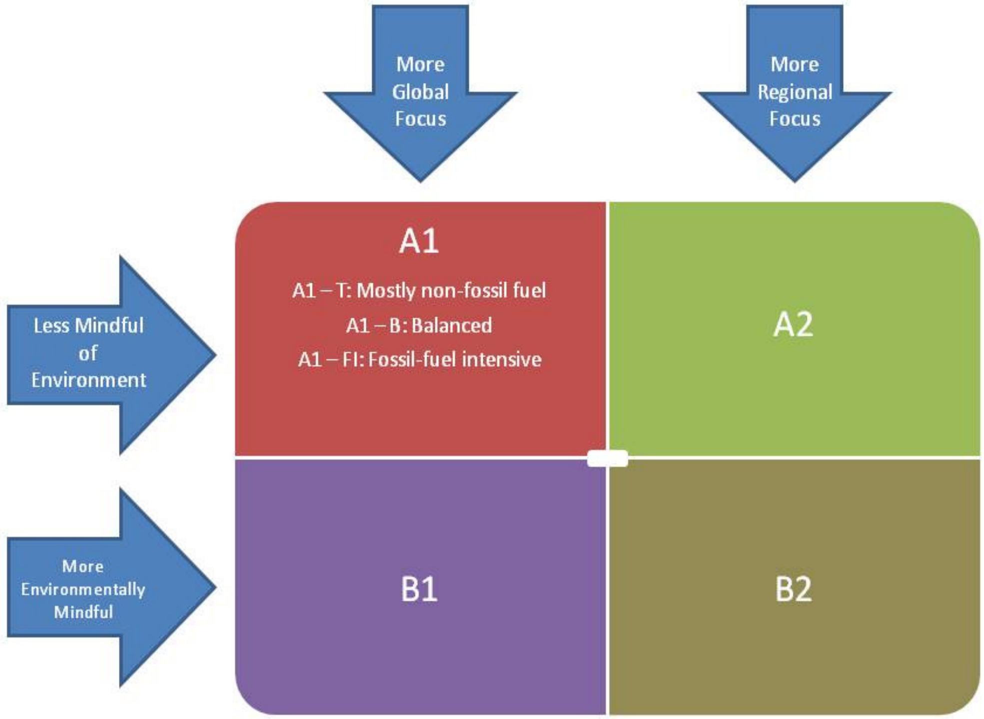


**Figure 2** – SRES Scenario Families (adapted from IPCC, 2007a).

## *2.4 – Climate Change Impacts on Tornadoes*

Among the many findings in AR4, an important conclusion is that warming temperatures will create more evaporation, greater amounts of low level moisture, and more instability – in turn, causing an increase in CAPE, and possibly an increase in severe storms. However, at the same time, a possible decrease in wind shear over some mid-latitude regions could offset the projected increase in CAPE and lead to a decrease in severe weather (Trapp et al., 2009). While the effect of climate change on tropical storms and hurricanes receives ample attention at the moment, impacts on the much smaller-scale mid-latitude severe environments – and the future changes in the seasonality, intensity, location and frequency of tornadoes in particular – receive considerably less attention. This inattention is due in large part to the aforementioned spatial resolution limitations of contemporary global climate models (IPCC, 2007b; Diffenbaugh et al., 2008).

This increase in instability projected to accompany higher temperatures and greater amounts of atmospheric water vapor has already prompted some climate change researchers to look into the possible effects a changing climate may have on the frequency of severe storm environments. The prevailing research on this topic has utilized an “ingredients-based” method that favors using proximity soundings as the basis for determining the CAPE and shear measures that have most favored severe weather in the past (as in Brooks et al. 2003a), and then using GCM output data to analyze how these specific ingredients might change in the future under different scenarios (Trapp et al., 2007, 2009; Marsh et al., 2009; Van Klooster and Roebber, 2009). Generally, these studies have shown an increase in days that are favorable for severe weather development (NDSEV) in the future, and as greenhouse gas emissions increase, so too do the amount of days that are favorable for severe weather.

Where these studies are lacking, however, lies in the fact that they do not account for processes such as migrating frontal boundaries (Brooks et al., 2003a), and an acknowledged lack of attention is paid to storm initiation (Trapp et al., 2007, 2009). Additionally, the nature of basing these studies solely on the specific ingredients of CAPE and shear that are present near the formation of a storm, ignores the large-scale atmospheric circulation patterns and the complex interaction between air masses that are so critical to the initiation of severe weather – and all extratropical weather in general.

Furthermore, low-level moisture estimates that go into a calculation of CAPE are based off of variables that can sometimes be poorly represented in both the NCEP/NCAR data set (outlined below) and GCM representations of historical climates, because it is a parameter either *completely derived* from model processes (a Class C variable), or at least is an output value *strongly influenced* by the model processes (a Class B variable) – depending on the specific variable used for an approximation of low-level moisture (Kalnay et al., 1996).

Considering both the abilities of GCMs (large-scale circulation, atmospheric pressure, and temperature distributions, and storm tracks) and the shortcomings (small-scale processes within a single grid box, estimates of moisture) mentioned above, looking directly at the role that large-scale atmospheric circulation plays in creating favorable environments for tornadoes could be the most useful approach to analyzing the impacts climate change might have on future tornadoes (Van Klooster and Roebber, 2009).

### *2.5 – Synoptic Climatology*

Synoptic climatology offers a potential supplement to previous research on the topic of climate change and severe weather by playing into the strengths of GCMs. Because the circulation of the atmosphere plays so heavily into the weather of the ground below, synoptic climatology is an entire subfield of the discipline that is devoted to relating general atmospheric circulation to surface environments (Yarnal, 1993). Synoptic climatologists are interested in finding methods to classify daily atmospheric circulation patterns (of individual atmospheric variables over a wide area) or weather types (many surface variables at individual locations) over a very long period of time in order to bring some order of utility to the unwieldy amount of climate data that exist.

As Yarnal (1993) delineated, all synoptic classifications can be undertaken with two differing approaches: circulation-to-environment or environment-to-circulation. The former approach classifies every day in the study period before even considering the surface event of interest. The latter approach classifies only the days on which that event (or environment) occurs. Although this is the first major divide between synoptic *approaches*, synoptic climatological classifications are broadly carried out using one of two *methods* as well – termed either manual or automated (by Yarnal, 1993).

Manual methods came about well before computers became popular tools for use in climatological research. These methods often involved the time-intensive process of a number of researchers going through hundreds of daily weather maps to pick out 'types' of patterns. The researchers then met as a team to discuss the patterns and if they were correct, or whether there were too many, or too few. Researchers then would go back over the maps and re-classify each day individually, before meeting again to make the final classification (ibid.). These classifications were often reused in later research (i.e. the Lamb, Muller, or Grosswetterlagen classifications), thus, bringing about some synergy between studies that used the same classification. Some of these manual classifications have undergone revisions since their original creation in order to be updated for usage in a more automated world. Besides the time-intensive nature of manual methods, another major drawback is that the results are not repeatable – often even by the same researcher using the same method.

Automated methods on the other hand are more popular in contemporary synoptic climatology and have been used in conjunction with GCMs (as discussed in section 2.5.5 below). Automated methods use computers to assist in determining the classes and classifying the days into one of those classes (Yarnal, 1993). These automated methods can take on a variety of forms themselves, and each type of method has its own benefits and drawbacks. Automated methods are often considered to be more objective and more repeatable than manual methods, despite the many subjective decisions that still inherently go into them (which will be discussed throughout this thesis). Additionally, since powerful computers capable of handling and running statistics on extremely large data sets have become more readily available, automated classifications are becoming the more popular method (Yarnal, 1993).

Like with all methods in the sciences, synoptic climatology has assumptions inherent to its methodology. One of the underlying assumptions fundamental to the discipline is that the atmospheric circulation plays a major role in influencing the surface event of interest (Yarnal, 1993). While certainly not encompassing every ingredient that goes into creating a tornado friendly environment, as discussed previously (in section 2.1), atmospheric circulation has been shown to have an important association to tornadic weather. A synoptic classification of patterns that are tornado friendly would provide a valuable and holistic complement to previous research on the topic.

Another assumption is that both time and space are accurately resolved into finite periods or areas (Yarnal, 1993). While daily classifications are based upon a snapshot of a day, the weather at any level of the atmosphere is a dynamic entity. At the same time, weather in the study area, especially the edges, is constantly being influenced by unaccounted-for factors outside the study area. Further complicating this second assumption is that these spatial and temporal intervals must be harmoniously partitioned between both the atmospheric variable(s) and the surface event of interest.

A third assumption is that the variability that exists within a class is not a problem (Yarnal, 1993). Certainly there are no two patterns (or types) that will be exactly alike; yet hundreds of days are lumped into a class. Variability will inherently exist within a class, and measures must be taken to reduce it as much as possible.

A fourth major assumption is that the classification developed captures all of the actual patterns (or types) that occur – and, vice versa, does not define more patterns than actually occur (this will be discussed further below).

Taking these assumptions into consideration, this thesis proceeds using a standard automated synoptic climatological technique to create a map pattern classification of daily atmospheric circulation. This standard technique uses a common two-part process involving a principal components analysis (PCA) and a cluster analysis (CA).

### *2.5.1 – Principal Component Analysis*

Yarnal (1993) describes the proper process to use when creating automated map pattern classifications with this two-part process. The first part in the process is to perform a PCA, both for data reduction purposes and to create principal component

(PC) variables that are completely uncorrelated with each other – a characteristic necessary of variables entering a clustering algorithm (Yarnal, 1993). PCA is a necessary precursor to clustering because of the issues presented from temporal and spatial autocorrelation of many climatological variables. That is, weather observations (such as a temperature) taken today are going to be closely correlated to the temperature that was observed yesterday, and similarly, will influence the temperature tomorrow (Wilks, 2006). Furthermore, in a spatial sense, the temperature observed in any one location is going to be more closely related to the temperatures nearby than it will to temperatures that are further apart. Thus, these types of data, observed closely in space and time, will always be highly correlated to each other. If these autocorrelated variables are allowed to enter separately into a clustering algorithm, they will likely bias the clustering procedure, by being given an overly-influential weight. Additionally, this data does not give the researcher any greater understanding of the underlying processes of the atmosphere (as common sense suggests that these observations would be closely correlated). The benefits of PCA in removing autocorrelation from large data sets with these characteristics is discussed below.

The first step in preparing a PCA to classify atmospheric circulation maps (as opposed to taking a synoptic typing approach) involves choosing a mode of decomposition of the data. The most common mode of decomposition for classification purposes is termed the “s-mode” – which emphasizes a single variable as it changes though space (Yarnal, 1993). The s-mode sets up the time (days in this study) as rows, and the stations (latitude and longitude coordinates in this study) as columns. Using the s-mode of decomposition of the data requires the use of a correlation matrix as the dispersion matrix that is entered into the PCA algorithm (ibid.).

The principal components derived from the PCA are created such that the first PC accounts for the greatest amount of the variability of the data set, the second PC accounts for the second most variability, and so forth. Thus, the first few PCs account for a large majority of the variability in the data set and are the only variables necessary to retain for further analysis – thereby reducing total data volume. However, the total number of PCs to keep for further analysis is one of the two major subjective decisions that go into an automated synoptic map classification.

A standard practice in synoptic climatological research has been to retain only the PCs with eigenvectors greater than one. Presumably, the reason behind this routine is because this threshold value delineates between a PC that accounts for more of the data set's variance than the mean amount of variance of the individual variables it is replacing (Yarnal, 1993). The total variance accounted for with the retained PCs when using this standard usually falls somewhere between 85% to 95% (Cuell and Bonsal, 2009). Cuell and Bonsal (2009), however, tested this standard practice and concluded that even retaining PCs all the way up to 99% of the variance accounted for, still could significantly change the outcome of a cluster analysis for creating synoptic types. Additionally, the investigators surmised that due to the computing power of most standard-issue contemporary computers, PCA for the sole purposes of data reduction and/or noise reduction might not even be necessary. The reasons for using PCA in this thesis, however, are threefold: to account for the most amount of variance possible in order to reduce any approximation error (Cuell and Bonsal, 2009); reduce data volume; and, most importantly, create uncorrelated variables for use in further analysis.

### *2.5.2 – Cluster Analysis*

As mentioned above, the retained PCs will then undergo a cluster analysis (CA) in order to determine both the *number* of typical atmospheric circulation patterns for each variable, and the *classification* of each day into one of those patterns (analogous to clusters). Clustering is necessary for a map-pattern classification because each PC carries with it minute amounts of variance from each grid-point in the data, which makes the spatial pattern of the PCs difficult to interpret (Yarnal, 1993). Instead, the clustering algorithm is performed on the component scores matrix after the PCA is completed, which will cluster the days that have similar combinations of PC scores (and thus similar atmospheric patterns) into the same group. In this case, CA is also a useful tool because neither the number of ‘typical’ atmospheric circulation patterns is known ahead of time, nor are the actual shapes of the patterns.

There are a number of different clustering procedures that can be used (Wilks, 2006; Yarnal, 1993), but hierarchical agglomerative clustering (HAC) techniques and k-means clustering are two of the more widely used in climatological analyses. HAC methods – which have been favored in similar past studies – take a set of data and assume that it has no group structure. In the first stage of the process, a HAC algorithm proceeds to group the two 'closest' observations (or days in this thesis) in Euclidean space, and then groups the next two closest observations in the next stage, and so on, in each subsequent stage until there is one large group with all observations included in the final stage. One drawback of this method is that once an observation is grouped, it cannot be relocated into another group, even if it may have been incorrectly grouped in a previous stage (Wilks, 2006).

After the selection of the *number of PCs* to retain, the second major subjective decision that goes into an automated synoptic climatology is the selection of the *number of clusters* to use for the classification (i.e. knowing at what intermediate stage in a HAC method does one stop grouping before getting to one group with all observations in it). Ideally, the main goal of any classification is to limit the variability within each group (or pattern), while at the same time maximizing the variability between groups (Davis and Rogers, 1992; Yarnal, 1993). One of the more common methods used (although still subjective; Wilks, 2006) is to examine a scree plot of the variances to find breaks the in the data that mark points at which unlike clusters are being forced to merge (Yarnal, 1993). However, due to the nature of the atmosphere never exactly replicating the same flow pattern twice, an approximation of likeness to other daily patterns ultimately has to be made in order to group multiple patterns. Thus, while this main goal is kept in mind, both the applicability and utility of the classification have to be considered as well when deciding on the total number of clusters in a synoptic classification. Although the actual atmosphere might have hundreds of patterns that are all quite different from each other, the utility of a classification with 100s of different classes would be null. Additionally, if the classification created does not actually resolve the surface event you are attempting to relate it to, then its immediate applicability is limited (Yarnal, 1993).

Another clustering technique used is called the k-means method – which is a non-hierarchical method. While this method allows for the reallocation of an observation into a group after it has been placed there, the drawback is that the number of groups must be specified in advance. The first step in k-means clustering is to define ‘seed points’ (or seed days) for the pre-specified number of groups. The next step is to calculate means for the seed points, where after, every other observation is assigned into one of the pre-specified groups based on how closely its mean is correlated to the means of those seed points. After each observation is classified, the means of the new group are re-calculated, and the process starts all over again with the first observation – thus allowing an observation to be re-classified (Wilks, 2006). When used together in some form (such as in Davis and Rogers, 1992) the benefits of each of these two clustering methods (k-means clustering and hierarchical agglomerative clustering) can be maximized while the drawbacks of each are minimized.

A relatively new type of cluster analysis will be used in this research: the two-step clustering component (as in Sheridan et al., 2009; Michailidou et al., 2009). The two-step clustering (TSC) component in SPSS Statistical Software (SPSS Inc., Chicago, IL) is suited to handle large data sets and involves an initial pre-clustering of the data (principal component scores in this thesis) into sub-sets and then uses a HAC technique to create the actual clusters from the pre-clustered subsets (SPSS Inc., 2001; Michailidou et al., 2009).

### *2.5.3 – Discriminant Function Analysis*

This thesis also uses discriminant function analysis (DFA) as a means of combining similar atmospheric circulation patterns into a group. While DFA is used to group observations, fundamentally DFA is not a clustering technique because a sample of the data must have already been grouped in order to use DFA (i.e. both the number of patterns and the shape of the patterns must already be known). The procedure in DFA builds functions (or ‘rules’) based off of the sample of the data set for which group membership is already known. These rules relate a set of independent variables to the grouping variable in the sample, before being applied to the rest of the data set for every observation for which each of those independent variables exist (Wilks, 2006).

More simplistically, DFA sorts observations into pre-defined groups based off of their similarity to previously grouped observations. Thus, when used after a CA has already been performed for a sample of the data (such as historical climate data), DFA is a great tool to use after new data are added (such as GCM output data) to the data set, and need to be classified into similar groups.

*2.5.4 – Applications of Synoptic Climatology with Severe Weather*

Synoptic climatological approaches to analyzing severe weather events at the surface are a standard strategy in climatology. Romero et al. (1999) used a synoptic classification to associate circulation patterns to heavy rain events over Mediterranean Spain. Perrin et al., (2009) discussed the association between planetary-scale oscillations (such as El Nino, La Nina, etc.) and tornadoes in the United States. Holt (1999) looked into the relationship of the overlying climatic conditions and severe surge events in Europe; Kunz et al. (2009) analyzed circulation patterns and their relationship to thunderstorm and hail frequency in Germany; and Kounkou et al. (2009) used reanalysis data to look at cool-season tornado environments over Australia. Additionally, Yarnal (2001) outlines a litany of different studies that use the synoptic climatological methods to classifying circulation patterns and their association to surface events.

Regional-scale synoptic climatologies of severe storms and tornadoes have been done for the Northeastern U.S. (Leathers, 1993) and Virginia (Davis and Rogers, 1992; Davis et al., 1997), and synoptic types and patterns were analyzed in their association to severe weather environments in parts of the Midwest (Miller, 1972). Larger-scale synoptic climatologies have also been done on derecho (episodes of strong straight-line winds) producing storms (Coniglio et al., 2004), and a more focused synoptic climatology has been done on severe weather outbreaks across the US that occurred along with northwesterly flow at the 500mb level (Johns, 1982; 1984). However, none of these studies looked at the relationship of tornadoes (specifically) to continental-scale atmospheric circulation patterns, or utilized their synoptic classifications in order to assess the impacts of climate change.

*2.5.5 – Synoptic Climatologies using GCM Output Data*

Due to the very coarse spatial resolution of today's GCMs and their inability to accurately project certain variables such as low-level moisture and precipitation, synoptic climatological methods have become an increasingly useful tool for use with GCM output data because of their ability to take large-scale and well-modeled features and downscale them to help describe local-scale phenomena (Sheridan and Lee, 2010; Cheng et al., 2007a, 2007b). Based largely on statistical associations to past environments, synoptic methods – although not yet extensively employed – are useful in this type of research because they take advantage of the variables GCMs are best at replicating in order to predict those that GCMs poorly project. GCMs have become increasingly accurate at replicating *historic* atmospheric temperature and flow patterns;

naturally leading researchers to project *future* atmospheric circulation patterns as well, and then apply synoptic methods to project impacts on weather events such as future freezing rain events, heavy precipitation events, monthly precipitation, air pollution, heat waves and more. Often in the case of precipitation, the results derived from utilizing synoptic methods to project future precipitation is more accurate than the precipitation projected by the GCM itself (Sheridan and Lee, 2010).

No known published research, however, has incorporated synoptic climatological techniques with GCM output data in order to project the future occurrence of tornadoes.

## CHAPTER 3

## DATA AND METHODOLOGY

### *3.1 – Data*

Among the more commonly used variables in synoptic classifications are the 500mb level geopotential heights (500z), 700mb level geopotential heights (700z), and 850mb level temperatures (850t) (Sheridan and Lee, 2010; Vrac et al., 2007). Geopotential height fields represent a topographic surface of the height (in meters; m) above mean sea level at which the atmospheric pressure can be approximated to reach a specific value (either 500mb or 700mb in this thesis). Roughly, the 500z represents atmospheric pressure at around 5,500m above sea level, while the 700z field represents the atmospheric pressure at about 3,000m. The 850mb level is roughly located at about 1,500m.

The daily maps of both the 500z and 700z values are used to look for the overall trough and ridge pattern across the region and to locate shortwaves. Often, cooler than normal temperatures and precipitation can be found on the surface below a trough, while warmer than normal temperatures and mostly fair conditions persist under ridges. Most important to this thesis, is that the greatest amount of severe weather and the highest likelihood of tornadoes is found just to the east of the trough at both levels. Generally, meridional flow has been shown to be more favorable than zonal flow in regards to creating a severe environment, though in some areas, westerly flow at these heights can be associated to severe weather as well (Miller, 1972). The 500z map in specific is useful in finding positive vorticity maximums in the atmosphere – under which severe storms are more favorable for development. The daily 700mb map of geopotential heights is more useful for identifying the shortwaves and frontal boundaries aloft. Generally, stormy weather is found in the exit region, or just east of the shortwave at 700mb.

While the 850t values give a good indication of the surface temperatures without the interference of planetary boundary layer friction, their daily maps are also useful for identifying areas of warm air advection which often signals an area of underlying surface convergence and the potential for severe weather.

While no individual daily maps are analyzed in automated classifications, the mean values of the variables (the 850t, 500z and 700z, in this study) for each cluster can be mapped in order to get an indication of type of daily pattern that each cluster represents. Using a fundamental meteorological understanding of the type of weather a particular pattern is associated with on a daily weather map can help determine the validity of any classification at resolving the surface event of interest.

*3.1.1 – NNR Data Set*

In order to get a uniform grid of data to derive accurate historical atmospheric circulation patterns that are easily comparable to GCM output data, the National Centers for Environmental Prediction (NCEP) and National Center for Atmospheric Research (NCAR; together, NCEP/NCAR) reanalysis data set (hereafter referred to as the NNR data set) was used in this study (Kalnay et al., 1996). This data set, which has since been updated for the years following 1996, is the result of a cooperative effort to create a global data set of atmospheric variables which unites historical records from a variety of sources (including, rawinsondes, aircraft, ships, and land surface observations from many countries) for the purpose of eliminating data quality problems in climatological research (Kalnay et al., 1996). The more reliable variables (in the A-Class; such as geopotential heights and temperatures) are resolved at 2.5° x 2.5° latitude and longitude in the horizontal, at 17 vertical levels in the atmosphere, and at a six-hour temporal resolution (Kalnay et al., 1996).

In this study, the 850t, the 700z and the 500z variables were taken from the NNR data set at a once-daily temporal resolution (at 1200 UTC, or 8 a.m. Eastern Daylight Time) over a 45-year period (from 1 September 1957 through 31 August 2002 – 16,436 days – hereafter referred to more simply as 1957-2002) at 5° by 5° latitude/longitude spatial resolution spanning the US from 66°N to 21°N latitude and 163°W to 58°W longitude (220 points; hereafter referred to as the 'full domain'). Again, the s-mode of decomposition of the data was used for analysis purposes, and thus, this NNR data is imported with each individual day as a row, the grid-points as the columns, and the values representing the daily value of either temperature or geopotential height at each grid point.

These three atmospheric variables were chosen for three reasons. First, these variables are among the most well-replicated in the NNR data set and the most well-represented in the GCM data sets, and therefore, as mentioned above, are among the most widely used in synoptic climatological research (Sheridan and Lee, 2010; Vrac et al., 2007). Secondly, the analysis of the three maps will give a good indication of the synoptic-scale favorability for tornadic activity through multiple levels of the atmosphere. And lastly, these three data sets were the most readily available and easily attained through all models (NNR and all GCMs) used herein.

### *3.1.2 – Tornado Data*

In order to associate the atmospheric circulation patterns to historic tornadic activity, tornado data were collected from the National Atmospheric and Oceanic Administration (NOAA)'s Storm Prediction Center (SPC; SPC, 2009) for every tornado touchdown in the US from 1950-2007. The state, date, and intensity (as rated by the Fujita Scale) of each tornado was of primary importance. Tornado data from Alaska and Hawaii were not included; and to allow for direct association with NNR data, the original 57-year full data set was trimmed down to the 1957-2002 time period of interest for all further analyses. The intensity of tornadoes in this data set is based off of the F-Scale prior to January 2007, and the EF-scale afterwards (referred to more simply as the F-Scale, from F0 through F5, hereafter).

Tornado text data were imported into SPSS with the days as rows, each state as a column, and the values representing the Fujita Scale number of the strongest tornado in a state on each day (a day with no tornadoes in a state was given a value of -1). In order to prevent an outbreak of scores of tornadoes all in the same day and in the same state from overwhelming the results, a binary variable was created for each state so that ‘tornado days’ are used for all further analyses, as opposed to ‘total tornadoes.’ This binary was created for all 48 states for each of the 16,436 days in the study. Furthermore, this binary was revised to count only days that had an F2+ tornado in a state as a ‘tornado day.’ Thus, for every day, either a zero was entered in the cell if there were no F2+ tornadoes in that state, or a one was entered into the cell if there were one or more F2+ tornadoes in that state on a particular day. Combined with using only F2+ tornadoes, using tornado days instead of total tornadoes helps mitigate the impact of temporal trends and the tornado reporting bias over the 45-year study period that was discussed earlier (and in Doswell et al., 2007). This data set is hereafter referred to as the F2-Binary data set and is not used again until after the circulation patterns are created.

### *3.1.3 – GCM Data*

Two GCMs are used in this research – both of which are GCMs used for IPCC assessment reports. The first GCM is the Community Climate System Model 3 (CCSM3); a GCM that combines four different models that separately project the atmosphere, the land surface, sea ice, and the oceans; which are then integrated through a fifth component, a coupler, which coordinates the entire system (Collins et al., 2006). The resulting model is able to project temperature, precipitation, pollution, cloud behavior, energy fluxes and other measures by considering variables as complex as albedos, sea-ice melting, snow and ice thickness, interactions though 40 layers of the ocean, the topography of the land surface, the biogeophysics of overlying vegetation and many other complex factors (ibid.). Additionally – and what makes the CCSM3 particularly attractive to this study – is the ability to analyze the chemistry, temperature, humidity, wind shear, pressure and more through 26 layers of the atmosphere. The CCSM3 is able to model stable climates for thousands of years under future scenarios (Collins et al., 2006; Sheridan et al., 2009).

The second model used in this thesis is from the Canadian Centre for Climate Modeling and Analysis (CCCma) and is the third generation Coupled Global Climate Model, or the

CGCM3. The CGCM3 also incorporates and couples four different models into its projections of future climates. With the latest atmospheric component (the Atmospheric GCM or AGCM) being the main update since the second generation of this model (CGCM2), the CGCM3 includes resolution at 32 layers in the vertical, three different soil layers that account for both solid and liquid moisture, a snow layer, a vegetation canopy layer, surface roughness, surface albedos, and even updrafts and downdrafts at sub-grid spatial scales (Environment Canada, 2009a, 2009b).

Although many vertical layers and differing temporal resolutions and horizontal spatial resolutions can be used from each GCM, both 20th Century and future atmospheric circulation patterns were created using 500z, 700z and 850t output data from the two GCMs. Both models were run for a historical period for verification purposes to check their ability to replicate past observed climates, and then run under different future emissions scenarios (outlined above). The CCSM3 was run under the A1FI, A2 and B1 scenarios, while the CGCM3 was only run under the A2 and B1 scenarios for this thesis (data from a GCM’s 20th Century run are hereafter referred to as GCM20c data, while data that come from a GCM’s run into the future under one of the SRES scenarios are more generally referred to as GCM-Future data). Output data from the CCSM3 in the historical run spanned the 1957-2002 time period of interest; and in the three future SRES runs, from 2000-2099. The CGCM in the historical run spanned the years 1961-2000, and two separate future runs for each SRES scenario from 2046-2064 and from

2081-2100. For ease of comparison with the NNR data set, every set of GCM data were taken at a once-daily resolution on a 5° by 5° latitude and longitude grid for the same full domain grid as outlined above.

## *3.2 – Methodology*

### *3.2.1 – Trimming the Domain of NNR & All GCM Atmospheric Data*

Among other conclusions in their review paper, Sheridan and Lee (2010) surmised that total grid domain is dependent upon the specific research question being asked. While some research has obtained better results with larger grid domains, other questions are more suitable to a smaller total grid domain (e.g. Hope et al., 2006).

After importing the raw text data from all NNR and GCM data sets at all three levels into SPSS, the first step was to trim each data set (Figure 3) into a domain that was most applicable to studying tornadoes in the US. The original 220-point data sets were trimmed to 72 grid points that spanned an area from 56°N to 21°N latitude and 108°W to 68°W longitude (hereafter referred to as the 'small domain') in 5° by 5° increments – roughly covering the US from the Rocky Mountains eastward into the Atlantic Ocean, and from central Canada south past the southern tip of Florida.

For this study, the full domain (mentioned in section 3.1.1) and a ‘medium domain’ (from 56°N to 21°N latitude and 133°W to 58°W longitude) were also analyzed for possible classification, but oceanic influences and the high topography of the Rocky Mountains were found to weigh too heavily in the circulation pattern results in the prime area of interest of the Great Plains and eastward. That is, some of the main differences between patterns were merely over the ocean or over the mountains, and did not change the pattern shape over the areas of interest. Thus, the aforementioned 72-point small domain was selected based upon its relative location to the majority of tornadic activity in those areas of the US.

*3.2.2 – Data Considerations for Seasonality Shifts & Methods for Removing Model Bias*

Due to the fact that many studies have found that climate change impacts on weather could manifest themselves as changes in seasonality (Sheridan and Lee, 2010; IPCC, 2007b), raw data are often preferred for analysis in impact studies because assessing climate change seasonality impacts are more difficult using any sort of seasonal standardization of the data. However, after a number of unsuccessful permutations using a trial and error method with raw data to find the most accurate GCM representation of the NNR circulation patterns, for each data set, the NNR data and every GCM’s 20th Century (GCM20c) data were combined in order to subtract out the monthly mean GCM bias at each grid point from the GCM20c data of each model (Figure 3). When this GCM bias was removed (or debiased), substantially better correlations between GCM20c and NNR circulation patterns were found (as in Hope, 2006; Demuzere et al., 2008) and these debiased data are used in all further analyses.

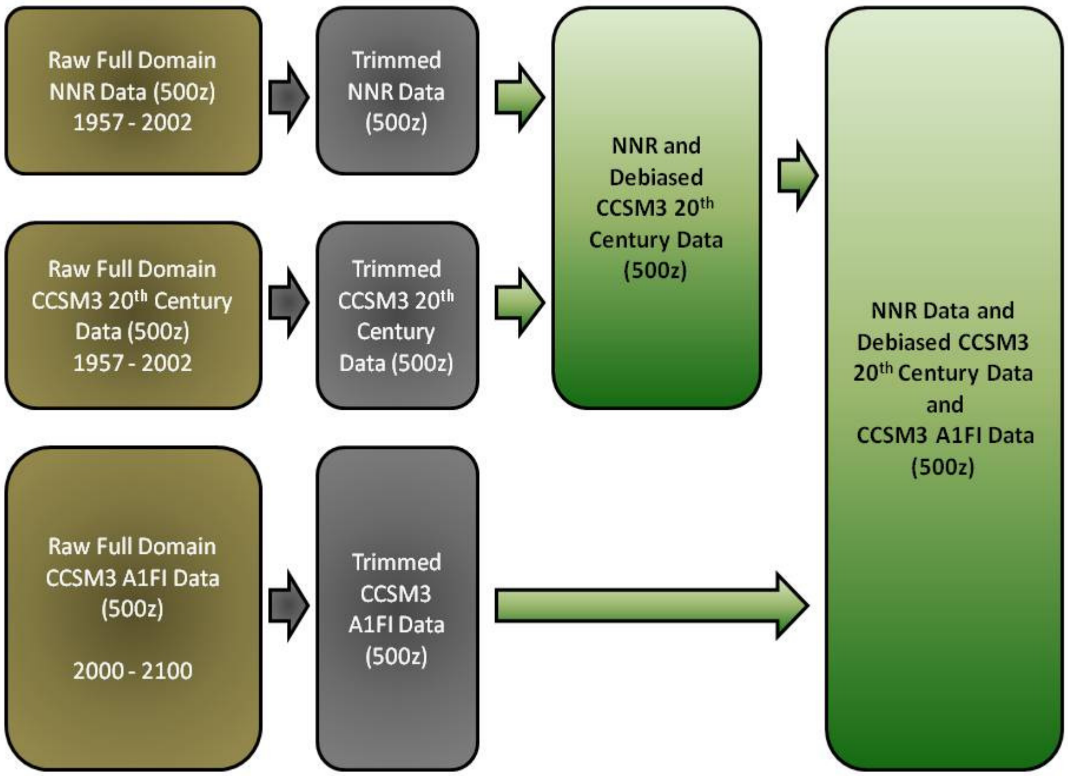


**Figure 3** – One iteration of the data preparation process. Brown boxes are raw data, gray boxes represent raw data that have been trimmed to the small domain, and green boxes represent trimmed data that have been merged and debiased. This process was repeated once for each level's data (500z, 700z, 850t) and once for each GCM's future scenarios (CCSM3: A1FI, A2 and B1; and CGCM3: A2 and B1).

This model bias must then also be removed from the GCM-Future data sets as well. Thus, for each of the scenarios in each GCM (the CCSM3 model has A1FI, A2 and B1, and the CGCM3 has A2 and B1), the future data set was combined with the GCM20c/NNR data set and the same mean monthly model bias at each grid point exhibited between the NNR and the GCM20c data was also removed from each of the data sets representing the future. These new data sets containing the NNR data, a GCM's 20th Century output data with the mean monthly model bias removed, and the future data of a scenario with that same bias removed, are used for all further analyses.

Removing this bias from each data set results in patterns showing less seasonality (i.e. they occurred more frequently throughout the year), and thus, in order avoid a 'tornado-favorable' pattern from shifting right out of a season-by-season analysis (the aforementioned expected impact of climate change), a year-long analysis was decided to be the most appropriate. Therefore, patterns were created using data for all 12 months, while tornado days were evaluated over a seven-month span from February through August (hereafter referred to as the TSeason).

Although the NNR, GCM20c and GCM-Future data sets are now merged, they are still kept separate for analysis purposes by adding a new variable into the data set that classifies the case into either NNR data, GCM20c data, or GCM-Future data.

### *3.2.3 – Six-Part Process for Creating Atmospheric Circulation Patterns*

After preparation of the atmospheric data is completed, circulation patterns are created using a six-part process (Figure 4). This six-part process is repeated for each of the 15 sets of merged NNR, GCM20c, and GCM-Future data involved in the investigation. The six-part method outlined below represents *one iteration* of this process (i.e. CCSM3-A1FI in which the 500z data is used). All analyses are run with SPSS.

*i. Principal Components Analysis of NNR Data*

The **first** part in the process is to perform a PCA on just the NNR data (Figure 4, arrow 1). The 500z values at each of the 72 grid points were entered into the PCA as the variables. The resulting PC scores were saved as variables. No rotation was necessary because the PCs are going to undergo a cluster analysis in a later step.

The primary purposes of performing the PCA in this study are both for data reduction needs, but also for creating uncorrelated variables to enter into the clustering algorithm. Thus, the PCA is necessary despite the aforementioned findings of Cuell and Bonsal (2009). However, many permutations of PCA with different numbers of PCs retained were tried in this research, including retaining PCs that accounted for up to 99.95% of the variance. The resulting synoptic patterns created from these different permutations varied minimally with each additional PC retained, and thus the standard method (of retaining only those PCs with eigenvalues greater than one) was adopted. Additionally, the final patterns that emerged when utilizing this standard method were the best at resolving tornadoes when compared to the other permutations.

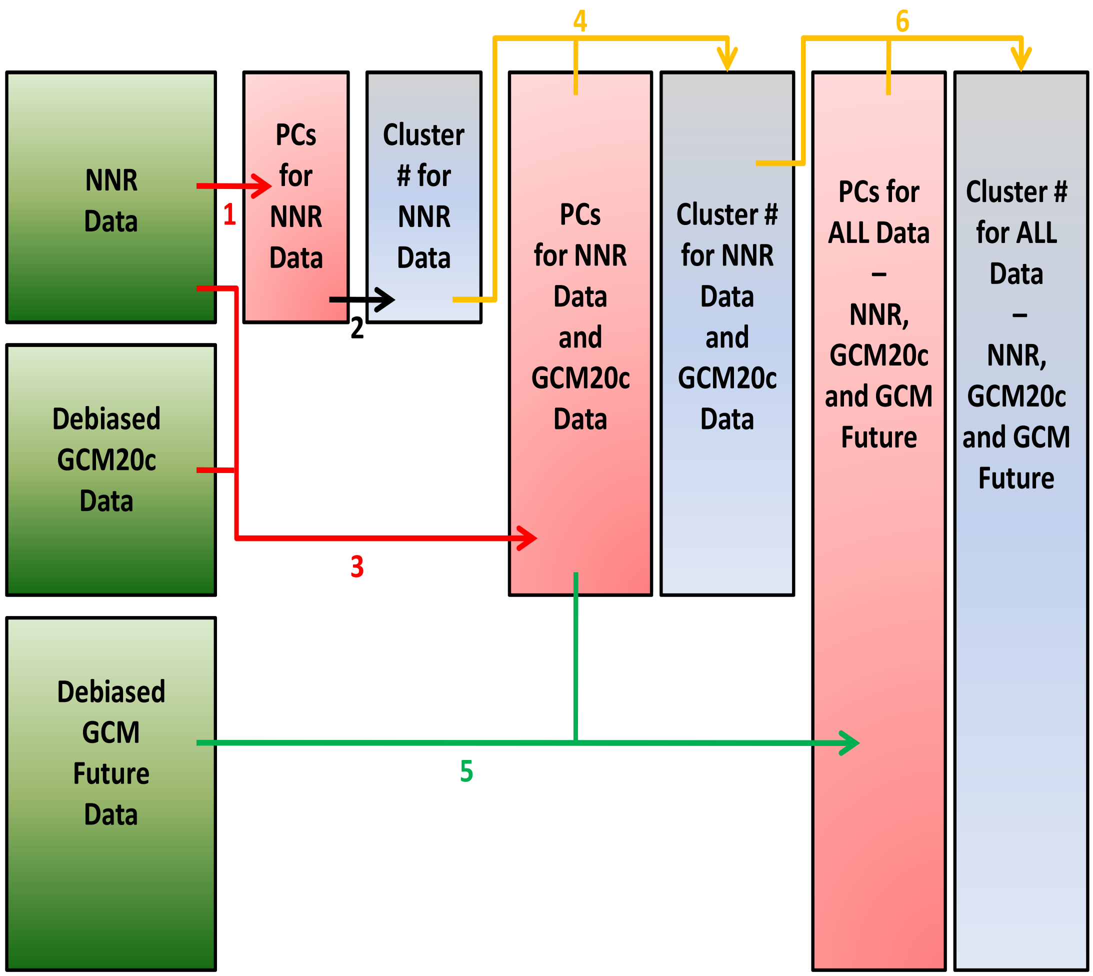


**Figure 4** – Flow chart diagramming the six-part process for creating the atmospheric circulation patterns. The six parts are the six numbered arrows: red arrows represent a PCA, orange arrows represent a DFA, the green arrow is a stepwise linear regression, and the black arrow is a TSC. Green boxes represent model data sets, red boxes are the derived principal component scores from the data sets, and the blue boxes are derived cluster numbers from the PC scores.

*ii. Two-Step Clustering of NNR Data*

The **second** part of this six-part process is to perform a Two-Step Clustering (TSC) on the retained PCs of the NNR data set (Figure 4, arrow 2). In SPSS, the TSC is set so that the principal components are inserted as continuous variables and are assumed to be standardized; the number of clusters is specified at 15 (this decision is discussed in section 3.2.4 below); the distance measure used is the log-likelihood; and the clustering criterion is Schwarz's Bayesian Criterion.

*iii. PCA of Both Data Sets*

The **third** part of this process is to perform a second PCA, this time including the 500z in both the NNR data set and the GCM20c data set (Figure 4, arrow 3) as variables entered into the PCA. A linear regression (to create a model from the NNR data set to predict the PCs of the GCM20c data set – similar to what is used in part 5 below) was not used here because the variability of both data sets needed to captured in the PCs in order to help validate the GCM's ability to replicate NNR patterns. Furthermore, because PCA is used here, when the final clusters are defined, they will be based off of the variability in the GCM and the NNR, and not just the NNR. The same settings are used as in the previous PCA, and again no rotation is necessary because the PCs will later be grouped using DFA. This PCA again creates uncorrelated PCs, but this time for both the NNR and the GCM20c data sets.

*iv. DFA of NNR and GCM20c Data Sets*

The PCs created from the previous step are then subjected to a DFA (the **fourth** part in the process; Figure 4, arrow 4). The DFA uses the TSC cluster variable created in part two as the grouping variable, and the newly created PCs (from part three) as the independents. The stepwise method is used with the F-score of Wilks' lambda as the criteria for entry into the DFA. Entry is based on the variable that minimizes Wilks' lambda. The entry criterion is set at 3.84 and removal is set at 2.71 (this is the default setting). Additionally, the classification of the prior probabilities is computed using the group sizes from the TSC groups. The predicted group membership number is saved as a variable in the data set. This DFA results in each case in both the NNR data set and the GCM20c data set being classified into one of 15 groups (as described in section 2.4.3 above).

*v. Linear Regression to Create PCs for Future Data*

The **fifth** part in the process for creating the atmospheric circulation patterns is to perform a linear regression on the data of all three data sets (NNR, GCM20c, and GCM-Future) in order to predict the PCs for the future data (Figure 4, arrow 5). The PCs created in third step of this process were used as the dependent variables to be predicted, while the 500z values for all data sets were used as the independent variables. The stepwise method of linear regression was used (with the significance values set at below .05 for entry and above .10 for removal), and the un-standardized predicted values for each PC were saved as variables in the data set. The linear regression was repeated for each PC that was created in step 3.

Linear regression was chosen instead of a third PCA in order to create future patterns that were similar to historical patterns, as opposed to allowing the future patterns to be taken into consideration when making the final patterns. Thus, if by the 2090s, the patterns are significantly warmer over the region – as is predicted by many studies (IPCC, 2007b), using PCA would most likely result in a pattern (or more than one pattern) that occurs mostly in the future and rarely in the past – which would significantly hinder comparability between the two time periods. The explicit assumption to using linear regression in this case is that future patterns will remain similar in shape and intensity in the future, while allowing for changes in frequency and seasonality.

*vi. Final DFA of All Data Sets*

The final circulation patterns are created in the **sixth** part of this process – a DFA of the PCs created from the linear regression in the previous step (Figure 4, arrow 6). The DFA cluster number variable created in part four is used as the grouping variable and the predicted group membership is saved as a variable in the data set. Once again the stepwise method is used and the entry and removal criteria are set at 3.84 and 2.71 respectively. Additionally, the classification of the prior probabilities is computed using the group sizes from the previous DFA groups. This DFA results in every day's 500z values (in the NNR, GCM20c and GCM-Future data sets) being classified into one of 15 patterns.

To visualize the circulation patterns that these groupings represent, the mean 500z field for each of the 15 clusters is then mapped. The resulting patterns are described in section 4 below. Again, this six-part process then starts over for each of the other 14 iterations representing other GCM scenarios and the other variables.

### *3.2.4 – Methods for Mapping*

Although patterns were *created* using only the data from the 72-point small domain, for easier interpretation purposes, the patterns were *mapped* using the mean temperature (or height) at each grid point for each cluster using the 128-point medium domain (outlined in section 3.2.1). This was accomplished simply by adding the data from the 56 additional grid points back to the data set after the six-part process had been completed and each day had already been grouped into one of the 15 clusters at each level.

The Kriging method of spatial interpolation (Johnston et al., 2001) was used to create the patterns in ArcMap 9.3.1. Spatial interpolation uses data at specific points (in this thesis, geopotential height or temperature values at 5° by 5° coordinate points of latitude and longitude) in order to estimate the spatial pattern throughout the entire domain. The contour maps were then made from the results of the interpolation. The contours were set at 60 meter intervals (running through the 5400-meter contour) for the 500z patterns, 30 meter intervals (running through the 3000-meter contour) for the 700z patterns, and at 2°C intervals (running through the 0°C contour) for the 850t patterns.

### *3.2.5 – Considerations in Deciding on the Number of Clusters*

As Yarnal (1993) and Wilks (2006) both note, the decision on the number of clusters is ultimately subjective and depends on the goals of the analysis. Ultimately, in this study, the applicability and utility goal (outlined in section 2.4.3 above) had the deciding influence on the number of clusters chosen. After using trial and error with many different numbers of clusters, this research proceeded using daily temperature and height data for the entire calendar year (instead of a season-by-season analysis – due to the possible future shift in the seasonality of patterns as discussed above) and determined that 15 clusters had the greatest applicability in accounting for the greatest resolution of tornado days. When a 16th cluster was added, it was noted that the main difference was in the addition of a wintertime pattern – with little change to the patterns of interest in the spring and summer. Using additional clusters for even better resolution of tornadoes was also thought to result in an unwieldy amount of patterns. When 14 clusters were used, it resulted in one less pattern that occurred most often in spring and summer – which was an undesirable result because it caused poorer resolution of tornado days. Additionally, once mapped, 15 distinct patterns emerged from the classification.

### *3.2.6 – Considerations in Deciding on the use of DFA*

The use of DFA was chosen after a number of permutations using TSC with the NNR and GCM20c merged data sets. When experimenting with the use of separate TSCs, it is worth noting that the TSC must be performed completely independently for the NNR and then for the GCM20c. Because of this, if separate TSCs were used instead of a DFA, the actual cluster numbers themselves would not equate to the same atmospheric circulation pattern in the two data sets (i.e. pattern 1 in the NNR data set would not look anything like pattern 1 in the GCM20c data set). Furthermore, it was realized that some patterns formed by the GCM20c TSC experimentations did not end up correlating well with any pattern from the NNR TSC when looking at the Pearson correlation coefficients of each of the NNR patterns to each of the GCM20c patterns. Additionally, some NNR patterns correlated almost equally well with two or more GCM20c patterns. However, when DFA is used, fundamentally, the groups created represent the same mean pattern in both data sets because the GCM20c patterns are grouped based upon their likeness to the NNR patterns (i.e. pattern 1 in GCM20c is calculated based off of the PCs in pattern 1 in the NNR – and is therefore representing the same pattern). The correlation tables presented in the section 4.2 of this thesis depict how well the patterns from the GCM20c match up statistically to the patterns in the NNR data set when using DFA.

*3.2.7 – Preparation of All Data for Binary Logistic Regression*

After the tornado data have been prepared and the atmospheric circulation patterns have been created, in five new data sets (one for each of the scenarios used), the 48 tornado binary variables are merged with the DFA cluster numbers for all three levels of the atmosphere – each on a day-by-day basis (Table 1). Since the DFA cluster numbers themselves are only used as a means of separating one atmospheric circulation pattern from another, and thus are categorical and not continuous variables, a binary is created for each of the DFA cluster numbers for each level of the atmosphere – creating 45 new variables (one for each of the 15 clusters at each of the 3 levels) – termed dummy variables (Table 1).

Additionally, one-day lag variables that represent the circulation pattern on the previous day, and one-day lead variables that represent the circulation pattern on the following day were created and added to the data set (Table 1). Each of these lag and lead variables (one for each level) also had to be created as dummy variables. In conjunction with ‘today’s’ dummy variables, the one-day lag and lead variables were found to better the predicting ability of the binary logistic regression discussed in the following section. Additionally, the belief was that in theory, ‘today’s’ pattern is a function of yesterday’s pattern, just as tomorrow's pattern is a function of today's pattern. Strings of days with similar patterns were also thought to give an approximation of seasonality, in that, if a May-dominant pattern happens to occur on a warm February day, it is less likely to occur on three straight days in February than it is to occur on three straight days in May. Furthermore, with the geopotential height and temperature values all being a snapshot of a pattern at 1200 UTC time (or the early morning of the different time zones of the US), tomorrow's pattern might be just as relevant to the actual pattern occurring in the late-afternoon of today – the time period of most severe weather (Ashley et al., 2008).

**Table 1** – Variables in each of the five data sets ready to be used for BLR analysis. The yellow highlighted row represents the 48 states and the USA F2 binary variables used as the dependant variable in each BLR iteration. The red variables were used in the final BLR permutation. The gray variables were extra variables used in other BLR permutations. The black variables are used to separate observations.

| Variable Name | Number | Description |
|---|---|---|
| Year | 1 | Year of the observation |
| Month | 1 | Month of the observation |
| Day | 1 | Day of the observation |
| TSeason | 1 | Binary Variable that delineates between TSeason and non TSeason |
| VAR00001 | 1 | Categorical variable that delineates between NNR, GCM20c and GCM-Future |
| Decade | 1 | Categorical variable that delineates between decades |
| **DFA_500** | **1** | **Categorical Variable that represents the 500z cluster numbers** |
| **DFA_700** | **1** | **Categorical Variable that represents the 700z cluster numbers** |
| **DFA_850** | **1** | **Categorical Variable that represents the 850t cluster numbers** |
| **D501 - D515** | **15** | **Binary variables that are dummy variables for each of the 15 500z clusters** |
| **D701 - D715** | **15** | **Binary variables that are dummy variables for each of the 15 700z clusters** |
| **D801 - D815** | **15** | **Binary variables that are dummy variables for each of the 15 850t clusters** |
| **LG501 - LG515** | **15** | **Binary varibales representing the one day lag of the 500z dummy variables** |
| **LG701 - LG715** | **15** | **Binary varibales representing the one day lag of the 700z dummy variables** |
| **LG801 - LG815** | **15** | **Binary varibales representing the one day lag of the 850t dummy variables** |
| **LD501 - LD515** | **15** | **Binary varibales representing the one day lead of the 500z dummy variables** |
| **LD701 - LD715** | **15** | **Binary varibales representing the one day lead of the 700z dummy variables** |
| **LD801 - LD815** | **15** | **Binary varibales representing the one day lead of the 850t dummy variables** |
| AL_F2Binary - USA_F2Binary | 48 | Binary variables marking an F2+ tornado day in each of the 48 states |
| PC1_500 - PC7_500 | 7 | Continuous variables of the seven PCs of the 500z data |
| PC1_700 - PC7_700 | 7 | Continuous variables of the seven PCs of the 700z data |
| PC1_850 - PC7_850 | 7 | Continuous variables of the seven PCs of the 850t data |
| LGPC1_500 - LGPC7_500 | 7 | One-day lags of the continuous variables of the seven PCs of the 500z data |
| LGPC1_700 - LGPC7_700 | 7 | One-day lags of the continuous variables of the seven PCs of the 700z data |
| LGPC1_850 - LGPC7_850 | 7 | One-day lags of the continuous variables of the seven PCs of the 850t data |
| 51_108 | 1 | The 850t value at 51N, 108W coordinate |
| 46_103 | 1 | The 850t value at 46N, 103W coordinate |
| 41_98 | 1 | The 850t value at 41N, 98W coordinate |
| 36_93 | 1 | The 850t value at 36N, 93W coordinate |
| 31_88 | 1 | The 850t value at 31N, 88W coordinate |
| 26_83 | 1 | The 850t value at 26N, 83W coordinate |
| AvgT | 1 | The average value of the six 850t values above |
| Diff1 - Diff5 | 5 | Differences between two of the 850t values above (two closest) |

*3.2.8 – Predicting Tornadoes Using Binary Logistic Regression*

Binary logistic regression (BLR) uses any number of independent variables in order to create an equation by which a dependent binary variable can be modeled to occur. In this study, the independent variables are the circulation patterns at each level and their one-day lags and their one-day leads. Each of these have been turned into binary variables, for a total of 135 variables entered into the BLR as independents. The dependent variable in each BLR iteration was each state's F2-Binary variable – thus the BLR was iterated 48 times per scenario, once for each of the 48 states in the area of interest. An additional BLR iteration was used on a binary variable created to represent whether or not there was an F2+ tornado day over the entire US as a whole (hereafter referred to as the USA F2 binary).

The BLR was set to run using the forward (stepwise) conditional method in SPSS. This method allows the entry and removal of a variable into the equation at each step based upon the significance of that variable's score statistic (SPSS, 2003). For this research, the significance of the statistic was left in the default setting (0.05 for entry, and 0.10 for removal). The probabilities for each day, for each state's BLR were saved as variables. These probabilities each represented the model's projection of a single state's likelihood of an F2+ tornado day occurring on each day in the data sets (NNR, GCM20c and GCM-Future). These probabilities are then summed in order to get monthly, yearly or decadal tornado days. These results are discussed in chapter four.

It should be noted, that over 35 sets of different independent variable combinations were tried before the aforementioned set of 135 variables was ultimately decided upon. Among these permutations, the 700z and 850t PCs (anywhere from one to seven PCs at each level) were tried, some 850t values at certain grid-points were tried, along with the averages and the differences of these temperatures at multiple grid-points (Table 1). The variables chosen represent tornado predictions that are purely based upon synoptic classifications. Adding other variables (such as PCs and specific 850t values) created less consistent results across the different states.

# CHAPTER 4

# RESULTS

The results portion of this thesis is divided into six sections. The first section will discuss the actual observed tornado climatology of the US derived from the tornado data – both total tornadoes and tornado days. The second section will outline the atmospheric circulation patterns (created by the six-step process discussed in section 3.2.3) and the association that these patterns have to tornado activity – delineating intuitively between favorable and unfavorable patterns for tornadic weather. The third section will analyze the accuracy of the BLR in modeling the observed tornado record in the CCSM3 GCM. The fourth section will compare and contrast the results of the previous two sections between the two GCMs used. The fifth section will compare the frequency and seasonality of the circulation patterns between the 20th Century and the future. The final section of the results will discuss the future projections of tornado days in both GCMs, with the frequency and the seasonality of each being highlighted.

### *4.1 – Observed Tornado Climatology of the United States*

#### *4.1.1 – Total Tornado Climatology (February – August)*

The greatest concentration of TSeason F2+ tornadoes in the US lies between central Oklahoma and East-Central Texas (Figure 5). Secondary areas of noted concentrations of F2+ tornadoes are the Texas Panhandle, spots throughout Kansas, central Nebraska, southeast South Dakota, central and western Iowa, central Indiana, central Arkansas and northern Alabama. While the rest of this study uses F2+ *tornado days* on a state-by-state basis for analysis purposes, this initial figure that displays each F2+ tornado in the study period will be useful in interpreting some of the later results.

#### *4.1.2 – Climatology of F2+ Tornado Days (February – August)*

Unsurprisingly, the F2+ tornado day (hereafter referred to more simply as a tornado day) map (Figure 6) is very similar to the total tornado map mentioned in the previous paragraph and is in line with many other studies looking into the states with the most tornadoes (Concannon et al., 2000; Brooks et al., 2003b). Overall, there were 2,498 tornado days in the US over the course of the study period, or a mean of 555.1 tornado days per decade. Every state in the study area experienced at least one F2+ tornado day during the study period with the exception of Nevada (Alaska and Hawaii were not included in the study).

Oklahoma and Texas are the only two states with more than 250 tornado days over the course of the study period. Due to its massive size and its location at the southern end of Tornado Alley, Texas has nearly double the number of tornado days (116.9 per decade) compared to Oklahoma (at 61.6 per decade). Four other states in the Midwest or Great Plains round out the top six states, each having more than 150 tornado days over the 45-year period: Kansas (48.7 per decade), Iowa (45.8 per decade), Illinois (41.1 per decade), and Nebraska (39.8 per decade).

**F2+ Tornado Days in Study Period**
**February - August**

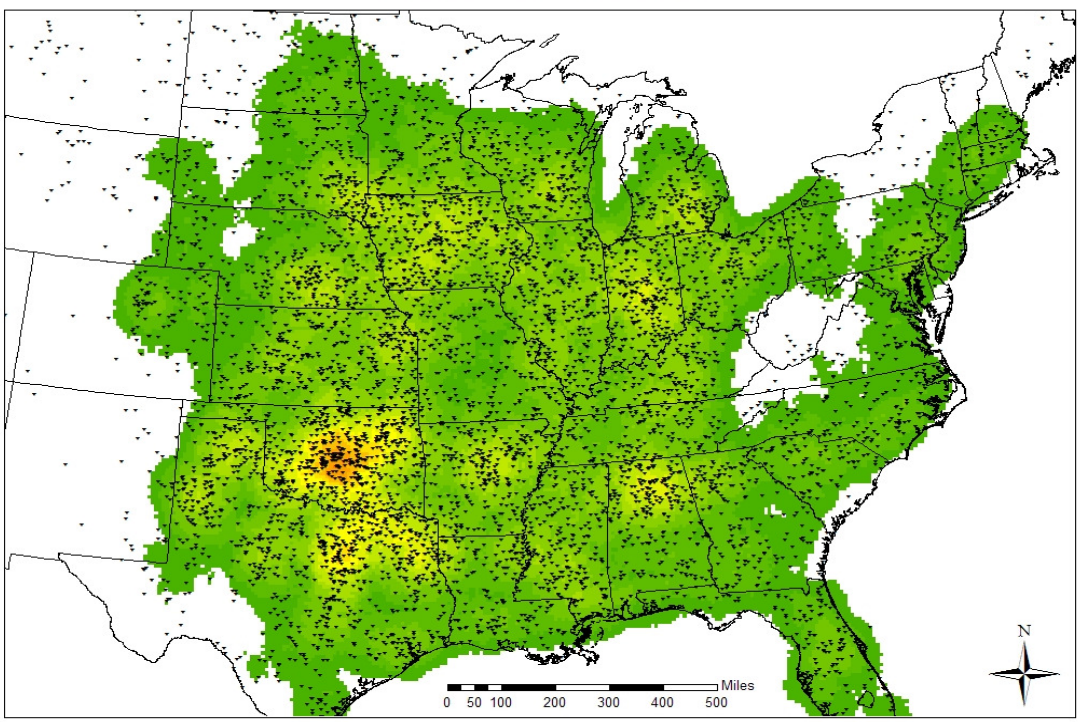


**Figure 5** – Total observed F2 and stronger TSeason tornadoes in the study period. Each black dot represents the location of an F2+ tornado touchdown. Dense regions of tornado touchdowns are marked in yellows, oranges and reds (greatest), while green and white (least) areas are less dense.

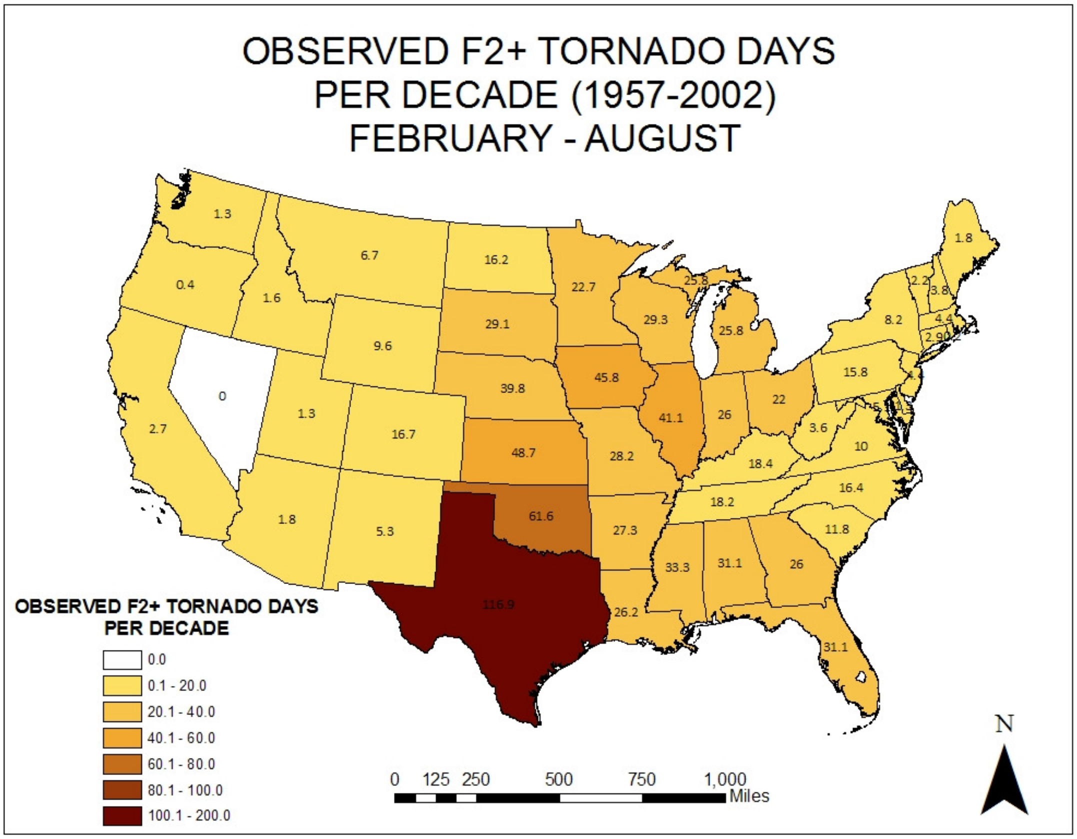


**Figure 6** – Observed F2+ tornado days in the US during the study period.

## *4.1.3 – Monthly Climatology of Observed F2+ Tornado Days*

The TSeason F2+ tornado days map discussed above has also been broken up by month in order to allow for direct comparisons to be made with later results in regards to the possible future changes in the seasonality of tornadoes. When broken down by month, vague regions of tornado days also begin to show up.

Quite a few of the states with a considerable number of TSeason tornadoes get an early start to the season on the February map (Figure 7). The first region is the southern states, especially the ones bordering the Gulf of Mexico. Mississippi (5.8 per decade), Texas (5.1 per decade), Florida (3.8 per decade), Alabama (3.6 per decade), a Louisiana (3.6 per decade) each have more than 15 tornado days in February over the study period, while the US as a whole had 108 (or 24.0 per decade). The other region worth noting is the Northern Plains and Upper Great Lakes area (NPUGL) whose states were shown to have at least 20 tornado days per decade each during the entire study period (except for North Dakota), but none of which have had a single F2+ tornado day in February.

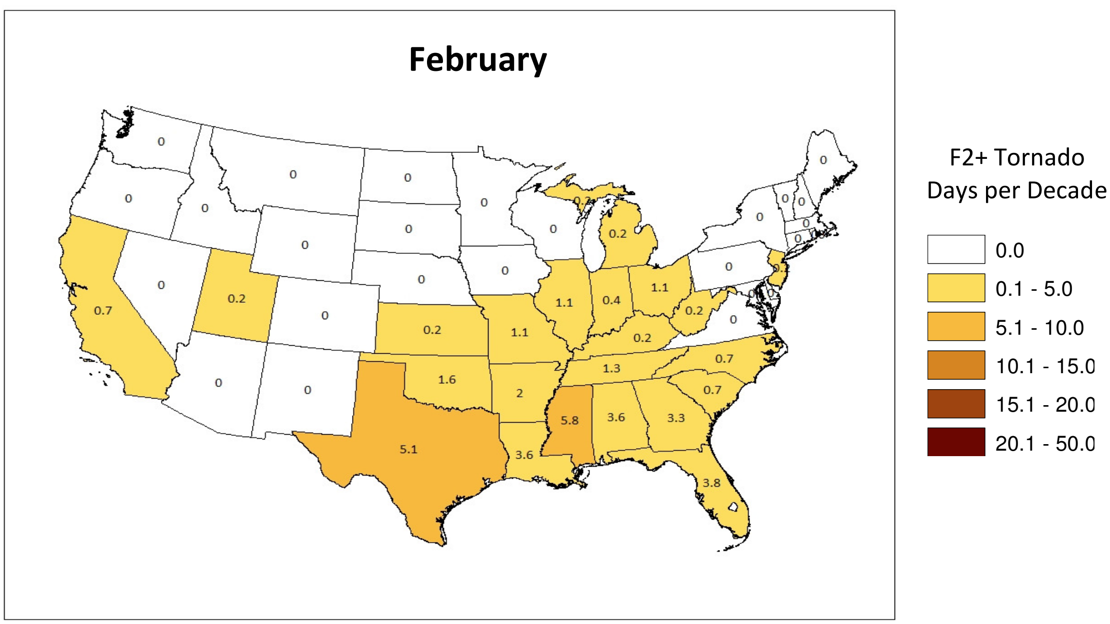


**Figure 7** – Observed monthly climatology of F2+ tornado days in the US during the study period (continued on the next page).

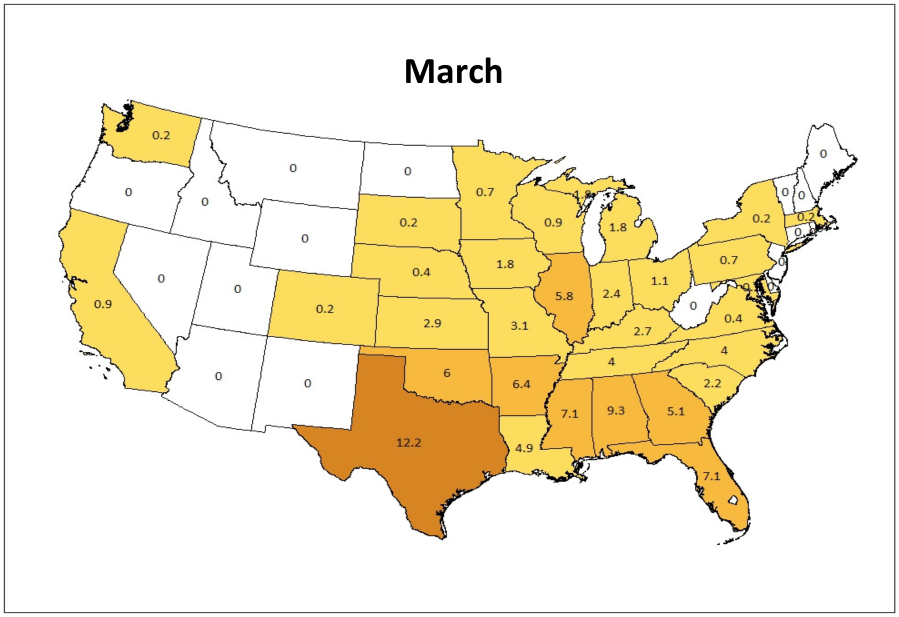


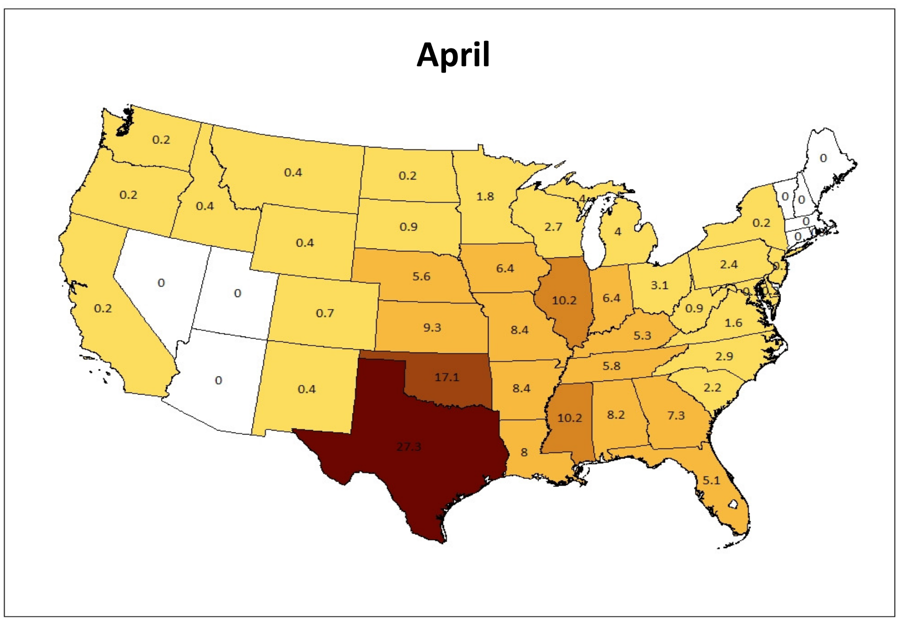


**Figure 7 (continued)** – Observed monthly climatology of F2+ tornado days in the US during the study period (continued on the next page).

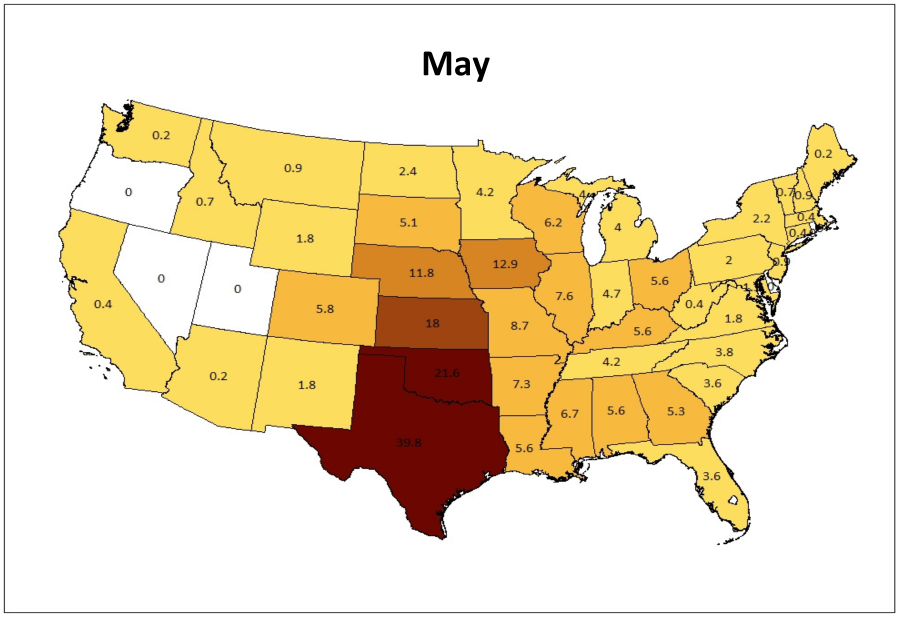


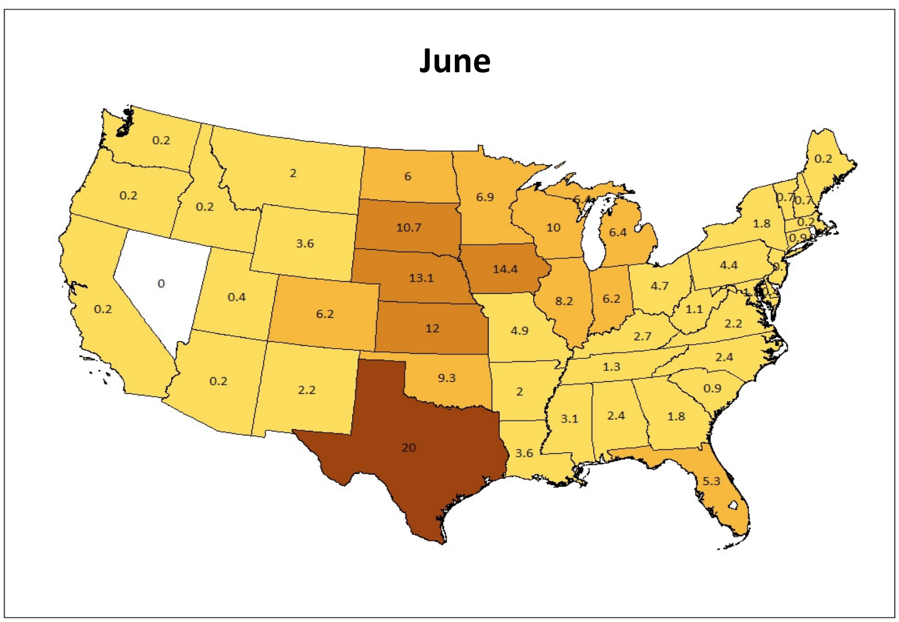


**Figure 7 (continued)** – Observed monthly climatology of F2+ tornado days in the US during the study period (continued on the next page).

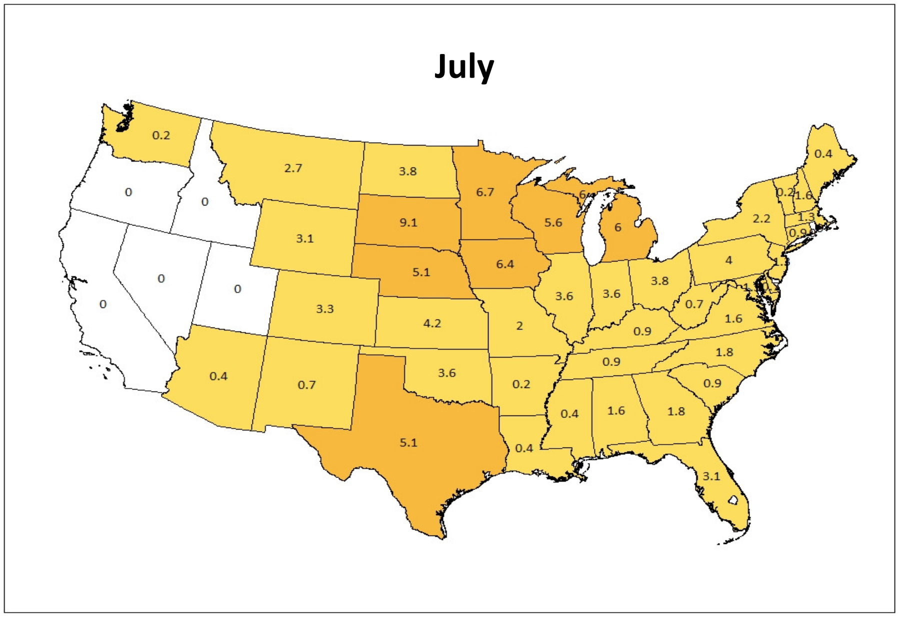


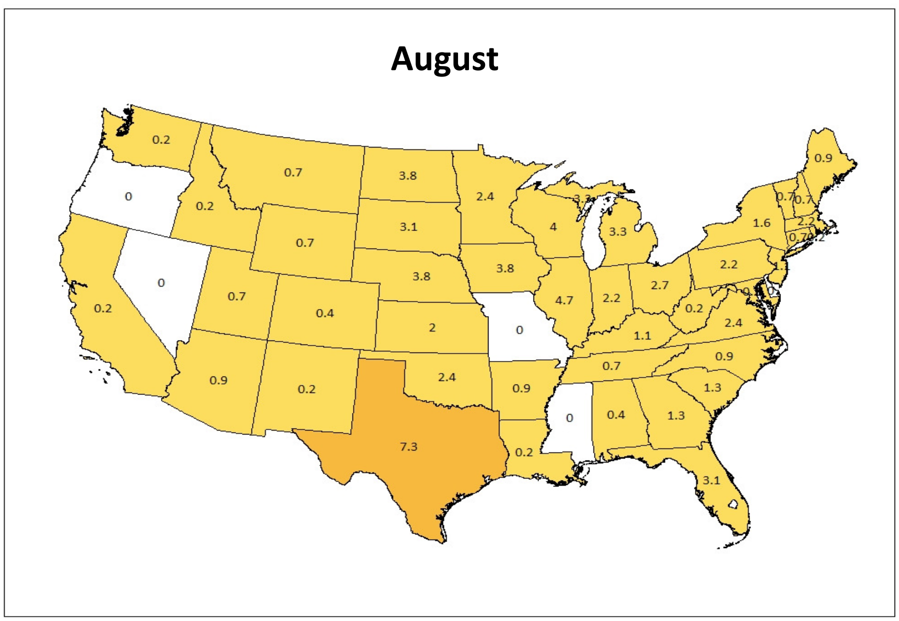


**Figure 7 (continued)** – Observed monthly climatology of F2+ tornado days in the US during the study period.

The March map (Figure 7) appears to be an extension of the February map, with greater numbers of tornado days in some southern states, while the first few tornado days begin to appear in the NPUGL. Illinois stands out from its bordering states as one of only seven states with more than 25 tornado days in March (with 5.8 per decade) – all of the others are completely south of the 37th parallel. Texas also stands out as the state with the most tornado days in March with 12.2 per decade. As a whole, the US had 264 tornado days in March or 58.7 per decade.

April (Figure 7) marks the peak of the tornado season in the more southerly states, especially in the Southeast, and the rise of the tornado season in the northern states. Texas (27.3 per decade) and Oklahoma (17.1 per decade) each have over 75 tornado days during the 45-year period. Mississippi (10.2 per decade), Illinois (10.2 per decade) and Kansas round out the top 5 in April – each experiencing more than 40 tornado days during the study period. The Mississippi River valley states begin to experience an increase in activity, as do the Northern Rockies states. The US as a whole has its third most active month in April with 424 tornado days or 94.2 per decade.

May (Figure 7) is the peak of the tornado season throughout the Southern Great Plains and Tornado Alley, as well as being the peak month for the US as a whole (561 total days; 124.7 per decade). Texas (39.8 per decade), Oklahoma (21.6 per decade), Kansas (18.0 per decade), Iowa (12.9 per decade) and Nebraska (11.8 per decade) each have at least 50 tornado days in May. The states immediately bordering this region to the east – Missouri (8.7 per decade), Illinois (7.6 per decade), and Arkansas (7.3 per decade) – also have more activity than their bordering states to the west.

With 527 tornado days, June (Figure 7) is the second most active month in the US as a whole (117.1 per decade). While Texas again leads the way due to its size with 20.0 per decade, the warmer conditions likely shift a majority of the tornado activity northward into the NPUGL region. Texas is followed by Iowa (14.4 per decade), Nebraska (13.1 per decade), Kansas (12.0 per decade), South Dakota (10.7 per decade), and Wisconsin (10.0 per decade). June is also the month in the TSeason with the broadest range of activity, with each state except for Nevada experiencing at least one F2+ tornado day in June during the study period. Noticeably fewer tornado days (compared with previous months) are depicted in the Southeastern US (with the exception of Florida) and along the Mid-Atlantic coast.

Compared to the previous month, a marked decrease in F2+ tornado days across the country is the most noticeable feature of the July map (Figure 7). South Dakota, however, leads the way in July as the only state with more than 45 tornado days over the study period (9.1 per decade), followed by Minnesota (6.7 per decade), Iowa (6.4 per decade), Michigan (6.0 per decade), and Wisconsin (5.6 per decade). The entire Southeast also stands out as having fewer tornado days than the bordering regions to the north and west. Over the entire US, there were 352 tornado days, or 78.2 per decade in the month of July.

Texas again leads the way in August (Figure 7) with 33 tornado days (and 7.3 per decade), but the majority of the activity remains in the NPUGL region, with each state except Minnesota experiencing at least three tornado days per decade. Behind Texas, seven states from the NPUGL region follow: Illinois (4.7 per decade); Wisconsin (4.0 per decade); Iowa, Nebraska and North Dakota (each with 3.8 per decade); Michigan (3.3 per decade); and South Dakota (3.1 per decade). In the US as a whole, August has the second fewest tornado days (behind February) with 262 days, or 58.2 per decade.

## *4.2 – Historic Synoptic Patterns and Tornado Association*

### *4.2.1 – Overview*

In total, 15 atmospheric circulation patterns were created at each of the three levels for each GCM. For a more intuitive interpretation of the results, each pattern's association to historic tornado activity is provided on the same map as each pattern. The tornado choropleths are mapped using the percentage point difference between *actual* tornadoes and *expected* tornadoes in each state for that pattern (e.g. if there are 15,000 days in the data set and there are 15 clusters, then each cluster would be *expected* to occur 1,000 times. If there were 500 *actual* tornado days in Texas over those 15,000 total days, then 33.33 tornado days would be *expected* per cluster and Texas would have an *expected* tornado day probability of 3.33% - and each cluster would then have an *expected* tornado day probability of 3.33% as well. But, if cluster A only *actually* happened 300 times – instead of the 1000 *expected* times – but had 50 *actual* tornado days in it instead of the 33.33 *expected* tornado days, then it would have an *actual* tornado day probability of 16.66%. Now, although this is a 500% increase in tornado days over what would be expected, the choropleth map merely represents the <u>percentage point difference</u> between the *actual* tornado day probability of 16.66% and the *expected* tornado day probability of 3.33%, and would therefore be mapped as a +13.33%.). This method was chosen to prevent some states that have very few tornado days from being over-represented in the results merely as an artifact of the statistical methods. Again, tornado days represented in this map are only those occurring from February through August (TSeason).

The patterns discussed below are mapped using the data from the 20th Century run of a GCM. The correlations between the GCM20c patterns and the NNR patterns are all very high (above 99%) and can be considered analogous while initially reviewing the results (though full correlation tables and mean absolute error tables are provided in tables 2 through 4).

Due to many similarities between the two GCMs (CCSM3 and CGCM3) in the historic synoptic patterns that they produce, only the CCSM3 patterns will be outlined in detail below. While general comparisons between the two models' historic patterns will be made in later sections of the results, a comprehensive collection of the maps of the CGCM3 patterns, their tornado associations, and their seasonality, can be found in Appendix B.

The 15 patterns were given letters (A through O) as identifiers (instead of the numbers created from the six-step process), as well as short titles for a more intuitive interpretation. Additionally, the patterns were re-ordered after creation in order to list the 'tornado-favorable' patterns before the 'tornado-unfavorable' patterns – though these monikers are only intended to be helpful for qualitative analyses. All patterns – favorable or unfavorable – are included when calculating future tornado projections in section 4.5 below. The legend that corresponds with the maps in figures 9 through 11 is represented in Figure 8 below.

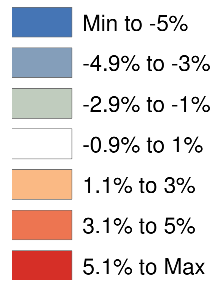


**Figure 8** – Tornado association legend. This legend is to be used for the synoptic pattern and tornado association maps presented throughout the rest of section 4.2. The legend is in terms of the percentage point difference between actual tornado days and expected tornado days.

*4.2.2 – CCSM3 20th Century Synoptic Patterns and Tornadoes – 500mb Level*

Patterns A through F are considered favorable for tornado activity across the US as a whole, while patterns G through O are considered unfavorable at the 500mb level (Figure 9).

**Pattern A (A500) – Rocky Mountain Trough** – Pattern A at the 500mb level features a trough over the Rocky Mountains with the 5460 line dipping southward into central Montana. Due to the meridional nature of this pattern, along with its seasonality (occurring most frequently in the peak of the tornado season from March through May), pattern A is favorable for tornado development throughout the Southern Great Plains, the Midwest, and the Upper Great Lakes regions.

**Pattern B (B500) – Southwest Trough** – A trough that has an axis running from the four corners region through Northern Mexico creates favorable conditions in Pattern B for tornado development just downwind in the Southern Plains states, as well as just north and just east of this area. Like pattern A, this pattern occurs most frequently in the peak tornado season, but only about half as often. A ridge in the Northern Plains makes this pattern unfavorable for tornado development in that area.

**Pattern C (C500) – Deep High Plains Trough** – Compared to the previous two patterns, pattern C features a much more pronounced trough that extends the length of the continent on a southwest axis, from Hudson Bay in Canada to Baja California in Mexico. This pattern occurs most frequently in the winter and early spring months, and the exit region of the trough is in line with increased tornado activity in the Southeast US and Illinois, while below normal activity is evident in the Plains states and Florida.

**Pattern D (D500) – Summer Weak Plains Trough** – While fairly zonal in nature, a weak trough can be identified in pattern D over the Canadian Shield, as well as over the West Coast states. Pattern D occurs nearly 30% of the time in May and June before dipping in the middle of summer and peaking again in September. Although this pattern does occur most often in autumn, the choropleth only represents tornado days from February through August. This pattern is favorable for tornadoes in the Cornbelt.

**Pattern E (E500) – Spring Shortwave Trough** – At first glance, Pattern E looks fairly zonal, but a shortwave trough can be identified in the Northern Plains region. This pattern's seasonality is limited mostly to the shoulder seasons – most often in April and May, and is relatively warm for that time of year. Pattern E is quite favorable for tornado activity in the Southern Plains, while a more muted favorability is exhibited in the Southeast and northwards into Indiana.

**Pattern F (F500) – Plains Trough** – Pattern F is a mild and quite infrequent winter pattern with a trough extending on a south-southeast axis from the Northern Plains through Texas. Although unfavorable for tornadoes in the Northern Plains, the Southeast again sees increased activity under this pattern.

**Pattern G (G500) – Weak East Coast Trough** – At the 500mb level, Patterns G through O are all considered 'unfavorable' for tornado activity. Pattern G features a fairly weak trough along the Eastern seaboard. This pattern occurs most often in winter and is unfavorable for tornadoes throughout the Plains.

**Pattern H (H500) – Weak Great Lakes Trough** – While favorable for tornadoes in three states, overall in the US, this pattern is considered 'tornado-unfavorable.' Pattern H is another winter pattern that occurs most often towards the early winter before leveling off in the spring. This pattern's weak trough is most noticeable in the Great Lakes region.

**Pattern I (I500) – Spring Rocky Mountain Ridge** – While Pattern I occurs throughout winter, its peak seasonality is actually in early spring. As a fairly meridional pattern, a broad ridge can be seen over the Rockies along with a noticeable trough from Maine southward into the western Atlantic Ocean. Decreased tornado activity is present throughout much of the Plains, Midwest and Southeast.

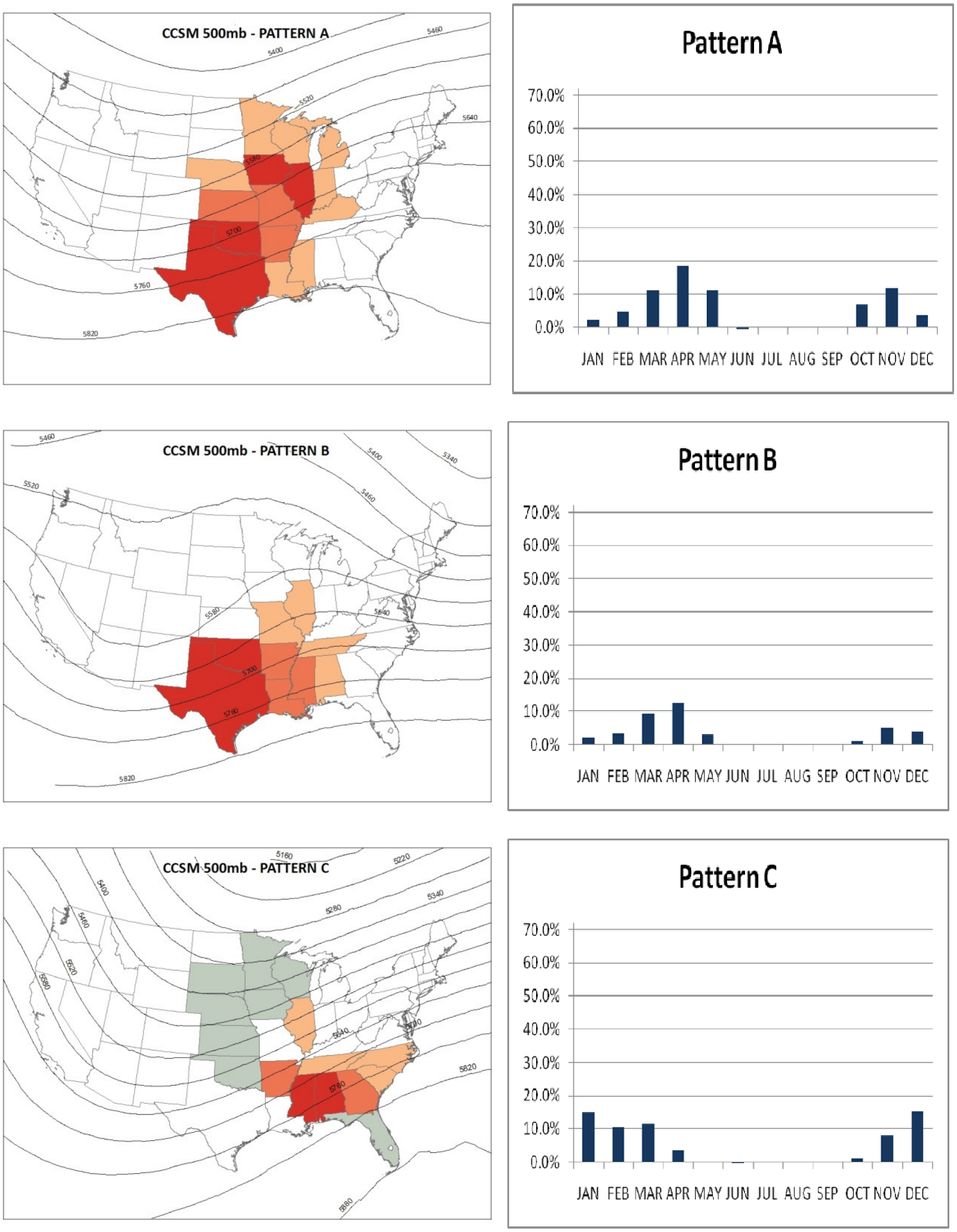


**Figure 9** – The 15 CCSM3 synoptic patterns at the 500mb level with the associated tornado activity for each pattern (on the left); and percent frequency of occurrence by month of each pattern during the GCM20c time period (on the right). Color coding for the tornado association on the map on the left can be taken from figure 8 (Continued on the next page).

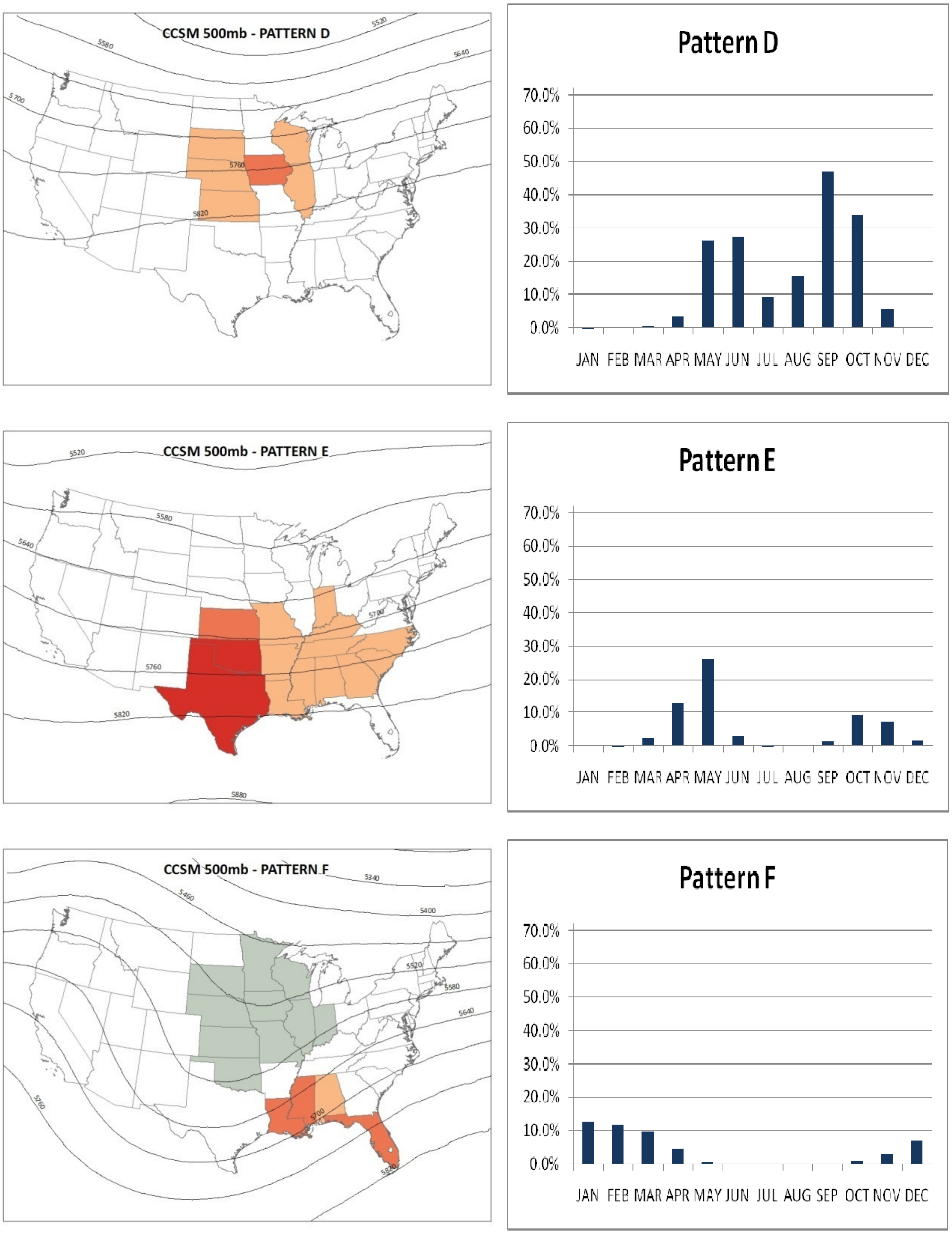


**Figure 9 (continued)** – The 15 CCSM3 synoptic patterns at the 500mb level with the associated tornado activity for each pattern (on the left); and percent frequency of occurrence by month of each pattern during the GCM20c time period (on the right). Color coding for the tornado association on the map on the left can be taken from figure 8 (Continued on the next page).

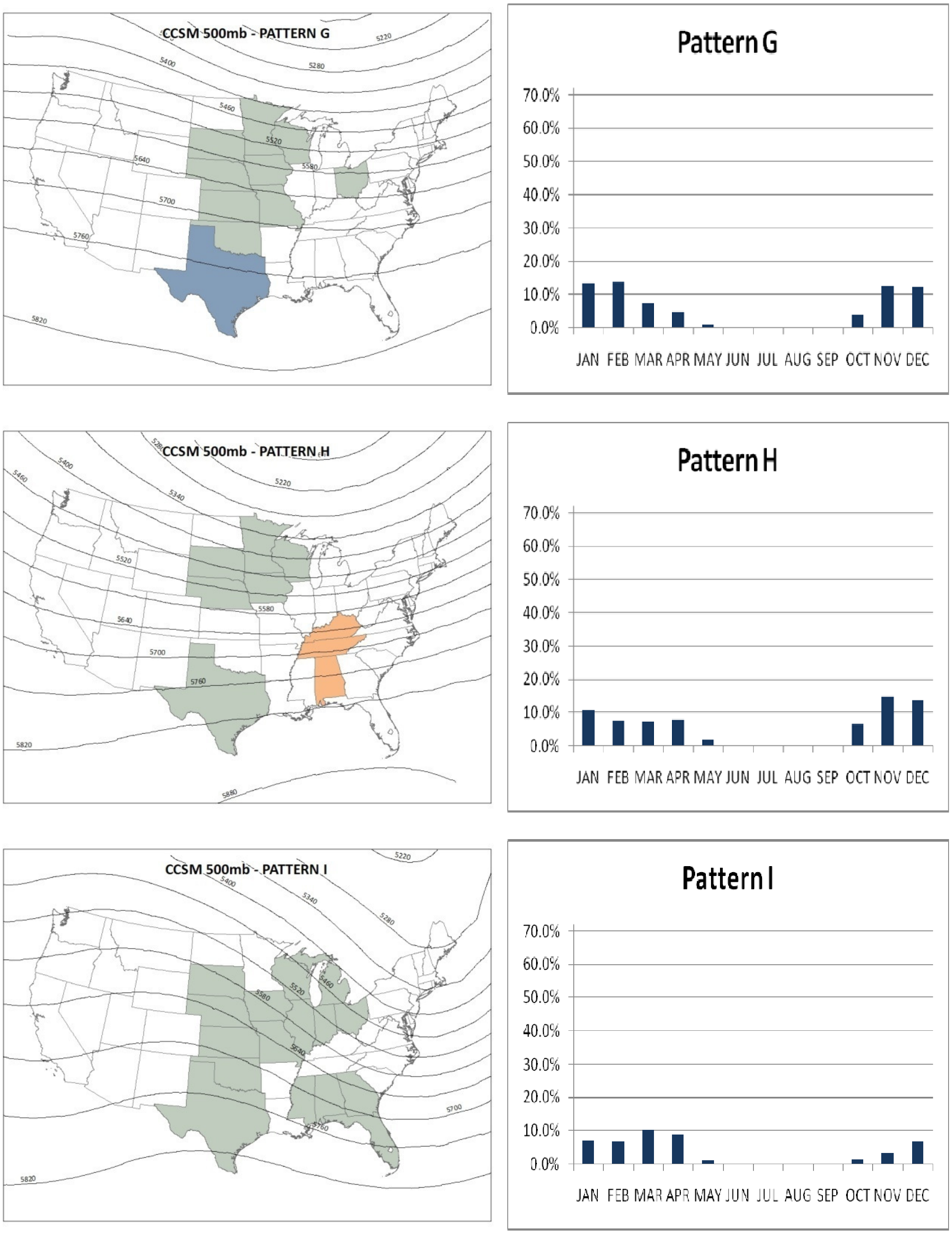


**Figure 9 (continued)**– The 15 CCSM3 synoptic patterns at the 500mb level with the associated tornado activity for each pattern (on the left); and percent frequency of occurrence by month of each pattern during the GCM20c time period (on the right). Color coding for the tornado association on the map on the left can be taken from figure 8 (Continued on the next page).

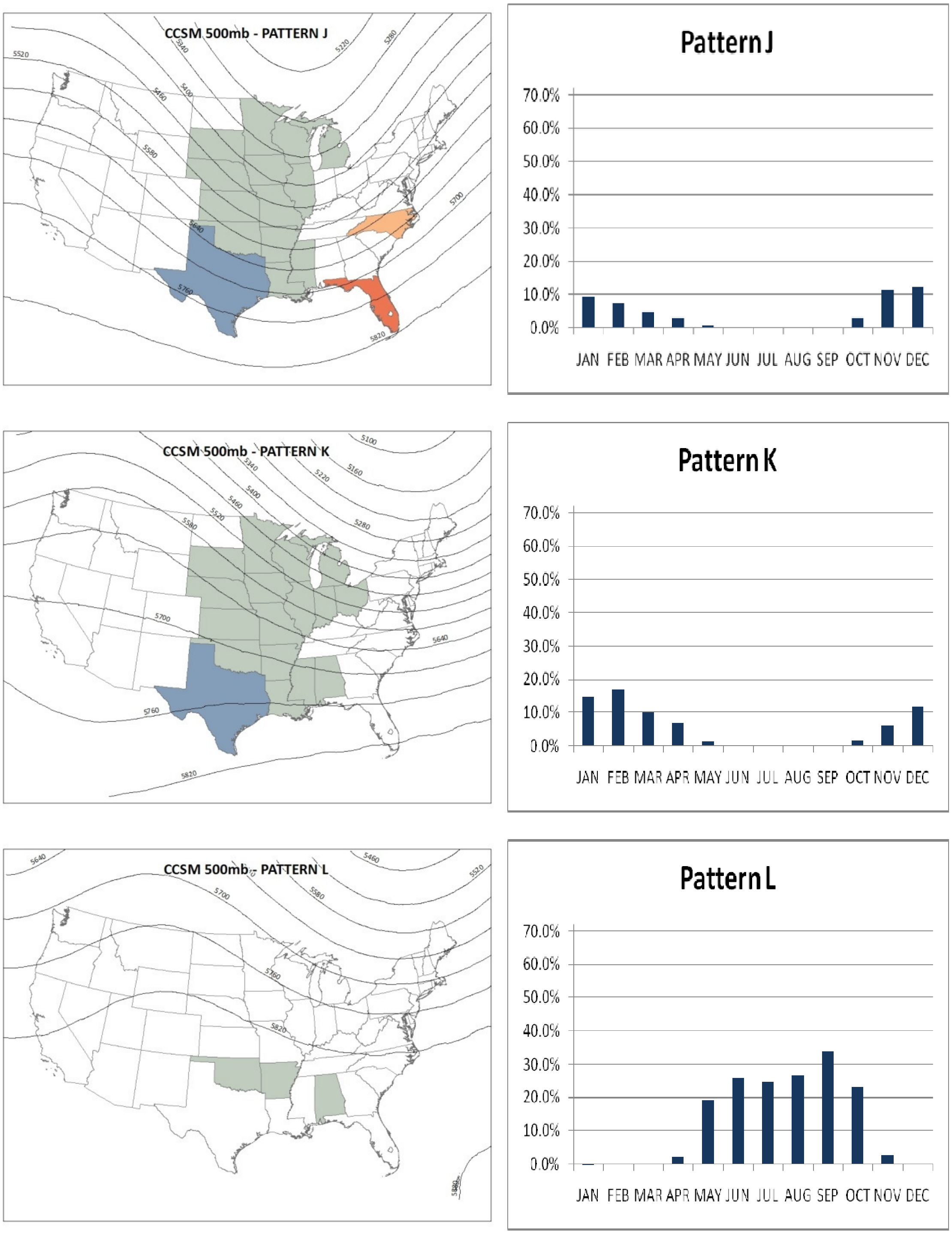


**Figure 9 (continued)** – The 15 CCSM3 synoptic patterns at the 500mb level with the associated tornado activity for each pattern (on the left); and percent frequency of occurrence by month of each pattern during the GCM20c time period (on the right). Color coding for the tornado association on the map on the left can be taken from figure 8 (Continued on the next page).

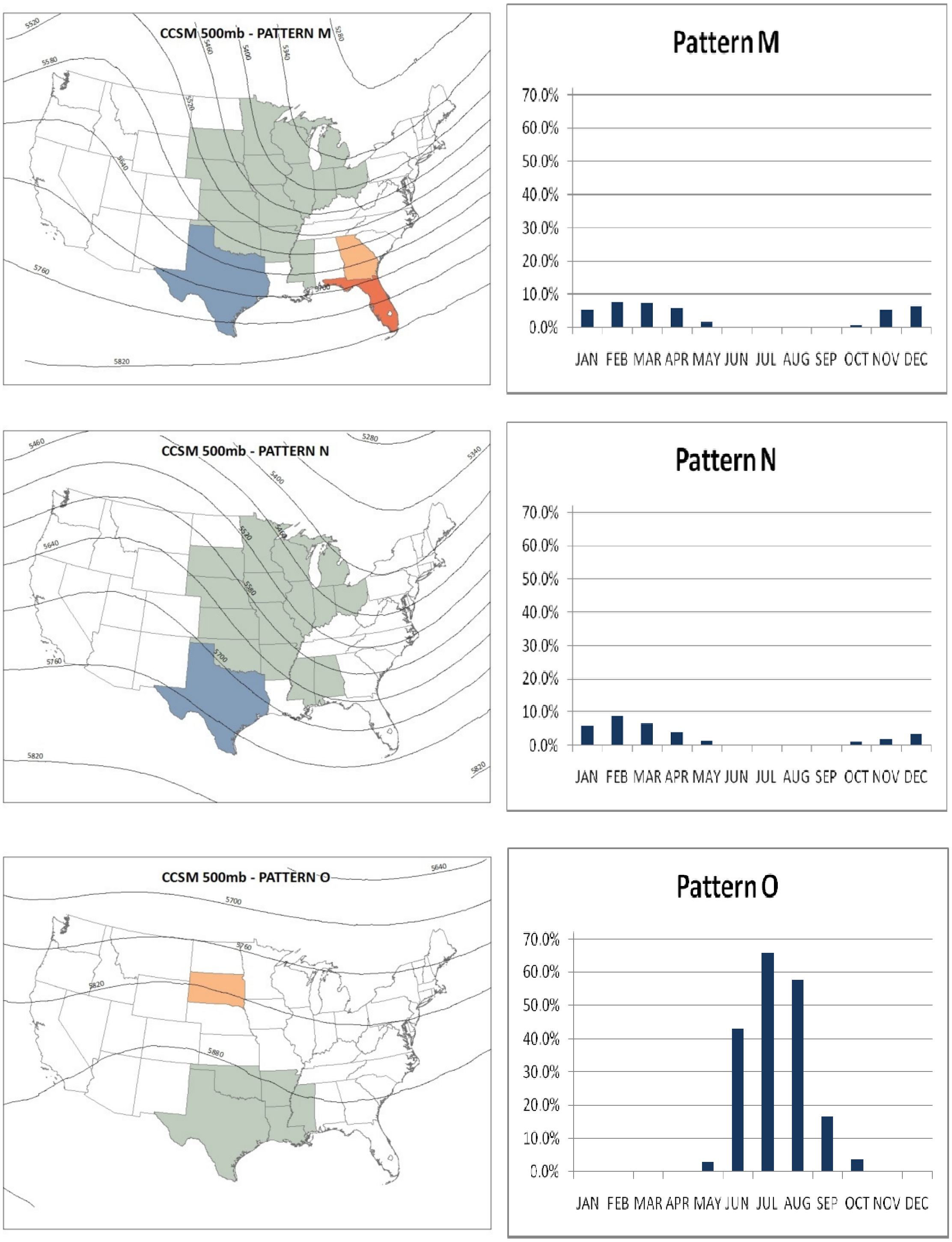


**Figure 9 (continued)** – The 15 CCSM3 synoptic patterns at the 500mb level with the associated tornado activity for each pattern (on the left); and percent frequency of occurrence by month of each pattern during the GCM20c time period (on the right). Color coding for the tornado association on the map on the left can be taken from figure 8.

**Table 2** – Pearson correlation coefficients (top) and mean absolute error (MAE, in meters; bottom) of the mean 500z values of each CCSM3 pattern in the NNR portion of the 20th Century to each pattern in the GCM20c portion of the 20th Century. Green boxes indicate the best match for each row.

| PEARSON | GCM-A | GCM-B | GCM-C | GCM-D | GCM-E | GCM-F | GCM-G | GCM-H | GCM-I | GCM-J | GCM-K | GCM-L | GCM-M | GCM-N | GCM-O |
|---|---|---|---|---|---|---|---|---|---|---|---|---|---|---|---|
| NNR-A | 0.9953 | 0.9086 | 0.9446 | 0.9559 | 0.9671 | 0.9188 | 0.9284 | 0.9348 | 0.8472 | 0.8740 | 0.8228 | 0.8499 | 0.8237 | 0.8261 | 0.9068 |
| NNR-B | 0.9262 | 0.9972 | 0.9245 | 0.8603 | 0.9469 | 0.9627 | 0.9150 | 0.9219 | 0.9358 | 0.8487 | 0.9227 | 0.8817 | 0.9104 | 0.8962 | 0.8675 |
| NNR-C | 0.9550 | 0.9179 | 0.9956 | 0.9403 | 0.9465 | 0.9566 | 0.9496 | 0.9721 | 0.8592 | 0.9383 | 0.8880 | 0.8679 | 0.9082 | 0.8623 | 0.8978 |
| NNR-D | 0.9689 | 0.8597 | 0.9413 | 0.9980 | 0.9405 | 0.9099 | 0.9638 | 0.9479 | 0.8521 | 0.8973 | 0.8640 | 0.9183 | 0.8239 | 0.8474 | 0.9717 |
| NNR-E | 0.9813 | 0.9496 | 0.9493 | 0.9408 | 0.9987 | 0.9603 | 0.9520 | 0.9588 | 0.9234 | 0.9225 | 0.8901 | 0.8866 | 0.9077 | 0.9133 | 0.9283 |
| NNR-F | 0.9307 | 0.9528 | 0.9711 | 0.9199 | 0.9551 | 0.9976 | 0.9640 | 0.9609 | 0.9220 | 0.9448 | 0.9498 | 0.9187 | 0.9563 | 0.9356 | 0.9213 |
| NNR-G | 0.9519 | 0.9241 | 0.9620 | 0.9757 | 0.9631 | 0.9666 | 0.9985 | 0.9854 | 0.9468 | 0.9501 | 0.9608 | 0.9642 | 0.9273 | 0.9461 | 0.9818 |
| NNR-H | 0.9645 | 0.9356 | 0.9831 | 0.9645 | 0.9765 | 0.9660 | 0.9872 | 0.9981 | 0.9355 | 0.9625 | 0.9399 | 0.9251 | 0.9387 | 0.9307 | 0.9523 |
| NNR-I | 0.8600 | 0.9391 | 0.8812 | 0.8558 | 0.9156 | 0.9310 | 0.9390 | 0.9332 | 0.9963 | 0.8954 | 0.9793 | 0.9238 | 0.9484 | 0.9766 | 0.9024 |
| NNR-J | 0.8926 | 0.8618 | 0.9488 | 0.9084 | 0.9346 | 0.9388 | 0.9459 | 0.9638 | 0.8937 | 0.9986 | 0.9038 | 0.8575 | 0.9574 | 0.9370 | 0.8965 |
| NNR-K | 0.8325 | 0.9143 | 0.9008 | 0.8583 | 0.8802 | 0.9354 | 0.9449 | 0.9352 | 0.9591 | 0.9009 | 0.9973 | 0.9489 | 0.9517 | 0.9550 | 0.9064 |
| NNR-L | 0.8578 | 0.8741 | 0.8889 | 0.9085 | 0.8809 | 0.9124 | 0.9537 | 0.9202 | 0.9129 | 0.8667 | 0.9669 | 0.9964 | 0.8831 | 0.9106 | 0.9600 |
| NNR-M | 0.8132 | 0.8987 | 0.9039 | 0.8091 | 0.8945 | 0.9390 | 0.9083 | 0.9277 | 0.9354 | 0.9506 | 0.9531 | 0.8619 | 0.9963 | 0.9659 | 0.8426 |
| NNR-N | 0.8354 | 0.8984 | 0.8755 | 0.8499 | 0.9098 | 0.9317 | 0.9353 | 0.9265 | 0.9770 | 0.9339 | 0.9706 | 0.9152 | 0.9696 | 0.9968 | 0.9009 |
| NNR-O | 0.9337 | 0.8737 | 0.9170 | 0.9776 | 0.9375 | 0.9207 | 0.9725 | 0.9433 | 0.8996 | 0.8934 | 0.9181 | 0.9725 | 0.8571 | 0.8947 | 0.9987 |

| MAE | GCM-A | GCM-B | GCM-C | GCM-D | GCM-E | GCM-F | GCM-G | GCM-H | GCM-I | GCM-J | GCM-K | GCM-L | GCM-M | GCM-N | GCM-O |
|---|---|---|---|---|---|---|---|---|---|---|---|---|---|---|---|
| NNR-A | 20.0611 | 76.2653 | 104.8147 | 124.9293 | 78.9555 | 83.4177 | 95.6325 | 104.6549 | 119.0369 | 107.9357 | 142.5336 | 156.9290 | 120.3393 | 110.5403 | 190.9508 |
| NNR-B | 67.7331 | 14.7766 | 106.9086 | 153.4491 | 95.0492 | 55.0998 | 96.9830 | 106.7995 | 82.3432 | 113.0865 | 107.8809 | 166.1310 | 86.7793 | 81.2855 | 208.0597 |
| NNR-C | 111.6447 | 106.1486 | 21.5229 | 205.1262 | 162.3602 | 79.3294 | 73.6278 | 56.8871 | 116.0459 | 83.4934 | 108.5470 | 231.1051 | 96.4806 | 118.0329 | 271.1341 |
| NNR-D | 110.8535 | 160.2104 | 201.0220 | 8.7265 | 69.0212 | 173.6647 | 178.3457 | 191.1763 | 198.6911 | 178.2779 | 209.9637 | 55.8387 | 193.6903 | 180.4054 | 73.2602 |
| NNR-E | 58.9082 | 96.9726 | 155.0574 | 73.6390 | 8.8739 | 115.3066 | 135.7077 | 146.6512 | 141.3742 | 131.8300 | 164.8465 | 97.6146 | 135.9607 | 122.8435 | 128.7049 |
| NNR-F | 73.7934 | 51.7818 | 79.1130 | 158.4065 | 106.7063 | 19.8143 | 69.6764 | 83.8744 | 81.3350 | 74.3877 | 89.6273 | 175.1698 | 61.2435 | 63.1653 | 218.0130 |
| NNR-G | 91.8163 | 90.3004 | 65.3184 | 174.3941 | 134.9898 | 64.4786 | 12.2608 | 42.0632 | 72.0295 | 67.5309 | 65.8056 | 193.3892 | 81.2274 | 76.5404 | 238.2204 |
| NNR-H | 111.7911 | 106.0700 | 43.9183 | 201.3450 | 158.6557 | 82.0543 | 43.8918 | 18.4540 | 87.5475 | 70.4192 | 81.3612 | 223.6745 | 86.8914 | 99.7087 | 266.0600 |
| NNR-I | 118.1161 | 76.5338 | 107.8881 | 194.8716 | 143.9092 | 73.8767 | 74.7151 | 84.9312 | 18.6492 | 95.8129 | 53.3212 | 202.2861 | 63.6051 | 48.8151 | 248.4057 |
| NNR-J | 111.8153 | 110.9717 | 74.0131 | 185.8616 | 141.2469 | 77.7275 | 70.6242 | 62.6954 | 97.3190 | 14.1817 | 99.4752 | 208.6588 | 62.7832 | 79.4812 | 246.8141 |
| NNR-K | 141.6560 | 105.2289 | 101.8994 | 207.6406 | 166.7195 | 89.1341 | 74.9371 | 82.9320 | 68.6207 | 100.3611 | 17.4235 | 210.9834 | 73.6186 | 81.3747 | 260.5407 |
| NNR-L | 145.3594 | 174.5779 | 225.4893 | 57.9742 | 94.2705 | 190.6982 | 197.7782 | 212.5080 | 207.9523 | 198.9695 | 212.3562 | 10.8001 | 202.4122 | 189.4991 | 58.7027 |
| NNR-M | 121.4972 | 85.3161 | 100.0091 | 189.1179 | 135.7036 | 66.1794 | 90.4329 | 89.6898 | 71.9893 | 66.1132 | 76.3306 | 197.6252 | 18.4099 | 51.2666 | 240.6095 |
| NNR-N | 106.6348 | 77.3198 | 114.8871 | 173.3158 | 121.2316 | 65.4792 | 81.3911 | 96.3002 | 50.3472 | 78.1490 | 75.9879 | 181.0710 | 50.9979 | 17.1178 | 225.3048 |
| NNR-O | 181.0702 | 218.9399 | 270.8699 | 74.2171 | 125.6503 | 237.1892 | 246.8128 | 259.5624 | 257.0608 | 242.5154 | 268.0203 | 58.5171 | 250.9242 | 237.4543 | 6.5582 |

**Pattern J (J500) – Deep Midwest Trough** – A deep trough that extends the 5460 line into Southern Illinois is the most noticeable feature of pattern J. This winter-dominant pattern is actually favorable for tornado activity in North Carolina and Florida (in the exit region of the trough), but is unfavorable for tornadoes throughout the middle-third of the country.

**Pattern K (K500) – Broad East Coast Trough** – Although very similar to pattern I, the East Coast trough coupled with a ridge over the Rockies in pattern K is slightly broader and not quite as cold. This pattern also has a similar seasonality, but is around twice as frequent as pattern I. The decreased tornado activity can again be seen in the Plains and Great Lakes regions.

**Pattern L (L500) – Summer Mountain Ridge –** Pattern L is the first summer-dominant pattern at the 500mb level – occurring in May and frequently thereafter through October. A broad ridge over the Rocky Mountains and very few height contours throughout the southern half of the country are the most noticeable features of this pattern. This pattern is relatively ‘tornado neutral,’ with only Oklahoma, Arkansas and Alabama showing a slight decrease in tornado activity.

**Pattern M (M500) – Strong Great Lakes Trough** – Pattern M features a positively tilted axis running from the Great Lakes southwest through Texas. This late winter pattern is quite infrequent, but does show some increased tornado activity in Georgia and Florida, while the Plains and Great Lakes states have fewer than expected tornado days.

**Pattern N (N500) – Winter West Coast Ridge** – This winter pattern is somewhat similar to both patterns I and K, however the ridge and the trough appear much more pronounced, are spatially much closer together, and exhibit a slightly different tilt. Decreased tornado activity is again evident in the Plains and Great Lakes.

**Pattern O (O500) – Weak Summer Mountain Ridge –** By far, the most frequent of all patterns at the 500mb level, Pattern O occurs in the peak of the summer season, accounting on average for nearly 50% of all summer days. A broad ridge over the High Plains and Rockies and a broad trough from the Great Lakes through the Southeast are the main features of this pattern. While South Dakota experiences slightly increased tornado activity, the Southern Plains experience a slight decrease.

*4.2.3 – CCSM 20th Century Synoptic Patterns and Tornadoes – 700mb Level*

Patterns A through G are considered favorable for tornado activity across the US as a whole, while patterns H through O are considered unfavorable at the 700mb level (Figure 10).

**Pattern A (A700) – Tight Spring Zonal** – While mostly a zonal pattern with tight contouring, a slight dip in the isohypses can be discovered over Southern California and into the eastern Pacific Ocean. Peak seasonality in pattern A is in the shoulder seasons and slightly increased tornado activity can be seen in the Mid-Mississippi River Valley. Florida and the Northern Plains states have a slight decrease in tornado activity.

**Pattern B (B700) – Baja Trough** – While a noticeable ridge over the Northwest US and British Columbia is apparent in Pattern B at the 700mb level, the more relevant feature is the trough over the Baja Peninsula. This Spring-dominant pattern is most frequent in May, and there is increased tornado activity in the Plains region.

**Pattern C (C700) – Deep High Plains Trough** – The slightly tilted deep trough that extends from Manitoba southward through New Mexico creates a widespread region of increased tornado activity just downwind of this trough in pattern C. From Michigan, southwest into Texas, and through the Southeastern US as well, substantially more tornado days occur in pattern C compared to average. This pattern occurs regularly from late autumn through spring, and has its peak in March and April.

**Pattern D (D700) – Spring Rocky Mountain Trough** – One of the more meridional patterns at the 700mb level, pattern D features a broad trough over the western third of the US before transitioning to a sharp ridge over the Great Lakes and Ontario, Canada. Throughout the Plains states, in the outflow region of the western trough, substantial increases in tornado activity are noticed, especially from Texas through Nebraska. This is a predominantly spring pattern with nearly equal peaks in April and May.

**Pattern E (E700) – Summer Plains Zonal** – This pattern is the most frequently occurring of any pattern at any level, peaking in July at over 70%, and accounting for about 60% of all summer days at the 700mb level. Although mostly a zonal pattern, a slight trough is noticeable off the west coast. The Northern Plains states have generally increased tornado activity, while the Southern Plains states have a decrease.

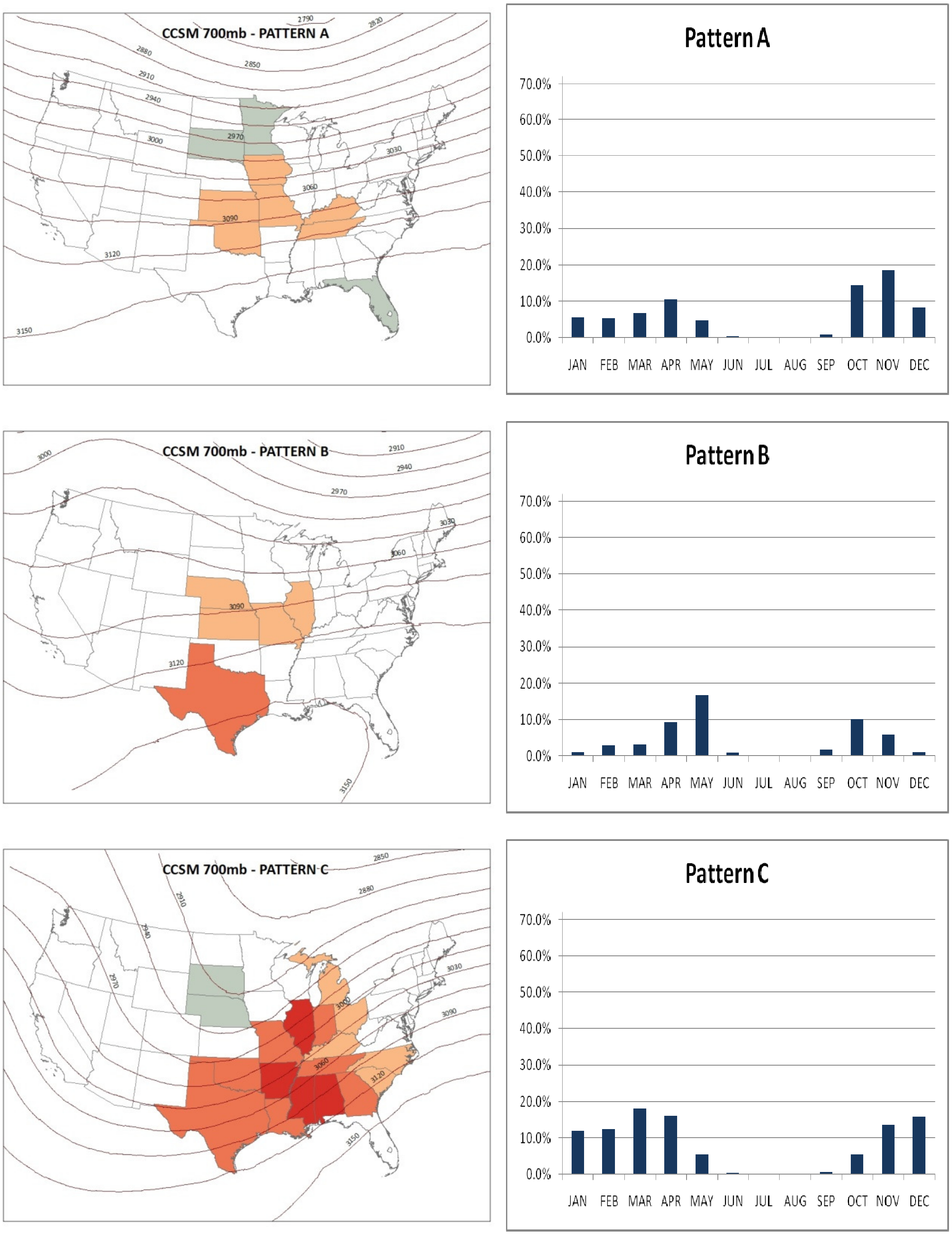


**Figure 10** – The 15 CCSM3 synoptic patterns at the 700mb level with the associated tornado activity for each pattern (on the left); and percent frequency of occurrence by month of each pattern during the GCM20c time period (on the right). Color coding for the tornado association on the map on the left can be taken from figure 8 (Continued on the next page).

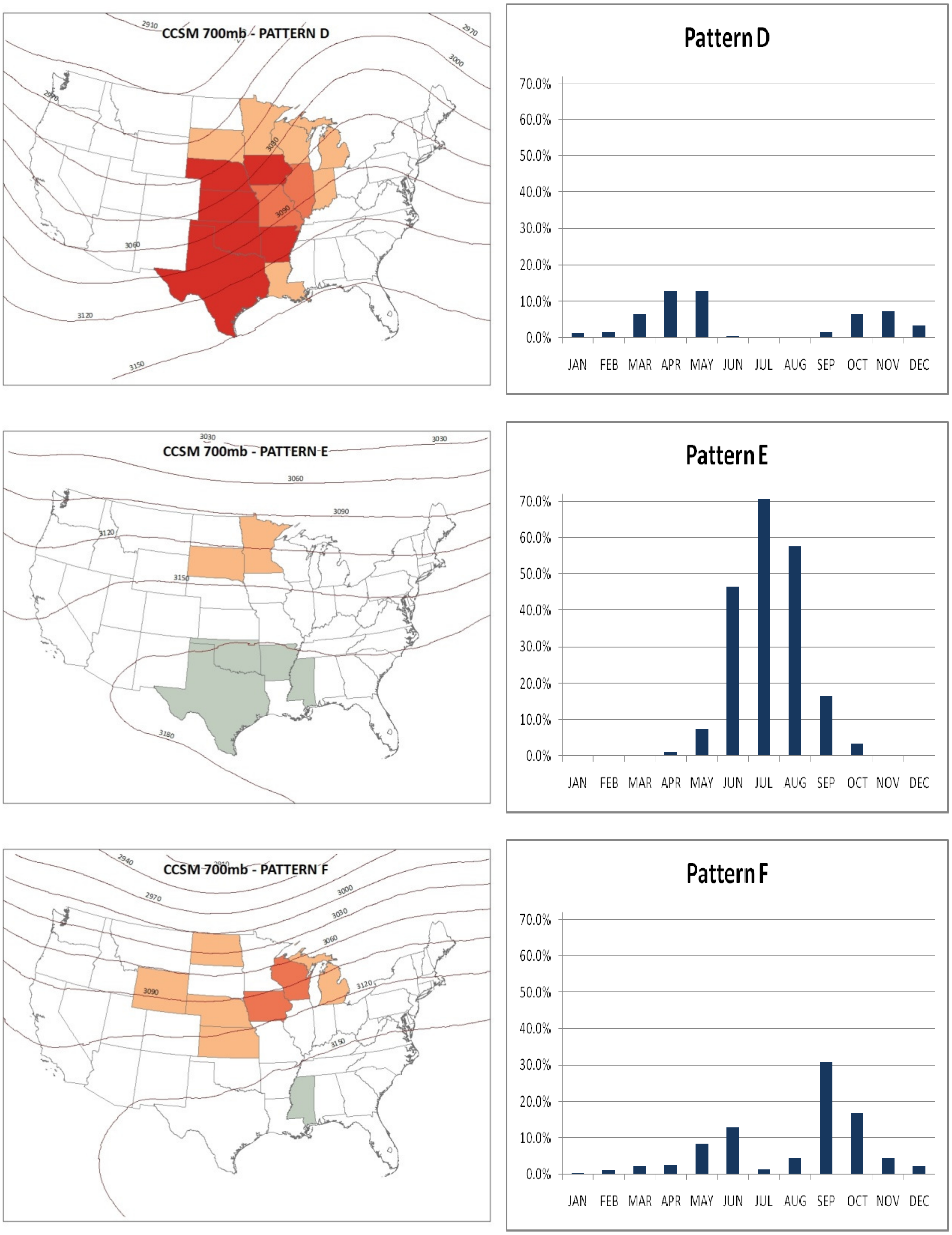


**Figure 10 (continued)** – The 15 CCSM3 synoptic patterns at the 700mb level with the associated tornado activity for each pattern (on the left); and percent frequency of occurrence by month of each pattern during the GCM20c time period (on the right). Color coding for the tornado association on the map on the left can be taken from figure 8 (Continued on the next page).

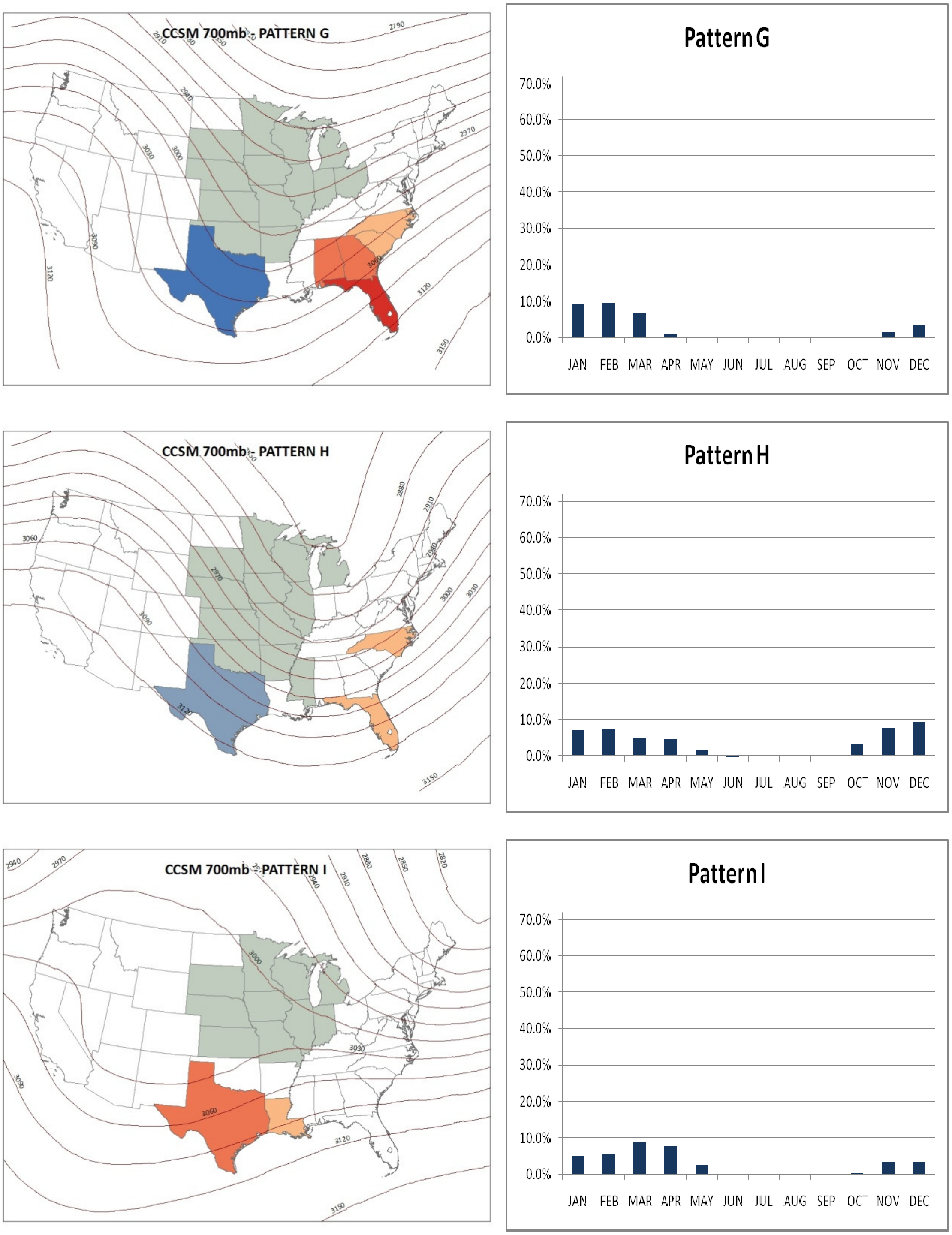


**Figure 10 (continued)** – The 15 CCSM3 synoptic patterns at the 700mb level with the associated tornado activity for each pattern (on the left); and percent frequency of occurrence by month of each pattern during the GCM20c time period (on the right). Color coding for the tornado association on the map on the left can be taken from figure 8 (Continued on the next page).

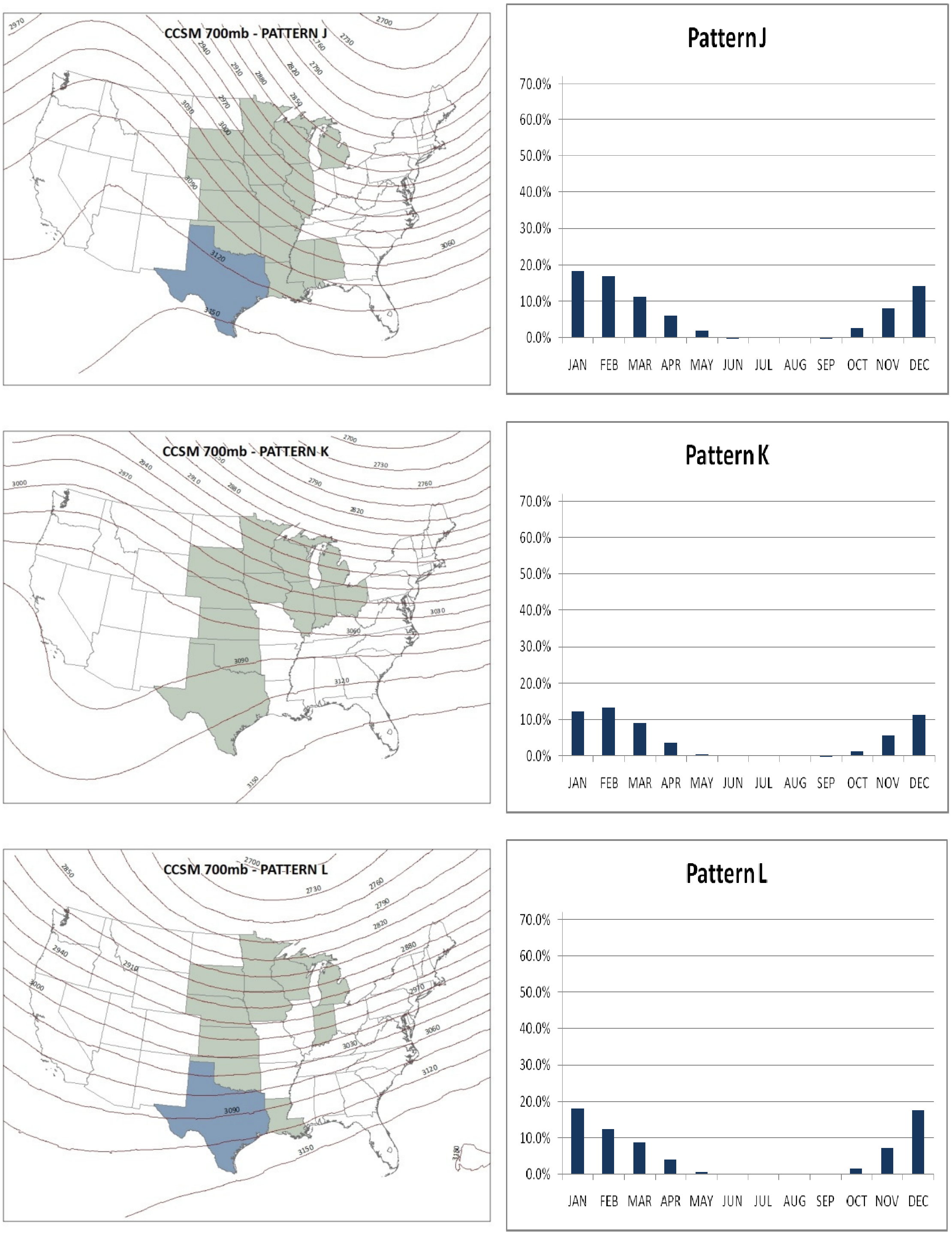


**Figure 10 (continued)** – The 15 CCSM3 synoptic patterns at the 700mb level with the associated tornado activity for each pattern (on the left); and percent frequency of occurrence by month of each pattern during the GCM20c time period (on the right). Color coding for the tornado association on the map on the left can be taken from figure 8 (Continued on the next page).

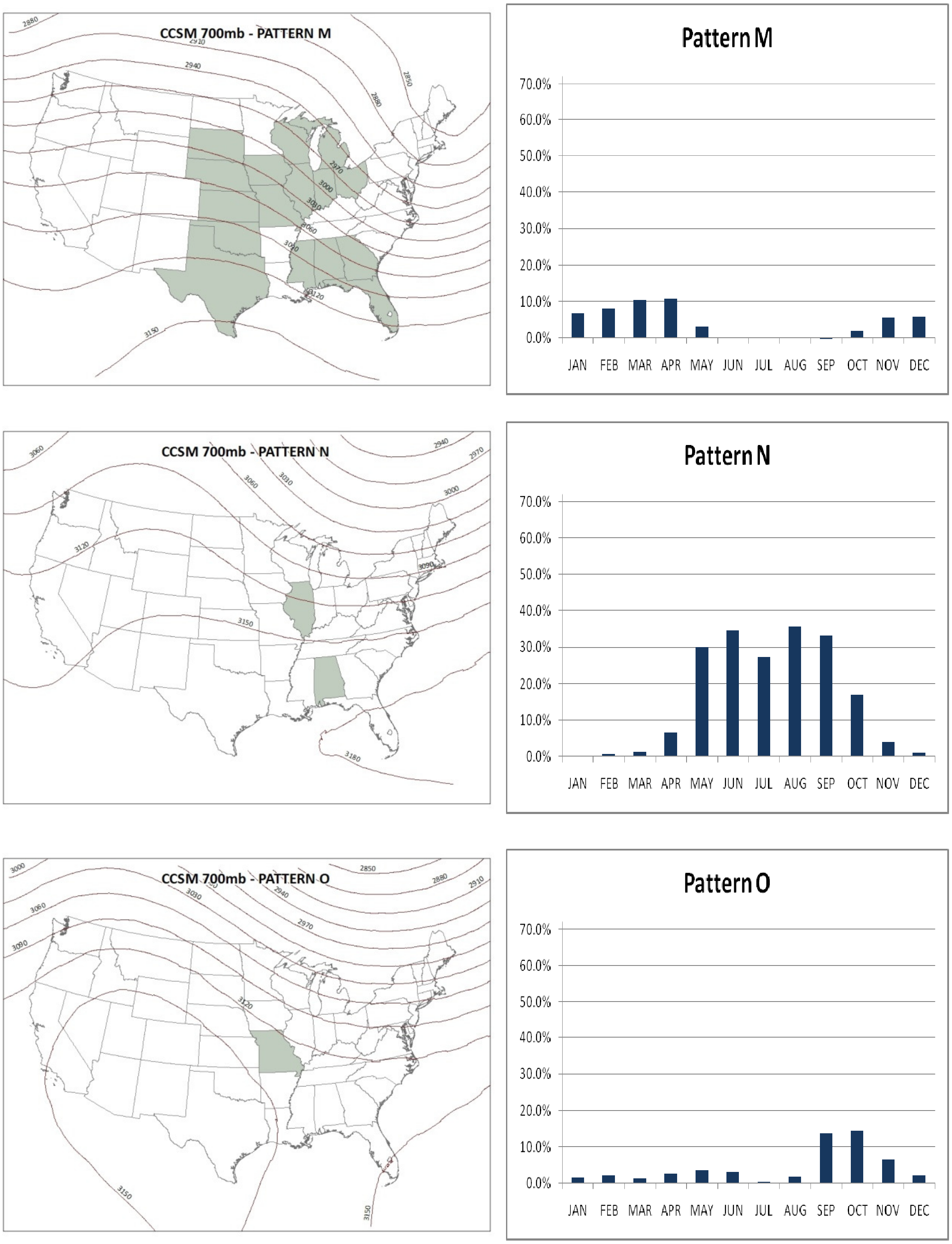


**Figure 10 (continued)** – The 15 CCSM3 synoptic patterns at the 700mb level with the associated tornado activity for each pattern (on the left); and percent frequency of occurrence by month of each pattern during the GCM20c time period (on the right). Color coding for the tornado association on the map on the left can be taken from figure 8.

**Table 3** – Pearson correlation coefficients (top) and mean absolute error (MAE, in meters; bottom) of the mean 700z values of each CCSM3 pattern in the NNR portion of the 20th Century to each pattern in the GCM20c portion of the 20th Century. Green boxes indicate the best match for each row.

| PEARSON | GCM-A | GCM-B | GCM-C | GCM-D | GCM-E | GCM-F | GCM-G | GCM-H | GCM-I | GCM-J | GCM-K | GCM-L | GCM-M | GCM-N | GCM-O |
|---|---|---|---|---|---|---|---|---|---|---|---|---|---|---|---|
| NNR-A | 0.9974 | 0.9768 | 0.9503 | 0.9280 | 0.9688 | 0.9717 | 0.9210 | 0.8991 | 0.8534 | 0.8650 | 0.9372 | 0.9685 | 0.8814 | 0.9183 | 0.9155 |
| NNR-B | 0.9765 | 0.9956 | 0.9323 | 0.8807 | 0.9675 | 0.9345 | 0.9166 | 0.8691 | 0.8724 | 0.8994 | 0.9656 | 0.9479 | 0.8838 | 0.9738 | 0.9636 |
| NNR-C | 0.9393 | 0.9102 | 0.9946 | 0.8979 | 0.8818 | 0.8881 | 0.9345 | 0.8861 | 0.8669 | 0.8346 | 0.9100 | 0.9656 | 0.8062 | 0.8625 | 0.8348 |
| NNR-D | 0.8909 | 0.8551 | 0.8921 | 0.9923 | 0.8495 | 0.8936 | 0.7774 | 0.7424 | 0.7989 | 0.6587 | 0.7813 | 0.8384 | 0.7919 | 0.7376 | 0.7060 |
| NNR-E | 0.9668 | 0.9708 | 0.9022 | 0.8821 | 0.9986 | 0.9747 | 0.8864 | 0.8442 | 0.8231 | 0.8456 | 0.9301 | 0.9278 | 0.8517 | 0.9481 | 0.9435 |
| NNR-F | 0.9502 | 0.9360 | 0.8863 | 0.9096 | 0.9539 | 0.9942 | 0.8368 | 0.8024 | 0.7364 | 0.7407 | 0.8513 | 0.8969 | 0.7778 | 0.8486 | 0.8594 |
| NNR-G | 0.9183 | 0.9064 | 0.9384 | 0.7823 | 0.8829 | 0.8498 | 0.9960 | 0.9618 | 0.8951 | 0.9446 | 0.9572 | 0.9634 | 0.8695 | 0.9060 | 0.9103 |
| NNR-H | 0.9012 | 0.8636 | 0.8903 | 0.7651 | 0.8409 | 0.8105 | 0.9590 | 0.9972 | 0.8589 | 0.9261 | 0.8989 | 0.9322 | 0.8894 | 0.8436 | 0.8510 |
| NNR-I | 0.8232 | 0.8257 | 0.8541 | 0.7978 | 0.7988 | 0.7046 | 0.8944 | 0.8375 | 0.9895 | 0.9094 | 0.9186 | 0.8506 | 0.9348 | 0.8596 | 0.8219 |
| NNR-J | 0.8468 | 0.8543 | 0.8124 | 0.6637 | 0.8263 | 0.7223 | 0.9220 | 0.9082 | 0.9038 | 0.9940 | 0.9488 | 0.8874 | 0.9170 | 0.9171 | 0.9172 |
| NNR-K | 0.9332 | 0.9415 | 0.9085 | 0.7968 | 0.9235 | 0.8572 | 0.9595 | 0.9045 | 0.9291 | 0.9747 | 0.9963 | 0.9540 | 0.9180 | 0.9685 | 0.9654 |
| NNR-L | 0.9843 | 0.9453 | 0.9751 | 0.9130 | 0.9365 | 0.9402 | 0.9481 | 0.9294 | 0.8722 | 0.8780 | 0.9366 | 0.9891 | 0.8736 | 0.8938 | 0.8847 |
| NNR-M | 0.8885 | 0.8742 | 0.8296 | 0.8352 | 0.8609 | 0.7901 | 0.8923 | 0.8967 | 0.9513 | 0.9289 | 0.9195 | 0.8751 | 0.9983 | 0.8700 | 0.8607 |
| NNR-N | 0.9167 | 0.9497 | 0.8754 | 0.7588 | 0.9393 | 0.8523 | 0.9074 | 0.8543 | 0.8691 | 0.9366 | 0.9700 | 0.9136 | 0.8656 | 0.9972 | 0.9827 |
| NNR-O | 0.9013 | 0.9403 | 0.8305 | 0.7152 | 0.9272 | 0.8500 | 0.9033 | 0.8534 | 0.8379 | 0.9413 | 0.9613 | 0.8933 | 0.8629 | 0.9814 | 0.9929 |

| MAE | GCM-A | GCM-B | GCM-C | GCM-D | GCM-E | GCM-F | GCM-G | GCM-H | GCM-I | GCM-J | GCM-K | GCM-L | GCM-M | GCM-N | GCM-O |
|---|---|---|---|---|---|---|---|---|---|---|---|---|---|---|---|
| NNR-A | 11.2141 | 60.7895 | 41.8514 | 64.5345 | 119.5694 | 83.2934 | 58.5079 | 56.2142 | 70.1632 | 75.8274 | 57.3469 | 56.7481 | 63.4029 | 102.3535 | 77.9899 |
| NNR-B | 56.1103 | 8.4922 | 60.8265 | 41.1315 | 66.7543 | 38.3368 | 87.3836 | 73.8160 | 76.1673 | 100.3290 | 94.2078 | 108.7698 | 78.7413 | 46.3116 | 28.6444 |
| NNR-C | 43.4779 | 66.0728 | 11.4832 | 59.1123 | 123.6218 | 89.3015 | 46.9851 | 51.2860 | 54.4774 | 81.4175 | 66.1450 | 62.4648 | 67.2582 | 105.5507 | 85.5966 |
| NNR-D | 61.4562 | 48.0029 | 55.7261 | 11.1663 | 90.4214 | 56.7241 | 89.8613 | 79.2126 | 72.0039 | 116.9756 | 104.7874 | 109.4736 | 77.4722 | 82.4647 | 73.0794 |
| NNR-E | 115.3390 | 68.4443 | 121.0217 | 86.3303 | 3.6471 | 43.0824 | 148.8495 | 129.6060 | 135.7740 | 157.8930 | 155.5248 | 168.2709 | 137.8143 | 32.6159 | 59.6146 |
| NNR-F | 71.7741 | 35.2264 | 80.6745 | 48.8482 | 51.8289 | 12.6789 | 110.1672 | 94.1936 | 103.5531 | 127.7414 | 118.8819 | 126.4988 | 103.5894 | 49.3999 | 45.4756 |
| NNR-G | 56.6420 | 85.1279 | 45.9920 | 89.7902 | 143.6912 | 111.8544 | 12.1827 | 36.2449 | 54.0085 | 50.0541 | 45.0087 | 49.9166 | 58.8811 | 121.9894 | 95.5932 |
| NNR-H | 54.2865 | 76.9230 | 51.7309 | 80.5109 | 130.8514 | 101.0503 | 38.2705 | 9.0640 | 58.3618 | 59.0103 | 66.1981 | 66.5350 | 52.6149 | 111.8472 | 88.3580 |
| NNR-I | 69.3550 | 72.6582 | 55.2825 | 66.1960 | 124.5375 | 100.3171 | 56.6806 | 59.5371 | 18.2076 | 70.6111 | 68.9169 | 90.2347 | 39.7642 | 102.9784 | 84.2797 |
| NNR-J | 79.5095 | 101.9039 | 84.9119 | 116.0827 | 154.3396 | 131.8675 | 58.4639 | 63.8286 | 69.3324 | 15.9784 | 46.1111 | 72.1087 | 61.7941 | 128.3244 | 102.4268 |
| NNR-K | 59.1425 | 92.7452 | 65.7653 | 103.2513 | 150.9643 | 122.1113 | 45.1505 | 64.5454 | 63.1460 | 32.1061 | 12.6084 | 47.1964 | 60.7080 | 126.3015 | 98.4514 |
| NNR-L | 67.5615 | 118.5806 | 71.0731 | 114.5121 | 177.9208 | 141.7862 | 60.7163 | 77.0147 | 89.3967 | 78.6304 | 58.5044 | 25.7841 | 85.1708 | 159.4589 | 134.1680 |
| NNR-M | 59.8998 | 80.5927 | 64.9984 | 76.0321 | 136.1542 | 108.1652 | 54.2378 | 50.8567 | 35.7774 | 57.5854 | 59.9066 | 78.0248 | 8.0371 | 116.1171 | 92.9193 |
| NNR-N | 96.3293 | 48.9038 | 101.2920 | 77.1385 | 32.6719 | 43.4520 | 125.4001 | 108.2710 | 112.7636 | 129.7389 | 129.3278 | 146.2716 | 115.8813 | 5.5963 | 33.1890 |
| NNR-O | 70.6252 | 35.0565 | 81.8253 | 72.5663 | 65.9535 | 51.8532 | 96.4666 | 83.5182 | 90.9377 | 96.8875 | 96.2756 | 117.2337 | 90.1004 | 39.7894 | 13.5633 |

**Pattern F (F700) – Autumn Northern Trough –** A very broad trough over the northern High Plains highlights pattern F. Although it occurs most frequently in autumn, and has a secondary peak in June, it does occur fairly infrequently through the rest of the year. This pattern has increased tornado activity associated with it in the Northern Plains and Upper Great Lakes – where the contours begin to turn north.

**Pattern G (G700) – Deep Winter Plains Trough** – This winter pattern features a deep trough from Northern Michigan to Texas. While the region under the trough is associated with decreased tornado activity, the Southeastern US states, especially Florida, have an up-tick in tornado days.

**Pattern H (H700) – Deep Winter Midwest Trough** – Although vaguely similar to pattern G, pattern H has a much more pronounced trough and tighter isohypses than the previous pattern. Additionally, the trough's axis in pattern H is shifted slightly eastward and is nearly due north/south in alignment which decreases the overall tornado activity. Although Florida and North Carolina have an increase, the Plains and Upper Great Lakes have a decrease leading this pattern to be unfavorable for tornado activity across the whole of the US.

**Pattern I (I700) – Spring Split Flow** – Pattern I occurs most frequently in winter and early spring and thus is favorable for tornadoes in some southern portions of the US where the temperatures are favorable as well, and the states are located downwind of the trough over Northern Mexico. Less favorable conditions occur in the Northern Plains and Upper Great Lakes on the downwind side of the ridge over the Canadian Rockies.

**Pattern J (J700) – Tight Winter Eastern Trough** – The broad trough over the eastern third of the country in pattern J has some of the tightest contours of any pattern at the 700mb level. A sharp ridge over the western third of the US and the winter seasonality of this pattern makes for a decrease in tornado activity over the Plains and Great Lakes regions.

**Pattern K (K700) – Northwest Ridge** – This pattern is similar to the previous one in its seasonality and shape, however, a broader trough is shifted north over the eastern half of the US, while the ridge in the west also broadens. Additionally, pattern K features a trough over the Baja Peninsula. Overall, the High Plains states and the Great Lakes all have slightly decreased tornado activity associated with this pattern.

**Pattern L (L700) – Tight Winter Plains Trough** – Like pattern J, this pattern also features some of the tightest isohypses of any at the 700mb level. Pattern L has a very broad trough over the entire US, with an axis through the entire length of the Plains states. This pattern peaks in December and January and has decreased tornado activity in the Plains and Great Lakes.

**Pattern M (M700) – Spring East Coast Trough** – Pattern M regularly occurs throughout the winter and spring months, peaking in the middle of spring. A very broad ridge over the entire western half of the US creates decreased activity for the Great Lakes, Plains and Southeast, while the axis of a fairly pronounced trough sits just off the East Coast.

**Pattern N (N700) – Summer Rockies Ridge** – A ridge from the four corners region north through the Canadian Rockies and a trough over Ontario and the Great Lakes are the main features of pattern N. Predominantly a summer pattern, the seasonality of pattern N features dual peaks in frequency in June and August, and is fairly tornado neutral.

**Pattern O – (O700) – Autumn Four Corners High** – Pattern O occurs throughout the year, peaking in mid-autumn. A high over the four corners region creates a ridge over the Northwest US and British Columbia, Canada. A trough sits over Quebec, Canada and into the New England states. This pattern is also considered neutral in its association to tornado activity.

*4.2.4 – CCSM 20th Century Synoptic Patterns and Tornado Association – 850mb Level*

Patterns A through G are considered favorable for tornado activity across the US as a whole, while patterns H through O are considered unfavorable at the 850mb level (Figure 11). As a reminder, 850mb level patterns are with temperatures (in °C) as opposed to the geopotential heights used at the 500mb and 700mb level.

**Pattern A (A850) – Autumn Great Lakes Cold Front** – Pattern A is mostly a late-summer and early-autumn pattern that features a thermal ridge extending from the Desert Southwest and a cold front moving south from the Great Lakes region. Favorable areas for tornadoes under pattern A are the Great Lakes states and parts of the Northern Plains, while the Southern Plains and Southeast are generally unfavorable.

**Pattern B (B850) – Southwest Thermal Ridge** – This pattern features warm air over Northern Mexico, tight isotherms, and perhaps a baroclinic environment over the areas of increased tornado activity in the Southern Plains. Pattern B is a late-spring dominant pattern, occurring over 40% of the time in May and nearly 20% of the time in April and June.

**Pattern C (C850) – Weak Summer Upper Great Lakes Cold Front** – This pattern features a weak cold front near the US/Canada border in the northern Great Lakes, and much like patterns A and B, warm air over the desert Southwest. This pattern, however, has a much different seasonality from the previous two, being a summer-dominant pattern – peaking from June through September. Thus, the increase in tornado activity under this pattern has shifted considerably northward into the Upper Great Lakes region.

**Pattern D (D850) – Spring Mild** – Pattern D occurs throughout the winter, but peaks in the spring. Fairly zonal isotherms across much of the country are the main features of this pattern, with a slight thermal ridge in Northern Mexico reaching into the southern and western portions of Texas. The pattern is favorable for tornadoes throughout the southern US.

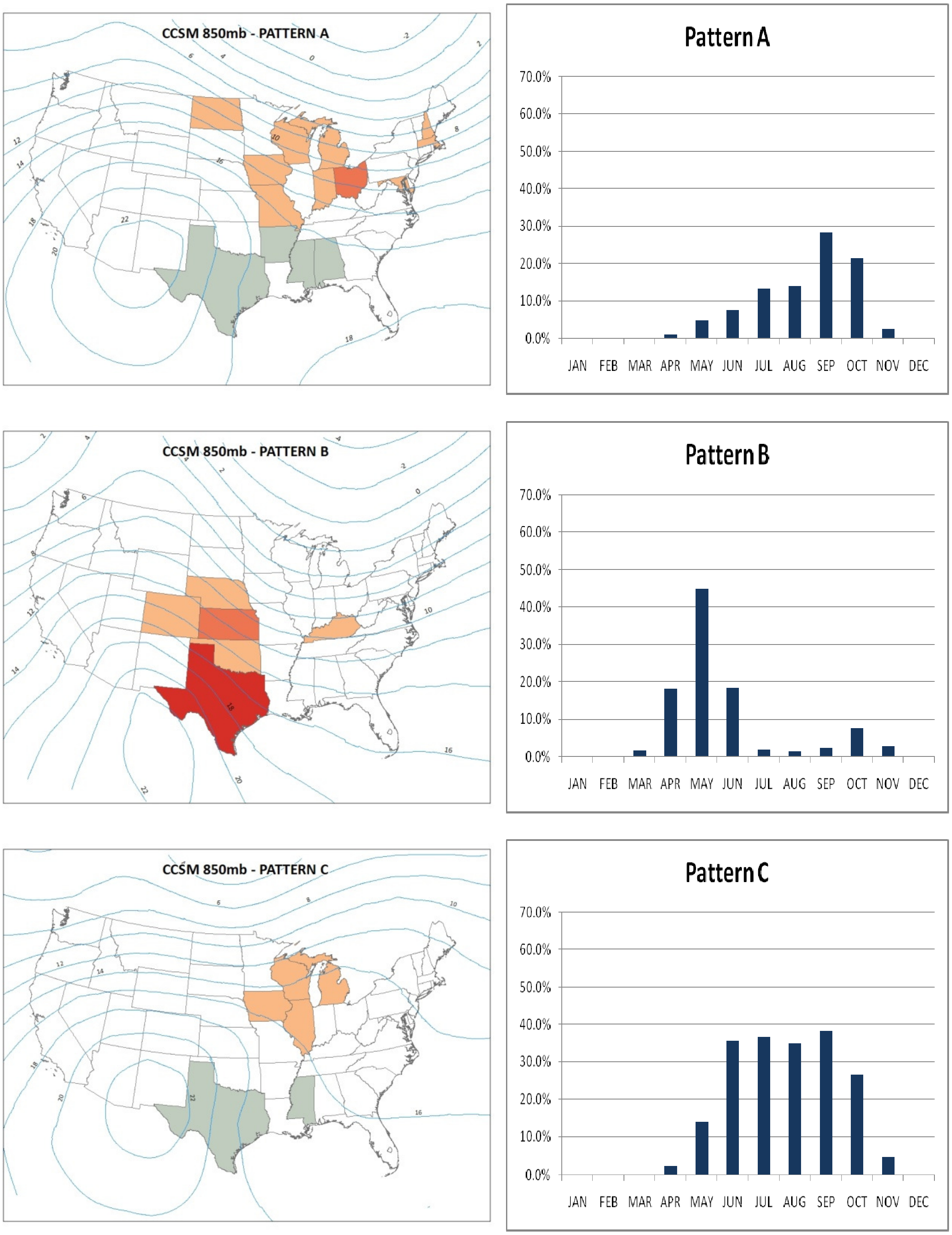


**Figure 11** – The 15 CCSM3 synoptic patterns at the 850mb level with the associated tornado activity for each pattern (on the left); and percent frequency of occurrence by month of each pattern during the GCM20c time period (on the right). Color coding for the tornado association on the map on the left can be taken from figure 8 (Continued on the next page).

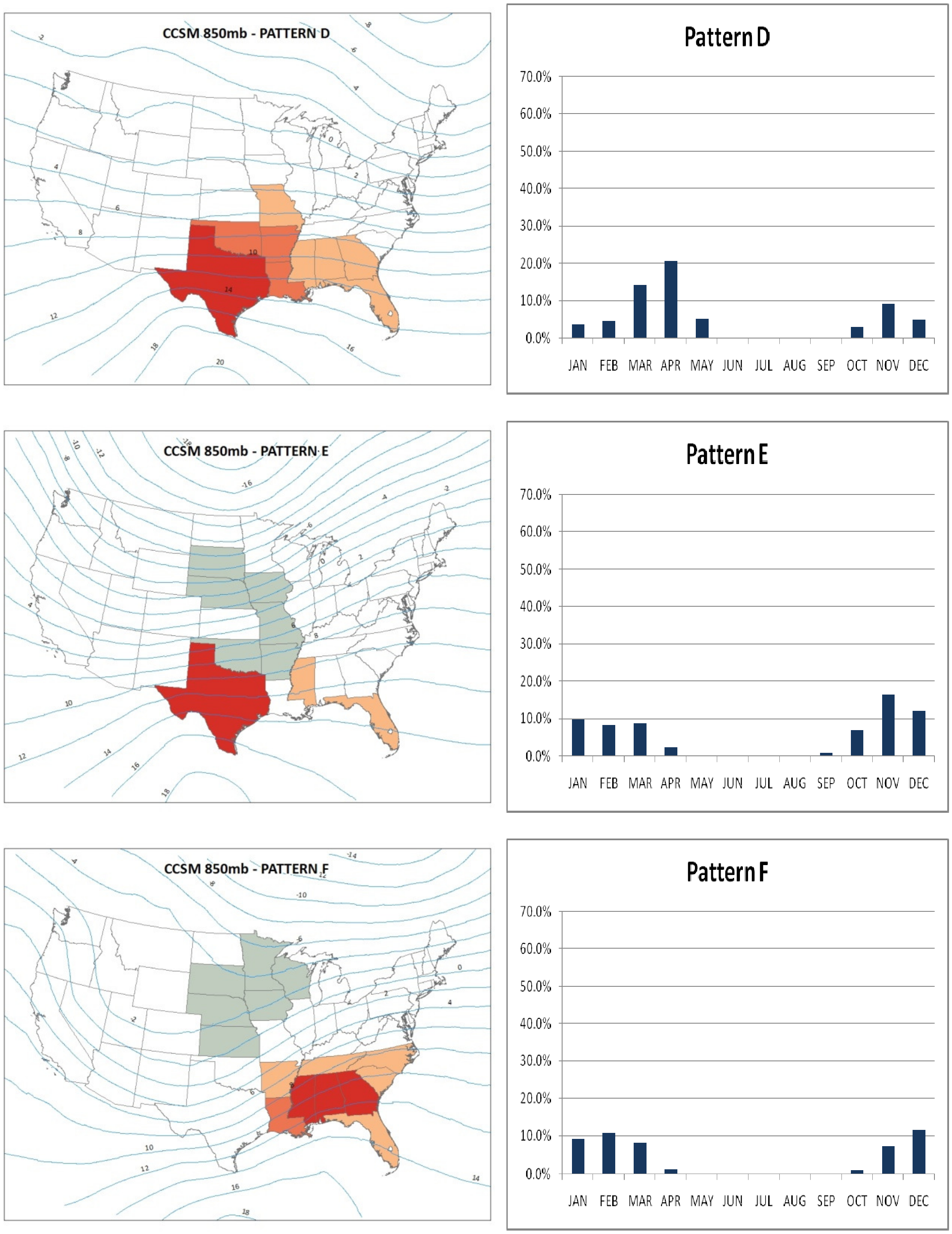


**Figure 11 (continued)** – The 15 CCSM3 synoptic patterns at the 850mb level with the associated tornado activity for each pattern (on the left); and percent frequency of occurrence by month of each pattern during the GCM20c time period (on the right). Color coding for the tornado association on the map on the left can be taken from figure 8 (Continued on the next page).

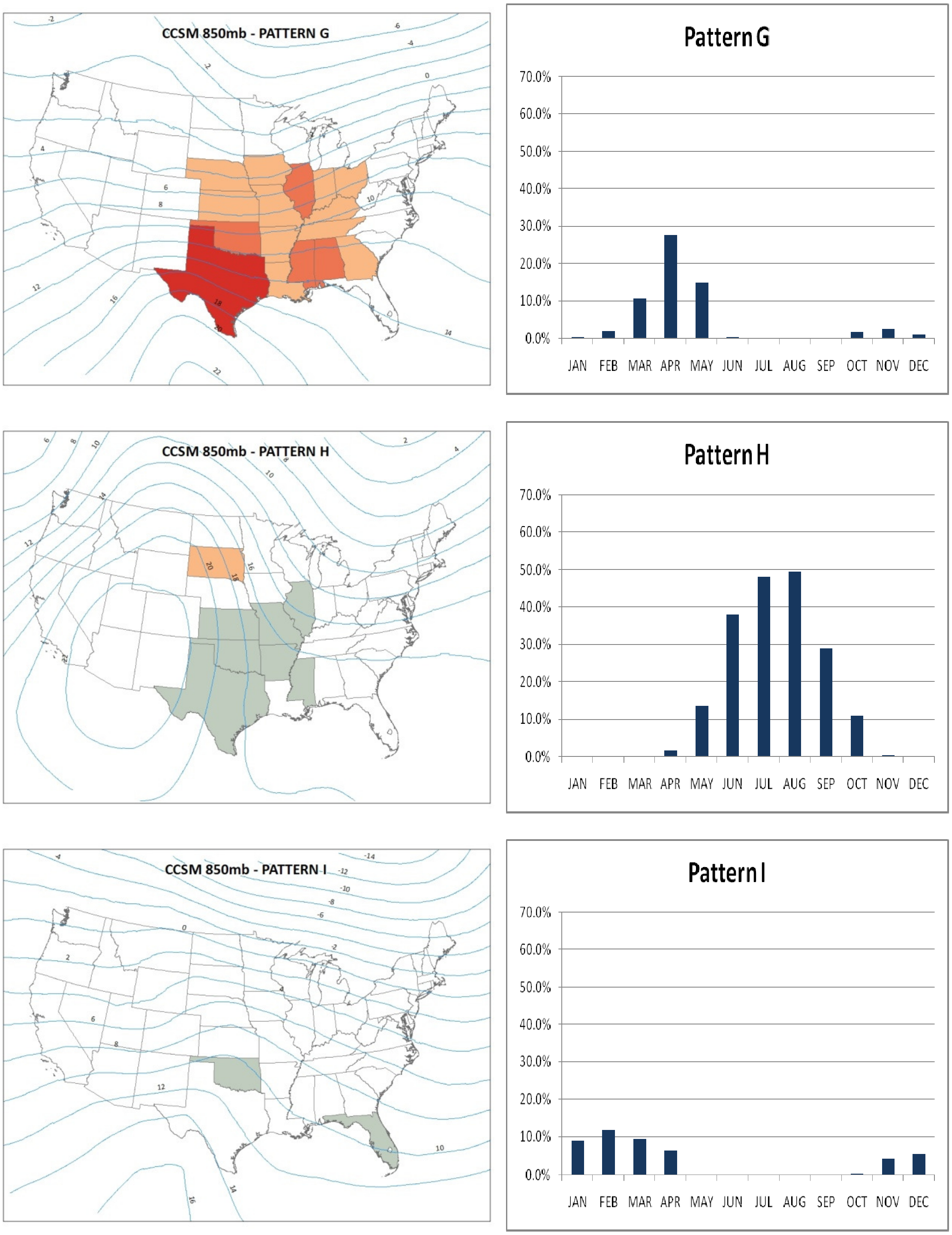


**Figure 11 (continued)** – The 15 CCSM3 synoptic patterns at the 850mb level with the associated tornado activity for each pattern (on the left); and percent frequency of occurrence by month of each pattern during the GCM20c time period (on the right). Color coding for the tornado association on the map on the left can be taken from figure 8 (Continued on the next page).

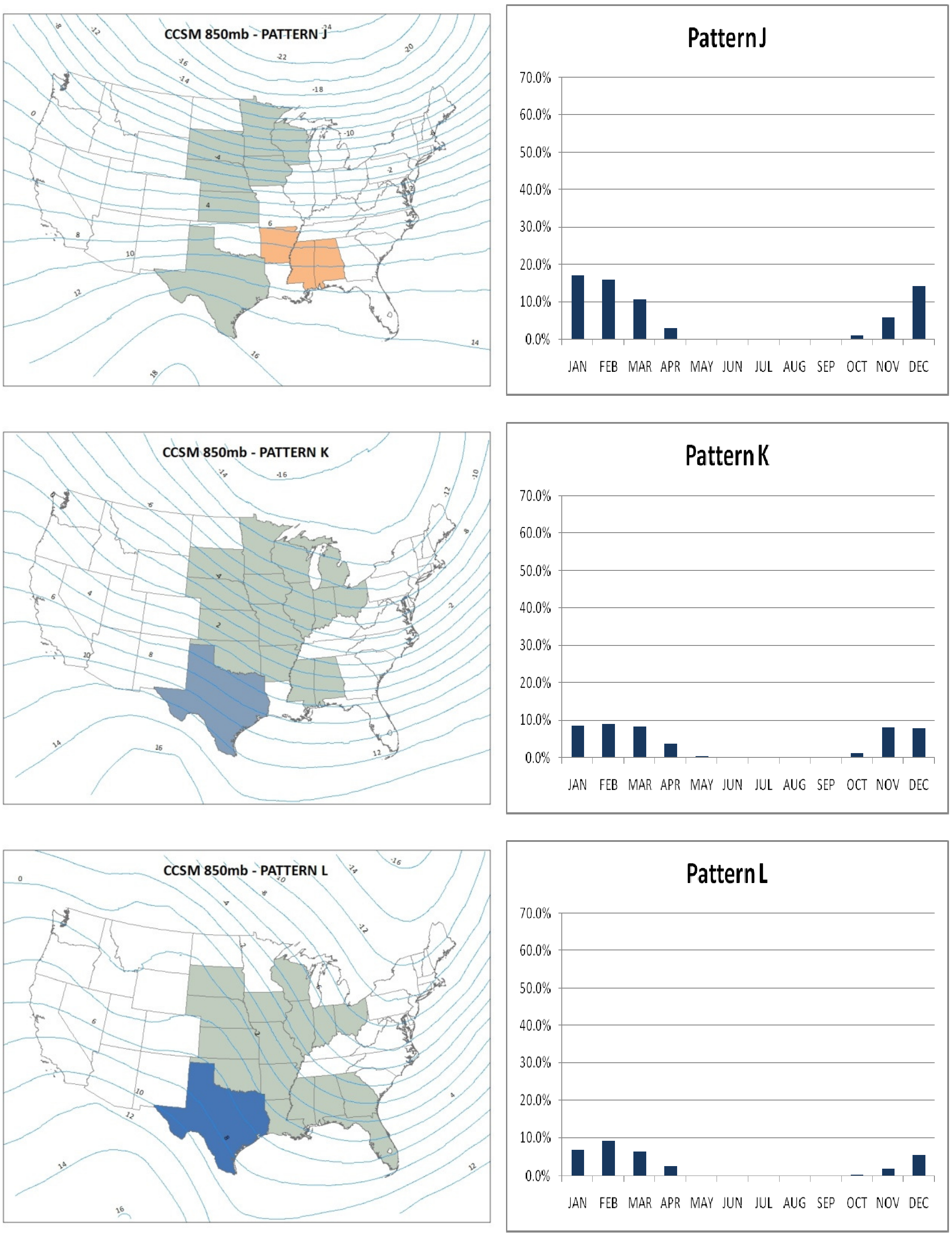


**Figure 11 (continued)** – The 15 CCSM3 synoptic patterns at the 850mb level with the associated tornado activity for each pattern (on the left); and percent frequency of occurrence by month of each pattern during the GCM20c time period (on the right). Color coding for the tornado association on the map on the left can be taken from figure 8 (Continued on the next page).

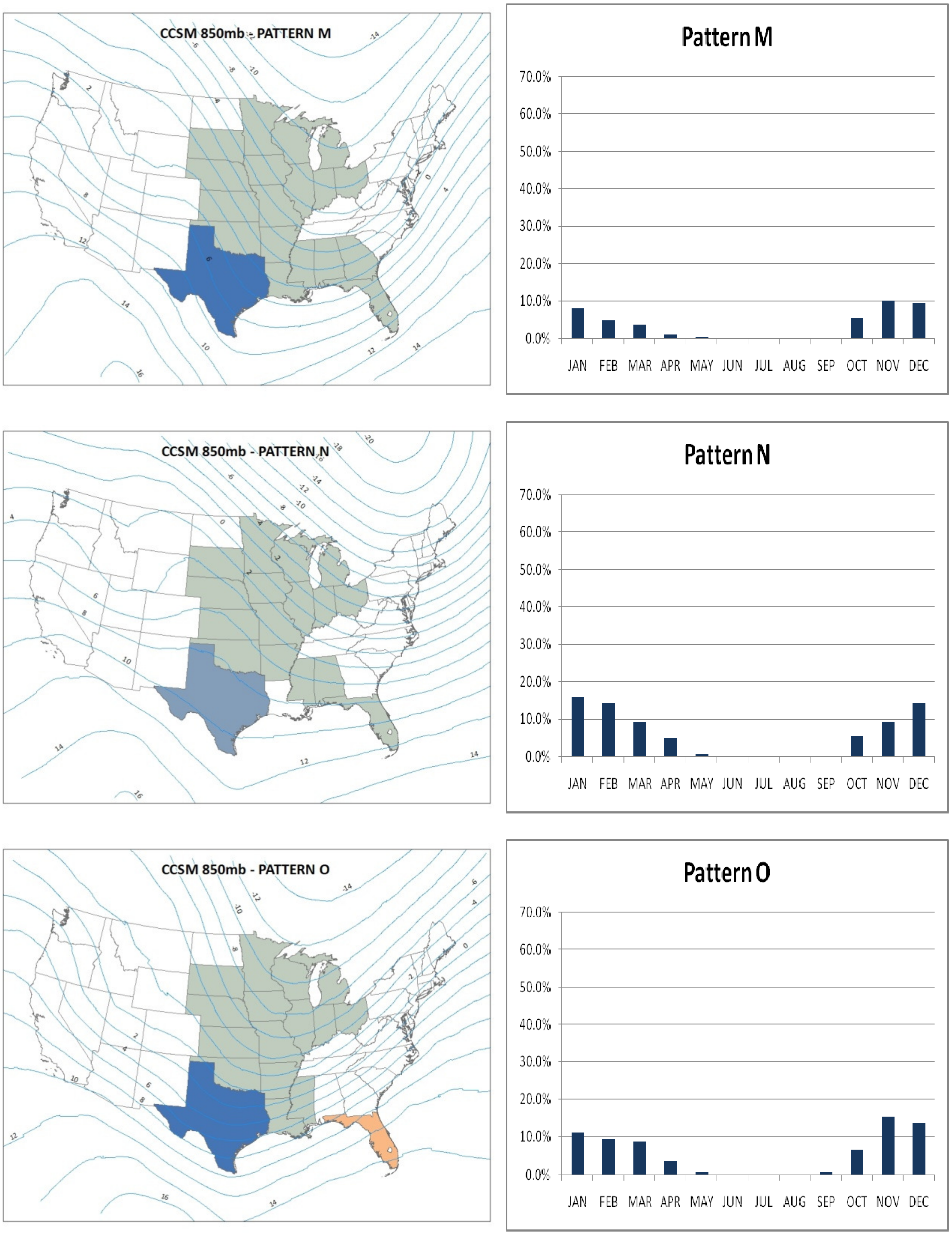


**Figure 11 (continued)** – The 15 CCSM3 synoptic patterns at the 850mb level with the associated tornado activity for each pattern (on the left); and percent frequency of occurrence by month of each pattern during the GCM20c time period (on the right). Color coding for the tornado association on the map on the left can be taken from figure 8.

**Table 4** – Pearson correlation coefficients (top) and mean absolute error (MAE, in °C; bottom) of the mean 850t values of each CCSM3 pattern in the NNR portion of the 20th Century to each pattern in the GCM20c portion of the 20th Century. Green boxes indicate the best match for each row.

| PEARSON | GCM-A | GCM-B | GCM-C | GCM-D | GCM-E | GCM-F | GCM-G | GCM-H | GCM-I | GCM-J | GCM-K | GCM-L | GCM-M | GCM-N | GCM-O |
|---|---|---|---|---|---|---|---|---|---|---|---|---|---|---|---|
| NNR-A | 0.9978 | 0.9583 | 0.9514 | 0.8854 | 0.8300 | 0.8517 | 0.9174 | 0.9480 | 0.9530 | 0.9173 | 0.8699 | 0.8857 | 0.8493 | 0.9317 | 0.8318 |
| NNR-B | 0.9676 | 0.9974 | 0.9311 | 0.9431 | 0.8667 | 0.8883 | 0.9648 | 0.9142 | 0.9579 | 0.9339 | 0.9164 | 0.9157 | 0.8805 | 0.9339 | 0.8846 |
| NNR-C | 0.9099 | 0.9089 | 0.9913 | 0.8252 | 0.8352 | 0.7634 | 0.9017 | 0.8752 | 0.8848 | 0.8249 | 0.7683 | 0.7417 | 0.7191 | 0.7626 | 0.7132 |
| NNR-D | 0.8928 | 0.9418 | 0.8583 | 0.9989 | 0.8972 | 0.9501 | 0.9567 | 0.7917 | 0.9587 | 0.9377 | 0.9231 | 0.8982 | 0.8389 | 0.9291 | 0.8858 |
| NNR-E | 0.8349 | 0.8543 | 0.8471 | 0.8865 | 0.9963 | 0.9299 | 0.9339 | 0.6411 | 0.8886 | 0.9407 | 0.8819 | 0.7615 | 0.8278 | 0.7920 | 0.8904 |
| NNR-F | 0.8636 | 0.8779 | 0.7997 | 0.9451 | 0.9497 | 0.9989 | 0.9411 | 0.7023 | 0.9297 | 0.9660 | 0.9162 | 0.8512 | 0.8779 | 0.9073 | 0.9535 |
| NNR-G | 0.9100 | 0.9577 | 0.9058 | 0.9531 | 0.9492 | 0.9421 | 0.9968 | 0.7976 | 0.9478 | 0.9469 | 0.8884 | 0.8301 | 0.8341 | 0.8682 | 0.8931 |
| NNR-H | 0.9170 | 0.8997 | 0.8835 | 0.7816 | 0.6266 | 0.6928 | 0.8082 | 0.9971 | 0.8460 | 0.7499 | 0.7192 | 0.8060 | 0.7153 | 0.8443 | 0.6770 |
| NNR-I | 0.9598 | 0.9548 | 0.9270 | 0.9580 | 0.9006 | 0.9315 | 0.9620 | 0.8668 | 0.9987 | 0.9578 | 0.9139 | 0.9175 | 0.8650 | 0.9535 | 0.8762 |
| NNR-J | 0.9370 | 0.9290 | 0.8810 | 0.9404 | 0.9662 | 0.9624 | 0.9552 | 0.7750 | 0.9642 | 0.9987 | 0.9612 | 0.9022 | 0.9217 | 0.9343 | 0.9472 |
| NNR-K | 0.8937 | 0.9064 | 0.8190 | 0.9271 | 0.8987 | 0.9174 | 0.8923 | 0.7496 | 0.9266 | 0.9626 | 0.9987 | 0.9681 | 0.9680 | 0.9525 | 0.9563 |
| NNR-L | 0.8885 | 0.8877 | 0.7890 | 0.8965 | 0.7742 | 0.8554 | 0.8353 | 0.8132 | 0.9196 | 0.8964 | 0.9411 | 0.9944 | 0.9299 | 0.9788 | 0.8866 |
| NNR-M | 0.8659 | 0.8575 | 0.7646 | 0.8438 | 0.8389 | 0.8739 | 0.8289 | 0.7416 | 0.8749 | 0.9198 | 0.9618 | 0.9570 | 0.9972 | 0.9358 | 0.9627 |
| NNR-N | 0.9273 | 0.9051 | 0.8130 | 0.9173 | 0.8088 | 0.9027 | 0.8711 | 0.8387 | 0.9474 | 0.9318 | 0.9348 | 0.9723 | 0.9186 | 0.9983 | 0.9036 |
| NNR-O | 0.8488 | 0.8614 | 0.7546 | 0.8787 | 0.9034 | 0.9402 | 0.8782 | 0.6949 | 0.8774 | 0.9475 | 0.9575 | 0.9047 | 0.9728 | 0.9132 | 0.9989 |

| MAE | GCM-A | GCM-B | GCM-C | GCM-D | GCM-E | GCM-F | GCM-G | GCM-H | GCM-I | GCM-J | GCM-K | GCM-L | GCM-M | GCM-N | GCM-O |
|---|---|---|---|---|---|---|---|---|---|---|---|---|---|---|---|
| NNR-A | 0.9933 | 3.2019 | 2.8782 | 8.2950 | 11.0509 | 10.7941 | 6.4253 | 3.4460 | 9.4696 | 13.5918 | 12.1986 | 11.2858 | 10.8389 | 10.6767 | 10.6625 |
| NNR-B | 2.4762 | 0.5429 | 4.7233 | 5.5743 | 8.7147 | 8.3189 | 3.7282 | 5.6716 | 7.0748 | 11.3202 | 9.6452 | 8.7835 | 8.4491 | 8.4224 | 8.1277 |
| NNR-C | 3.8704 | 4.8774 | 0.7303 | 9.8425 | 12.4719 | 12.5206 | 7.8451 | 2.8865 | 11.3610 | 15.7730 | 14.1417 | 13.2841 | 12.8038 | 13.0946 | 12.5246 |
| NNR-D | 7.7306 | 5.9277 | 9.8941 | 0.5116 | 5.0183 | 3.4921 | 3.1140 | 11.0870 | 2.8970 | 7.1462 | 5.3707 | 4.8505 | 5.5434 | 4.5755 | 4.6609 |
| NNR-E | 10.5501 | 9.1621 | 12.5765 | 5.5173 | 0.9399 | 3.9446 | 5.8192 | 14.3119 | 4.8763 | 5.0567 | 5.2679 | 6.9652 | 5.9716 | 6.7228 | 4.7982 |
| NNR-F | 9.7357 | 8.2728 | 12.0554 | 3.6132 | 3.3790 | 0.4710 | 4.9361 | 13.3303 | 3.3885 | 5.2005 | 4.4509 | 5.0140 | 4.6278 | 4.3593 | 2.8502 |
| NNR-G | 5.7811 | 3.9392 | 7.7598 | 2.9871 | 5.3114 | 5.0921 | 0.6260 | 9.1896 | 4.4292 | 8.5006 | 7.2496 | 6.9718 | 6.5680 | 6.6266 | 5.6044 |
| NNR-H | 4.2619 | 5.5729 | 2.8765 | 10.7629 | 14.0402 | 13.5147 | 9.0251 | 0.4695 | 12.2390 | 16.7232 | 15.0272 | 13.7733 | 13.5156 | 13.4117 | 13.3700 |
| NNR-I | 8.0927 | 6.6949 | 10.5382 | 2.7556 | 4.6257 | 3.5055 | 3.7716 | 11.7243 | 0.6993 | 6.0074 | 4.9343 | 4.1186 | 4.9452 | 3.5209 | 4.6288 |
| NNR-J | 12.8000 | 11.5860 | 15.5128 | 7.5066 | 4.6230 | 5.2495 | 8.5711 | 16.8171 | 5.6001 | 0.6527 | 4.1070 | 6.1932 | 5.9009 | 5.3053 | 5.5484 |
| NNR-K | 11.4513 | 10.0119 | 14.0222 | 5.7270 | 5.0307 | 4.4867 | 7.4225 | 15.1824 | 4.5753 | 3.8532 | 0.5828 | 2.9628 | 3.1271 | 3.4961 | 3.6401 |
| NNR-L | 10.2000 | 8.8013 | 12.7140 | 4.8054 | 6.6798 | 4.8514 | 6.6873 | 13.5436 | 3.7754 | 6.3292 | 3.7013 | 1.0063 | 3.5945 | 2.4598 | 4.4919 |
| NNR-M | 9.6526 | 8.3917 | 12.1674 | 5.3020 | 5.6724 | 4.6163 | 6.3410 | 13.1436 | 4.5745 | 6.0601 | 3.3616 | 2.9259 | 0.8160 | 3.6765 | 2.5572 |
| NNR-N | 9.8653 | 8.7129 | 12.7066 | 4.9162 | 6.3885 | 4.4208 | 6.5598 | 13.4718 | 3.4439 | 5.3068 | 3.9400 | 2.6622 | 4.0620 | 0.5981 | 4.4164 |
| NNR-O | 9.9366 | 8.5333 | 12.3943 | 4.9532 | 4.4475 | 3.2413 | 5.9227 | 13.5080 | 4.6071 | 5.3459 | 3.3947 | 4.1963 | 2.2330 | 4.2114 | 0.4732 |

**Pattern E (E850) – Cold Season Frontal System** – Strong temperature gradients and a cold front swinging down from Canada are the main features associated with pattern E at 850mb. Because this is a winter-dominant pattern, where the temperatures are still warm enough for tornadoes, increased activity is present in Texas and portions of the Southeast. Decreased tornado activity is exhibited in the central Plains.

**Pattern F (F850) – Winter Midwest Cyclone** – This winter pattern features a thermal trough over much of Texas and a thermal ridge over the Southeast and Mid-Atlantic states. This most likely is bringing warm moist air up from the Gulf of Mexico and swinging a cold front over the southeastern portions of the US where substantially increased tornado activity is associated with this pattern. The Northern Plains states see a slight decrease in tornado activity.

**Pattern G (G850) – Spring Weak Plains Frontal** – This pattern occurs most often in the spring, peaking in April at nearly 30% of all days and flanked by over 10% frequency in both March and May. While there is some slight cold air advecting from Canada, it does not reach far enough south to get into a favorable tornado area for April. The broad area of increased tornado activity might be due simply to the seasonality of the pattern, or a stationary front through the middle of the country.

**Pattern H (H850) – Summer Four Corners High** – This pattern accounts for nearly 50% of all days in both July and August and is characterized by a sharp thermal ridge from the four corners northward over the Rockies, and a thermal trough over the Great Lakes moving mild air south from Canada. This pattern is associated with less-than-expected tornado activity through much of the Plains, Midwest and Great Lakes.

**Pattern I (I850) – Winter Southern Plains Warm Front** – For the seasonality of Pattern I – being quite winter-dominant – it is a rather mild pattern, with the 0°C line only approaching the US/Canada border until it reaches into the Northeast where it dips southward. The most noticeable feature is the slight thermal ridge in the Southern Plains. This pattern is fairly neutral in its association with tornadoes.

**Pattern J (J850) – Strong Winter Polar Front** – The obvious features of Pattern J are the tightly-spaced isotherms and the thermal trough over the eastern half of the US bringing cold air southward. The 0°C line extends all the way to Southern Ohio on average in this pattern. This pattern is quite frequent in the winter months, but also into the early spring. This seasonality may lead to the slight increase in tornado activity in some portions of the Southeast, but overall, much of the country experiences decreased tornado activity.

**Pattern K (K850) – Strong Winter East Coast Cold Front** – Pattern K is marked by a strong cold front moving into the northeast US, dipping the 0°C line into South Carolina and Georgia. This winter-dominant pattern is unfavorable for tornadoes through the Plains, Great Lakes, and parts of the southeastern US as well.

**Pattern L (L850) – Winter Mid-Atlantic Cold Front** – This very cold winter pattern dips the freezing line into southern Georgia, while relatively warmer air is moving into Texas from central Mexico. This pattern is associated to a considerable reduction in tornado activity in Texas, with slight decreases in much of the Southeast, Plains, and Great Lakes regions.

**Pattern M (M850) – Early Winter Polar Front** – Similar to patterns L and K in shape, this pattern features a strong polar front moving its way to the east coast, but a seasonality that is shifted towards the beginning of the cold season. This pattern has the southernmost freezing line of any

850mb pattern – reaching as far south as southern Alabama and Mississippi.

**Pattern N (N850) – Winter Rocky Mountain Cyclone** – The twisting of the isotherms on this pattern perhaps indicate a mid-latitude cyclone moving through the Rocky Mountains, while colder air is over the Northeast at 850mb. Pattern N is another winter pattern, peaking in December and January with decreased tornado activity in the Plains, Northeast and Great Lakes.

**Pattern O (O850) – Winter Southeast Cold Front** – This pattern occurs throughout the cold season, but peaks in frequency in November and December. The axis of the main thermal trough leans slightly southwest to northeast as a cold front pushes through the southern states. As with most of the winter patterns, pattern O is unfavorable for tornadoes in the Plains and Great Lakes, but interestingly is associated with a slight increase in tornado activity in Florida as the front makes its way through, and where the temperatures are still favorable for development.

*4.3 – Summary and Comparison of BLR Results*

After examining each individual pattern at each of the levels and the associated tornado activity, the next step is to combine the three levels. Using a separate binary logistic regression (BLR) for each of the 48 states, tornado days are predicted using the circulation patterns created for each day at each level. It is important to note here that there are two separate portions of 20th Century predictions with BLR, one being with the NNR data and the other being with the GCM20c data – this is true for both GCMs used (CCSM3 and CGCM3). The results discussed below depict the NNR's and the CCSM3's ability to predict 20th Century tornadoes using these circulation patterns; thus serving as a validation of the method used in this research to predict future tornado activity. These results will also allow for direct comparisons to the results presented in section 4.6 below. The following results are in terms of F2+ tornado days per decade (and per month where noted).

Overall, the NNR BLR model is very accurate at predicting the observed record of tornado days throughout the TSeason of the 20th century. A clear 'tornado alley' is visible on the map of the NNR tornado days (Figure 12) from Texas northward through to South Dakota and then eastward into Illinois. The Southeastern US is also accurately represented as a secondary area of tornado day occurrence. Over the US as a whole, the NNR BLR overpredicts tornado days by 0.1% - or less than a single tornado day per decade.

Because only the GCMs (and not the NNR) can be used to make future projections of synoptic patterns – and therefore tornado days as well – a more detailed comparison of GCM ability to replicate the observed tornado climatology is provided (hereafter) than was for the NNR.

Upon first glance at the map of the GCM20c portion of the CCSM3 BLR results (Figure 13), the choropleth looks nearly identical to the observed map (Figure 6). The shading of every state is in the same color as it was for both the NNR results (Figure 12) and the observed tornado results (Figure 6). However, a closer look at the actual numbers predicted by the CCSM3 in each state reveals some of the minor discrepancies between the observed record and the BLR method used for prediction.

Generally, the Great Lakes region and parts of the Midwest are slightly over-predicted by the BLR method with the CCSM3 (Figure 14), while some Southern Plains states are slightly under-predicted as are Florida and South Carolina. None of the states have a tornado day difference of more than 3.5 days per decade. Additionally, the states that have the greatest total number of tornado day differences also have quite a few tornado days in general, and thus the percentage difference in tornado days (as seen in Figure 15) is not more than 9% different in any of the Great Plains or Midwestern states, and not more than 17% different in any of the Great Lakes or Southeastern states of interest with the CCSM3 BLR predictions.

A month-by-month TSeason breakdown of the absolute difference (instead of percent difference) between the CCSM3 BLR predictions and the observed record is provided in Appendix A to allow for easier comparison to future results as well. Generally, the middle months of April and May are the best predicted across the map with April only having three states with more than a +/- 1 day difference between the model and the observed tornado climatology per decade. The extreme months of the TSeason (February and August) seem to be the least accurately predicted, with wide areas of slight over-prediction throughout the map. June stands out as the only month with a wide area of under-prediction of actual tornado days, with negative or neutral values in a vast majority of the states.

Out of the 2,498 observed tornado days (555.1 per decade) in the US over the 45-year study period, the US as a whole is over-predicted by the CCSM3 BLR by 2.0% (50.3 days; or 11.2 days per decade) over the entire TSeason (Table 5). The majority of that over-prediction comes in February (+52.1%) and August (+42.1%), while June tornado days are under-predicted by nearly 22.8%. However, March (+6.0%), April (-0.7%), and May (-4.7%) – months in the peak of the US tornado season – are some of more accurately predicted months by the model.

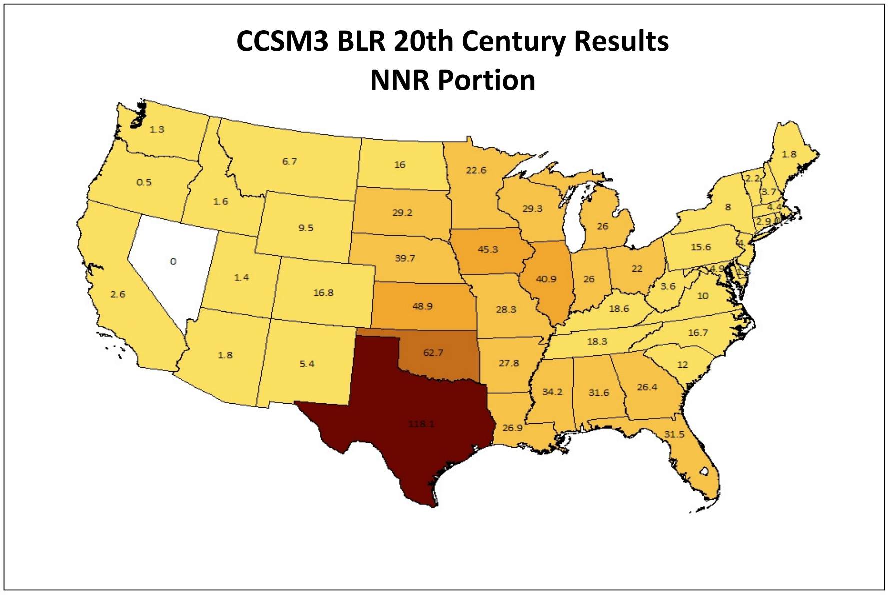


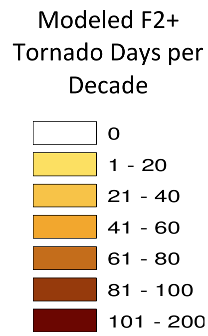


**Figure 12** – BLR tornado prediction results for NNR portion of the 20th century for the CCSM3 global climate model. Labeled and colored in terms of F2+ tornado days per decade.

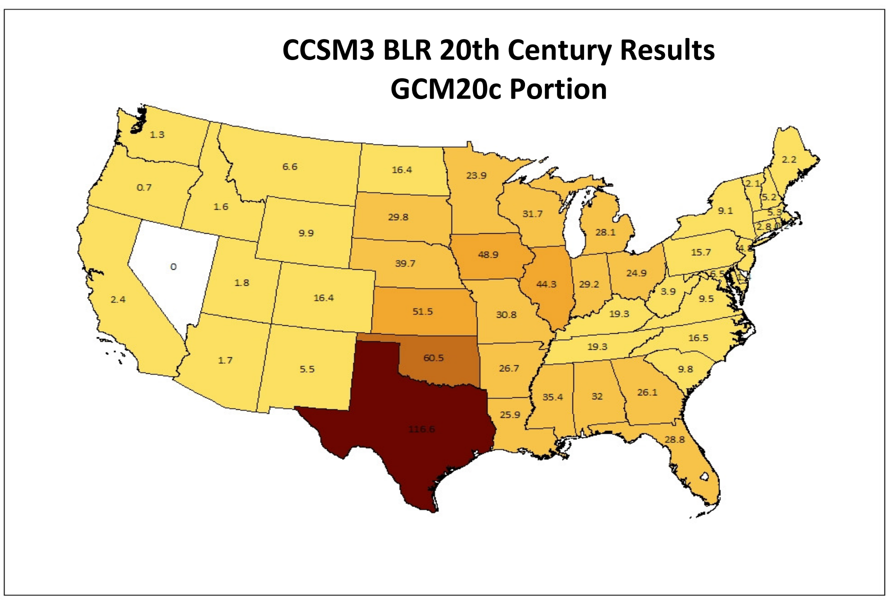


**Figure 13** – BLR tornado prediction results for GCM20c portion of the 20th century for the CCSM3 global climate model. Labeled and colored in terms of F2+ tornado days per decade.

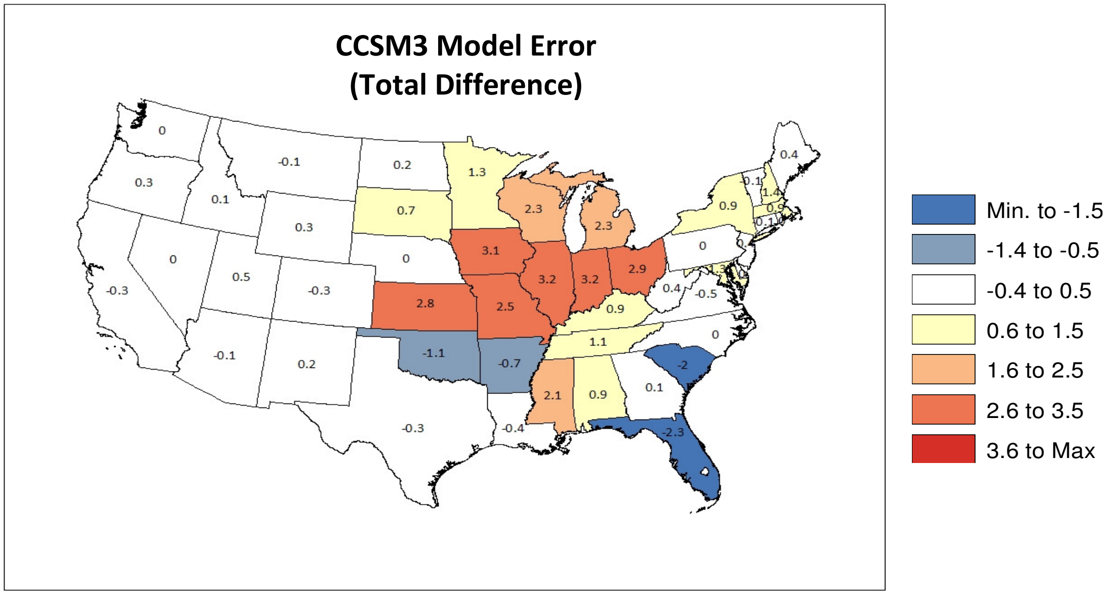


**Figure 14** – Model error between GCM20c BLR results and observed tornado climatology (for the TSeason) for CCSM3. Labeled and colored in terms of F2+ tornado days per decade.

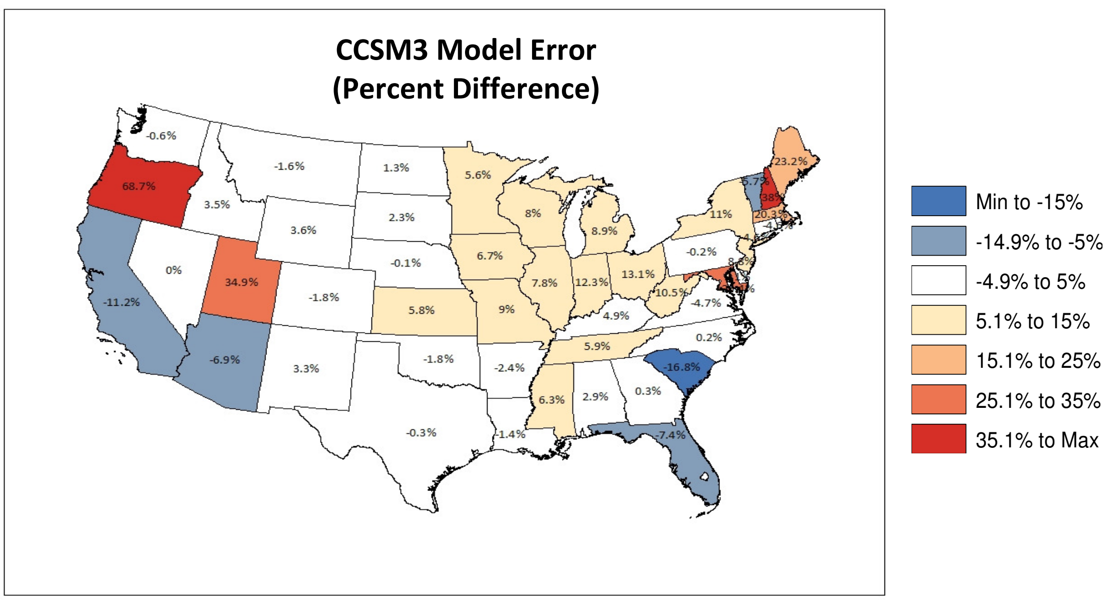


**Figure 15** – Percentage difference between GCM20c BLR results and observed tornado climatology (for the TSeason) for CCSM3.

**Table 5** – Comparison of results by month of the observed tornado climatology, the NNR portion of the BLR of the CCSM3, and the GCM20c portion of the BLR for CCSM3 over the US as a whole. Numbers represent monthly F2+ tornado days per decade.

| Over the Entire US as a Whole | FEB | MAR | APR | MAY | JUN | JUL | AUG | TOT |
|---|---|---|---|---|---|---|---|---|
| Actual Observed | 24.0 | 58.7 | 94.2 | 124.7 | 117.1 | 78.2 | 58.2 | 555.1 |
| | | | | | | | | |
| CCSM3 BLR 20c Results (NNR portion) | 36.3 | 61.1 | 89.5 | 124.0 | 90.5 | 76.6 | 77.8 | 555.7 |
| | | | | | | | | |
| CCSM3 BLR 20c Results (GCM20c portion) | 36.5 | 62.2 | 93.5 | 118.9 | 90.4 | 82.1 | 82.7 | 566.3 |
| Difference b/w Observed and GCM20c | 12.5 | 3.5 | -0.7 | -5.8 | -26.7 | 3.9 | 24.5 | 11.2 |
| Percent Difference b/w Observed and GCM20c | 52.1% | 6.0% | -0.7% | -4.7% | -22.8% | 5.0% | 42.1% | 2.0% |

## *4.4 – Short Discussion on CCSM3 vs. CGCM3 Historical Results*

Before comparing and contrasting the two GCMs in their ability to model the observed tornado record, it is worth reiterating that while the CCSM3 was based on the years of 1957-2002 (45 year period), the CGCM3 was based on the years 1961-2000 (40 year period). This results in the actual observed number of tornado days being slightly different between the two models (555.1 in CCSM3; 561.5 in CGCM3), but because the numbers are standardized by decadal averages, the maps allow for a direct comparison.

While the shading in average tornado day numbers per decade is similar in the NNR portion of both the CCSM3 and the CGCM3 (Figure 16), the labels show the slight differences between the GCMs – this holds true for the GCM20c portion of the results as well (Figure 17). While the NNR portion of both GCMs showed nearly equal accuracy at predicting the observed record, the GCM20c portion had slightly diverging results between GCMs. On a state-by-state basis, the CGCM3 appears a bit more accurate than the CCSM3 at modeling 20th Century tornado days (Figure 18 vs. Figure 14). Much like the CCSM3, the CGCM3 generally over-predicted the states of interest, however, this over-prediction showed up most noticeably in the Southern Plains and Southeastern states (in the CGCM3) instead of around the Great Lakes (in CCSM3; Figure 16). The CGCM3 GCM20c results also showed a region of under-prediction in the Central Plains states.

On a state-by-state basis, in terms of the model error between actual tornado days and predicted tornado days, results were very similar between the two models used; in that the states with the greatest amount of over prediction usually corresponded to states with a substantial amount of tornado days in the first place. Thus, the percentage of model error (Figure 19) was actually quite low in many tornado-prone states. February and August were the months with the greatest number of states showing considerable over-predictions, while June had the greatest number of under-predicted states. April was slightly more under predicted in the CGCM3 compared to the CCSM3. Using the USA F2 Binary variable, over the entire US, however, the CGCM and the CCSM were nearly identical in the in the GCM20c portion of the results (Table 6) – both over-predicting total TSeason tornado days. However, the CGCM3 only over predicted tornado days by 0.9% across the US as a whole compared to the 2.0% over prediction by

CCSM3. CGCM3 appears to be slightly more accurate over the US as a whole in the peak of the tornado season from March through May (with all months being within a +/- 2.0% range of the observed tornado days), with July being the next most accurate month (at +1.2%). Much like in CCSM3, February and August had the greatest amount of over-prediction in the CGCM3, with June being the only month with a substantial under-prediction of tornadoes across the US.

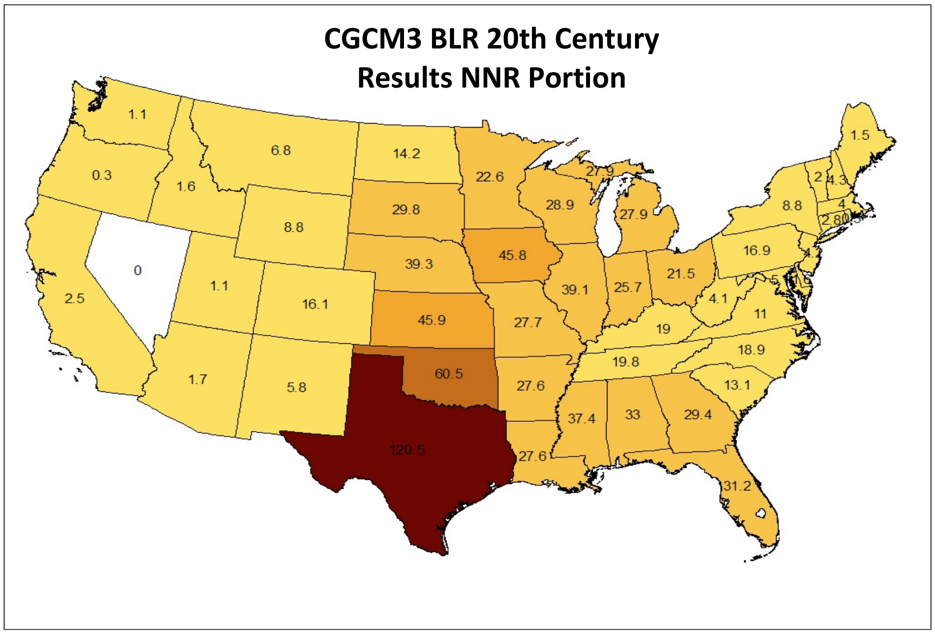


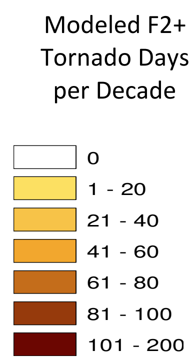


**Figure 16** – BLR tornado prediction results for NNR portion of the 20th century for the CGCM3 global climate model. Labeled and colored in terms of F2+ tornado days per decade.

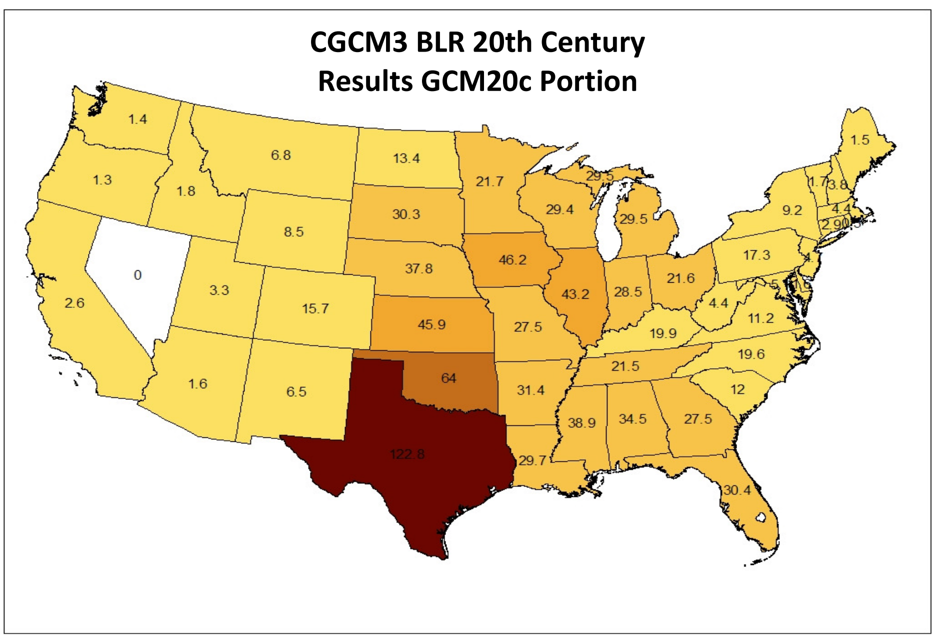


**Figure 17** – BLR tornado prediction results for GCM20c portion of the 20th century for the CGCM3 global climate model. Labeled and colored in terms of F2+ tornado days per decade.

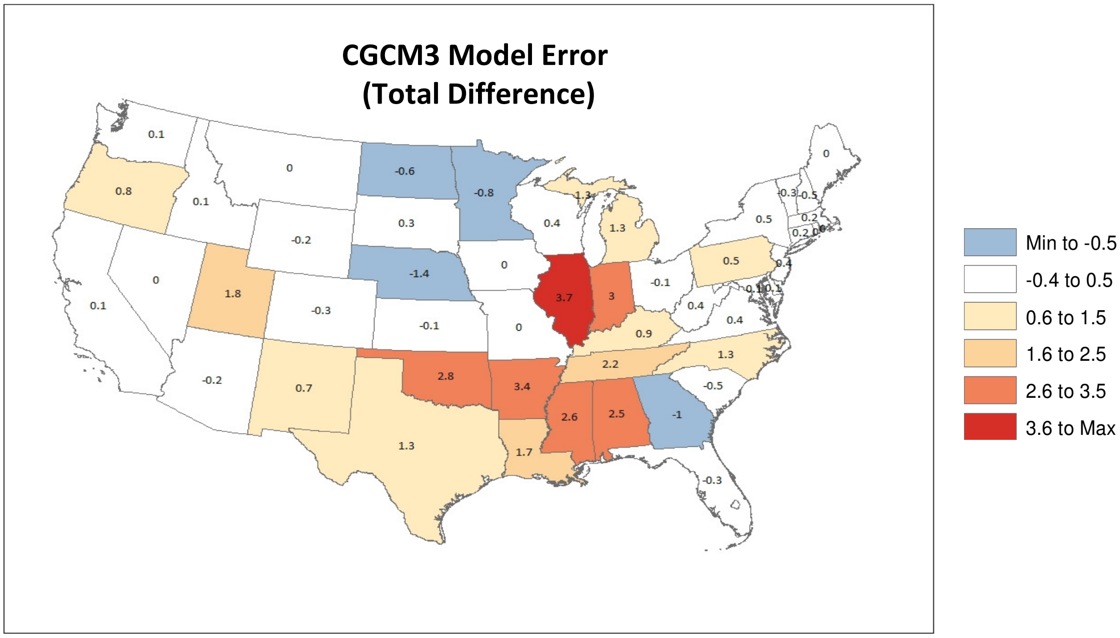


**Figure 18** – Model error between GCM20c BLR results and observed tornado climatology (for the TSeason) for CGCM3. Labeled and colored in terms of F2+ tornado days per decade.

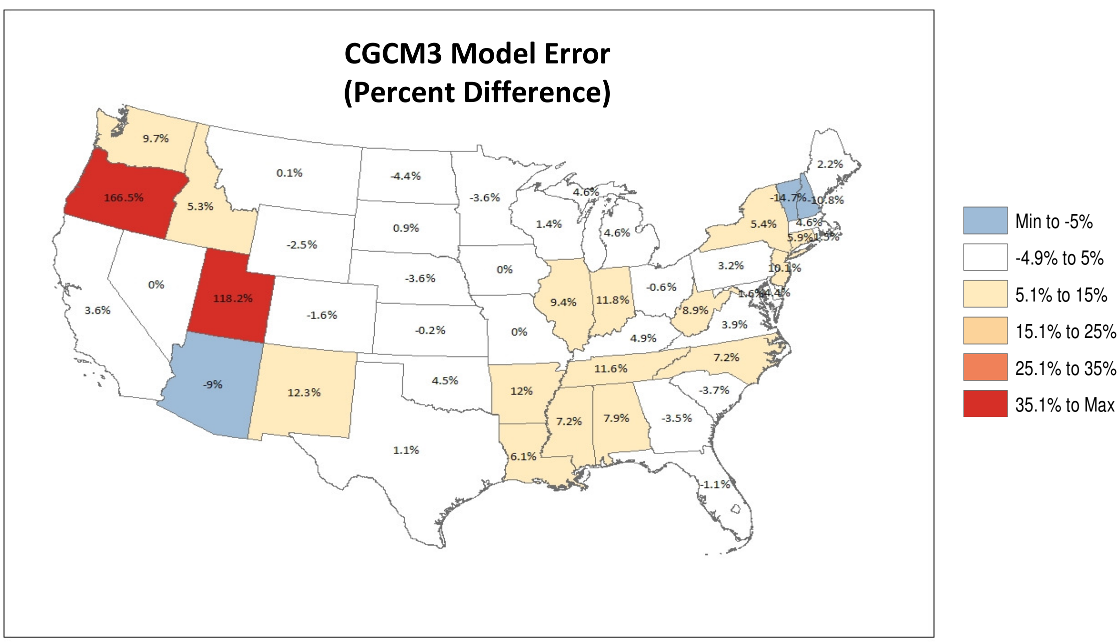


**Figure 19** – Percentage difference between GCM20c BLR results and observed tornado climatology (for the TSeason) for CGCM3.

**Table 6** – Comparison of results by month of the observed tornado climatology, the NNR portion of the BLR of the CGCM3, and the GCM20c portion of the BLR for CGCM3 over the US as a whole. Numbers represent monthly F2+ tornado days per decade.

| **Over the Entire US as a Whole** | **FEB** | **MAR** | **APR** | **MAY** | **JUN** | **JUL** | **AUG** | **TOT** |
|---|---|---|---|---|---|---|---|---|
| Actual Observed | 24.5 | 60.8 | 95.5 | 125.5 | 118.8 | 79.0 | 57.5 | 561.5 |
| | | | | | | | | |
| CGCM3 BLR 20c Results (NNR portion) | 35.6 | 63.5 | 90.0 | 125.4 | 90.1 | 80.4 | 77.2 | 562.2 |
| | | | | | | | | |
| CGCM3 BLR 20c Results (GCM20c portion) | 37.6 | 61.9 | 94.3 | 124.6 | 89.5 | 80.0 | 78.7 | 566.6 |
| Difference b/w Observed and GCM20c | 13.1 | 1.2 | -1.2 | -0.9 | -29.3 | 1.0 | 21.2 | 5.1 |
| Percent Difference b/w Observed and GCM20c | 53.6% | 1.9% | -1.3% | -0.7% | -24.6% | 1.2% | 36.9% | 0.9% |

### *4.5 – Future Projections of Synoptic Patterns*

Due to the method used, the shapes of the future synoptic patterns are nearly identical to their respective patterns in the 20th Century. The matrices of Pearson correlation coefficients between the GCMs 20th Century pattern and the GCM's future patterns (for each scenario) over the course of the entire run of the GCM future, as well as the mean absolute error (MAE) between these patterns, are provided as evidence in Appendix C. A brief discussion on some of the more minor changes to these patterns will be provided in the discussion section of this thesis, however for the remainder of the results section, the shapes of the future patterns can be assumed to be identical to the shapes of the 20th Century patterns, and thus only changes to the frequency and seasonality of the each pattern will be discussed below.

In order to directly compare to data in the CGCM3 model (which was only available for the complete future decades of the 2050s and 2090s), the CCSM3 patterns' frequency and seasonality were analyzed and graphed for the 2050s and the 2090s only (although tables with the frequency on a decade by decade basis are available in Appendix D of this thesis). Additionally, only the patterns that were considered 'tornado-favorable' in the 20th Century will be discussed in detail below – as the scope of this thesis is to analyze the potential impacts climate change may have on future tornadoes, and not necessarily on all synoptic patterns (although, the monthly future frequency graphs of 'tornado unfavorable' CCSM3 patterns in the 2050s and 2090s can also be found in Appendix D).

### *4.5.1 – Future Changes to Tornado-Favorable 500z Patterns*

**Pattern A** – Overall, pattern A decreases quite substantially in total frequency in the future – and decreases more as time passes (Figure 20). Under the A1FI and the A2 scenarios pattern A nearly disappears in the 2050s and occurs less than 5% of the time when it does occur in spring and winter. By the 2090s, the pattern no longer occurs in any scenario except for B1. The seasonality of the pattern also shifts slightly. In the GCM20c, pattern A peaked in April and then again in November, under the B1 scenario the peak moves to March in the 2050s and then skips ahead to May by the 2090s. The secondary peak in the autumn months nearly completely disappears as well.

**Pattern B** – Pattern B at the 500mb level is not nearly as consistent as A500 is in their respective future frequencies and seasonalities (Figure 20). Under the A1FI scenario in the 2050s, B500 peaks nearly two months earlier that it did in GCM20c. By the 2090s, however, the pattern has been somewhat muted in its frequency in the A1FI scenario during all late winter and early spring months. In the A2 scenario, B500 also shifts to February as its peak month in the 2050s, but occurs often in March as well, before tapering off in April and May. By the 2090s this pattern occurs about half as often, and the peak again shifts to March. In the B1 scenario, pattern B's seasonality is similar to its GCM20c seasonality, although it becomes slightly more frequent in most spring months for both the 2050s and the 2090s. Additionally, a slight double peak shows up in B500 in the 2050s (February and April), while by the 2090s, the pattern occurs nearly an equal percent of the time from February through April.

**Pattern C** – Again in pattern C, the changes in frequency and seasonality are quite different depending on the scenario (Figure 20). In the 2050s of both the A2 and the A1FI scenario, C500 is much less common than it was in GMC20c in nearly every month – and, although muted, the seasonality is the same as GCM20c. By the 2090s however, C500 rarely occurs at all in those scenarios. The B1 scenario, however, is quite different, with the peak seasonality of C500 also being in December and January in the 2050s, but being nearly twice as frequent in those months. In the spring months of the B1 scenario, by the 2050s, C500 is not nearly as frequent as it was in GCM20c, but does make a comeback in those months by the 2090s.

**Pattern D** – Pattern D does not occur nearly as often in the future as it did in the past – in any scenario (Figure 20). In the 2050s, this dual-peaked pattern (in late spring and early autumn) occurs most often in the B1 scenario out of the three future scenarios – and with roughly the same peak months as in GCM20c. However, by the 2090s, D500 rarely occurs at all in any scenario except for B1 – and even there, its frequency is muted in every month except October.

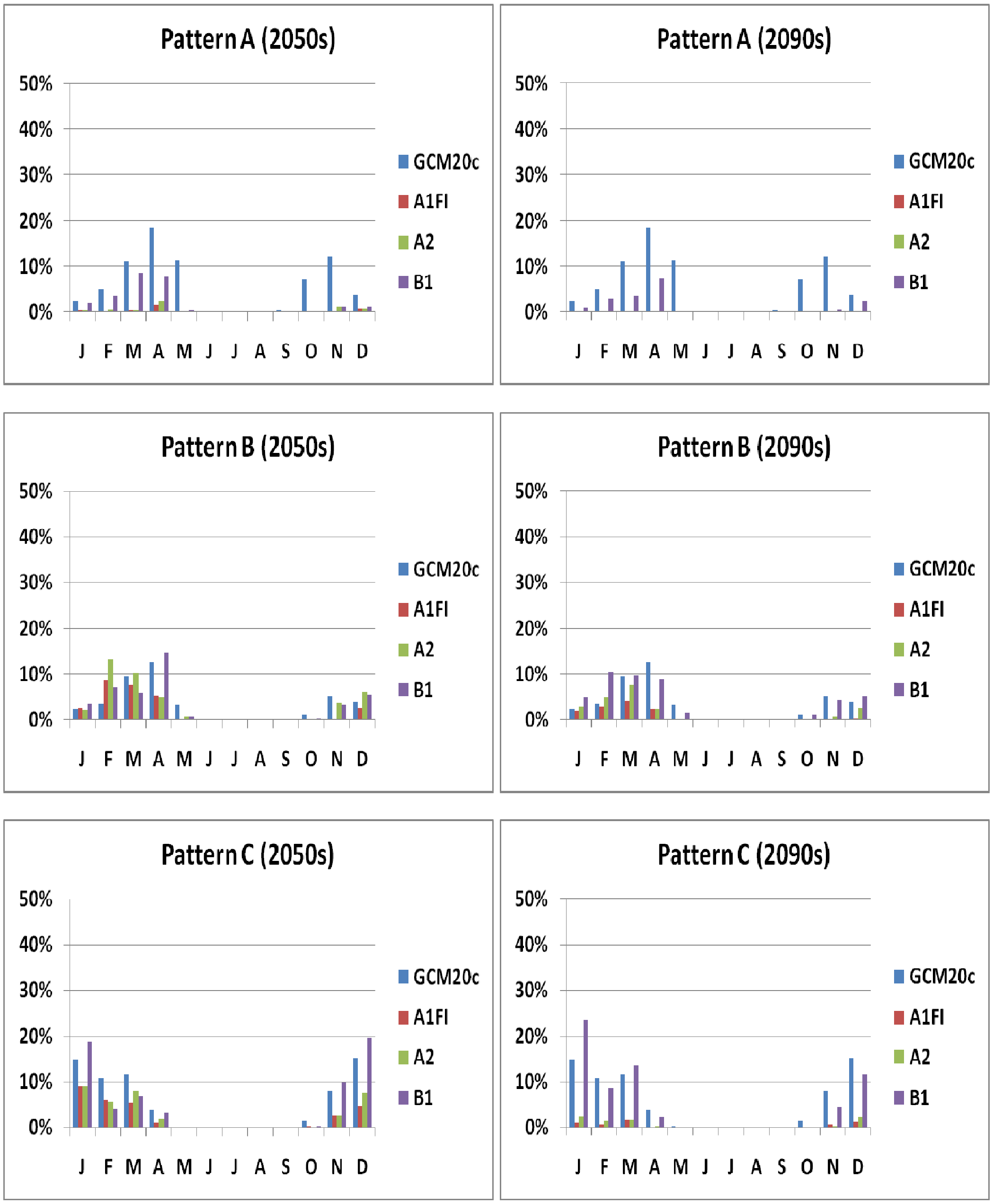


**Figure 20** – Percentage of occurrence of tornado-favorable CCSM3 500z synoptic patterns per month; 2050s (left) and 2090s (right). The blue bar is the GCM20c frequency, red is the A1FI future scenario frequency, green is A2, and purple is B1. Continued on the next page.

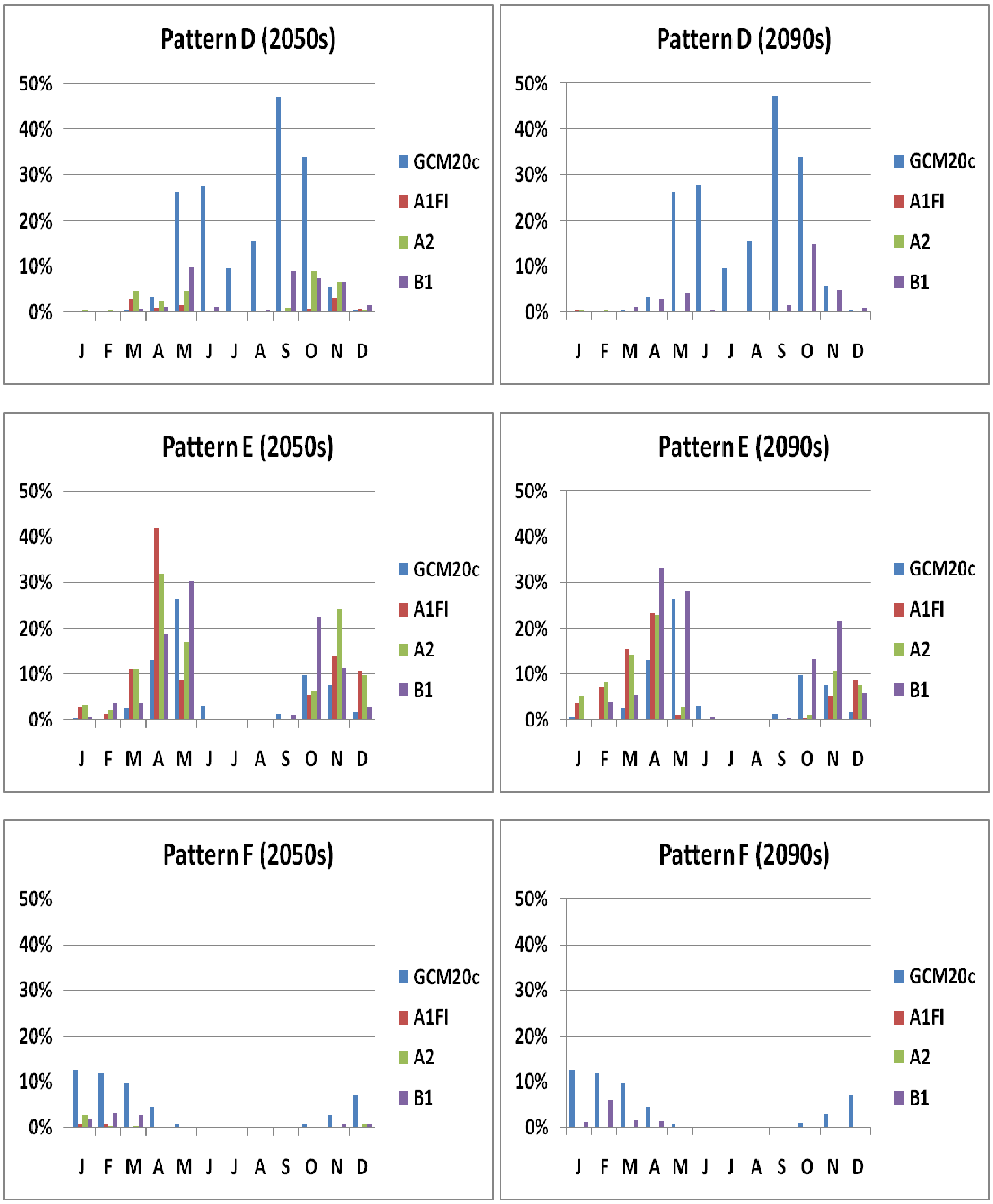


**Figure 20 (continued)** – Percentage of occurrence of tornado-favorable CCSM3 500z synoptic patterns per month; 2050s (left) and 2090s (right). The blue bar is the GCM20c frequency, red is the A1FI future scenario frequency, green is A2, and purple is B1.

**Pattern E** – Among all of the tornado favorable patterns at the 500mb level, Pattern E is the only one that becomes considerably more frequent in the future in nearly every scenario (Figure 20). In both the 2050s and the 2090s under the A1FI and A2 scenarios, the peak seasonality shifts one month (from May in GCM20c to April in the future). In the autumn months, it is slightly more common in both decades under the A2 scenario. Under the B1 scenario, however, the peak seasonality of the pattern is nearly identical to the GCM20c seasonality (peaking in April), except quite a bit more frequent in all months of spring and autumn. In the 20th Century, the pattern did not occur at all in February. Under every future scenario, however, the pattern does occur some, especially in the 2090s under the A1FI and A2 scenarios.

**Pattern F** – Although a winter-dominant pattern, the climate change projections for pattern F are similar to those in A500 (Figure 20). Overall, the pattern occurs much less frequently, especially in the A1FI and A2 scenarios. By the 2090s, the pattern has nearly disappeared entirely from the A1FI and A2 scenarios, but makes a comeback under the B1 scenario. In the 2090s under the B1 scenario, peak seasonality shifts back one month, but overall F500 occurs less than half as often in the peak tornado months of March – May.

*4.5.2 – Future Changes to Tornado-Favorable 700z Patterns*

**Pattern A** – The seasonality of pattern A at the 700mb level in nearly every scenario of both decades is similar to its GCM20c seasonality – although slightly more frequent – especially in the peak tornado months (Figure 21). In the 2050s, under the A1FI and A2 scenarios, the pattern is a bit more frequent in the spring months than it is in the B1 scenario, but less frequent in the late winter months than with B1. In the 2090s, overall the pattern decreases in frequency in both the spring and autumn when compared to the 2050s – especially in the A1FI and A2 scenarios – but less of a decrease is noticed in the B1 scenario.

**Pattern B** – Much like patterns A500 and F500, pattern B at the 700mb level maintains its seasonality from the GCM20c into the future, but becomes markedly less frequent in all months (Figure 21). In the 2050s, pattern B700 is rare in all months of the A1FI and A2 scenarios, but sees a minor spike in frequency in May under the B1 scenario. By the 2090s however, the pattern nearly disappears from the A1FI and A2 scenarios; and while the seasonality of the pattern in B1 has shifted peaks from May back to April, it is also much less frequent under this scenario in the 2090s as well.

**Pattern C** – Pattern C at the 700mb level is quite chaotic between scenarios and decades in regards to its response to climate change (Figure 21). Compared to GCM20c, in the 2050s under the A1FI and A2 scenarios, C700 maintains a similar seasonality, but occurs slightly less often in every month (except for February in A2). This relationship is maintained through the 2090s as well with these two scenarios, except C700 occurs much less often in every month (including February in A2). Under the B1 scenario, however, in the 2050s, a dual peak is noted in frequency in January and again in April (while the GCM20c peak was in March). In the 2090s under B1, this dual peak shifts to January and March, and overall the pattern becomes more frequent than GCM20c for every month from January through April.

**Pattern D** – Under the A1FI and A2 scenarios, pattern D at the 700mb level steadily decreases into the future and generally develops a much sharper peak in April, especially in the 2090s (Figure 21). Overall, D700 is a bit more frequent in the spring months under the A2 scenario than it is in the A1FI scenario. In both decades of the B1 scenario, the pattern nearly mimics the seasonal pattern of the 20th Century, although it becomes quite a bit less frequent by the 2090s.

**Pattern E** – Much like E500, pattern E at the 700mb level is the one tornado-favorable pattern that becomes noticeably more frequent in the future – more so than any other 700z pattern – favorable or not (Figure 21). This summer-dominant pattern shows a much broader seasonality as well, especially in the A1FI and A2 scenarios. In A1FI, this pattern occurs more than 30% of the time from May through October in the 2050s (including over 80% of the time from June through August), and by the 2090s, the pattern's seasonality has grown to include 30% of the days from April through November (including over 80% of the days from May through October). The frequency and seasonality of E700 in A2 is very similar to A1FI, and while B1's seasonality is the same as the other two scenarios, it is comparably quite a bit less frequent than under the A1FI or A2 scenario, but still considerably more frequent than GCM20c.

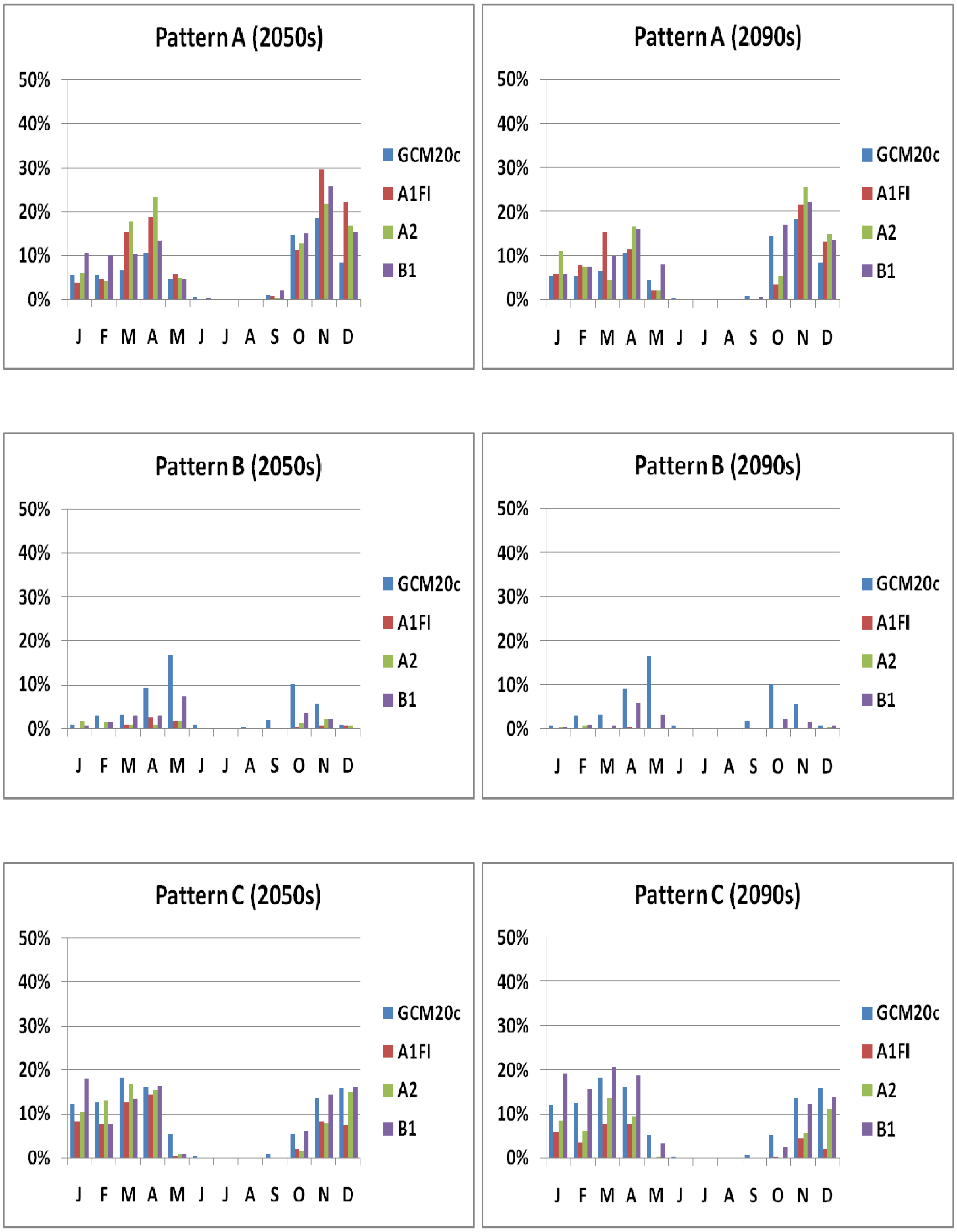


**Figure 21** – Percentage of occurrence of tornado-favorable CCSM3 700z synoptic patterns per month; 2050s (left) and 2090s (right). The blue bar is the GCM20c frequency, red is the A1FI future scenario frequency, green is A2, and purple is B1. Continued on the next page.

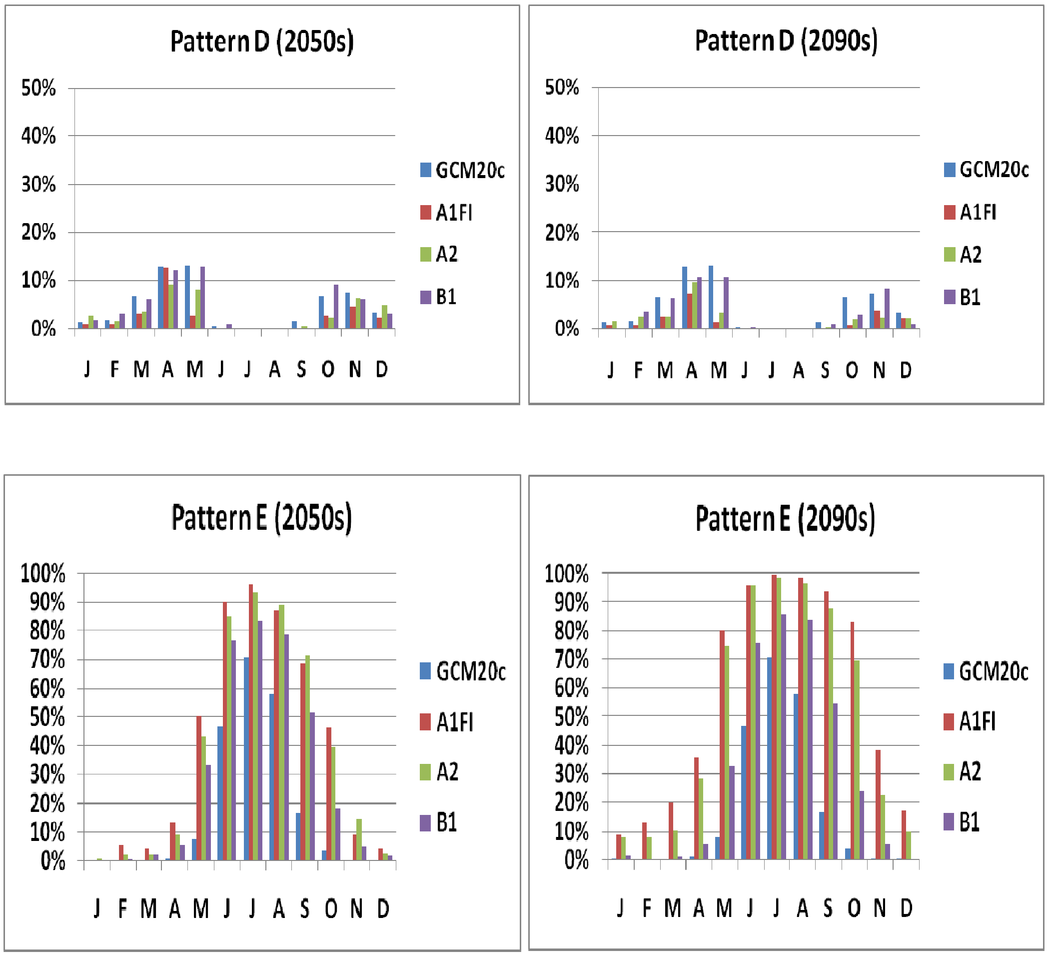


**Figure 21 (continued)** – Percentage of occurrence of tornado-favorable CCSM3 700z synoptic patterns per month; 2050s (left) and 2090s (right). The blue bar is the GCM20c frequency, red is the A1FI future scenario frequency, green is A2, and purple is B1. (Note the change of the vertical axis in Pattern E because it occurs more often than 50% of the time in at least one month). Continued on the next page.

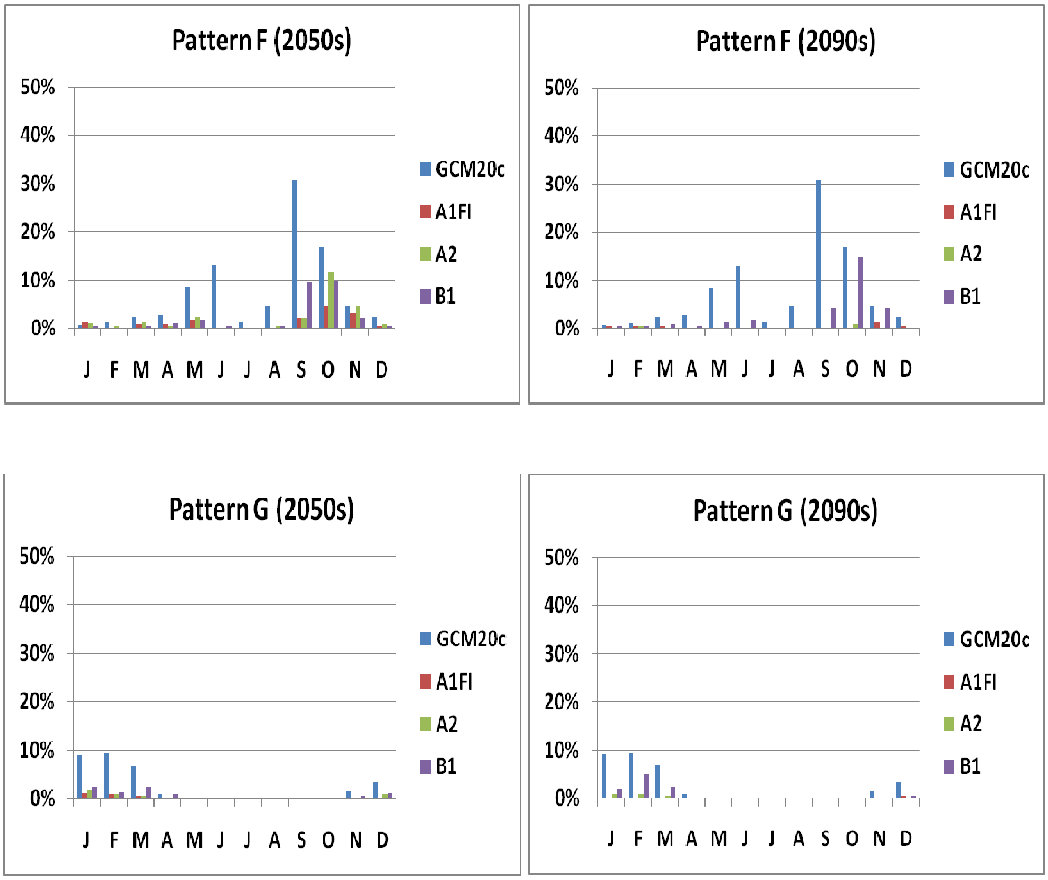


**Figure 21 (continued)** – Percentage of occurrence of tornado-favorable CCSM3 700z synoptic patterns per month; 2050s (left) and 2090s (right). The blue bar is the GCM20c frequency, red is the A1FI future scenario frequency, green is A2, and purple is B1.

**Pattern F** – Both the seasonality and frequency of pattern F change under all future scenarios – though the largest portions of this change are outside of the TSeason in autumn (Figure 21). In the months of interest in the spring, F700 decreases substantially under all scenarios and in both future decades.

**Pattern G** – Pattern G at the 700mb level has a different response in the future scenarios depending on the decade (Figure 21). In the 2050s, G700 occurs rarely in any spring month under any scenario. In the 2090s, however, while the pattern almost completely disappears in the A1FI and A2 scenarios, under the B1 scenario there is a slight increase from the 2050s in frequency, and peak occurrence is in February. Compared to GCM20c, however, even under the B1 scenario in the 2090s, the overall frequency of G700 is much less.

### *4.5.3 – Future Changes to Tornado-Favorable 850t Patterns*

**Pattern A** – At the 850mb level, pattern A displays a slight increase in frequency when compared to GCM20c – especially in the later months of the TSeason and autumn, more so in the 2090s than in the 2050s, and more so in A1FI than in any other scenario (Figure 22). The seasonality of this increase within the TSeason, peaks in June in every scenario and in both decades – about a month earlier than the two-month peak of the pattern in GCM20c. This pattern also begins to appear in February and March in the 2090s, whereas it did not occur in those months in the past.

**Pattern B** – Pattern B at the 850mb level occurs more frequently in the future as well – especially in the 2090s and especially in A1FI (Figure 22). This spring-dominant pattern sees a change in peak seasonality from May to April in A1FI (in both decades) and in the A2 scenario (in the 2090s). This pattern does maintain its May peak in the 2050s of the A2 scenario, and in both decades under the B1 scenario. Additionally, February and March occurrences of B850 become more frequent in both A1FI and A2 – especially in the 2090s. Overall, the increase in frequency over GCM20c is quite large in every late winter and spring month.

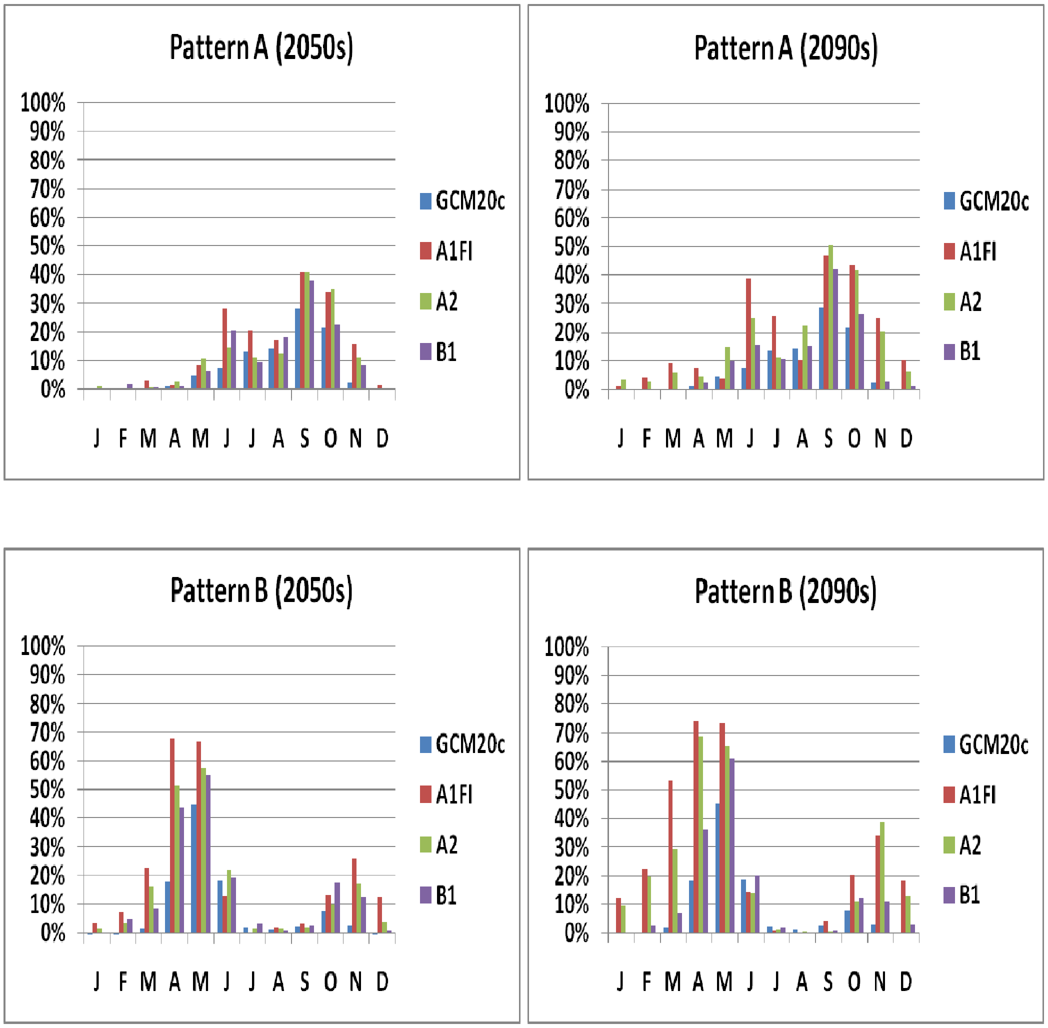


**Figure 22** – Percentage of occurrence of tornado-favorable CCSM3 850t synoptic patterns per month; 2050s (left) and 2090s (right). The blue bar is the GCM20c frequency, red is the A1FI future scenario frequency, green is A2, and purple is B1. (Note the change of the vertical axis in Patterns A and B because they occur more often than 50% of the time in at least one month). Continued on the next page.

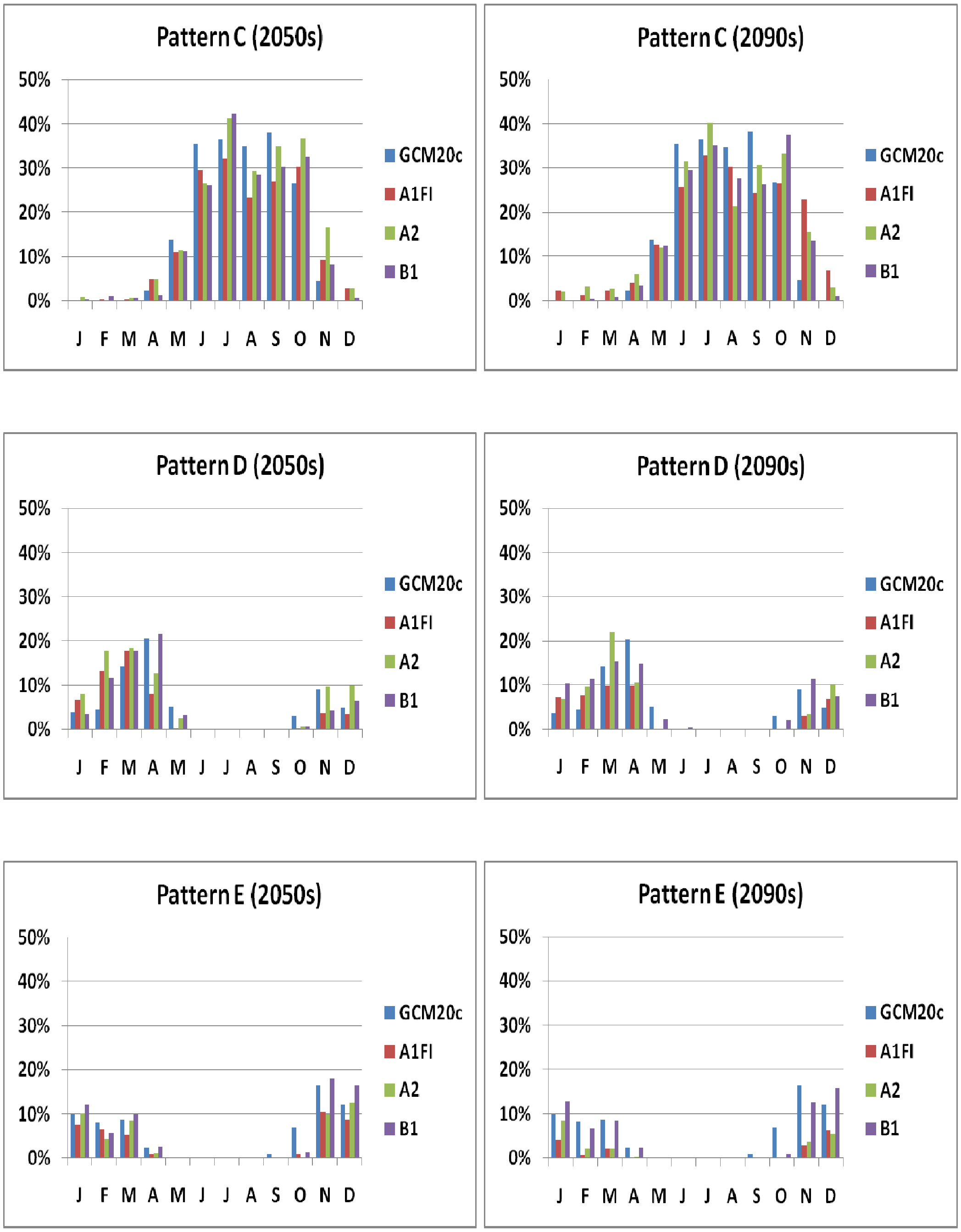


**Figure 22 (continued)** – Percentage of occurrence of tornado-favorable CCSM3 850t synoptic patterns per month; 2050s (left) and 2090s (right). The blue bar is the GCM20c frequency, red is the A1FI future scenario frequency, green is A2, and purple is B1. Continued on the next page.

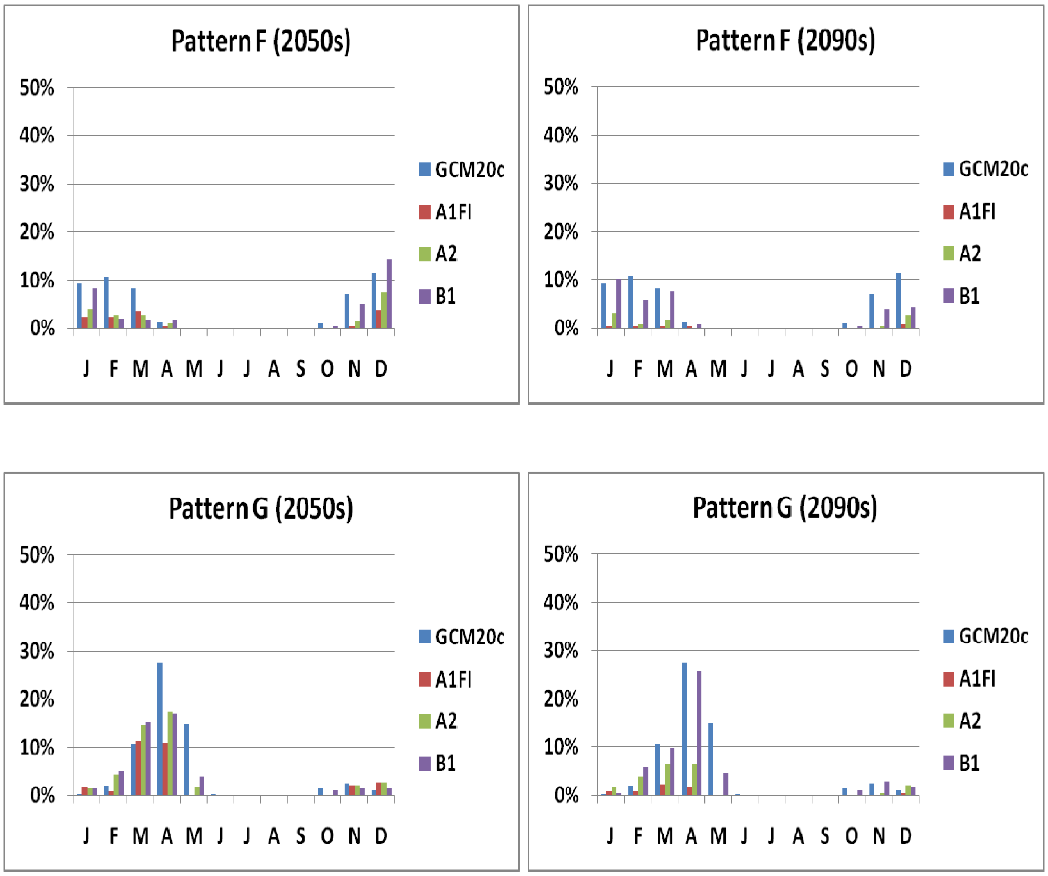


**Figure 22 (continued)** – Percentage of occurrence of tornado-favorable CCSM3 850t synoptic patterns per month; 2050s (left) and 2090s (right). The blue bar is the GCM20c frequency, red is the A1FI future scenario frequency, green is A2, and purple is B1.

**Pattern C** – Frequency and seasonality changes of C850 from the 20th Century are quite minimal in both decades and all scenarios (Figure 22). Generally, the pattern in GCM20c was slightly more frequent than it was in any future scenario, although under A2 and B1, C850 is a bit more frequent than under A1FI. A slightly sharper peak in seasonality – as well as a dual peak in July and October (amplified in the 2090s) – is noticed in every future scenario, whereas there was a broad seasonality from June through September in GCM20c.

**Pattern D** – Pattern D is quite chaotic by decade and by scenario in the future (Figure 22). Under the A1FI scenario, in the 2050s, D850 shows a clear peak seasonality in March – a month earlier than GCM20c – but also occurs quite frequently in February. By the 2090s, that peak is gone, and the pattern occurs a bit less frequently in February. In the A2 scenario, a two-month peak is observed in February and March of the 2050s, but by the 2090s, a sharper peak in March occurs. Under the B1 scenario, in the 2050s, the seasonality is similar to GCM20c – in that it peaks in April – but D850 is slightly more frequent from February through April. In the 2090s under B1, pattern D seems to have a two month peak from March through April, and occur slightly more frequently from February through March than it did in the 2050s.

**Pattern E** – In the 2050s, under the A1FI and A2 scenarios, the seasonality of E850 in GCM20c is kept intact, although the frequency is slightly decreased from that of GCM20c (Figure 22). By the 2090s, however, E850 in both of these scenarios decreases quite a bit, and becomes rare in the late winter and early spring. Under the B1 scenario, however, a double-peak emerges in the 2050s in November and (less-so) in March, before shifting slightly to December and (less-so) in March in the 2090s. During the TSeason months, however, only February and March see many occurrences of E850.

**Pattern F** – The frequency and seasonality changes from GCM20c in F850 are similar to those in E850 (Figure 22). The biggest difference however is that under the B1 scenario, this pattern actually becomes more frequent in the 2090s than it was in the 2050s, especially February and March. The peak also changes from February (in GCM20c) to January under the B1 scenario in the 2090s. Under the A1FI and A2 scenarios, F850 rarely occurs in the 2050s, and decreases even further in the 2090s.

**Pattern G** – Pattern G at the 850mb level was spring-dominant in GCM20c and remains that way under future scenarios (Figure 22). Under the A1FI scenario in the 2050s, however, a broader peak is noticed in March and April, rather than the April peak that occurred over the 20th Century. By the 2090s, G850 becomes rare in any month. In the A2 scenario, the pattern becomes more frequent earlier, but much less frequent later in the TSeason. While the pattern also decreases in overall frequency by the 2090s in A2, it is still over twice as frequent as it was in A1FI. Under the B1 scenario, peak seasonality of the pattern in GCM20c is maintained in both future decades, but muted. This pattern, however, does increase substantially in frequency in April in the 2090s compared to the 2050s under the B1 scenario.

#### *4.5.4 – Future Changes in Tornado-Favorable Synoptic Patterns – CCSM3 vs. CGCM3*

An important note before discussing the comparison between GCMs is that the patterns in each GCM are not identical. Although there are 15 patterns at each level in both GCMs, pattern A at 500z in CCSM3 is not meant to be similar in shape or seasonality to pattern A at 500z for CGCM3, nor are any of the other patterns. CGCM pattern shapes and seasonalities (for both the 20th century and for all future scenarios) can be found in Appendix B of this thesis.

Although the individual shapes of the patterns between GCMs are different and not directly comparable, some broad similarities can be made regarding the future frequency and seasonality of the patterns when compared between the two GCMs used. Primarily, there are a select few of the 15 patterns at each level that show a trend towards happening more frequently in the future, while the rest show an overall decrease in frequency. These select few patterns represent the warmer patterns at each level, with peak seasonality occurring in the summer. Additionally, the seasonality of these patterns is broadened in the future – occurring more often in the months just outside of their 20th century seasonality. This increase is more pronounced in the 2090s than it is in the 2050s, and is more pronounced in the ‘higher emissions’ scenarios (A1FI and A2; the A1FI scenario is not used with the CGCM3 model in this research) than it is in the B1 scenario in both GCMs.

On a level-by-level basis, more nuanced differences are exhibited between the two GCMs. At the 500z level of the CGCM, two of the six tornado-favorable patterns show a considerable uptick in total frequency (patterns B and F) into the future, while one pattern remains relatively stable into the future (pattern A) and the rest decrease in frequency in the future. This is quite a bit different than CCSM3, where only pattern E is predicted to increase markedly into the future, while the other five tornado-favorable patterns generally decrease.

At the 700z level, one tornado-favorable pattern (pattern A) in the CGCM3 model is forecast to increase substantially, one pattern seems to shift seasonality, while maintaining its yearly frequency (pattern D), while the other four tornado favorable patterns decrease in overall frequency. In comparison, CCSM3 pattern E increases its frequency and seasonality greatly in the future, while patterns A, C and D all are relatively stable into the future (depending on the scenario) and only patterns B, F and G (of the tornado-favorable patterns) are predicted to decrease substantially.

With the 850mb temperature fields, the CGCM projects pattern C to increase in frequency, especially in the spring months, and pattern E to increase in frequency and broaden in seasonality – but more in the summer and autumn months. Four patterns (patterns B, D, F and G) will remain relatively stable in their frequency, but will differ in their seasonality depending on scenario, while only one pattern (pattern A) is projected to decrease substantially among tornado-favorable patterns in this model. This differs from CCSM3, in that two patterns show a considerable uptick in frequency and a broader seasonality (patterns A and B), while the other tornado favorable patterns are a bit more chaotic in regards to their future frequencies.

### *4.6 – Future Projections of Tornadoes*

All patterns were included in the BLR to predict future tornado day occurrences. The labels of ‘tornado-favorable’ or ‘not tornado favorable’ are used only for discussion purposes and qualitative analysis.

The Mann Whitney test (Wilks, 2006) was used to test for statistical significance in differences between a state's GCM20c tornado days (as described in section 4.3) and its future tornado days as modeled with BLR. This non-parametric test was performed individually for each state based upon that state's average number of tornado days per decade (and per month, where monthly results are displayed) in the GCM20c portion of the BLR results and the average per decade of either the 2050s or the 2090s. The test was run on a state's yearly BLR totals from 1960-1999 (n=40, compared with one decade in the future, where n=10). Because the data from 1960 were missing from the CGCM 20th Century data, only the BLR totals from 1970-1999 are used for this GCM, and thus n=30 for CGCM GCM20c.

*4.6.1 – Future Tornado Days – CCSM3 – A1FI*

The A1FI scenario is only available through the CCSM3 in this thesis, and thus, the results are not comparable between GCMs. Over the US as a whole, tornado days are projected to increase 7.6% by the 2050s and 12.6% by the 2090s under the A1FI scenario (Table 7). The majority of the increase in both decades can be accounted for in two general regions, the first being the Lower Great Lakes and eastern Mid-Atlantic states, and the second in the Northern Plains states (Figure 23). By the 2050s, South Dakota, Maryland, and Indiana southward to Alabama are expected to have significantly more tornado days under the A1FI scenario. By the 2090s, those states are joined by Nebraska, Colorado, West Virginia and Ohio, all with an increase of at least 6 tornado days per decade. A swath of states from the Upper Great Lakes south-southwestward through the Southern Plains are expected to have a decrease in tornado days under the A1FI scenario.

The majority of the total US increase in tornado days is accounted for in March and April when there is an over 35% increase in the 2050s in each month, and a 58.6% increase in March by the 2090s (Table 7). This early season increase is offset by slight decreases in tornado days from May through August in the 2050s, but by the 2090s, even June and July see an increase in tornado days. This marks a substantial shift in the peak tornado season of the US as a whole – from May back to April – and a broadening of the seasonality as well, from a one month peak (of May) in the 20th Century, to a three month peak (from April through June) by the 2090s (Figure 25).

The US total is reflected on a regional basis by early TSeason (February and March) increases in tornado days in the Southern Plains and northeastward through the Lower Great Lakes states in the 2090s (Figure 24). The two regions that showed the greatest overall increases in the 2090s (the Northern High Plains and the Mid-Atlantic to Midwest) gain the majority of their total TSeason tornado increases in March and April. August is the only month in which no state is projected to have a substantial increase in tornado days by the 2090s in the A1FI scenario.

**Table 7** – Monthly percent change from GCM20c in F2+ tornado days per decade for the US as a whole by GCM and scenario. Percents greater than 10% are shaded red; percents less than -10% are shaded green. The top table is the percent change in the 2050s; the bottom table is the percent change in the 2090s.

| USA - 2050s | | Feb | Mar | Apr | May | Jun | Jul | Aug | Total |
|---|---|---|---|---|---|---|---|---|---|
| CCSM3 | A1FI | 12.4% | 35.4% | 35.8% | -6.5% | -2.4% | -1.0% | -7.8% | 7.6% |
| | A2 | 19.4% | 33.0% | 28.7% | -4.3% | -3.2% | -2.3% | -6.3% | 7.0% |
| | B1 | 13.9% | 13.2% | 20.9% | -3.0% | -1.2% | -1.7% | -3.2% | 4.2% |
| CGCM | A2 | 16.2% | 24.9% | 15.4% | -5.3% | -7.0% | -1.5% | -0.6% | 3.8% |
| | B1 | 29.7% | 8.3% | 19.9% | 1.1% | -4.7% | -0.4% | 3.7% | 6.1% |

| USA - 2090s | | Feb | Mar | Apr | May | Jun | Jul | Aug | Total |
|---|---|---|---|---|---|---|---|---|---|
| CCSM3 | A1FI | 49.8% | 58.6% | 29.1% | -5.4% | 3.0% | 2.4% | -10.3% | 12.6% |
| | A2 | 47.7% | 38.4% | 29.5% | -4.0% | -1.6% | -3.0% | -2.8% | 10.2% |
| | B1 | 38.7% | 17.4% | 21.2% | 0.9% | -3.1% | -4.5% | -5.5% | 6.1% |
| CGCM | A2 | 70.8% | 66.9% | 23.6% | -13.3% | -7.8% | 2.5% | 4.1% | 12.7% |
| | B1 | 6.4% | 25.3% | 21.0% | -5.9% | -7.2% | -1.5% | -1.4% | 3.8% |

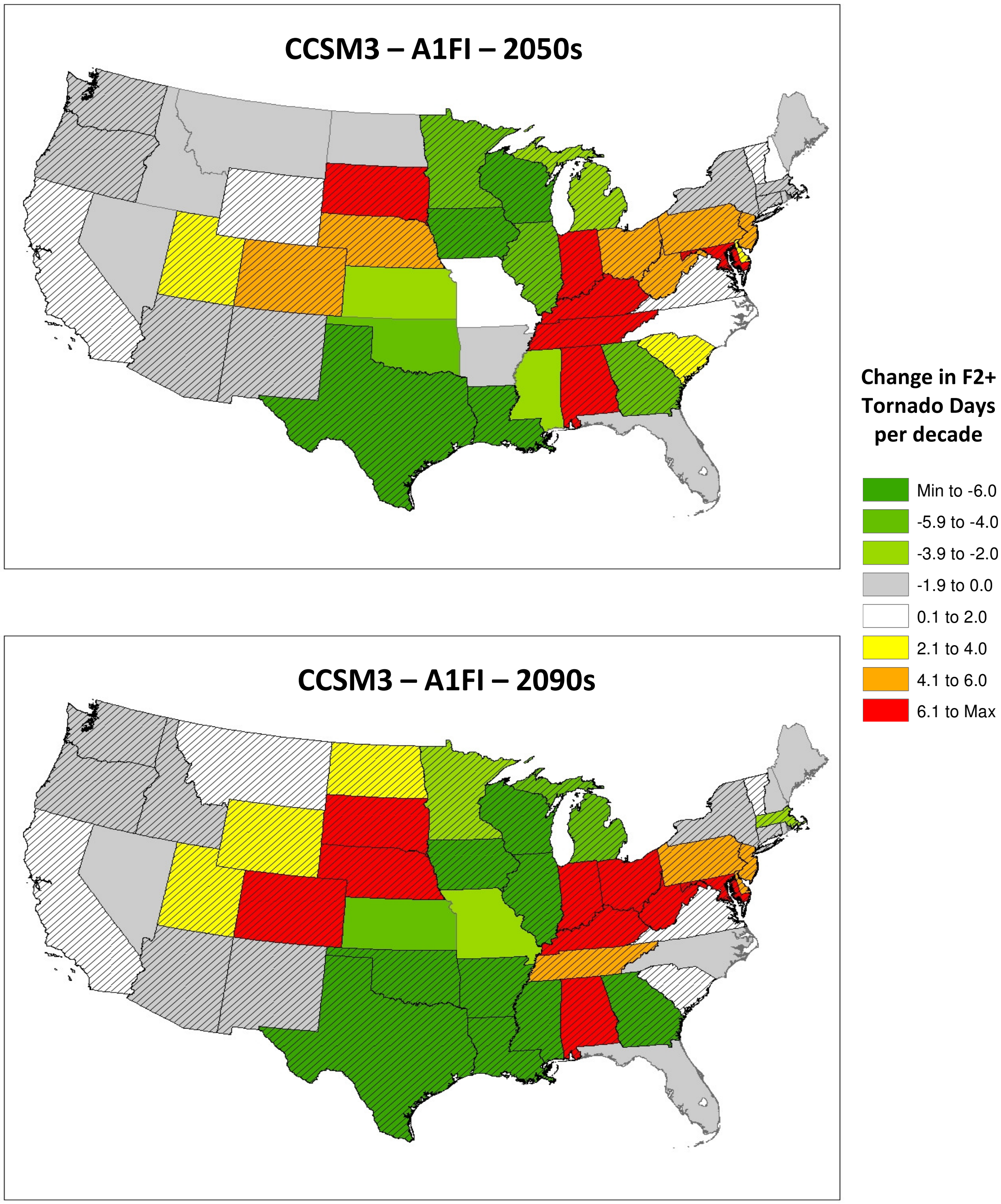


**Figure 23** – Total difference from GCM20c in F2+ tornado days per decade for CCSM3 – A1FI. Hatching indicates the difference in that state is significant at the 0.05 level.

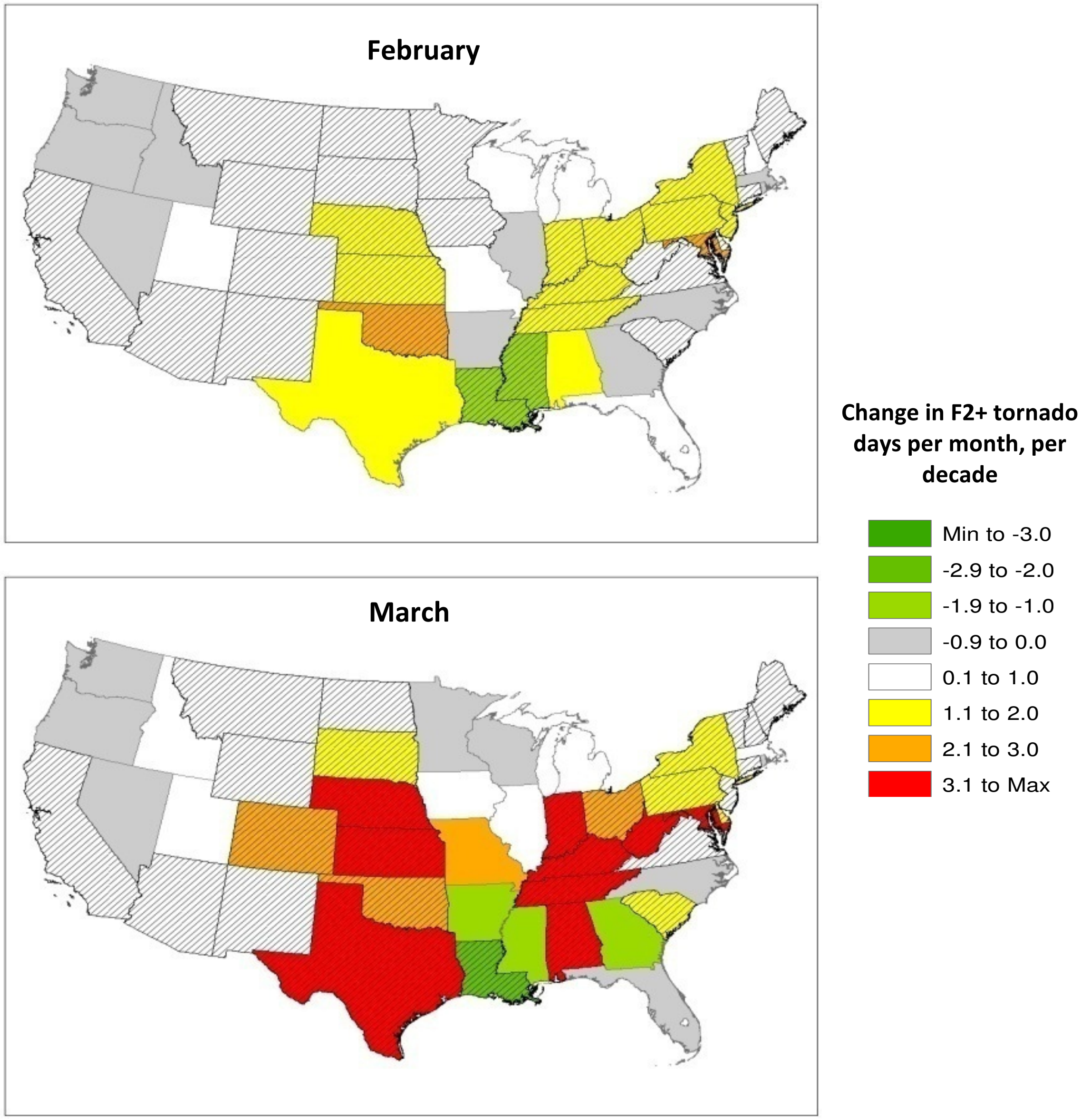


**Figure 24** – Monthly difference of the 2090s from GCM20c in F2+ tornado days per decade (February – August) for the CCSM3 – A1FI scenario. Hatching indicates the difference in that state is significant at the 0.05 level. Continued on the next page.

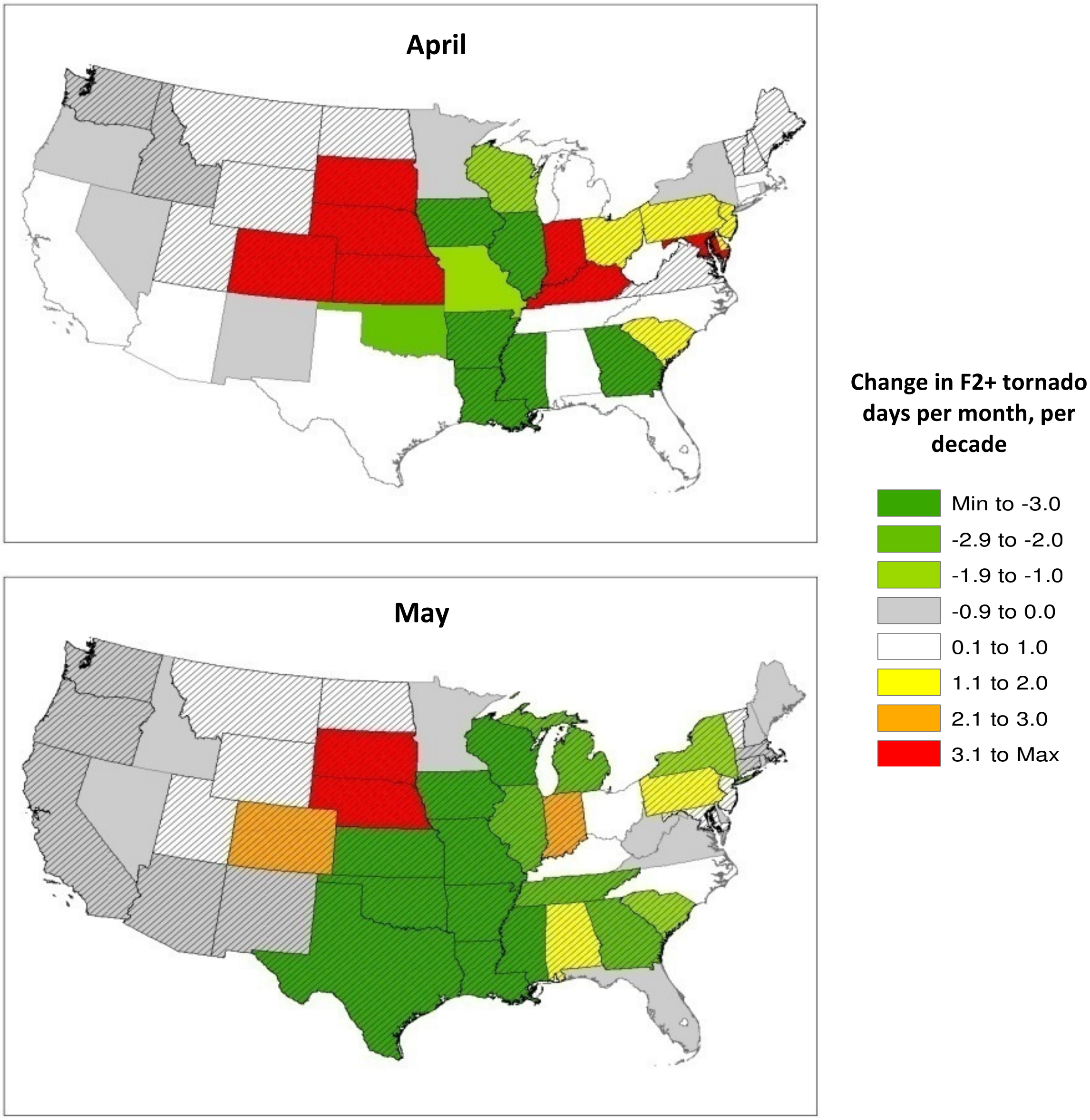


**Figure 24 (continued)** – Monthly difference of the 2090s from GCM20c in F2+ tornado days per decade (February – August) for the CCSM3 – A1FI scenario. Hatching indicates the difference in that state is significant at the 0.05 level. Continued on next page.

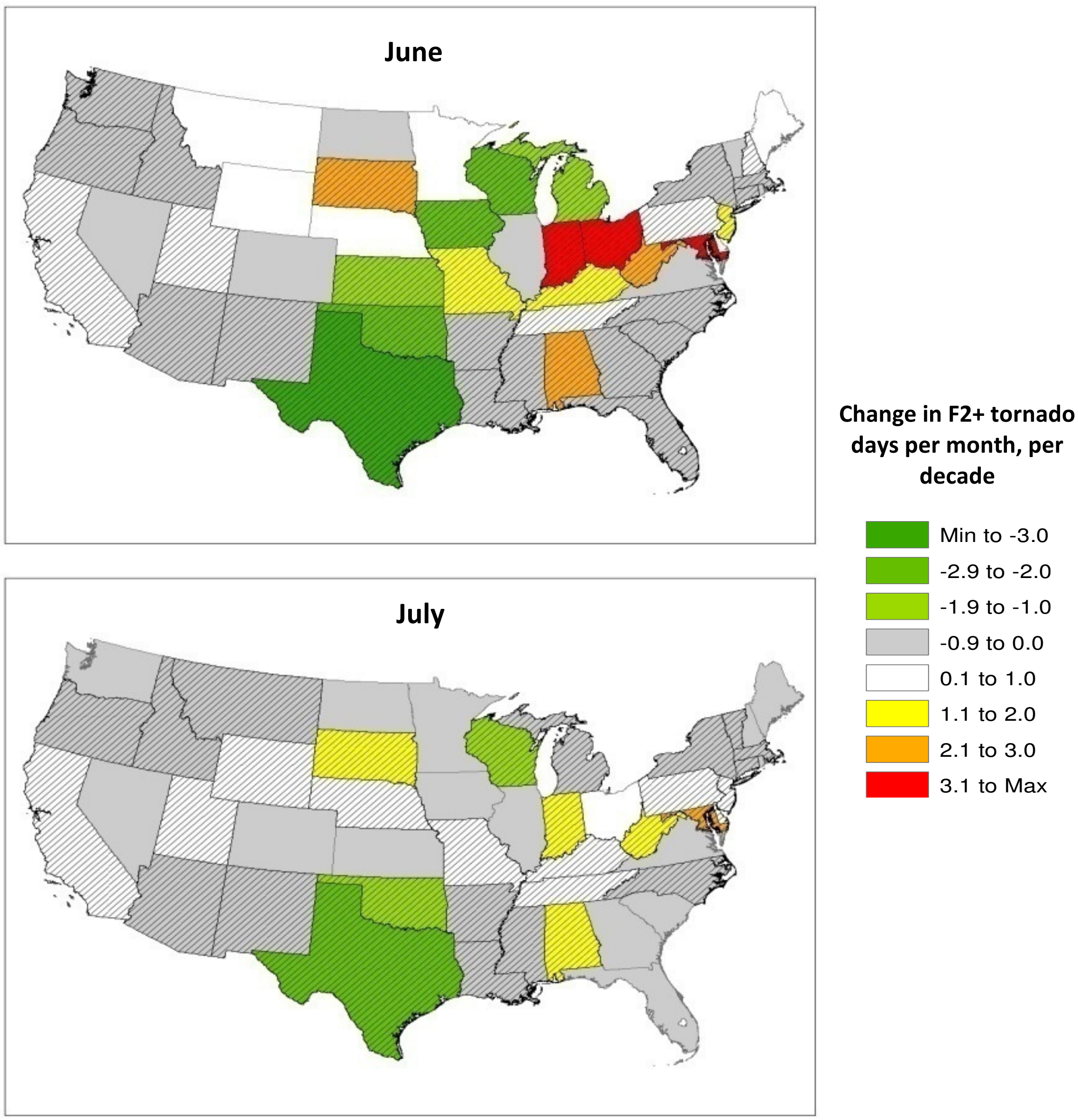


**Figure 24 (continued)** – Monthly difference of the 2090s from GCM20c in F2+ tornado days per decade (February – August) for the CCSM3 – A1FI scenario. Hatching indicates the difference in that state is significant at the 0.05 level. Continued on the next page.

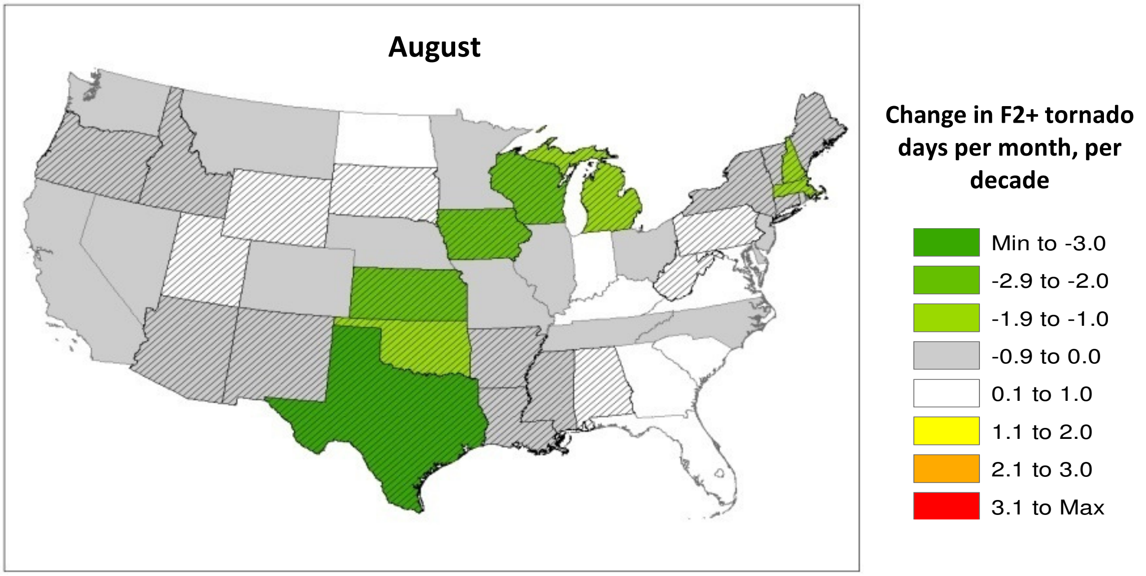


**Figure 24 (continued)** – Monthly difference of the 2090s from GCM20c in F2+ tornado days per decade (February – August) for the CCSM3 – A1FI scenario. Hatching indicates the difference in that state is significant at the 0.05 level.

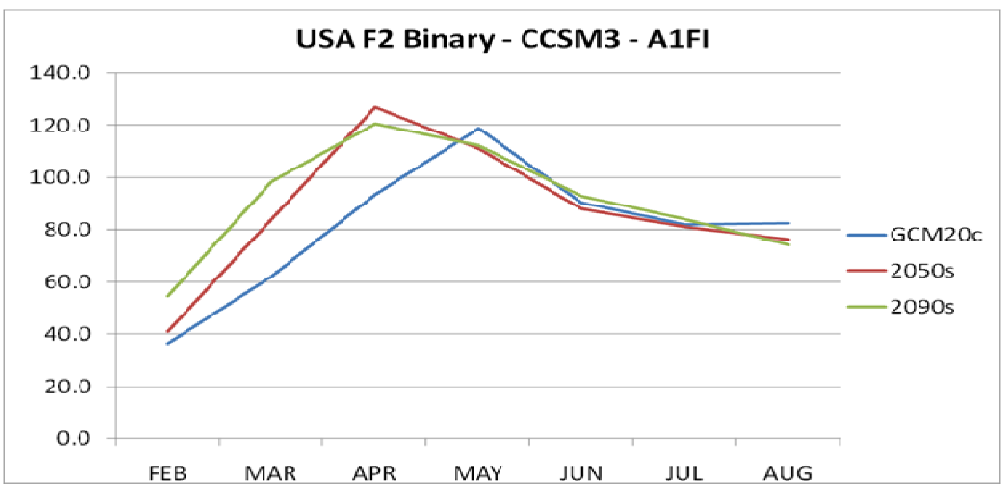


| | FEB | MAR | APR | MAY | JUN | JUL | AUG | TOT |
|---|---|---|---|---|---|---|---|---|
| **GCM20c** | 36.5 | 62.2 | 93.5 | 118.9 | 90.4 | 82.1 | 82.7 | 566.3 |
| **2050s** | 41.1 | 84.2 | 127.0 | 111.1 | 88.2 | 81.3 | 76.3 | 609.2 |
| **2090s** | 54.7 | 98.6 | 120.7 | 112.5 | 93.1 | 84.1 | 74.2 | 637.9 |

**Figure 25** – Change in seasonality of F2+ tornado days in the US as a whole from GCM20c to CCSM3 – A1FI. Table on the bottom represents the line graph at the top.

*4.6.2 – Future Tornado Days – CCSM3 – A2*

Under the A2 scenario in the CCSM3 model, tornado days are projected to increase 7.0% by the 2050s and 10.2% by the 2090s (Table 7). Similar to the A1FI results, in both the 2050s and the 2090s, the majority of the increase is in the eastern Mid-Atlantic states, into Appalachia and the Midwest, and a secondary area in the Northern High Plains (Figure 26). In the 2050s, the states from Indiana southward to Alabama, along with South Dakota and Maryland are each projected to have at least a 6 day increase. By the 2090s, however, the increase appears to shift slightly northward, as Ohio, Pennsylvania, Nebraska, Virginia, West Virginia and Colorado each are projected to have an even larger increase in total tornado days. These increases are slightly offset by Tennessee (which drops a category) and Missouri (which drops two categories and switches signs) – both of which have fewer tornado days in the 2090s compared to the 2050s.

On a month-by-month basis, over the entire US as a whole, the majority of the 7.0% increase in the 2050s is accounted for in the first three months of the TSeason – February is projected to see a 19.4% increase, March a 33.0% increase and April 28.7% increase (Table 7). By the 2090s however, this increase becomes more noticeable in February with a 47.7% rise in tornado days while March and April also are projected to increase by nearly 30% each. Similar again to the A1FI scenario, this increase is offset by

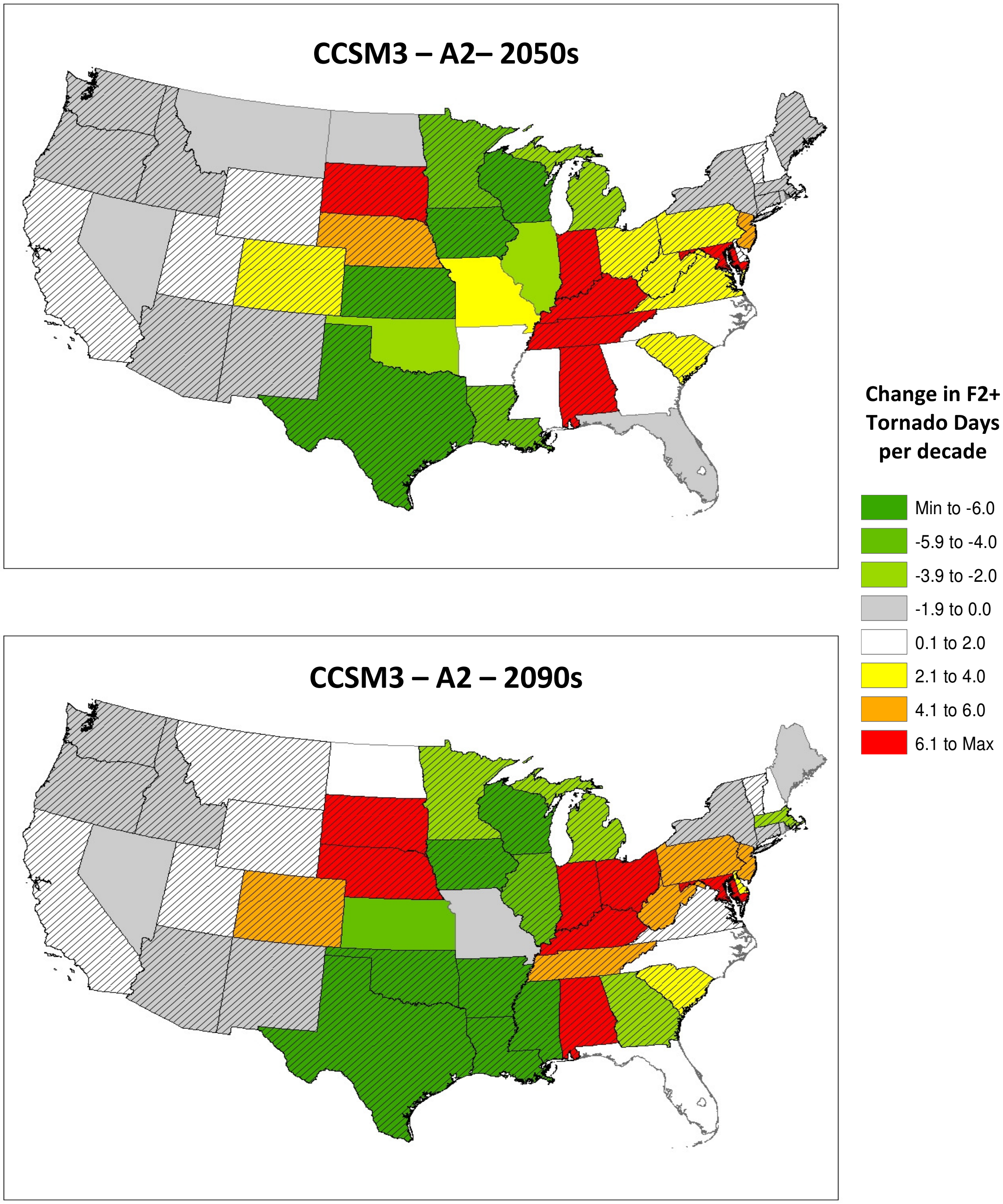


**Figure 26** – Total difference from GCM20c in F2+ tornado days per decade for CCSM3 – A2. Hatching indicates the difference in that state is significant at the 0.05 level.

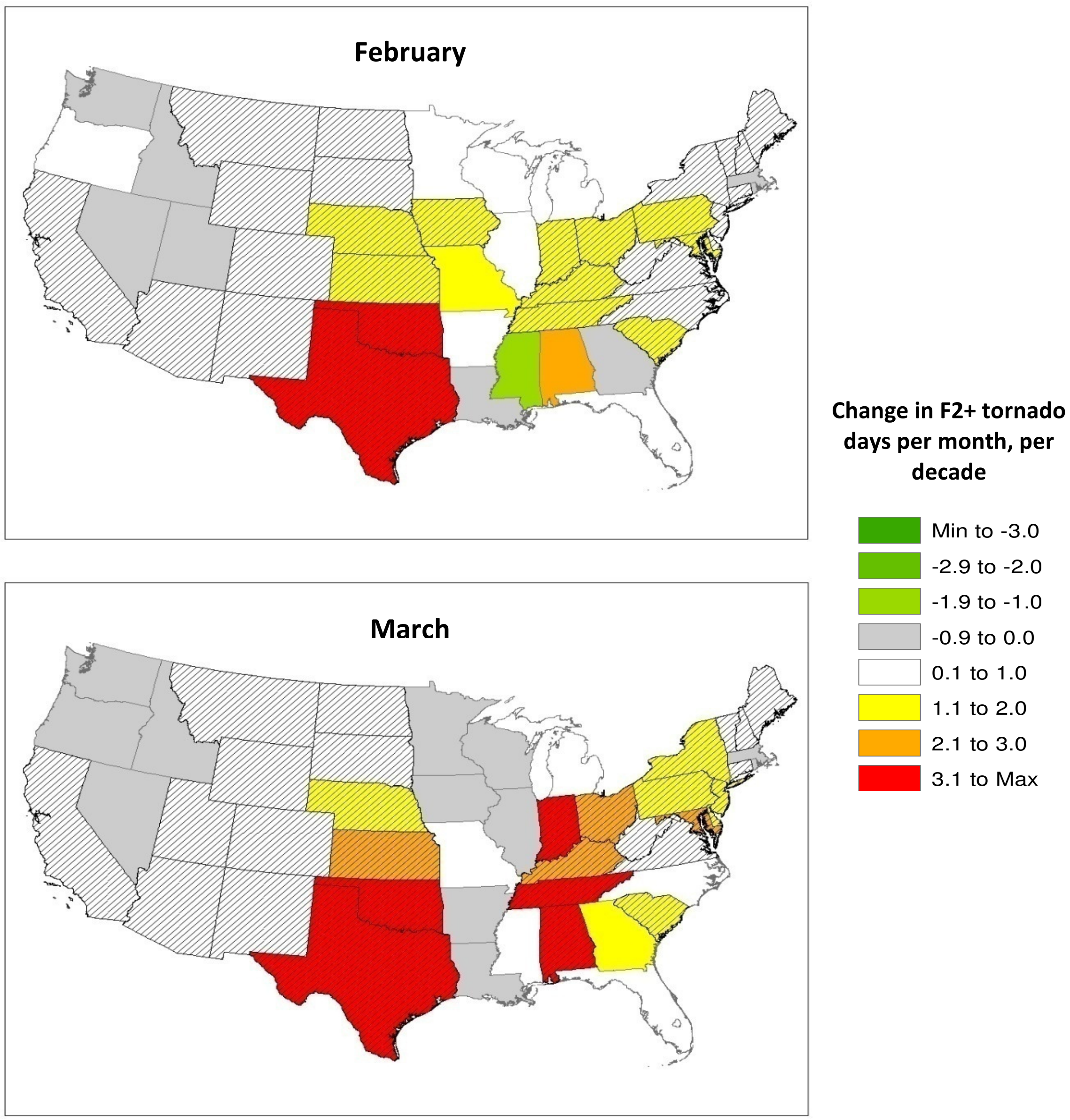


**Figure 27 –** Monthly difference of the 2090s from GCM20c in F2+ tornado days per decade (February – August) for the CCSM3 – A2 scenario. Hatching indicates the difference in that state is significant at the 0.05 level. Continued on the next page.

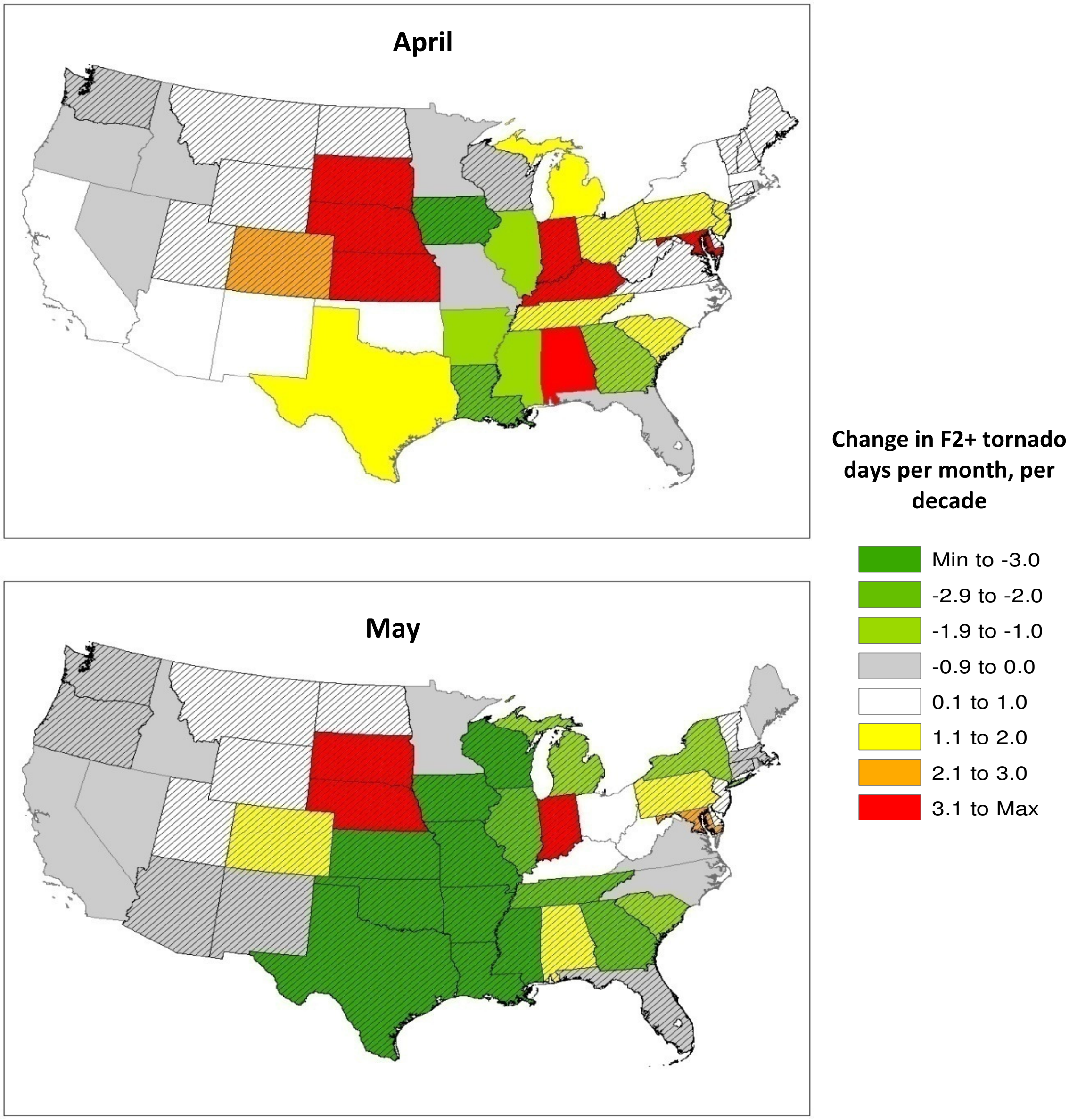


**Figure 27 (continued) –** Monthly difference of the 2090s from GCM20c in F2+ tornado days per decade (February – August) for the CCSM3 – A2 scenario. Hatching indicates the difference in that state is significant at the 0.05 level. Continued on the next page.

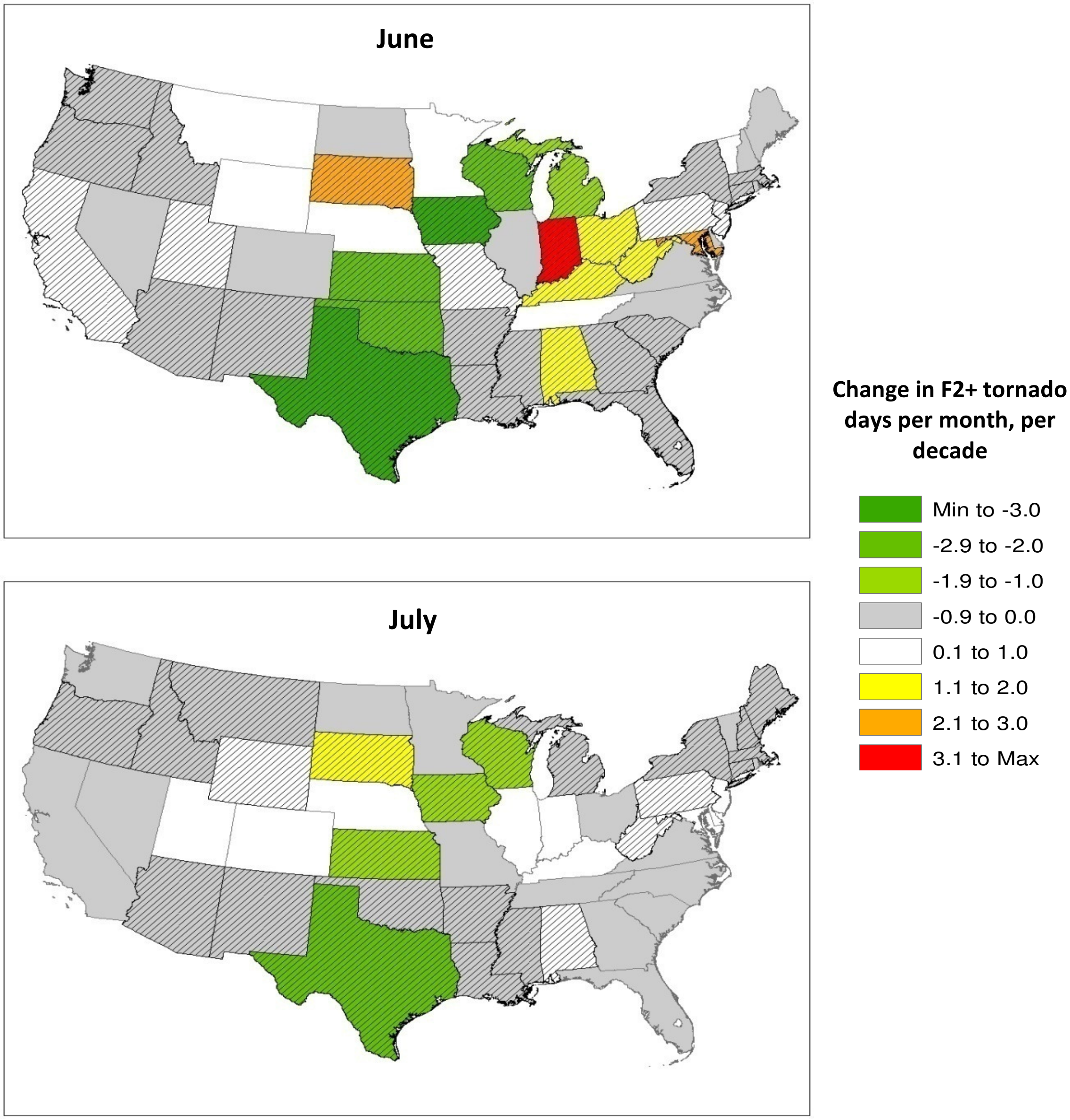


**Figure 27 (continued) –** Monthly difference of the 2090s from GCM20c in F2+ tornado days per decade (February – August) for the CCSM3 – A2 scenario. Hatching indicates the difference in that state is significant at the 0.05 level. Continued on the next page.

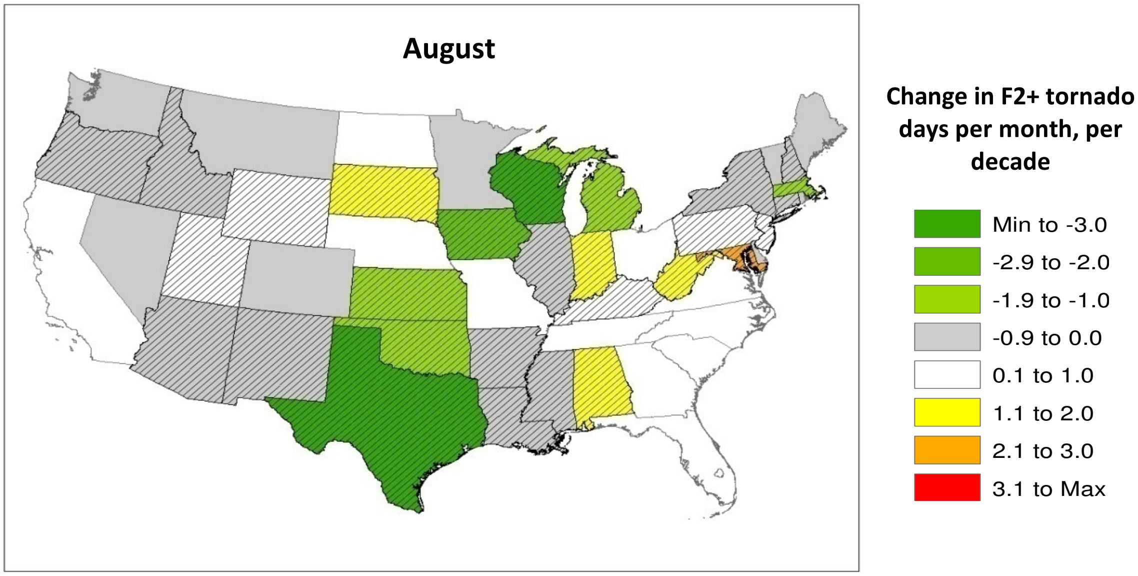


**Figure 27 (continued) –** Monthly difference of the 2090s from GCM20c in F2+ tornado days per decade (February – August) for the CCSM3 – A2 scenario. Hatching indicates the difference in that state is significant at the 0.05 level.

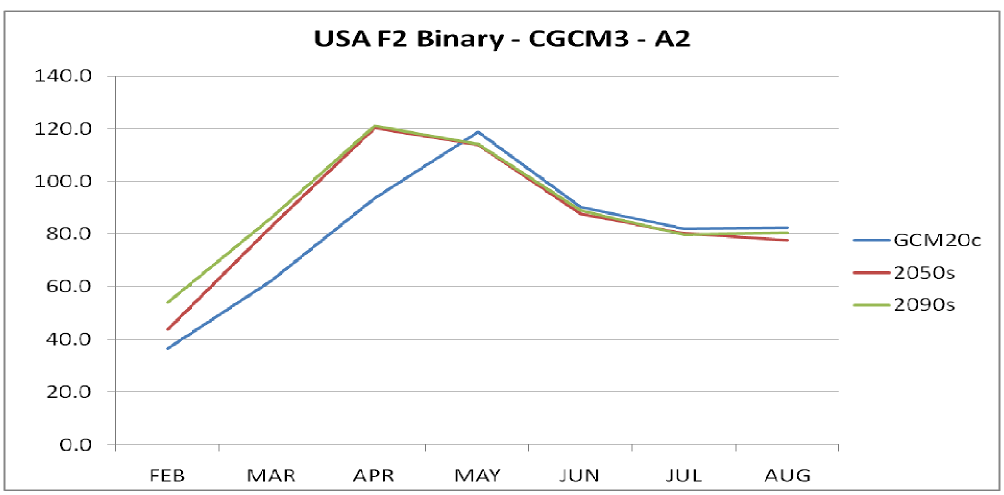


| | FEB | MAR | APR | MAY | JUN | JUL | AUG | TOT |
|---|---|---|---|---|---|---|---|---|
| **GCM20c** | 36.5 | 62.2 | 93.5 | 118.9 | 90.4 | 82.1 | 82.7 | 566.3 |
| **2050s** | 43.6 | 82.7 | 120.4 | 113.8 | 87.5 | 80.2 | 77.5 | 605.7 |
| **2090s** | 53.9 | 86.1 | 121.1 | 114.1 | 88.9 | 79.6 | 80.4 | 624.1 |

**Figure 28** – Change in seasonality of F2+ tornado days in the US as a whole from GCM20c to CCSM3 – A2. Table on the bottom represents the line graph at the top.

slight decreases in tornado days from May through August in both the 2050s and the 2090s. Noteworthy here is that while in the 2090s of the A1FI scenario there is a projected increase in tornado days in June and July, under the A2 scenario, every month from May to August is projected to have at least a 1% decrease in tornado days in both decades analyzed. This has an important effect on the seasonality of tornadoes in the future: the peak of the tornado season does move back to April (from May in GCM20c), and the breadth of the peak seasonality does increase; however the increase is only to a slight two-month peak (Figure 28), whereas it broadened to three months under the A1FI scenario (Figure 25).

On a monthly and state-by-state basis in the 2090s under the A2 scenario, while February sees a slight increase of tornado days in the Southern Plains, the Lower Great Lakes, and parts of the Southeast; the bigger increases come in March over these same areas (Figure 27). In April, much of the Southeast (with the exception of Alabama and South Carolina) is projected to have a slight decrease in tornado days, while the Central Plains and Lower Great Lakes regions are projected to have significant increases. By May, only a few Northern Plains states are projected to have an increase, but the majority of the South, Midwest and Upper Great Lakes states are beginning to usher in decreased tornado activity for the rest of the TSeason. Indiana, however, bucks this trend, and is projected to have an increase in F2+ tornado days in each of these months.

*4.6.3 – Future Tornado Days – CCSM3 – B1*

Over the US as a whole, under the B1 scenario for CCSM3, tornado days are projected to increase by 4.2% from GCM20c totals by the 2050s and 6.1% by the 2090s (Table 7). Each of these increases is less than each of their respective increases in the other two CCSM3 scenarios. Regionally, these increases are manifested predominantly in the southeastern US northward up to the Lower Great Lakes (Figure 29). In the 2050s, most of the increase is relegated to the eastern and northern portion of this area, with Indiana, Tennessee, Alabama, and Maryland seeing the greatest increases in tornado days (all with increases of 6 days or more). In the 2090s, however, this area expands towards the eastern seaboard – the region from Indiana southward to Mississippi and Alabama is projected to have an increase of at least 6 or more tornado days, while the region from Pennsylvania and New Jersey southward along the Eastern Seaboard is projected to increase significantly as well.

Much like the results from the other two CCSM3 scenarios, over the US as a whole, the greatest increase on a month-to-month basis occurs in the first few months of the TSeason (Table 7). With the exception of February in the 2050s, each month’s increase is markedly less than the increase in A1FI and A2, but does increase in the 2090s compared to the 2050s. In the 2050s, the biggest increase is seen in April (at 20.9%), followed by February (13.9%) and March (13.2%), however, by the 2090s, February sees the largest increase of any month (at 38.7%). Interestingly, in the 2090s, May actually is projected to see an increase (albeit only 0.9%) in tornado days under the CCSM3 – B1 scenario, where as May is projected to see a decrease in both the 2050s and 2090s in every other CCSM3 scenario. Because of this, the seasonality of F2+ tornado days under the B1 scenario is noticeably different than the seasonality of other scenarios. Overall, the peak month remains May (as it was in GCM20c), however, it broadens to a two-month-long peak of April and May before tailing off in June at a similar pace to the GCM20c (Figure 31).

Spatially, on a month-to-month basis in the 2090s, from February through April, increased tornado days in the Southern Plains, Southeast and some Appalachian states (both significant and not) can generally be noticed (Figure 30). By May, although most states are experiencing either a minor (and insignificant) decrease or little change at all from GCM20c tornado days, Indiana, Kentucky, Maryland, and Alabama are still projected to see a slight (and significant) increase. Additionally, of those four states, except for Kentucky in July, each is projected to see an increase in tornado days in each month of the 2090s. Furthermore, out of the seven month long TSeason, July is the only month in which no states are expected to see significant increases greater than one F2+ tornado day per decade in the 2090s under the B1 scenario of the CCSM3.

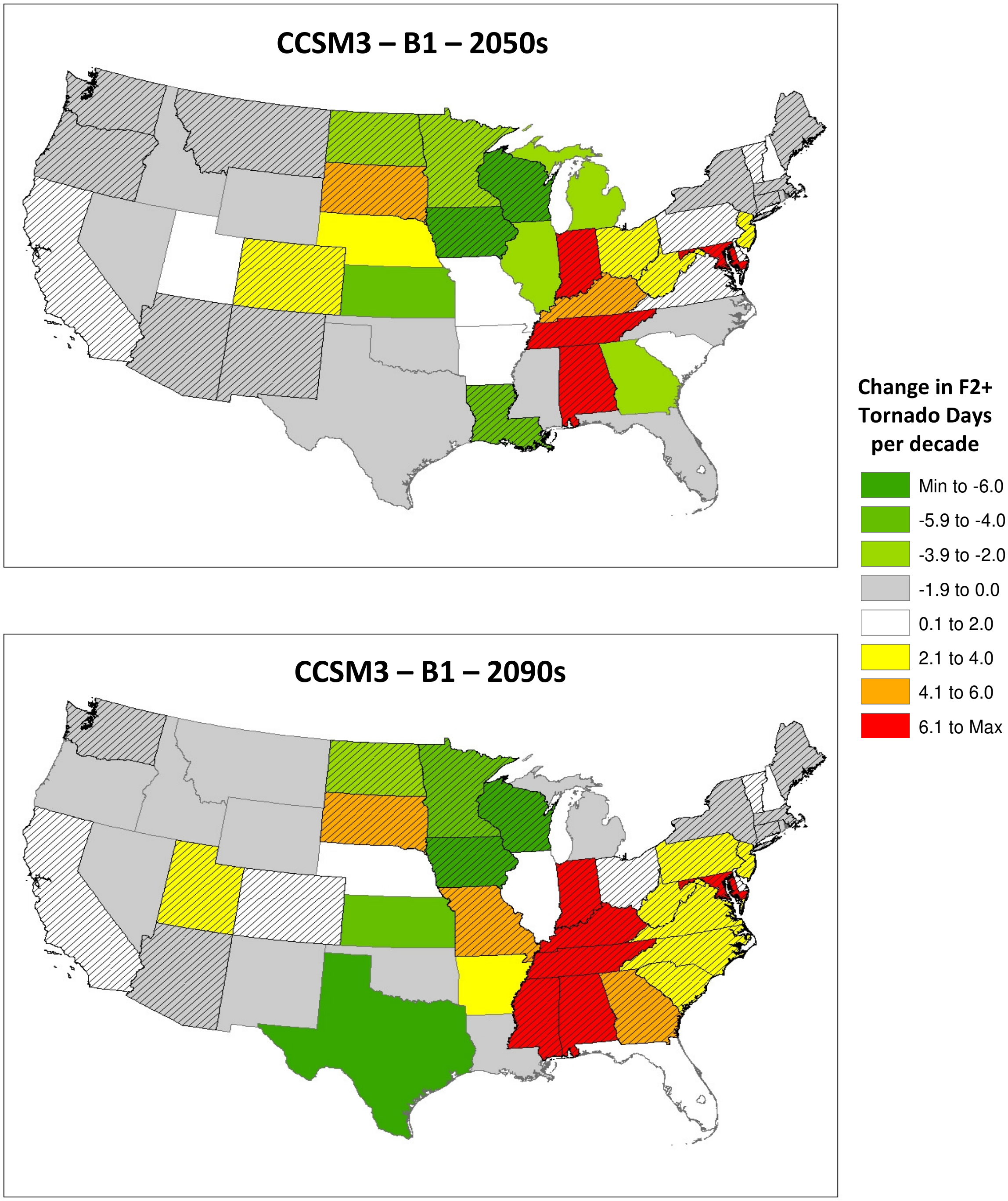


**Figure 29** – Total difference from GCM20c in F2+ tornado days per decade for CCSM3 – B1. Hatching indicates the difference in that state is significant at the 0.05 level.

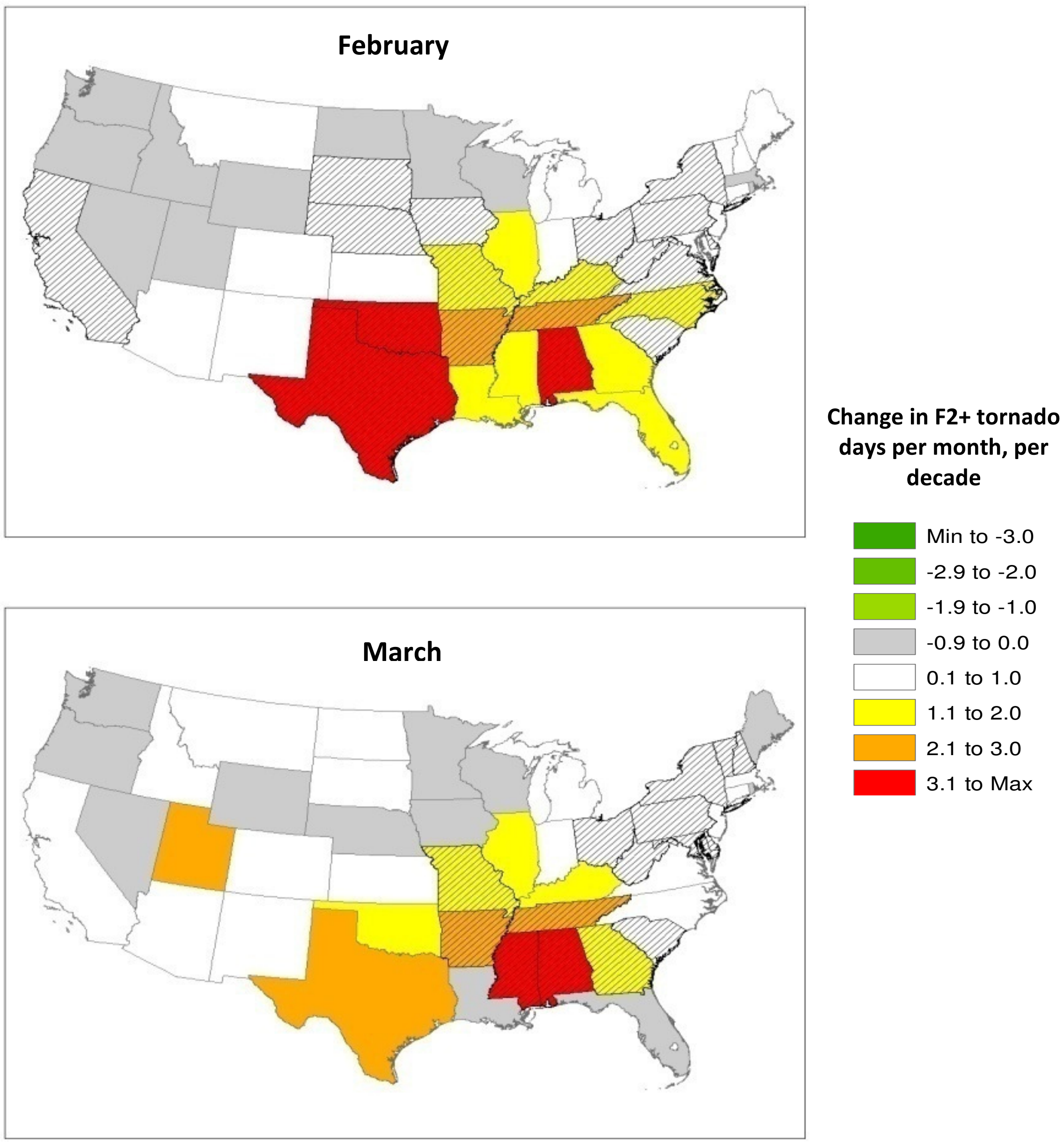


**Figure 30 –** Monthly difference of the 2090s from GCM20c in F2+ tornado days per decade (February – August) for the CCSM3 – B1 scenario. Hatching indicates the difference in that state is significant at the 0.05 level. Continued on the next page.

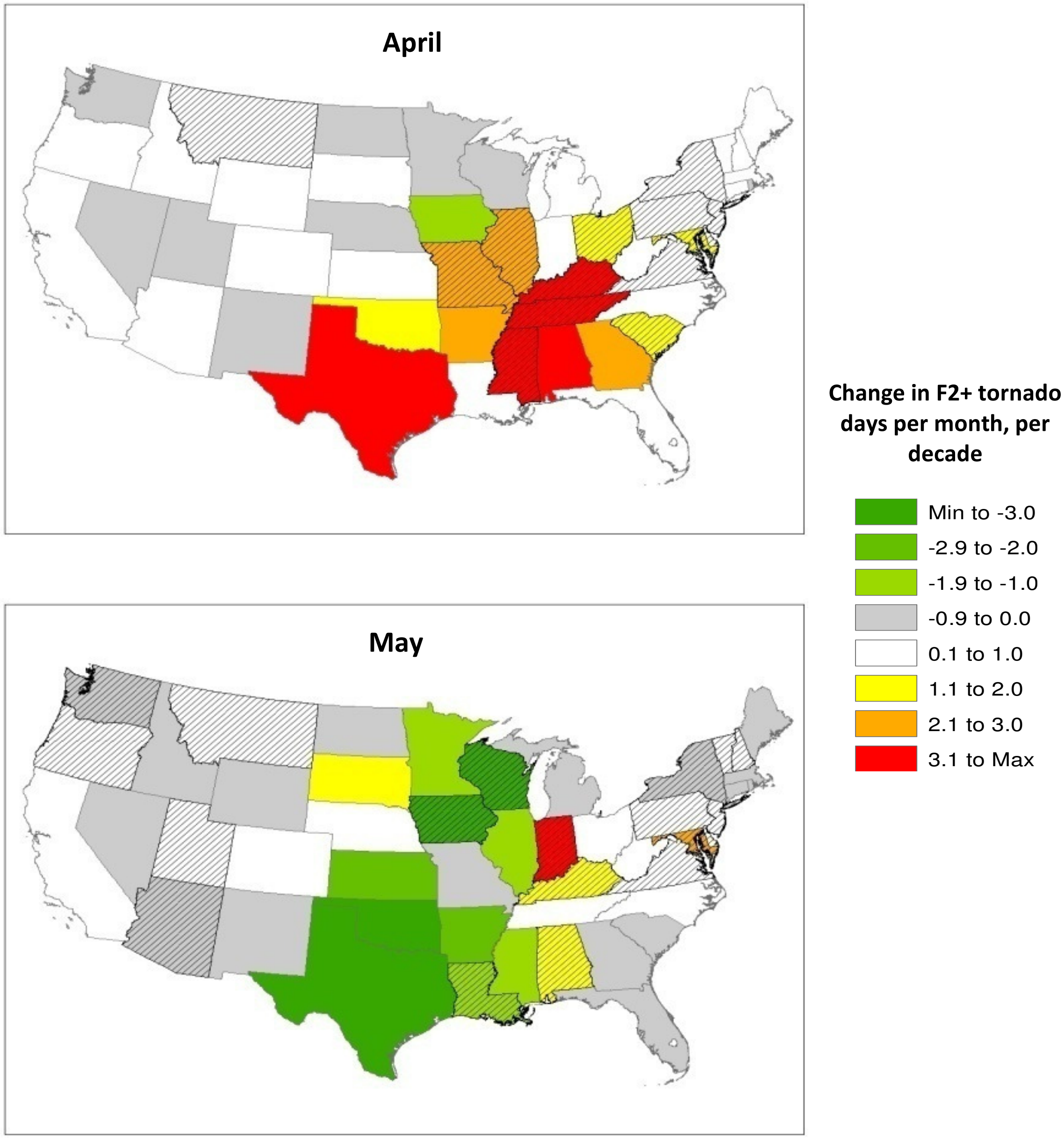


**Figure 30 (continued) –** Monthly difference of the 2090s from GCM20c in F2+ tornado days per decade (February – August) for the CCSM3 – B1 scenario. Hatching indicates the difference in that state is significant at the 0.05 level. Continued on the next page.

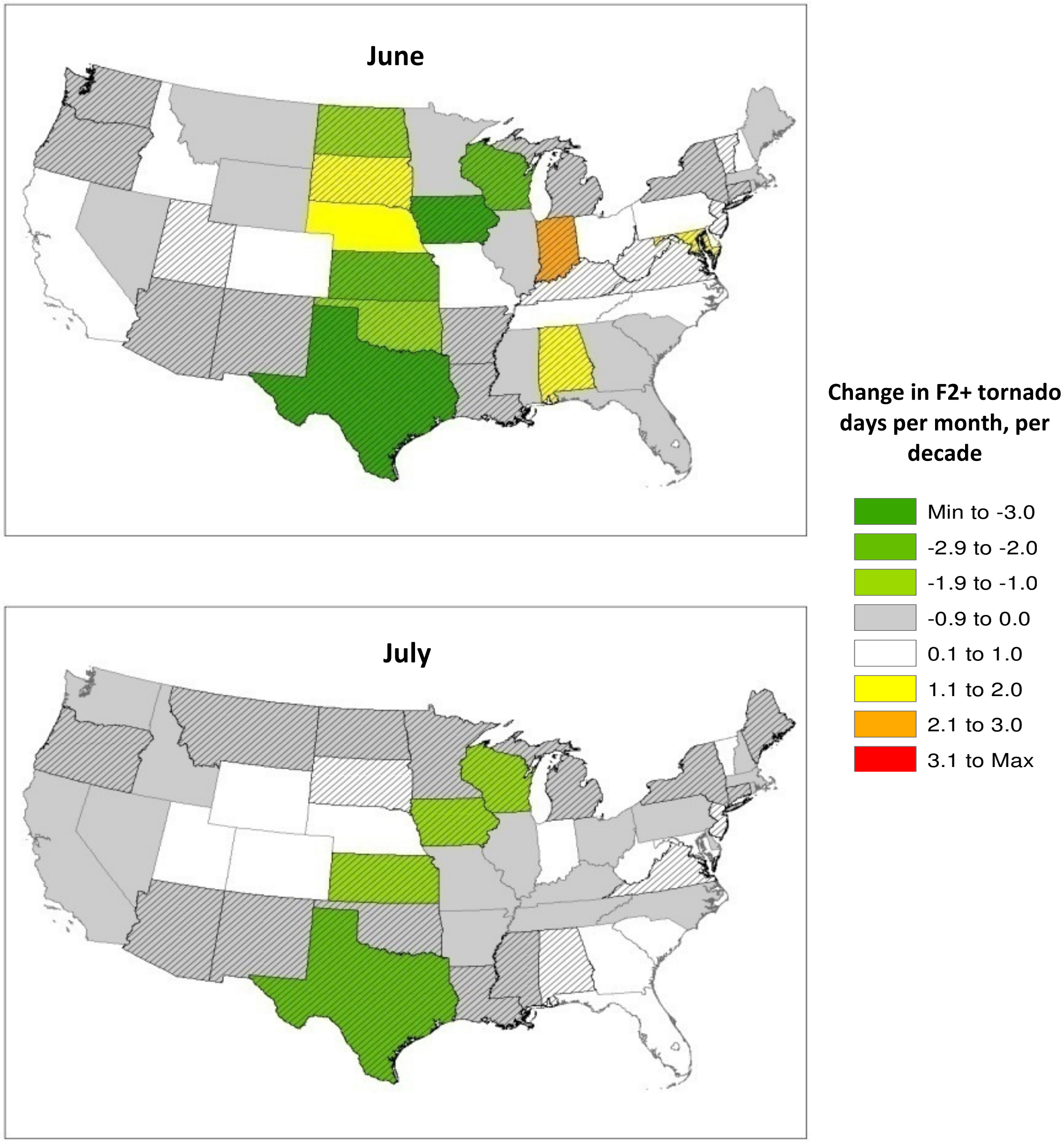


**Figure 30 (continued) –** Monthly difference of the 2090s from GCM20c in F2+ tornado days per decade (February – August) for the CCSM3 – B1 scenario. Hatching indicates the difference in that state is significant at the 0.05 level. Continued on the next page.

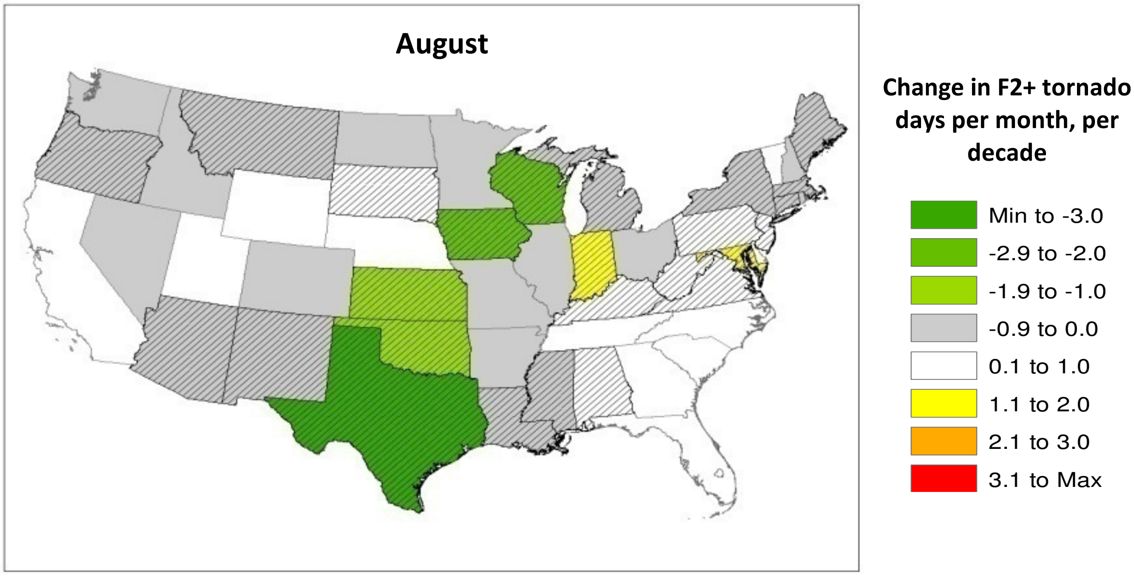


**Figure 30 (continued) –** Monthly difference of the 2090s from GCM20c in F2+ tornado days per decade (February – August) for the CCSM3 – B1 scenario. Hatching indicates the difference in that state is significant at the 0.05 level.

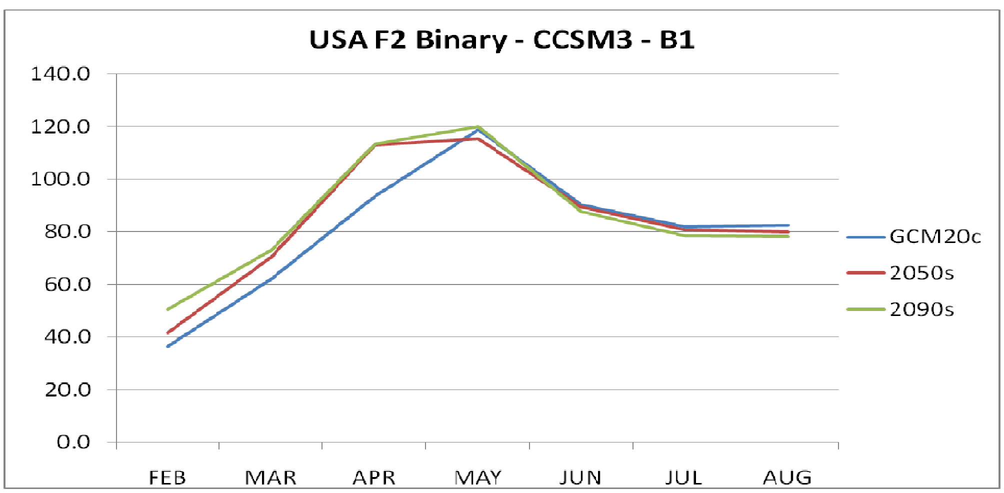


| | FEB | MAR | APR | MAY | JUN | JUL | AUG | TOT |
|---|---|---|---|---|---|---|---|---|
| **GCM20c** | 36.5 | 62.2 | 93.5 | 118.9 | 90.4 | 82.1 | 82.7 | 566.3 |
| **2050s** | 41.6 | 70.4 | 113.1 | 115.3 | 89.3 | 80.7 | 80.0 | 590.3 |
| **2090s** | 50.6 | 73.0 | 113.4 | 119.9 | 87.6 | 78.4 | 78.1 | 601.1 |

**Figure 31** – Change in seasonality of F2+ tornado days in the US as a whole from GCM20c to CCSM3 – B1. Table on the bottom represents the line graph at the top.

*4.6.4 – Future Tornado Days – CGCM3 – A2*

With the CGCM3 model, two SRES scenarios were available for this thesis, A2 and B1. Under the A2 scenario, the most drastic changes are noticed between the 2050s and the 2090s, as opposed to the 2050s and the GCM20c period. Over the US as a whole, in the 2050s a 3.8% increase in F2+ tornado days is projected – tied for the lowest of either decade, in any scenario, in either GCM – but by the 2090s, that increase has more than tripled to a 12.7% increase in tornado days over the US as whole – the most of any scenario, decade, or GCM (Table 7). Much like the CCSM3-B1, the Southeast and Lower Great Lakes states account for the majority of this nation-wide increase with a secondary area in the Central Plains (Figure 32). In the 2050s, Pennsylvania is projected to have the largest increase in tornado days in the decade, while bordering states (except New York), especially southward into the Southeastern US, are all projected to experience a significant increase as well, albeit less of one. Two Central Plains states are also projected to see substantial increases as well. By the 2090s, seven more states, and 12 total (spread between the Lower Great Lakes, Mid-Atlantic, and the Central Plains), are projected to experience a 6+ tornado day increase in the decade. Again, the Upper Great Lakes states and portions of the Southern Plains are projected to see the greatest decreases in tornado days.

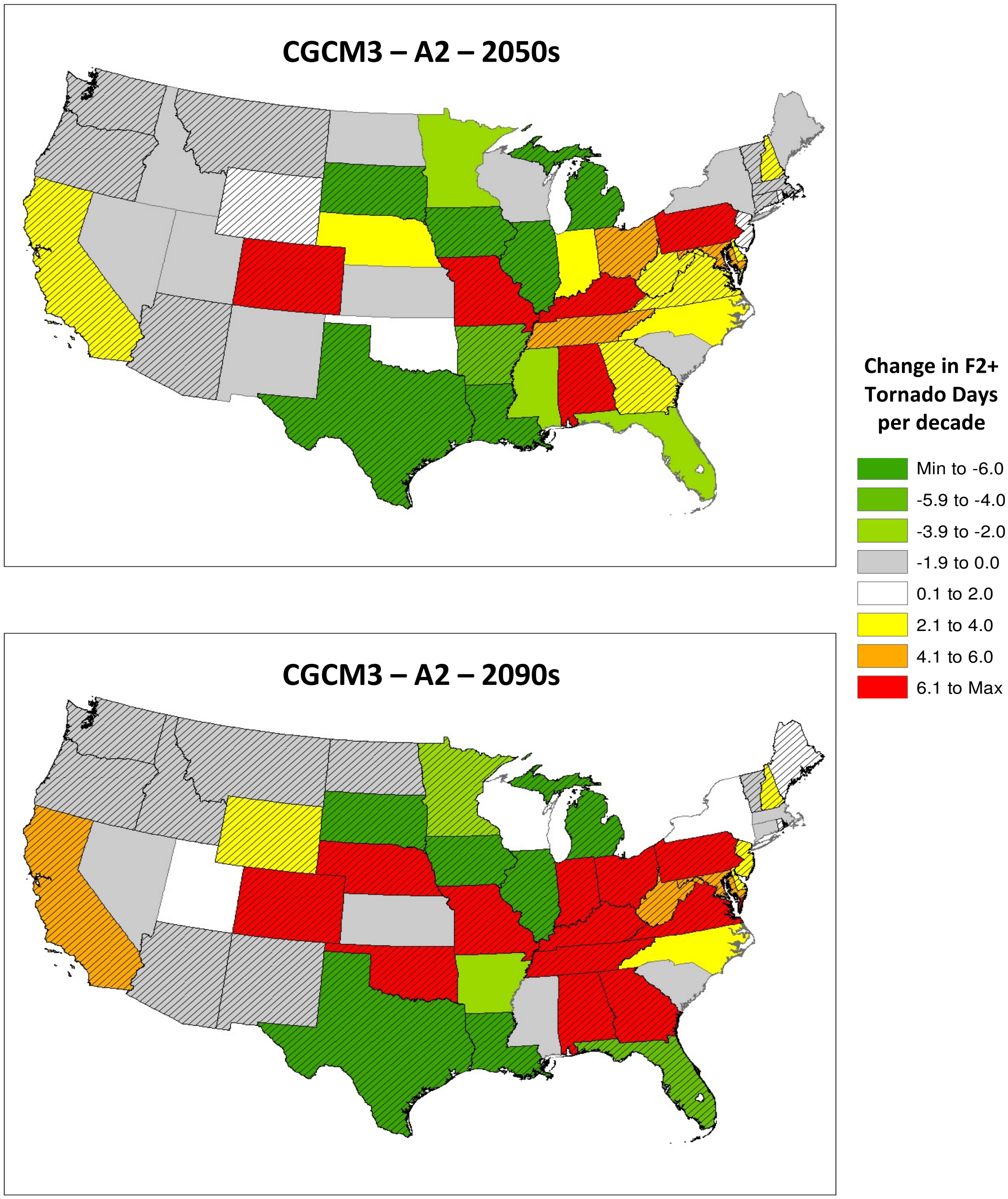


**Figure 32** – Total difference from GCM20c in F2+ tornado days per decade for CGCM3 – A2. Hatching indicates the difference in that state is significant at the 0.05 level.

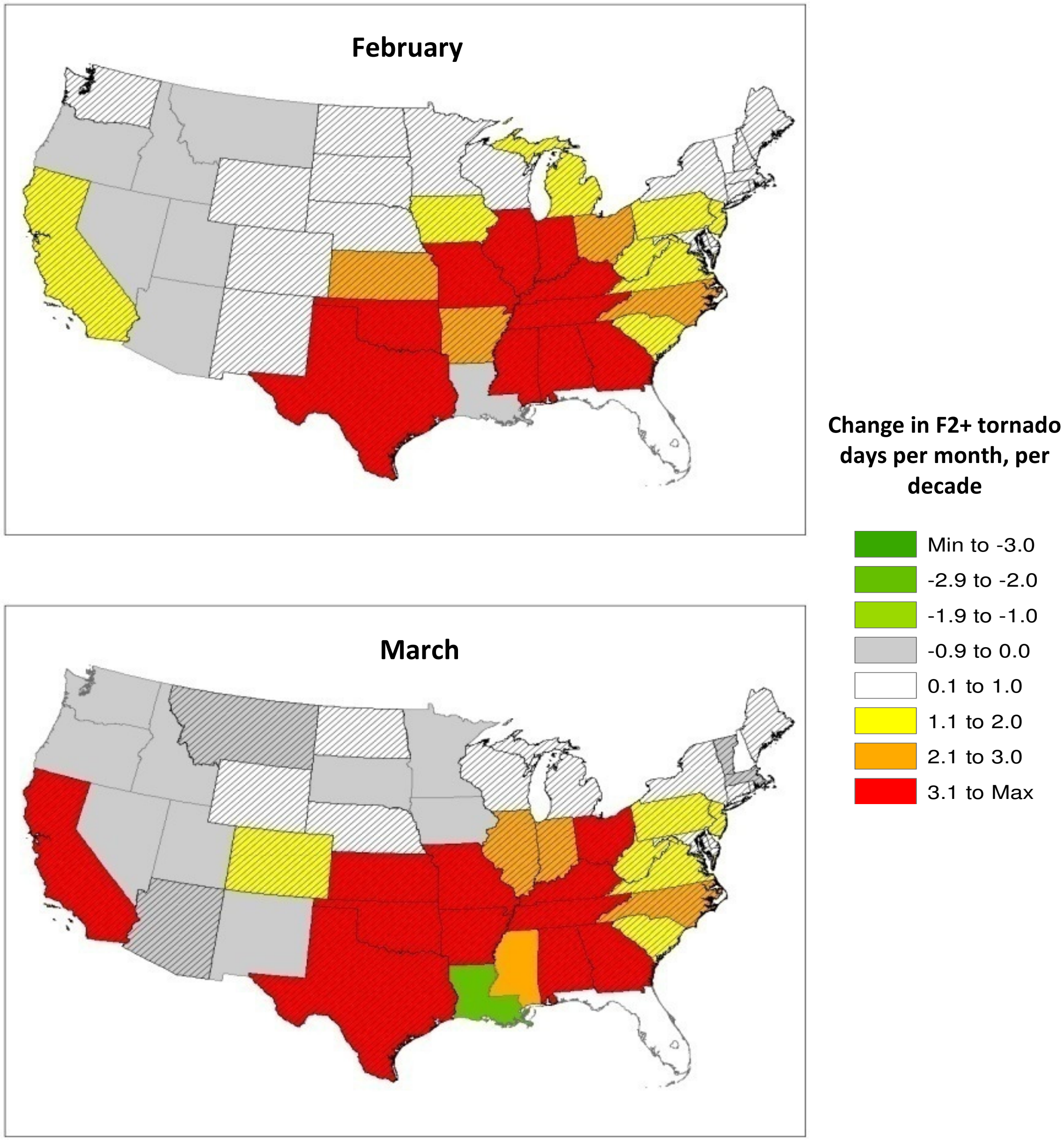


**Figure 33 –** Monthly difference of the 2090s from GCM20c in F2+ tornado days per decade (February – August) for the CGCM3 – A2 scenario. Hatching indicates the difference in that state is significant at the 0.05 level. Continued on the next page.

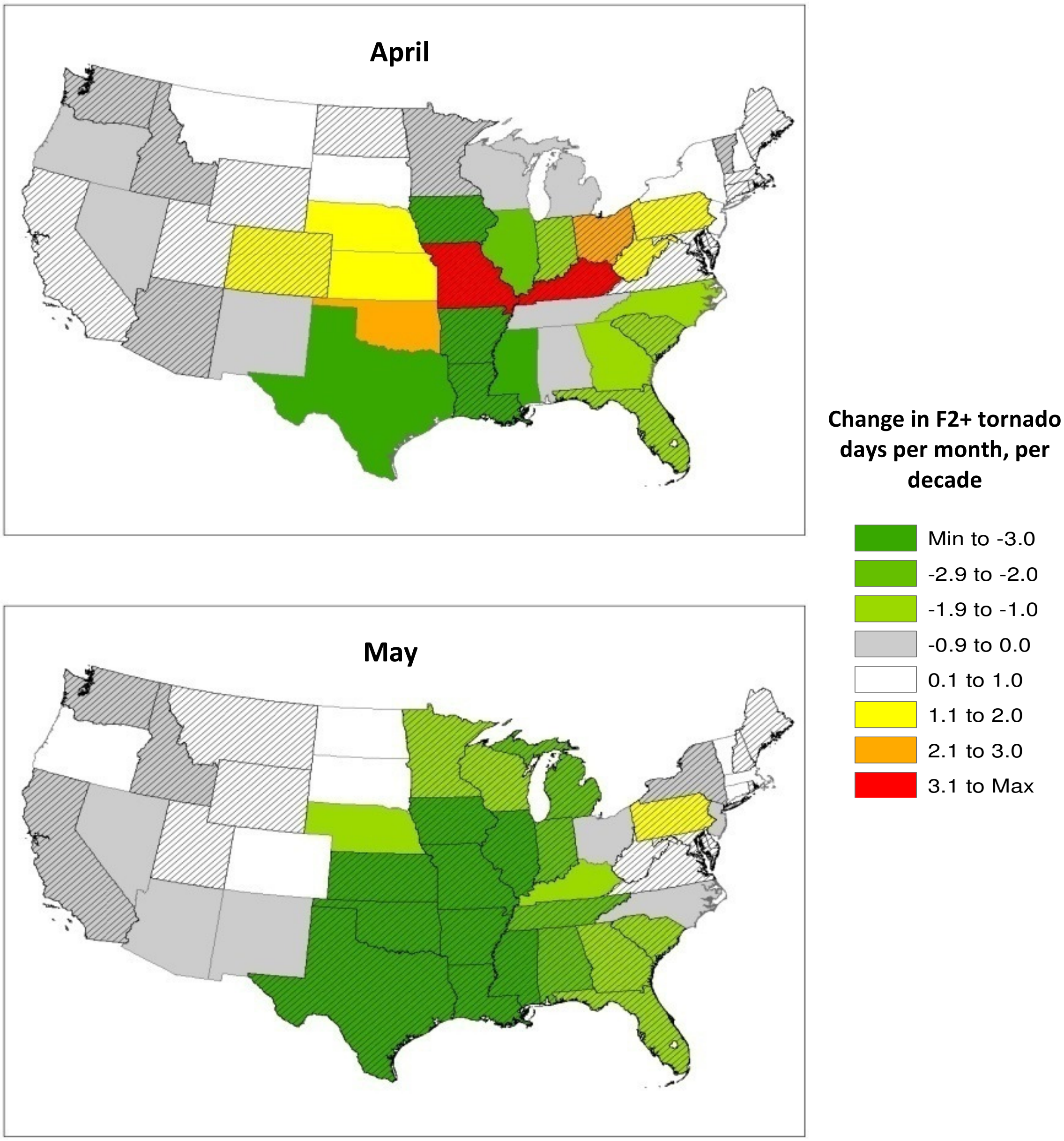


**Figure 33 (continued) –** Monthly difference of the 2090s from GCM20c in F2+ tornado days per decade (February – August) for the CGCM3 – A2 scenario. Hatching indicates the difference in that state is significant at the 0.05 level. Continued on the next page.

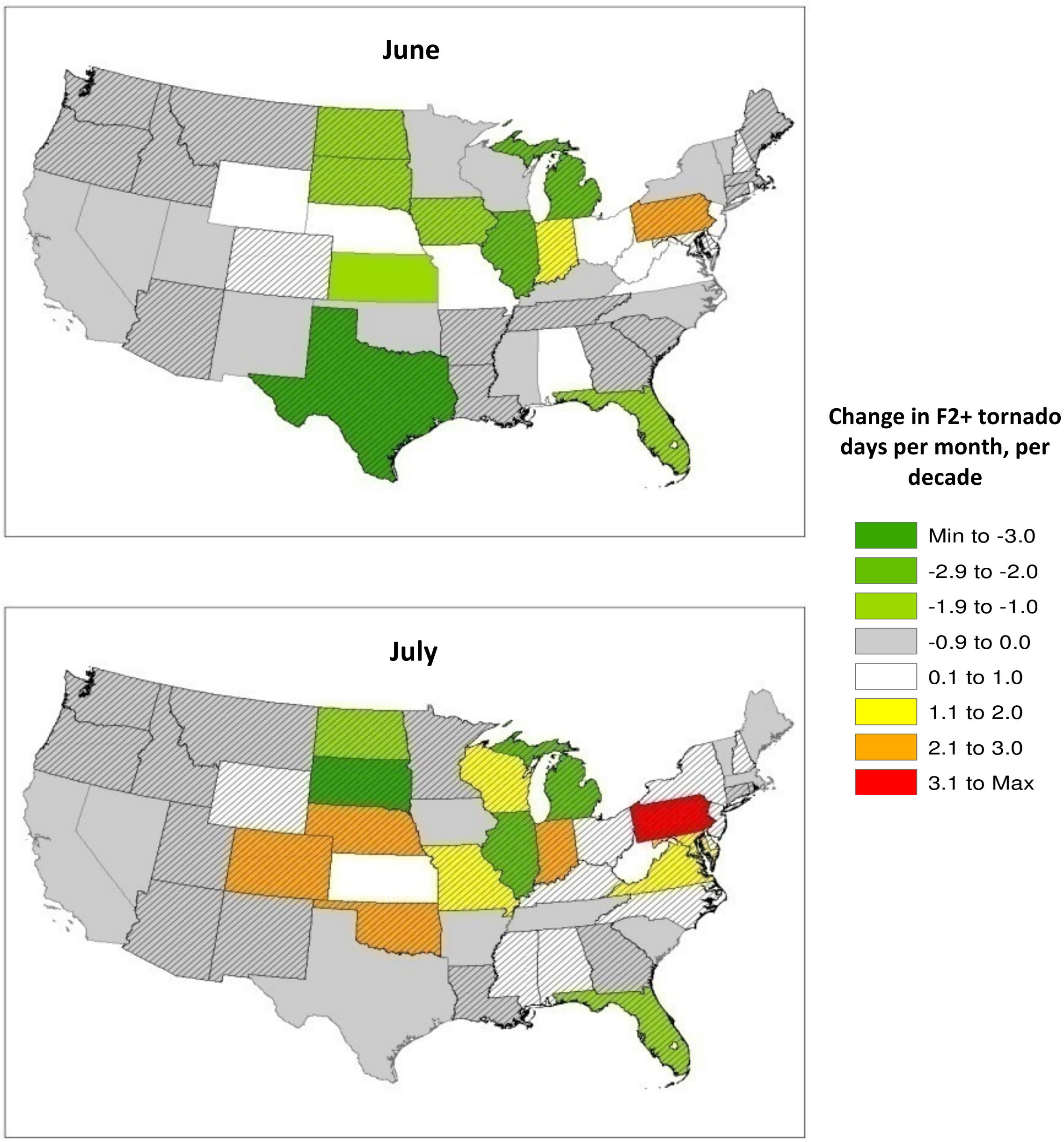


**Figure 33 (continued) –** Monthly difference of the 2090s from GCM20c in F2+ tornado days per decade (February – August) for the CGCM3 – A2 scenario. Hatching indicates the difference in that state is significant at the 0.05 level. Continued on the next page.

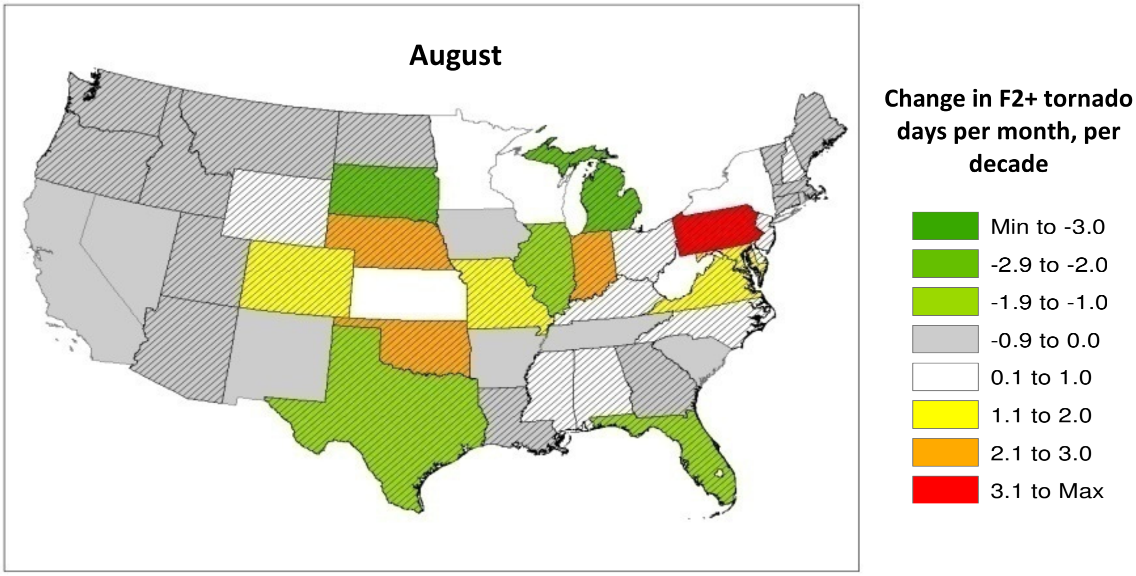


**Figure 33 (continued) –** Monthly difference of the 2090s from GCM20c in F2+ tornado days per decade (February – August) for the CGCM3 – A2 scenario. Hatching indicates the difference in that state is significant at the 0.05 level.

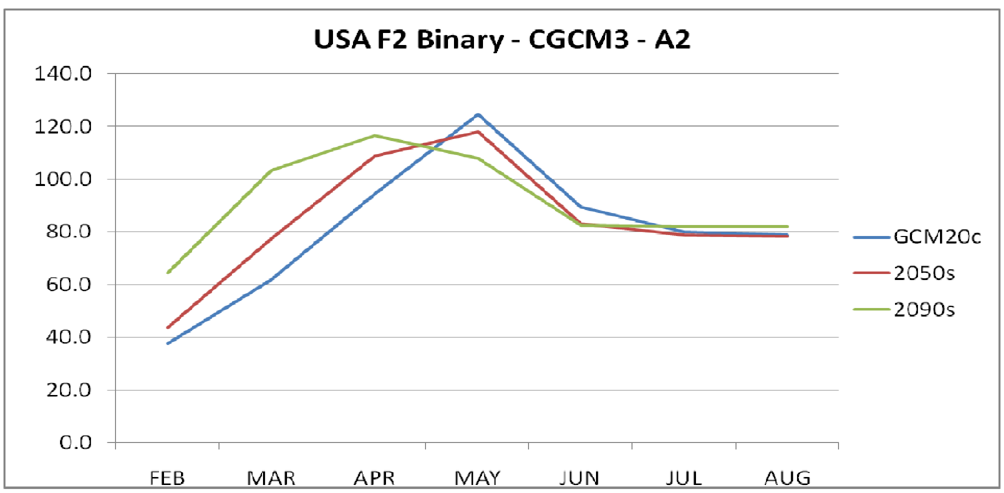


| | FEB | MAR | APR | MAY | JUN | JUL | AUG | TOT |
|---|---|---|---|---|---|---|---|---|
| **GCM20c** | 37.6 | 61.9 | 94.3 | 124.6 | 89.5 | 80.0 | 78.7 | 566.6 |
| **2050s** | 43.7 | 77.4 | 108.8 | 118.0 | 83.2 | 78.8 | 78.3 | 588.2 |
| **2090s** | 64.3 | 103.3 | 116.5 | 108.0 | 82.5 | 82.0 | 81.9 | 638.5 |

**Figure 34** – Change in seasonality of F2+ tornado days in the US as a whole from GCM20c to CGCM3 – A2. Table on the bottom represents the line graph at the top.

On a month-to-month basis over the US as a whole, March is projected to see the largest increase in tornado days in the 2050s at 24.9%, followed by February (at 16.2%) and April (at 15.4%; Table 7). This contrasts starkly to the 2090s, where a 70.8% increase of February tornado days is projected under the CGCM3 – A2 scenario, followed by a 66.9% increase in March and a 23.6% increase in April. These numbers have different effects on the seasonality of tornadoes depending on the decade. In the 2050s, peak tornado day occurrence remains in May, but broadens back into April as well, somewhat forming a two-month peak before tailing off in June (Figure 34). In the 2090s however, the peak broadens even further to three months – from March through May (with April at the apex). Tornado activity then tails off and becomes almost steady from June through August – which results in a monthly increase of 2.5% in July and 4.1% in August. Overall, this is a markedly earlier start to the peak tornado season in the US, and in comparison to other scenarios, a stronger finish as well.

In February, these increases in the 2090s are seen with significant results in nearly every Southern Plains, Southeast, Midwest, and Mid-Atlantic state (Figure 33). In March, each of these regions seems to intensify, with Oklahoma, Texas, Missouri, Kentucky, Tennessee, Alabama and Georgia all projected to have increases of at least five tornado days per decade in the month. By April, most of the aforementioned states begin to offset their increases, with the exception of Missouri and Kentucky. Much of the south and Southeast begin seeing decreases continuing into May and June. The 2.5% July increase is manifested most noticeably in the Central Plains (with the exception of Kansas) and around Pennsylvania. The maps of these two regions look nearly identical from July into August.

### *4.6.5 – Future Tornado Days – CGCM3 – B1*

Throughout the US as a whole under the B1 scenario for CGCM, F2+ tornado days are projected to increase 6.1% over the GCM20c average per decade by the 2050s, but only increase 3.8% by the 2090s (Table 7). This decrease in tornado days from the 2050s to the 2090s is in contrast to every other scenario in either model, where the total increase continues through the 2090s. The 6.1% increase is sharper than the increase of the other CGCM scenario's 2050s projections. Regionally, the areas of greatest increase are similar to those in the other CGCM scenario – the Lower Great Lakes states south into the Mid-Atlantic and Southeast, and a second area in the Central Plains (Figure 35). Interestingly, two high profile tornado states (Oklahoma and Kansas) in the Central Plains do not have *significant* differences from GCM20c averages, though each is projected to have an increase in tornado days in both decades. The main difference between the 2050s and the 2090s choropleths are the darker greens in Iowa, Illinois and Michigan (signifying greater decreases in tornado days), and a lessened increase in activity in Ohio and Missouri. These overall decreases likely offset the increases between the future decades in some Central Plains states.

Monthly, the 2050s under the B1 scenario is more like the 2090s in most other scenarios. February of the 2050s sees the largest increase throughout the US as a whole, up 29.7% from GCM20c numbers (Table 7). April follows with a 19.9% increase and then March at an 8.3% increase. Unlike any other scenario in the 2050s, CGCM3 – B1 projects increased tornado activity in May as well – up 1.1%. August also sees an increase of 3.7%, leaving June and July as the only months in the 2050s with an overall decrease in tornado activity. By the 2090s, March becomes the month with the largest increase in tornado activity (at 25.3%) but followed closely by April (at 21.0%). May and June see decreased activity, while July and August see the slightest decrease in tornado days in the 2090s of this scenario – both less than 2%. The 2050s and 2090s are projected to have similar seasonalities in tornado day occurrence with the peak broadening to two months (April and May) in each decade, and the season starting a bit sooner in the year before tapering off from June through August (Figure 37).

Geographically, on a month-by-month basis for CGCM – B1 in the 2090s, February, March and April see the largest increases, with the Southeast being highlighted in February, with a shift of focus to the Central Plains, Midwest, and Mid-Atlantic states in March and April (Figure 36). Noteworthy is the lack of significant differences in these months, including some states with large differences between the 2090s and the

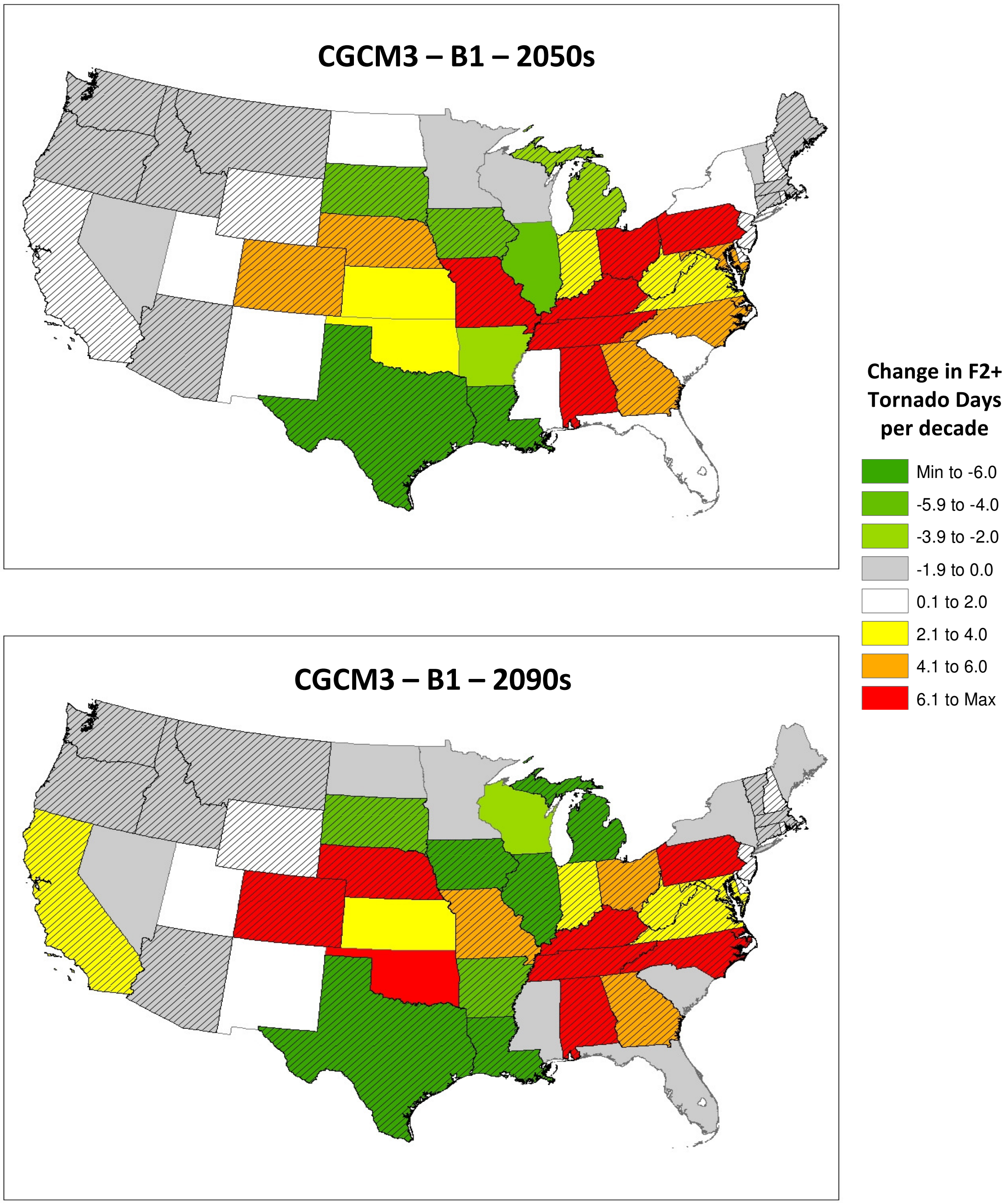


**Figure 35** – Total difference from GCM20c in F2+ tornado days per decade for CGCM3 – B1. Hatching indicates the difference in that state is significant at the 0.05 level.

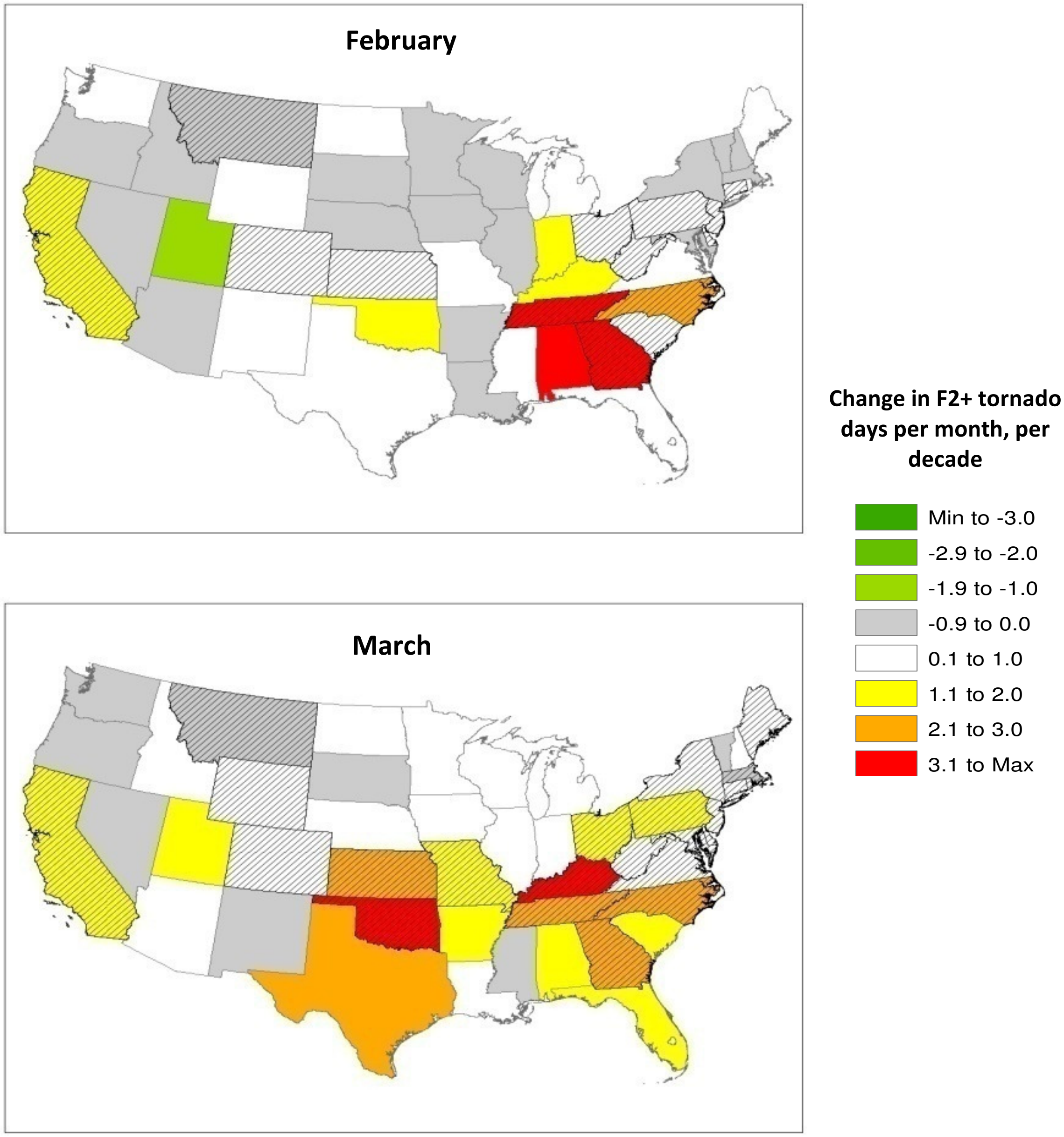


**Figure 36 –** Monthly difference of the 2090s from GCM20c in F2+ tornado days per decade (February – August) for the CGCM3 – B1 scenario. Hatching indicates the difference in that state is significant at the 0.05 level. Continued on the next page.

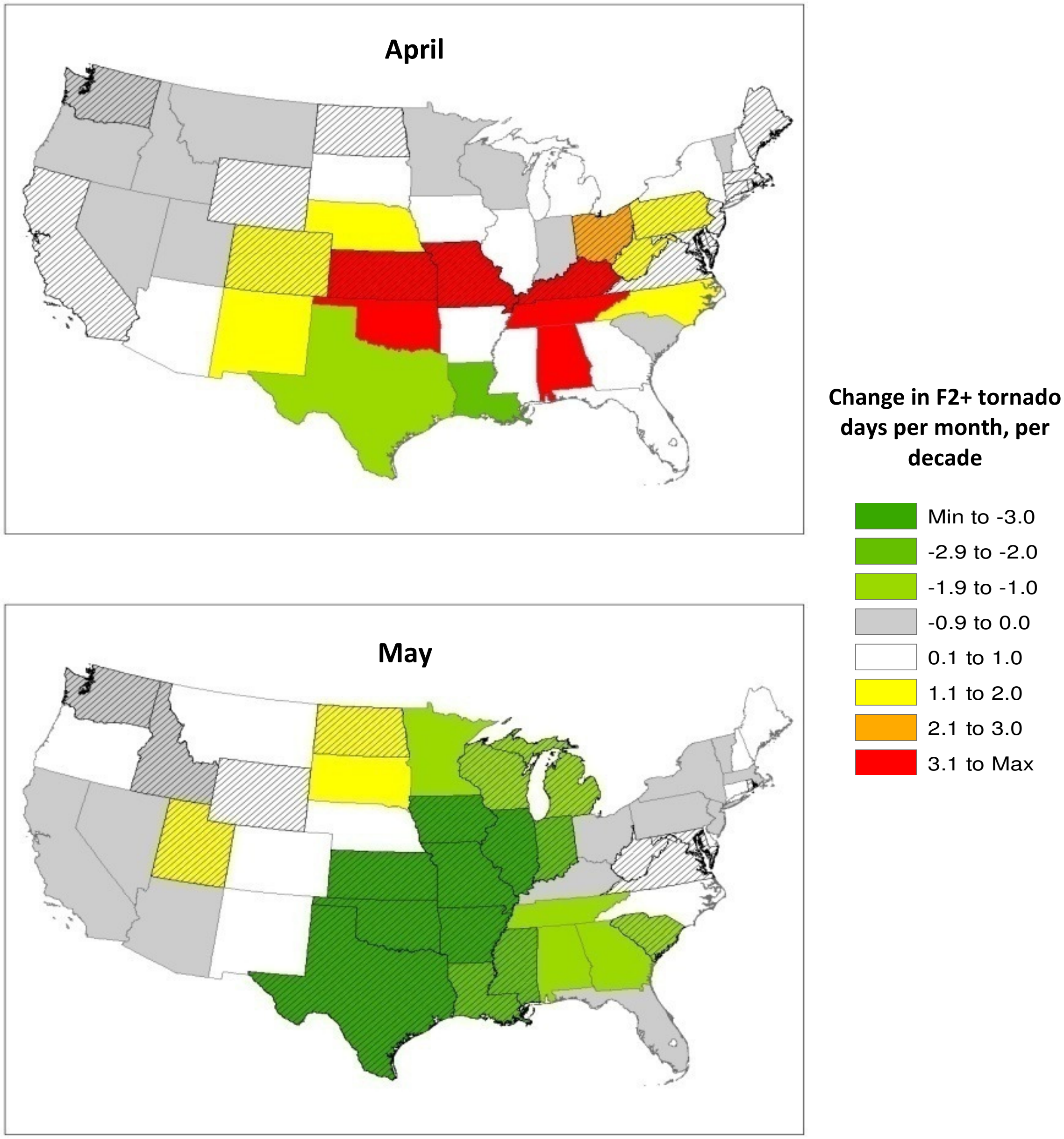


**Figure 36 (continued) –** Monthly difference of the 2090s from GCM20c in F2+ tornado days per decade (February – August) for the CGCM3 – B1 scenario. Hatching indicates the difference in that state is significant at the 0.05 level. Continued on the next page.

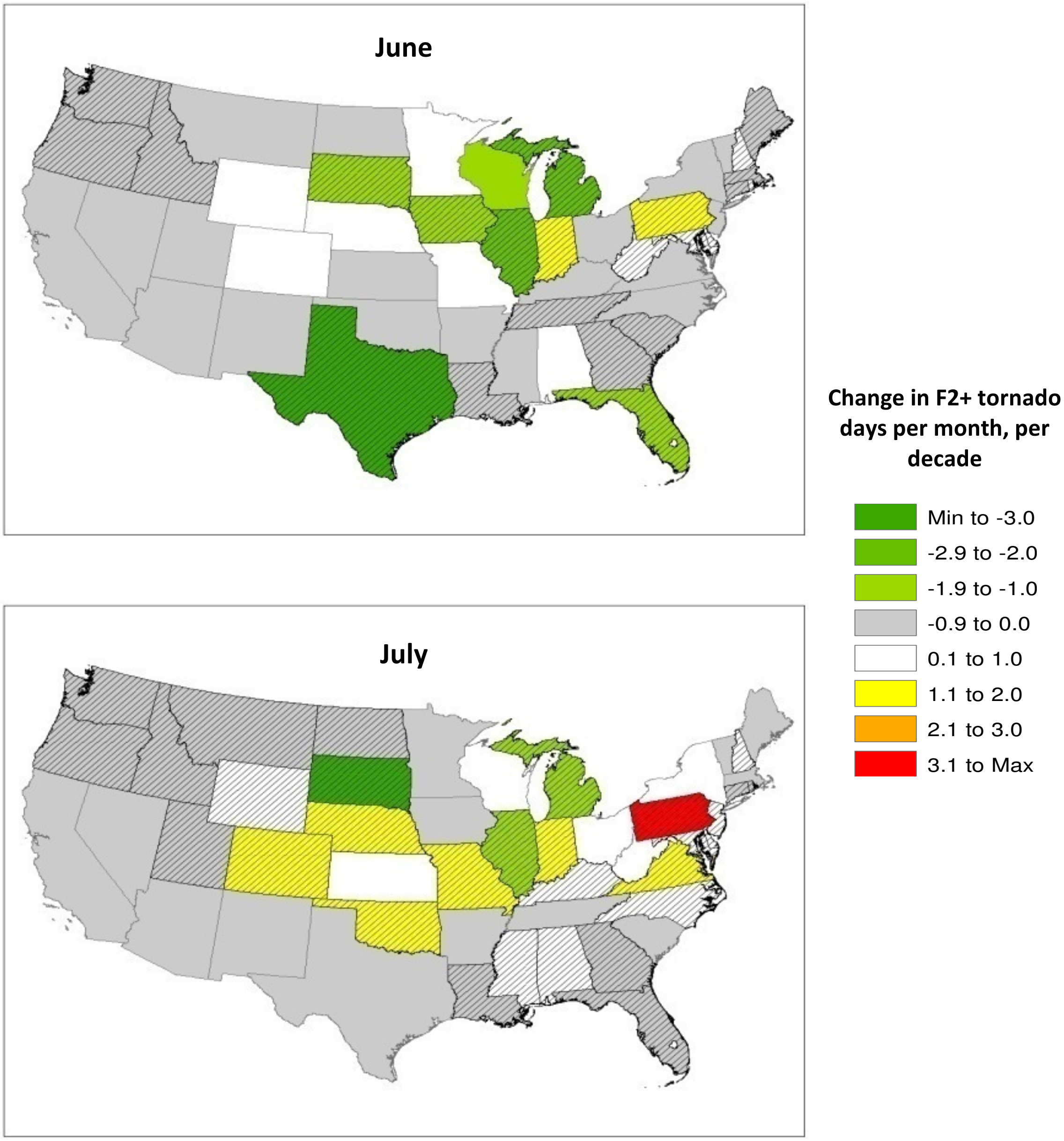


**Figure 36 (continued) –** Monthly difference of the 2090s from GCM20c in F2+ tornado days per decade (February – August) for the CGCM3 – B1 scenario. Hatching indicates the difference in that state is significant at the 0.05 level. Continued on the next page.

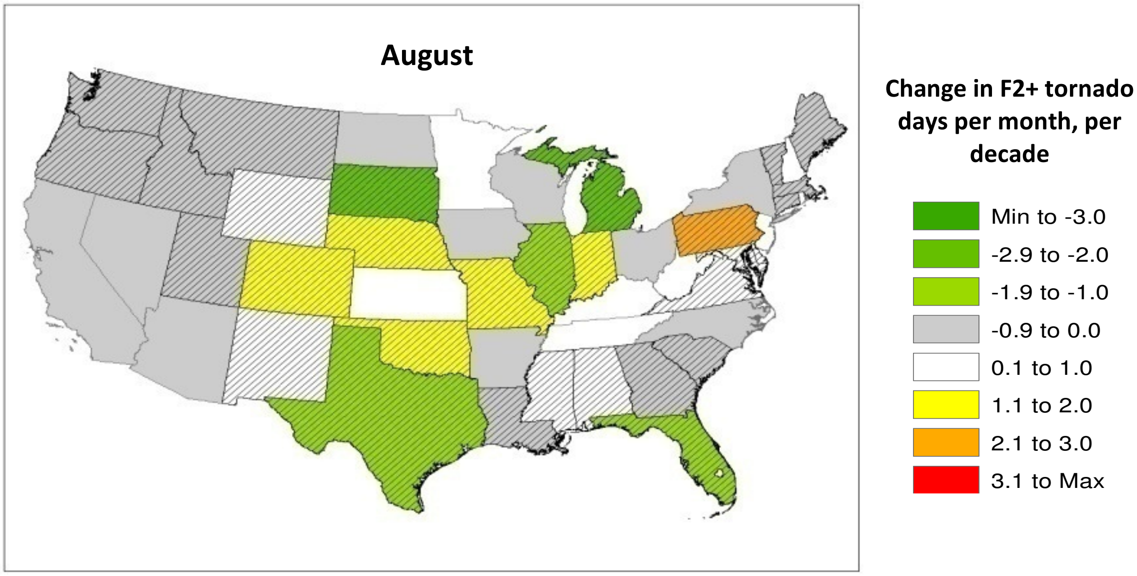


**Figure 36 (continued) –** Monthly difference of the 2090s from GCM20c in F2+ tornado days per decade (February – August) for the CGCM3 – B1 scenario. Hatching indicates the difference in that state is significant at the 0.05 level.

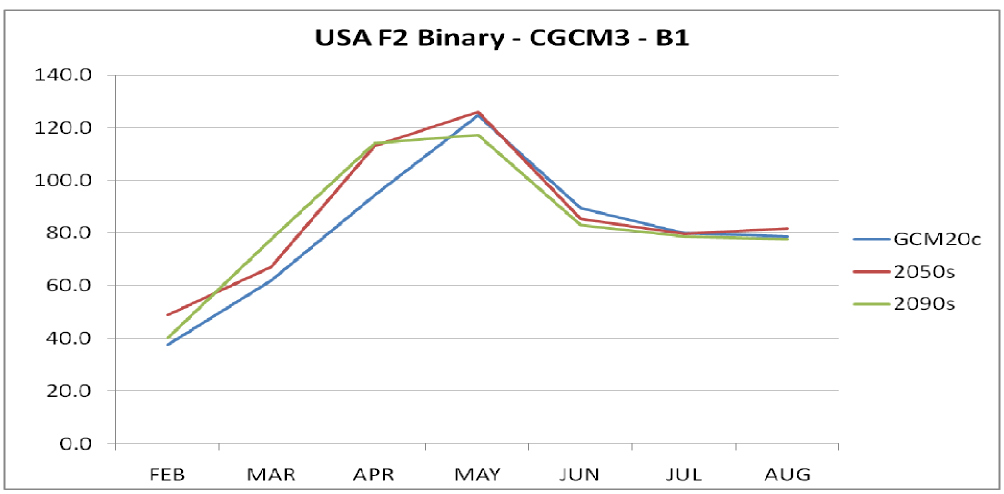


| | FEB | MAR | APR | MAY | JUN | JUL | AUG | TOT |
|---|---|---|---|---|---|---|---|---|
| **GCM20c** | 37.6 | 61.9 | 94.3 | 124.6 | 89.5 | 80.0 | 78.7 | 566.6 |
| **2050s** | 48.8 | 67.1 | 113.0 | 125.9 | 85.3 | 79.7 | 81.6 | 601.4 |
| **2090s** | 40.0 | 77.6 | 114.1 | 117.3 | 83.1 | 78.7 | 77.6 | 588.3 |

**Figure 37** – Change in seasonality of F2+ tornado days in the US as a whole from GCM20c to CGCM3 – B1. Table on the bottom represents the line graph at the top.

GCM20c period (i.e. most of the Southeast in all three months and Oklahoma in April). A large swath of significantly decreased activity is projected for May from the Upper Great Lakes southwest into Texas. June sees a decrease in the Upper Great Lakes and some of the Northern Plains states under this scenario, while the Central Plains states begin to show an increase in F2+ tornado days again in July and August, as well as Pennsylvania and Indiana.

# CHAPTER 5

# DISCUSSION

The discussion chapter of this thesis is divided into three sections. The first section will summarize the CCSM3 results from the previous chapter, and discuss the reasons these results might have occurred. The second section will discuss how both the results and the methods fit into the larger body of literature on both synoptic climatology and on climate change impacts on severe weather. The final section of this chapter will discuss the limitations and shortcomings of the research.

## *5.1 – Merging and Analyzing the Results*

Most of the scenarios in both GCMs produce similar overall results which supports the robustness of the methodology. Firstly, under any scenario, throughout the US as a whole, there is a projected increase in F2+ tornado days – anywhere from 3.8% to 12.7% depending on the scenario and/or GCM used (Table 8). Additionally, with the exception of CGCM – B1, the 2090s show a larger increase in tornado days when compared to GCM20c than the 2050s in the same scenario. Furthermore, in the CCSM3 GCM, both of the 'less environmentally-friendly' scenarios (A1FI and A2) generally show greater increases in tornado frequency than the ‘more environmentally-friendly’ scenario (B1). As documented in previous research (IPCC, 2007b; Sheridan and Lee, 2010), this trend towards future extreme events happening more frequently further into the future, and more frequently with the higher emissions scenarios, has been shown to occur in other synoptic research on such hazards (Cheng et al., 2007a, 2007b; Hope, 2006).

Another main conclusion that can be drawn from the results is that the bulk of the increase will be manifested in the early part of the tornado season, with substantial increases in February, March and April. Temporally, over a longer time frame, greater increases in February are projected for the 2090s than are for the 2050s. This suggests that the F2+ tornado season would start progressively earlier in the year.

Although some variance did occur between scenarios and models used, another important conclusion that can be drawn from these results is that, in addition to the shifting of the tornado season, a broadening of the peak of the tornado season is noticed as well. In some scenarios, the peak of the season occurs over a two month period; while in other scenarios, a three month peak is noticed. Coupled with this broadening, most future scenarios project a shift in the peak of the season back into April (from May in the GCM20c).

**Table 8** – Summary of changes in F2+ tornado days by GCM and scenario.

| GCM | Scenario | Geographic Impacts | Seasonality Impacts | Percent Change in US from 20th Century | |
|---|---|---|---|---|---|
| | | | | 2050s | 2090s |
| CCSM3 | A1FI - Highest Emissions | Increased tornado activity in Northern Plains and Lower Great Lakes Region; Kentucky, Tennessee and Alabama. Decreases in Upper Great Lakes southwest through Southern Plains. Stronger increases in the 2090s than the 2050s | Shift in the peak tornado season over the US as a whole from May back to April in both 2050s and 2090s. In the 2090s, a broadening of the peak of the tornado season from a one month peak in the 20th Century, to a three month peak from March through May | 7.6% | 12.6% |
| CCSM3 | A2 - Middle of the Road | Increased tornado activity in Northern Plains centered around South Dakota and Nebraska; and in Lower Great Lakes Region, Kentucky, Tennessee, and Alabama. Decreases in the Upper Great Lakes southwest through Southern Plains. Stronger changes in the 2090s than the 2050s, but not as intense as A1FI | Shift in the peak tornado season over the US as a whole from May back to April in both the 2050s and 2090s. Slight broadening of the peak of the tornado season to a two-month peak from April through May. | 7.0% | 10.2% |
| CCSM3 | B1 - Low Emissions | Increases in the 2050s, focused on the Central Plains and Lower Great Lakes. By the 2090s, Central Plains increase mostly disappears, while a new area of increased activity develops in the Southeast. Decreased activity in the Upper Great Lakes region in both decades | Peak month remains May in both future decades, but the peak broadens to a two month long peak from April through May | 4.2% | 6.1% |
| | | | | | |
| CGCM3 | A2 - Middle of the Road | Increased tornado activity in the Lower Great Lakes, extending into the Southeast; and a secondary increase in the Central Plains states. Decreased activity in the Upper Great Lakes states and in Texas, Louisiana and Arkansas. Very strong increases from 2050s to 2090s | In the 2050s, the peak tornado season remains May, but expands back into April - almost forming a two-month peak. By the 2090s, the peak has completely shifted back to April, and expanded to a three month peak from March through May | 3.8% | 12.7% |
| CGCM3 | B1 - Low Emissions | Increases in tornado activity in the Central Plains, Lower Great Lakes and Southeast states in the 2050s. The increase is greater into the 2090s, especially in the Central Plains, but significant areas of decreased activity in Upper Great Lakes, Texas, Louisiana and Arkansas are also amplified | Peak seasonality remains in May in both future decades, however, it does expand back into April to create a two month peak. | 6.1% | 3.8% |

Due to the method used, these general conclusions on the changes in frequency and seasonality of tornadoes in future climate scenarios are due entirely to the changes in the frequency and seasonality of the synoptic patterns. The overall increase in tornado activity throughout the US as a whole is likely due to the increase in the frequency of just a few of the tornado favorable patterns at each level. At 500z, the Spring Shortwave Trough pattern (E500) in the CCSM3 GCM substantially increases during the TSeason under every future scenario, bringing an increase in tornado days to some Southeastern and Appalachian Mountain states. At 700z, however, it was a combination of patterns that helped raise the frequency of tornadoes – the increase in the Tight Spring Zonal pattern (A700) helped spur the increase of tornado days in the A1FI and A2 scenarios – especially in Kentucky and Tennessee; the Deep High Plains Trough (C700) accounted for tornado day increases in the Southeast and Mid-Atlantic regions under the B1 scenario; and the Summer Plains Zonal pattern (E700) increases substantially in all three scenarios used, although the association to tornadoes under this pattern is not as evident as the other two 700z patterns. With the 850mb temperatures, the autumn Great Lakes Cold Front pattern (A850) increased under the A1FI and A2 scenario – accounting for an associated increase in tornado days in some of the Lower Great Lakes states, while the Southwest Thermal Ridge pattern (B850) increased under all three scenarios, which could account for some of the tornado day increase in some Central Plains states. Furthermore, the increases in frequency of these patterns are greater in the 2090s than they are in the 2050s, and there are more patterns that are increasing in frequency under the A1FI and A2 scenarios than there are under the B1 scenario. These two observations help explain the reasoning behind the increases in tornado activity being greater in the 2090s than in the 2050s, and why the A1FI and A2 scenarios have the greater increases in tornado days than the B1 scenario over the US as whole.

Many of these same synoptic patterns are also responsible for the shifting and broadening of the tornado season as well. Pattern E500 sees a substantial shift backwards one month (from May to April) under the A1FI and A2 scenarios in the 2050s. However, by the 2090s, the shift in these two scenarios has broadened to include more occurrences in February and March, while the pattern becomes much more frequent in April under the B1 scenario. At the 700mb level, pattern E is responsible for the majority of the shift and broadening of the tornado day seasonality in all scenarios – occurring much more frequently in every month of the TSeason. This is most noticeable in the A1FI and A2 scenarios, in the 2090s, and in February, March and April. Pattern B850 is most likely responsible for the changes in tornado seasonality among all the 850t patterns. Although more pronounced in the 2090s, in both future decades analyzed, the seasonality of B850 shifts back a month and broadens from its GCM20c seasonality.

In a geographic sense, a major conclusion that can be drawn from the results is that parts of the eastern Mid-Atlantic and Lower Great Lakes states are projected to be at the greatest risk for *increased* tornado activity. These states appear to be at the greatest risk for an increased number of F2+ tornado days, no matter which scenario is used in either GCM. Another main area for concern is the Central High Plains states – which, in most scenarios, in either decade, are also projected to see an increase in F2+ tornado days. Under some scenarios the Southeast is also projected to experience a significant increase in tornado days as well. The consensus area – among the scenarios used – of *decreased* tornado activity appears to be the Upper Great Lakes states, and parts of the Southern Plains (mainly Texas, Louisiana and Arkansas).

Other than the Southeast under the B1 scenario, most of the other geographic regions of projected future tornado day increases are difficult to interpret in regards to their association to the changes in synoptic patterns. In the 2090s, under the CCSM3 – B1 scenario, the southeastern US is projected to have several states with significant increases in tornado activity, and this is most likely due to the increase in frequency of pattern C700 and pattern D850 in February and March in the 2090s under the B1 scenario. In April and May, E500 is the likely pattern influencing the tornado day increase in the Southeast under the B1 scenario.

Although other *entire regions* have less consistent results, the projected changes for some *individual states* are more understandable. For example, under the A1FI and A2 scenarios in the 2090s, Kentucky and Tennessee both show an increase in tornado activity – likely due to the increased frequency of pattern A700, especially in March and

April, and an increase in pattern E500 as well. South Dakota is projected to have a significant increase in tornado days in the 2090s under the A1FI and A2 scenarios, and this is likely due to the increase in frequency of pattern E700. Indiana has an increase across all scenarios, which is most likely due to the increase in the frequency of pattern E500, and A850 in the 2090s. Under the A1FI and A2 scenarios in the 2090s, Ohio is expected to have a significant increase in tornado days due in large part to the increased frequency of pattern A850 throughout the TSeason. In the Northern High Plains region, Nebraska and Colorado are projected to have increased tornado activity in the 2090s under the A1FI and A2 scenarios, which corresponds to dramatic increases in the frequency of pattern B850 from February through May.

The regions showing overall decreases in tornado day activity in the future – the Upper Great Lakes states southwest into the Southern Plains – are more easily understood than the regions of increases. Most of the patterns that are favorable for tornado days in these areas decrease in overall frequency into the 2050s and 2090s. At the 500mb level, both the Rocky Mountain Trough (A500) and the Summer Weak Plains Trough (D500) decline substantially in the A1FI and A2 scenarios. While this decline is also present in the B1 scenario of both patterns, it is not nearly as sharp – thus, these states are not projected to have as much of a decrease in tornado days in the lower-emissions scenario. At the 700z level, the Autumn Northern Trough pattern (F700) decreases drastically as well in the 2050s and more so in the 2090s under the A1FI and A2 scenarios, as does the Baja Trough pattern (B700), which is favorable for tornadoes in Kansas, Missouri, Iowa and Texas. At the 850mb level, the sharp decline in the Spring Weak Plains Frontal pattern (G850) is the likely culprit for decreased activity in these regions, especially in the 2090s under the A1FI and A2 scenarios.

While the aforementioned patterns are responsible for the shifts in frequency and seasonality of tornadoes in certain states, no single individual pattern corresponds to above normal tornado activity in an entire region that is projected to have tornado day increases in future scenarios. The likely reasoning behind this difficulty in explaining the regional results is that in the 20th Century results (section 4.2), the states that have only a very slight above-normal tornado association to some patterns do not stand out on the map. However, if the future frequency of these patterns increases substantially from their 20th Century frequency, then these slight percentages essentially get multiplied (in the 2050s and 2090s) to the point of becoming a substantial increase in total tornado days as well.

A trend is also noticed in regards to the behavior of individual patterns as time progresses into the future. The patterns representing warmer weather, and thus happening most often in the summer, are the same patterns that show a marked increase in frequency and a broadening in seasonality in the future (most notably O500 and E700). This increase in one pattern is at the expense of most of the other patterns –

which decline substantially under the high-emissions scenarios, or even disappear in most months of the year. This trend has been documented previously as a potential impact of climate change, and leads generally to more zonal flow, and fewer meridional disturbances (and troughs) in the atmosphere (e.g. Hope, 2006). The effect of this trend on the patterns themselves in this thesis is relatively minor, and can be seen only in the warmest patterns. While the shape of most future patterns looks nearly identical to the shape of the same pattern in the 20th Century (as discussed in section 4.5 above), in the warmest pattern (O500 and E700), each contour is usually a bit higher at a given latitude than they were in the 20th century, while all the other 14 patterns remain nearly the same in this regard.

In comparing between the two GCMs used in this research, the regions of increases and decreases in tornado days appear similar in both of the comparable scenarios (A2 and B1), but not identical (Table 8). While the CCSM3 projects increases in the Northern High Plains states under the A2 scenario, the CGCM3 projects this increase to occur slightly more southward into the Central Plains. Both GCMs project an increase in tornado days in the Lower Great Lakes region under the A2 scenario, but the CGCM3 extends this area a bit further south into parts of the Southeastern US as well. The CGCM3-A2 also projects a slightly greater intensity of increased tornado activity in the 2090s, compared to the 2050s; and seasonality-wise behaves more like the CCSM3-A1FI scenario than the CCSM3-A2. In comparing areas of decreased activity, both GCMs project fewer tornado days in the Upper Great Lakes and Southern Plains, but the CGCM3 has two notable exceptions, Oklahoma and Missouri – both expected to increase substantially, especially in the 2090s.

Under the B1 scenario, the models are also very similar in most aspects – both geographically and seasonally. Two dissimilar traits, however, are noticed. The first is that the CCSM3 projects a greater increase in tornado days between the 2050s and the 2090s, while the CGCM3 actually projects a decrease in tornado days from the 2050s to the 2090s. The other major difference between the tornado day projections of the two models is that the CGCM3 projects an increase in the Central Plains states, while the CCSM3 does not. Both models, however, do project an increase in tornado days in the Lower Great Lakes and into the Mid-Atlantic and Southeastern US, along with decreases in the Upper Great Lakes states and parts of the Southern Plains under the B1 scenario.

*5.2 – Comparisons of Results and Methods to Previous Studies*

Although no other known similar studies (using synoptic climatological methods with GCM output data to analyze future tornado occurrence) have been done to date, comparisons between the results found in this thesis can be made to synoptic climatologies of severe storms and tornadoes, and to the 'ingredients-based' research done previously on climate change impacts on severe storm environments.

*<u>5.2.1 – Synoptic Climatological Research on Severe Weather and Tornadoes</u>*

In creating a synoptic climatology of severe storms in Virginia, Davis and Rogers (1992) used PCA and cluster analysis to create late spring and summer weather types (a type of synoptic climatology which classifies types of weather based on a number of meteorological variables at single individual stations) for a single site in the state that consisted of over 20 surface and atmospheric variables. The researchers then utilized this classification to analyze the occurrence of severe storms in the state; finding that nearly 80% of all severe storms were associated with two of the nine clusters. While the method used in their synoptic climatology differs from the method used in this thesis (weather typing versus a map pattern classification), it does help validate the utilization of the synoptic climatological approach and the ability of accurately delineating between synoptic climatological clusters that are favorable or unfavorable for severe storms.

Five years later, Davis et al. (1997) created a synoptic climatology specifically for tornadoes in Virginia using an environment-to-circulation approach (Yarnal, 1993) and a similar method to Davis and Rogers (1992). This research highlighted the fact that outside of the Great Plains, different regions of the US have differing synoptic situations that could potentially be favorable for the development of tornadoes. Similar to this thesis, Davis et al. (1997) experimented with the use of tornado days (as opposed to total tornadoes). Additionally, among a suite of variables and synoptic types, they underline the importance of 500mb flow as a key determining characteristic in the air mass associated with the most tornadoes in their study – the air mass having a deep trough just to the southwest of the state. The position of the 500mb troughs in the patterns created in this thesis have similar regions associated to increased tornado activity, just downwind of the axis of a trough. Interestingly in this thesis, specifically within the state of Virginia, there were no patterns created at the 500z level that corresponded to more than a 1% increase or decrease in actual tornado days versus expected tornado days.

Leathers (1993) used a synoptic technique with both 500mb geopotential heights and 850mb temperatures (and surface pressure, which was not used in this thesis) as variables in creating a synoptic climatology of tornadoes in the northeast US. Due to their relative infrequency, this thesis largely neglected the analysis of tornadoes in the northeastern US. However, some similar conclusions to tornadoes elsewhere in the country can be drawn from Leathers (1993); in that 500mb-level troughs and the passage of frontal boundaries (as indicated by 850t fields) throughout the season are quite common features in association to tornadic activity. Also similar to this thesis, Leathers (1993) finds that these synoptic features are more pronounced in the spring months than the summer months, although greater instability due to the summer heat can still trigger tornado outbreaks in these months whether the synoptic situation seems favorable or not. In this thesis, while most associated tornado activity makes sense climatologically in regards to its location relative to a trough, some rather zonal patterns were unexpectedly associated with increased tornado activity. As noted by Leathers (1993), this could be attributed merely to the seasonality of these patterns rather than their shapes.

In analyzing the association of synoptic patterns and weather types to severe weather and tornadoes, Miller (1972) also found that a variety of patterns and types can be associated to severe weather. Additionally, Johns (1982 and 1984) found that northwesterly flow at the 500mb level is often associated with severe weather and tornadoes along (and just to the south of) the 500mb jet from May through August. However, in this thesis, the two warm-season patterns exhibiting northwest flow at the 500mb level (L500 and O500) were considered 'tornado unfavorable,' and with the exception of South Dakota under O500, no states showed a substantial (more than +1%) increase in tornado activity compared to normal. This likely is a result of the relatively high frequency of those patterns in the summer months (as compared to any other pattern's frequency in any other month) compared to the relatively low number of F2+ tornado days in general. Furthermore, the actual piece of datum being analyzed in those two papers differs slightly from what was analyzed in this thesis – an outbreak of severe weather (in Johns, 1982 and 1984) versus an F2+ tornado day (in this thesis).

Again, some of these synoptic climatologies of severe weather and tornadoes in the US are very regional in nature, while this thesis attempted to classify multiple geopotential height and temperature patterns over a continental scale. The two synoptic climatologies specifically of tornadoes (Davis et al., 1997; Leathers, 1993) both took an environment-to-circulation approach to classification, which, not only is less-universal in its utility, but is also not applicable to use to classify future GCM days, nor attempt to project future tornado occurrence. However, because the aforementioned research did use synoptic techniques, despite these differences, some of the broad conclusions from those studies can be related to similar conclusions from this thesis – mostly in regards to the relationship between tornadoes and patterns of atmospheric circulation.

*5.2.2 – Climate Change Impacts Research on Severe Thunderstorm Environments*

Perhaps the most relevant literature available for a direct comparison of the results herein is the research specifically on the impacts of climate change on severe weather. As previously mentioned in section 2.4.3, of the very few studies that have been done on this topic, most use an ingredients-based methodology that aims to predict possible future days of severe environments based upon the calculations of instability (most often in terms of CAPE) and wind shear from GCM output data. Although this thesis uses a starkly contrasting *method*, similar *results* can be found between the two.

Trapp et al. (2007) used a number of different GCMs, including the CCSM3, and did project an increase in overall severe weather days (NDSEV) across the US. Worth noting in comparing and contrasting the results of Trapp et al. (2007) and this thesis, however, is that the fundamental event being predicted differs slightly – a day with a favorable severe weather environment (NDSEV; in Trapp et al., 2007) versus a state's F2+ tornado day probability (in this thesis). Although slight differences in tornado day changes are noticed from the results discussed in this thesis, the geographical regions and the seasonality of the changes are quite similar. Using the A1B scenario (not used in this thesis, but could probably be best estimated by the results from A1FI or A2), Trapp et al. (2007) found increases in NDSEV over the Northern and Central High Plains states, and in the Lower Great Lakes, Mid-Atlantic (and generally the Appalachian states) as well. Although the researchers projected an increase in the Upper Great Lakes states (where this thesis found a decrease), a slight decrease was noted in the summer in parts of the Midwest – from Illinois southward into Texas. Additionally, similar to the results in this thesis, the spring (March through May) results from the CCSM3 – A1B scenario used in Trapp et al. (2007) appear to show a greater increase in NDSEV than do the summer results (June through August), although the locations of the most intense spring increases differ slightly from the tornado day results discussed in section 4.6.. Furthermore, when other GCMs are used, the summer months appear to show a larger increase in NDSEV. Also, in comparison to the other two GCMs used in their research (neither of which were used in this thesis), two areas of overall *increases* in severe weather look relatively similar to the results of the A1FI scenario in this thesis – the Northern Plains and the Lower Great Lakes – although similar areas of *decreased* NDSEV are really only present in western Texas and parts of Oklahoma and Kansas.

In using the A2 scenario in a GCM that incorporates the CCSM3 model used in this thesis, Van Klooster and Roebber (2009) also found that significant changes in *severe convective potential* could be possible during the first half of the 21st Century, though changes in *convective initiation potential* are not found to be significantly different from its observed variability. Geographically, Van Klooster and Roebber (2009) projected an increase in severe convective potential in the northern half of the US, including the Lower Great Lakes, parts of the Northern and Central Plains states, the eastern Mid-Atlantic, and parts of the Southeast (much like the results of this thesis), but also in the Upper Great Lakes and parts of the Midwest (where this thesis projects decreases). Areas projected for decreased activity were in Louisiana and Texas (as in this thesis), and then extending slightly west and north into New Mexico and Colorado. Although they used an ingredients-based method, Van Klooster and Roebber (2009) also surmise that a more direct comparison of the association between severe weather and synoptic patterns could yield productive insights into the impacts of climate change on severe weather.

Only a few other known studies specifically on the topic have been published with results on increases or decreases in severe weather. Trapp et al. (2009) found that as time passes in the A1B scenario (and therefore as greenhouse gas emissions continue to rise) an association to the increase in the number of days of severe weather could be found – suggesting that if greenhouse gas emissions were to be tapered, that the increase in severe storm frequency could be lessened as well. Marsh et al. (2009) used the CCSM3 GCM under the A2 scenario to project the future occurrence of favorable severe weather environments over Europe. Their research generally found slight increases in favorable environments depending on location. Both of these results can be considered roughly similar to a trend in this thesis: increasing tornado days in some locations – amplified under the highest emissions scenario (A1FI in this thesis), and as time continues into the 2090s. And, while looking into projected convective updraft speeds, Del Genio et al. (2007) concluded that although the total amount of severe weather might not alter significantly into the future, the most intense storms could become more frequent.

### *5.2.3 – Implications of Methods*

The methods used to assess the impacts of climate change on tornadoes in this thesis have some associated ancillary benefits. First, because a circulation-to-environment (Yarnal, 1993) approach was taken to create this synoptic climatology, the daily atmospheric circulation classifications for each of these levels can directly be used for association to any other surface event/environment for which the variable(s) (500z, 700z, 850t) can be reasonably thought to help predict. Additionally, these same variables are classified for five different scenarios spanning two different GCMs for both the 20th Century (from 1957-2002) and for decades into the future. This classification, therefore, can also be used to help validate 20th Century associations of surface events to atmospheric circulation, *and* future associations as well.

Fundamentally, the methodology used in projecting the future regions, frequencies and seasonalities of tornadoes in the US is very different than previous methods. Only a handful of previous studies (as mentioned in section 2.5.4) have used synoptic methods with GCM output data specifically to help predict future extreme events. This thesis helps to validate such methods and studies, due to the similarities of the results across multiple scenarios and across two GCMs. In addition to the validity of such methods, the necessity of using the synoptic method is also important to note. There have been numerous studies on some of the shortcomings of contemporary GCMs – such as their spatial resolution; and their inability to accurately project values of moisture, precipitation, and any 'class-C variable;' and synoptic methods are well-suited to help downscale GCM output data into local-scale analyses, especially in regards to extreme (and, by nature, infrequent) events (Sheridan and Lee, 2010).

*5.3 – Limitations, Shortcomings, and Potential Future Directions of the Research*

As with any scientific project undertaken, some necessary assumptions are made during the course of this thesis research that create limitations to interpretations of the results. Many of these limitations are due to the inherent assumptions associated with synoptic climatological methods mentioned in section 2.5 above. One of the major assumptions discussed was that the variables used to create the classification (500z, 700z, and 850t) are accurate predictors of the surface event of interest. While the patterns at each of the levels classified in this research do play a role in the development of tornadoes, they certainly are not the only three factors that create a tornado-favorable environment, and were used partly because of the availability of the data. Because of this shortcoming, the interpretation of the results herein must take into account that important variables (such as CAPE, low-level moisture, and wind shear; Brooks et al., 2003a) are not directly accounted for in this analysis, and the results are meant to represent a more holistic view of the daily continental-scale circulation, and not necessarily the approximate nearby values of all important ingredients necessary for tornado development.

Therefore, one potential future research direction off of this thesis is to incorporate more atmospheric variables into the classification – both at different levels of the atmosphere, but especially at the surface as well. The inclusion of a weather typing procedure (as in Davis et al., 1997; or the Spatial Synoptic Classification; Sheridan, 2002) might be a good (and strictly synoptic) starting point in this direction. Important to note with the inclusion of such variables, however, is that if future projections are made with GCMs, they do model certain variables *much* more accurately than others.

Another major assumption discussed above was that the temporal and spatial aspects of the classification must be partitioned into finite intervals. Undoubtedly, factors from outside of the spatial domain used in this study might have had an influence (especially on the edges of the spatial domain) on the classifications made if they had been included. One must also consider that circulation patterns are constantly evolving from hour to hour. Thus, the patterns themselves are really just the 'snapshot' of the height/temperature field at a certain moment of each day, and some days' patterns might have changed significantly a few hours before or after this 'snapshot' was taken. Related to this point is the fact that some tornadoes might have occurred in the early morning hours of the following day and are probably more a product of the previous day's synoptic situation than they are of the day for which they were classified to have occurred. While both of these problems were partly mitigated due to the inclusion of the one day lag and one day lead variables into the BLR for each state, and because tornado days were used as opposed to total tornadoes, the exact synoptic situation at the exact time of a single tornado is probably rarely reflected in the climatology.

Another space-related limitation to these results stems from the choice of using political boundaries to delineate the area in which a tornado day occurred. Especially in a large state, such as Texas, a tornado day might have been the result of tornadoes only in the northeastern corner of the state, yet the entire state gets classified as a tornado day. This region of Texas has a far different climate than the west, yet it is confined by the same political boundary. Thus, the interpretation of the resulting synoptic patterns that correspond to increased tornado activity over some large states should consider that these synoptic patterns might be quite different for tornadoes that occurred in one part of the state compared to the other. One result of this situation in this thesis is that some of the larger – or climatologically varying – states have a number of differing patterns that correspond to tornado activity, and it is impossible to tell definitively which of these synoptic patterns is favorable for tornadoes in one portion of a state over another.

On a related note, in order to use tornado days as opposed to total tornadoes, a definition *must* be made as to the spatial area in which a tornado day occurred. Thus, a potential future direction from this thesis could be to re-define these areas by their climatological similarities rather than their political boundaries, use a defined grid to partition tornado days, or use a smaller spatial scale to delineate a tornado day (such as counties), and then using spatial interpolation for greater spatial resolution in the results. With any of these directions, however, the issue of sample size could present a problem (i.e. there might not be enough tornado days in any one county, grid cell, or climate region).

Another assumption of synoptic climatology discussed in section 2.5 above was that there will always be some measure of within-class (or within-pattern) variability, and that this is not a problem (Yarnal, 1993). The goal again is to reduce within-cluster variability of the daily patterns, while maximizing the between-cluster variability. The maps of the patterns presented in section 4.2 were created by averaging the mean values of the height/temperature at each grid point for that pattern. However, not every day that got classified into the same pattern will have the exact same shape, and within most clusters there are undoubtedly some outlier daily patterns (that were just very abnormal compared to others) that were forced into a group because that was the group that they most resembled. The possibility exists that these days patterns look nothing like the patterns displayed, and that some of them had F2+ tornado days associated with them. On the other end of this assumption, is that some group of patterns that actually exists was not accurately represented (i.e. too few clusters/patterns were ultimately decided upon). Again, a line must be drawn at some point before an unwieldy number of clusters are decided upon.

One possible direction to take for future research regarding this matter would be to create an ‘other’ group that is a collection of patterns that do not fit into a cluster due to their abnormal shapes, nor do they fit in with each other. The caveat to this method, however, especially when tornadoes are the surface event of interest, is that many of these ‘abnormal’ patterns might be associated to tornadoes, and once classified into the ‘other’ group, no real average map can be drawn, nor can broad conclusions be made. If the synoptic method is used for any further similar research, the limitations that these two assumptions present will always need to be considered in the interpretation of the results.

Two limitations to the research presented herein stem from the data used. The first of these data limitations is that of the well-documented reporting bias of 20th Century tornadoes (Doswell, 2007). While efforts were made to mitigate the effects of this bias by using tornado days instead of total tornadoes, and by using only (E)F2 and stronger tornadoes as those that qualify as tornado days, the reporting bias must still be considered when interpreting the results. The second data limitation stems from the reliability of GCM output data. While the variables used by the GCMs in this thesis are considered fairly well modeled in comparison to others (Sheridan and Lee, 2010), they are still only *projections* of future values with no real way of verifying their accuracy into the future. These projections are meant to be accurate over the course of rather long temporal scales. However, the day-to-day variability projected by the GCMs is not meant to be an accurate representation of a particular day’s pattern – in the 20th Century or in the future. Thus, sums of the probabilities of a tornado day occurrence over the course of a decade (either per month or throughout the TSeason) are more accurate than any one particular day's probability, and therefore were used in calculating the figures presented in sections 4.3, 4.4, and 4.6.

Another factor that must be considered in the interpretation of the results is that although certain synoptic patterns (and thus, their associated tornado activity) are projected to shift to earlier in the tornado season, the solar geometry during these months will not change into the future. Thus, the possibility exists that the total solar energy that reaches the earth in these months still may not be adequate to actually create a sufficiently unstable environment to trigger severe weather or tornadoes, despite how a GCM projects the future frequency and seasonality of a tornado favorable synoptic pattern.

Perhaps one of the more important inherent assumptions in this thesis, which may or may not be viewed as a limitation, is that the relationship between atmospheric circulation patterns and tornadoes will not change in the future. That is, in order to project future results using synoptic methods, one must assume that if a specific pattern is generally (un)favorable for tornadoes based upon the analysis of the 20th Century, it will remain (un)favorable (to the same degree in each state) into the future as well. If this relationship does change into the future, the future tornado results presented in section 4.6 would be invalid; though the shape, frequency and seasonality of the future synoptic patterns may still be quite accurate.

# CHAPTER 6

# SUMMARY AND CONCLUSION

This thesis expands the body of research on a largely neglected topic looking into the impacts of climate change on severe weather and tornadoes. Principal components analysis, cluster analysis and discriminant function analysis were used to classify daily patterns of 500mb and 700mb geopotential heights and 850mb temperatures from both the NCEP/NCAR reanalysis data set, and from a range of future scenarios in two GCMs (CCSM3 and CGCM3). Using binary logistic regression, these patterns were then associated to F2 and stronger tornado days across the continental US. This relationship between patterns and tornado activity was then applied to the projected patterns from GCM output in order to infer the future change in the frequency and seasonality of US tornado activity. While many previous studies have made future projections of extreme events, this thesis does mark the first use of synoptic climatological methods in looking at the frequency and seasonality of future tornado activity. Furthermore, this research represents the first synoptic climatology of tornadoes throughout the entire continental United States, the first done with a map pattern classification technique in the US, and the first to use a circulation-to-environment approach with tornadoes in the US.

The results of this thesis are that over the US as a whole, under each scenario used in both GCMs, the number of F2+ tornado days from February through August are projected to increase (anywhere from 3.8% to 12.7%) in response to climate change. Seasonally, future tornado activity is projected differently depending on the scenario used and the decade. In the 20th Century, across the US as a whole, a sharp peak in tornado activity is observed in May, with a slow drop-off thereafter until August. Depending on the scenario and decade, future tornado activity could see a shift to an earlier peak (in April instead of May) and/or a broadening of the peak of the tornado season – from a one month peak, to a two or three month peak. Among all scenarios in both GCMs, the greatest increase in tornado days is projected for the earlier part of the tornado season (February – April), with a slight decline from May through August.

Geographically, the regions projected to see the greatest increase in tornado days (compared to the 20th Century modeled tornado day activity) are the Lower Great Lakes states, the eastern Mid-Atlantic states, and either the Southeast or the Northern and Central Plains states – depending on the GCM and scenario used. Generally, the regions projected to experience a decrease in tornado activity in the future extend from the Upper Great Lakes states southwestward into the Southern Plains. These results are similar to the CCSM3 – A1B results from Trapp et al. (2007) that used CAPE and shear values in grid boxes (instead of states) and projected the number of days that would be favorable for any kind of severe weather – not just tornadoes.

Much like other synoptic climatologies of tornadoes, the resulting classifications were able to decipher generally between the patterns that were favorable for tornadoes and those that were unfavorable for tornadoes over the historical time period. As originally hypothesized, different regions of the US were favorable for above-normal tornado activity differently depending on the synoptic pattern. That is, there were regions of above-normal tornado activity and areas of below-normal tornado activity under the same pattern.

The warmer 500z, 700z, and 850t patterns that had summer seasonalities showed a trend towards an increased frequency and a broadened seasonality in the future. This trend was more pronounced in the 2090s than it was in the 2050s, and was more evident in the higher emissions scenarios than it was in the B1 scenario in both GCMs used. Unsurprisingly, these two trends carried over into the resulting tornado projections as well. In the CCSM3 model, the A1FI scenario projected the largest increase in US tornado days among the three scenarios used (in both the 2050s and the 2090s). In the CGCM3 model, tornado activity showed the greatest projected increase under the A2 scenario compared (only) to the B1 scenario, and this increase was greater in the 2090s as well (though under the B1 scenario for the CGCM3, the 2050s showed a greater projected increase than the 2090s). These results are similar to those in previous synoptic climatological research looking into the impacts of climate change on other extreme events.

The most likely direction for future research using synoptic methods to project future tornado activity will be to enhance the spatial resolution of the tornado association – using tornado data on a county-by-county basis (possibly with centroids and interpolation) or within small gridded cells instead of using state boundaries. Another opportunity for future research along these lines would be to include other important variables – either in creating the synoptic patterns, or in the regression equation used to model tornado activity.

# CHAPTER 7

# REFERENCES


Aguado, E. and J.E. Burt (2001): Understanding Weather and Climate, Second Edition. Prentice Hall, Upper Saddle River, New Jersey, USA, 505 pp.

Ashley, W.S. (2007): Spatial and Temporal Analysis of Tornado Fatalities in the United States: 1880-2005. *Weather and Forecasting* **22**, 1214-1228.

Ashley, W.S., A.J. Krmenec, and R. Schwantes (2008): Vulnerability due to Nocturnal Tornadoes. *Weather and Forecasting* **23,** 795-807.

Brazzell, J.R., D.J. Kellenbenz, and B.J. Bramer (1998): The Impact of Surface Boundaries on Tornadogenesis during the Northwestern Minnesota Event of 20 July 1998, Unpublished.

Brooks, H.E., J.W. Lee, and J.P. Craven (2003a): The spatial distribution of severe thunderstorm and tornado environments from global reanalysis data. *Atmospheric Research* **(67-68),** 73-94.

Brooks H.E., C.A. Doswell III, and M.P. Kay (2003b): Climatological Estimates of Local Daily Tornado Probability for the United States, *Weather and Forecasting* **18,** 626-640.

Brooks, H.E. and C.A. Doswell III (2001): Normalized Damage from major Tornadoes in the United States: 1890-1999. *Weather and Forecasting* **16**, 168-176.

Brooks, H.E. and C.A. Doswell III (2002): Deaths in the 3 May 1999 Oklahoma City Tornado from a Historical Perspective. *Weather and Forecasting* **17,** 354-361.

Changnon, S.A. (2003): Shifting Economic Impacts from Weather Extremes in the United States: A Result of Societal Changes, Not Global Warming. *Natural Hazards* **29,** 273-290.

Cheng, C.S., H. Auld, G. Li, J. Klaassen and Q. Li (2007a): Possible impacts of climate change on freezing rain in south-central Canada using downscaled future climate scenarios. *Natural Hazards and Earth System Sciences* **7,** 71-87.

Cheng C.S., M. Campbell, Q. Li, G. Li, H. Auld, N. Day, D. Pengelly, S. Gingrich and D. Yap (2007b): A Synoptic Climatological Approach to Assess Climatic Impact on Air Quality in South-central Canada. Part II: Future Estimates. *Water, Air and Soil Pollution* **182**, 117-130.

Collins, W.D., C.M. Bitz, M.L. Blackmon, et al. (2006): The Community Climate System Model: CCSM3. White paper, NCAR, Boulder, Colorado, USA.

Concannon, P.R., H.E. Brooks and C.A. Doswell (2000): Climatological Risk of Strong and Violent Tornadoes in the United States, White paper, Paper 9.4, 2nd Conference of Environmental Applications, Long Beach, California, USA, 8-12 January 2000, American Meteorological Society, 212-219.

Coniglio, M.C., D.J. Stensrud and M.B. Richman (2004): An Observational Study of Derecho-Producing Convective Systems. *Weather and Forecasting* **19**, 320-337.

Craven, J.P. and H.E. Brooks (2004): Baseline Climatology of Sounding Derived Parameters Associated with Deep Moist Convection, *National Weather Digest,* **28**, 13-24.

Cuell C. and B. Bonsal (2009): An assessment of climatological synoptic typing by principal component analysis and kmeans clustering. *Theoretical and Applied Climatology* **98**, 361-373.

Davis, R.E., T.M. Stanmeyer, and G.V. Jones (1997): A Synoptic Climatology of Tornadoes in Virginia. *Physical Geography* **18(5)**, 383-407.

Davis, R.E. and R.F. Rogers (1992): A Synoptic Climatology of Severe Storms in Virginia. *Professional Geographer* **44(3)**, 319-332.

Davis, S. and Walsh, K.J.E (2008): Southeast Australian Thunderstorms: Are they increasing in Frequency? *Australian Meteorology Magazine,* **57**, 1-11.

Del Genio, A.D., M.-S. Yao and J. Jonas (2007): Will moist convection be stronger in a warmer climate? *Geophysical Research Letters* **34**, L16703, 1-5.

Demuzere, M., M. Werner, N.P.M. van Lipzig and E. Roeckner (2008): An analysis of present and future ECHAM5 pressure fields using a classification of circulation patterns. *International Journal of Climatology* **29**, 1796-1810.

Diffenbaugh, N.S., R.J. Trapp, and H.E. Brooks (2008): Does Global Warming Influence Tornado Activity? *EOS, Transactions, American Geophysical Union* **89(53)**, 553-554.

Doswell, C.A. (2007): Small sample size and data quality issues illustrated using tornado occurrence data. *Electronic Journal of Severe Storms Meteorology* **2(5)**, 1-16.

Environment Canada (2009a): The Third Generation Coupled Global Climate Model (CGCM3), http://www.cccma.bc.ec.gc.ca/models/cgcm3.shtml, as accessed in January 2010.

Environment Canada (2009b): The Third Generation Atmospheric General Circulation Model (AGCM3), http://www.cccma.bc.ec.gc.ca/models/gcm3.shtml, as accessed in January 2010.

Fujita, T.T. (1971): Proposed characterization of tornadoes and hurricanes by area and intensity. SMRP Res. Paper 97, Univ. of Chicago, 42 pp.

Holt T. (1999): A classification of ambient climate conditions during extreme surge events off western Europe. *International Journal of Climatology* **19**, 725–744.

Hope, P.K. (2006): Projected future changes in synoptic systems influencing southwest Western Austrailia. *Climate Dynamics* **26** 765-780.

Hope, P.K., W. Drosdowsky and N. Nicholls (2006): Shifts in the synoptic systems influencing southwest Western Australia. *Climate Dynamics* **26**, 751-764.

Hyndman, D. and D. Hyndman (2009): Natural Hazards and Disasters, Second Edition. Brooks/Cole, Cengage Learning, Belmont, California, USA, 555 pp.

IPCC (2007a): Summary for Policymakers. In: *Climate Change 2007: The Physical Science Basis. Contribution of Working Group I to the Fourth Assessment Report of the Intergovernmental Panel on Climate Change* [Solomon, S., D. Qin, M. Manning, Z. Chen, M. Marquis, K.B. Averyt, M.Tignor and H.L. Miller (eds.)]. Cambridge University Press, Cambridge, United Kingdom and New York, New York, USA.

IPCC (2007b): The Physical Science Basis, Contribution of Working Group I to the Fourth Assessment Report of the Intergovernmental Panel on Climate Change, (Solomon, S., D. Qin, M. Manning, Z. Chen, M. Marquis, K.B. Averyt, M. Tignor, and H.L. Miller (eds.), Cambridge, United Kingdom and New York, New York, USA, 996 pp.

Johns, R.H. (1982): A Synoptic Climatology of Northwest Flow Severe Weather Outbreaks. Part I: Nature and Significance. *Monthly Weather Review* **110**, 1653-1663.

Johns, R.H. (1984): A Synoptic Climatology of Northwest Flow Severe Weather Outbreaks. Part II: Meteorological Parameters and Synoptic Patterns. *Monthly Weather Review* **112**, 449-464.

Johnston, K., J.M. VerHoef, K. Krivoruchko and N. Lucas (2001): Using ArcGIS Geostatistical Analyst. ESRI, Redlands, California, USA, 300 pp.

Kalnay, E., M. Kanamitsu, R. Kistler, W. Collins et al. (1996): The NCEP/NCAR 40-Year Reanalysis Project. *Bulletin of the American Meteorological Society* **77**, 437-471.

Kounkou, R., G. Mills and B. Timbal (2009): A Reanalysis Climatology of Cool-Season Tornado Environments Over Southern Australia, *International Journal of Climatology* **29(14)**, 2079-2090.

Kunz, M., J. Sander and Ch. Kottmeier (2009): Recent Trends of Thunderstorm and Hailstorm frequency and their relation to atmospheric characteristics in southwest Germany. *International Journal of Climatology* **29(15),** 2283-2297.

Leathers, D.J. (1993): A Synoptic Climatology of Northeastern United States Tornadoes. *Physical Geography* **14(2)**, 171-190.

Maddox, R.A. (1983): Large-Scale Meteorological Conditions Associated with Midlatitude, Mesoscale Convective Complexes, *Monthly Weather Review* **111(7)**, 1475-1493.

Maddox, R.A., R. Hoxit, and C.F. Chappell (1980): A Study of Tornadic Thunderstorms Interactions with Thermal Boundaries, *Monthly Weather Review* **108(3)**, 322-336.

Markowski, P.M., E.N. Rasmussen, and J.M. Straka (1998): The Occurrence of Tornadoes in Supercells Interacting with Boundaries during VORTEX-95, *Weather and Forecasting* **13(3)**, 852-859.

Marsh P.T., H.E. Brooks and D.J. Karoly (2009): Preliminary Investigation into the severe thunderstorm environment of Europe simulated by the Community Climate System Model 3. *Atmospheric Research* **93**, 607-618.

Michailidou, C., P. Maheras, A. Arseni-Papadimititriou, F. Kolyva-Machera and C. Anagnostopoulou (2009). *Theoretical and Applied Climatology* **97**, 163-177.

Miller, R.C. (1972): Notes on Analysis and Severe-storm Forecasting Procedures of the Air Force Global Weather Central. Air Weather Service Technical Report 200 (revised), Air Weather Service (MAC), United States Air Force, Scott Air Force Base, Illinois, USA, 190 pp.

Moran, J.M., M.D. Morgan, P.M. Pauley, (1997), Meteorology: The Atmosphere and Science of Weather, Fifth Edition, Prentice-Hall, Inc., Upper Saddle River, New Jersey, USA.

Perrin, B.L., D.B. Enfield, K.B. Hughes and A.R. Lupo (2009): Can Large Scale Climate Controls Help Predict Seasonal Tornado Activity?, 9A.1, 21st Conference on Climate

Variability and Change / 89th Annual Meeting of the American Meteorological Society, 11-25 Jan. 2009, Phoenix, Arizona, USA.

Romero, R., G. Sumner, C. Ramis and A. Genoves (1999): A Classification of the Atmospheric Circulation Patterns Producing Significant Daily Rainfall in the Spanish Mediterranean Area, *International Journal of Climatology* **19**, 765-785.

Romero, R., M. Gaya and C.A. Doswell III (2007): European climatology of severe convective storms environmental parameters: A test for significant tornado events. *Atmospheric Research* **83**, 389-404.

Rose, S.F., et al. (2004): A 10-yr Climatology Relating the Locations of Reported Tornadoes to the Quadrants of Upper-Level Jet Streaks, *Weather and Forecasting* **19**, 301-309.

Schultz, P. (1989): Relationships of Several Stability Indices to Convective Weather Events in Northeast Colorado, *Weather and Forecasting* **4**, 73-80.

Sheridan, S., K. Hayhoe, and L. Kalkstein (2009): Estimating climate change impacts from atmospheric circulation patterns and air masses. White paper.

Sheridan S.C. (2002): The redevelopment of a weather type classification scheme for North America. *International Journal of Climatology* **22**, 51-68.

Sheridan, S.C. and C.C. Lee (2010): Synoptic Climatology and the General Circulation Model. *Progress in Physical Geography* **34(1)**, 101-109.

SPSS (2003): Choosing a Procedure for Binary Logistic Regression Models, Help Topics, SPSS, Inc., Chicago Illinois, USA.

SPSS Inc. (2001): The SPSS Two-Step cluster component: a scalable component to segment your customers more effectively. White paper, technical report, SPSS, Chicago, Illinois, USA.

SPC (2009): Storm Prediction Center Severe Weather Database Files, available at http://www.spc.noaa.gov/wcm/index.html#data

Trapp, R.J., N.S. Diffenbaugh, H.E. Brooks, M.E. Baldwin, E.D. Robinson, and J.S. Pal (2007): Changes in severe thunderstorm environment frequency during the 21st Century caused by anthropogenically enhanced global radiative forcing. *Proceedings of the National Academy of Sciences* **104(50)**, 19719-19723.

Trapp, R.J., N.S. Diffenbaugh and A. Gluhovsky (2009): Transient response to thunderstorm forcing to elevated greenhouse gas concentrations. *Geophysical Research Letters* **36**, 6 pp.

Van Klooster, S.L. and P.J. Roebber (2009): Surface-Based Convective Potential in the Contiguous United States in a Business-as-Usual Future Climate. *Journal of Climate* **22**, 3317-3330.

Verbout, S.M., H.E. Brooks, L.M. Leslie, and D.M. Schultz (2006): Evolution of the U.S. Tornado Database: 1954-2003. *Weather and Forecasting* ***21,*** 86-93.

Vrac, M., K. Hayhoe and M. Stein (2007): Identification and intermodal comparison of seasonal circulation patterns over North America. *International Journal of Climatology* ***27,*** 603-620.

Whitney, Jr., L.F. (1977): Relationship of Subtropical Jet Stream to Severe Local Storms, *Monthly Weather Review* **105**, 398-412.

Wilby, R.L., S.P. Charles, E. Zorita, B. Timbal, P. Whetton, L.O. Mearns (2004): Guidelines for Use of Climate Scenarios Developed from Statistical Downscaling Models. Unpublished, (available from: http://unfccc.int/resource/cd_roms/na1/v_and_a/Resoursce_materials/Climate/StatisticalDownscalingGuidance.pdf).

Wilks, D.S. (2006): <u>Statistical Methods in the Atmospheric Sciences, Second Edition.</u> Academic Press, Elsevier, Burlington, Massachusetts, USA; San Diego, California, USA; London, UK.

Wilson, J.W. and R.D. Roberts (2006): Summary of Convective Initiation and Evolution during IHOP: Obeservational and Modeling Perspective. *Monthly Weather Review* **134 (1),** 23-47.

Yarnal, B. (1993): Synoptic Climatology in Environmental Analysis: A primer. Belhaven Press, London and CRC Press, Inc., Boca Raton, Florida, USA.

Yarnal, B., A.C. Comrie, B. Frakes and D.P. Brown (2001): Developments and Prospects in Synoptic Climatology. *International Journal of Climatology* **21**, 1923-1950.

## APPENDIX A

The maps in Appendix A represent the monthly absolute difference in tornado days per decade between the GCM20c portion of the BLR results and the actual observed tornado record of F2+ tornado days. The first section of maps is for the CCSM3 results, and the second section of maps is for the CGCM3 results. The following legend can be used for all maps in Appendix A, and is in terms of difference in F2+ tornado days per month and per decade between the observed record and the GCM20c portion of the BLR results.

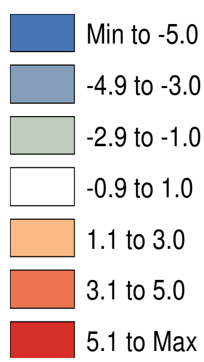

## *A.1 - CCSM3 Monthly Model Error*

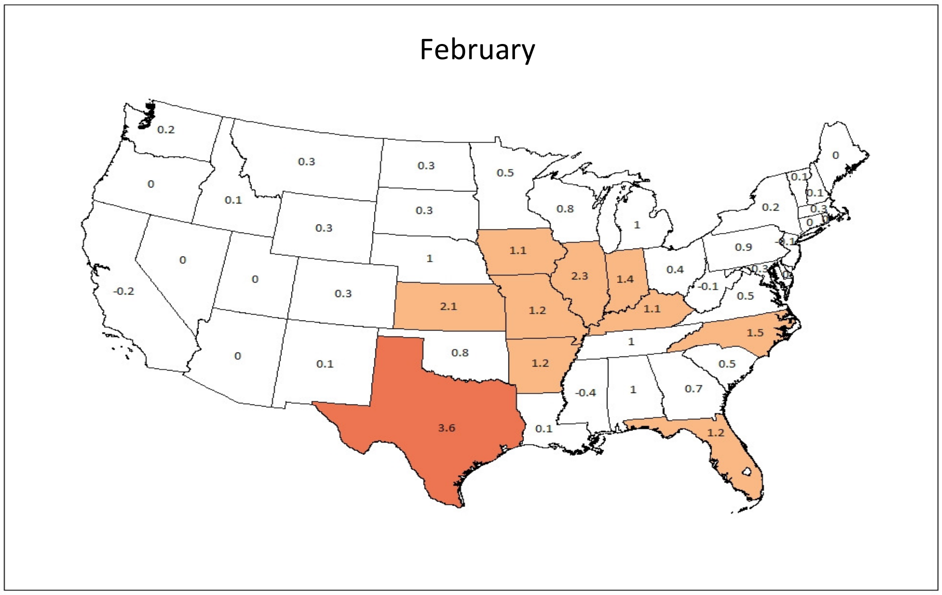


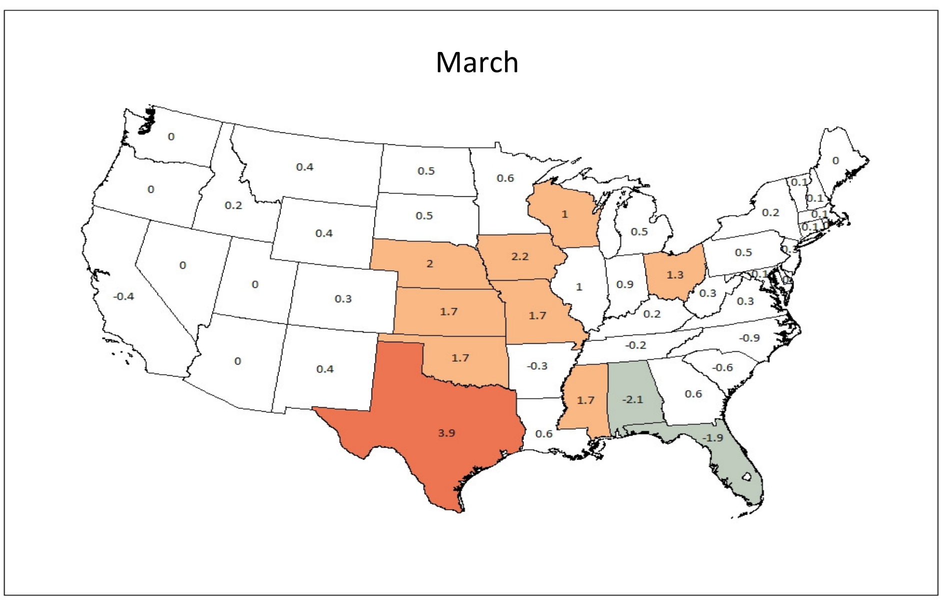


**Figure A.1 –** CCSM3 monthly model error in terms of F2+ tornado days per decade and per month. Continued on the next page.

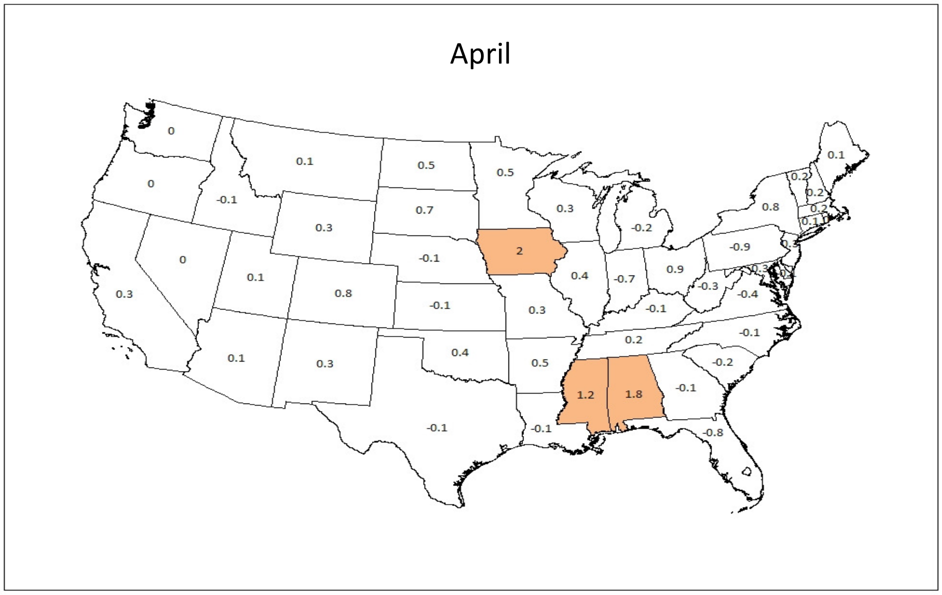


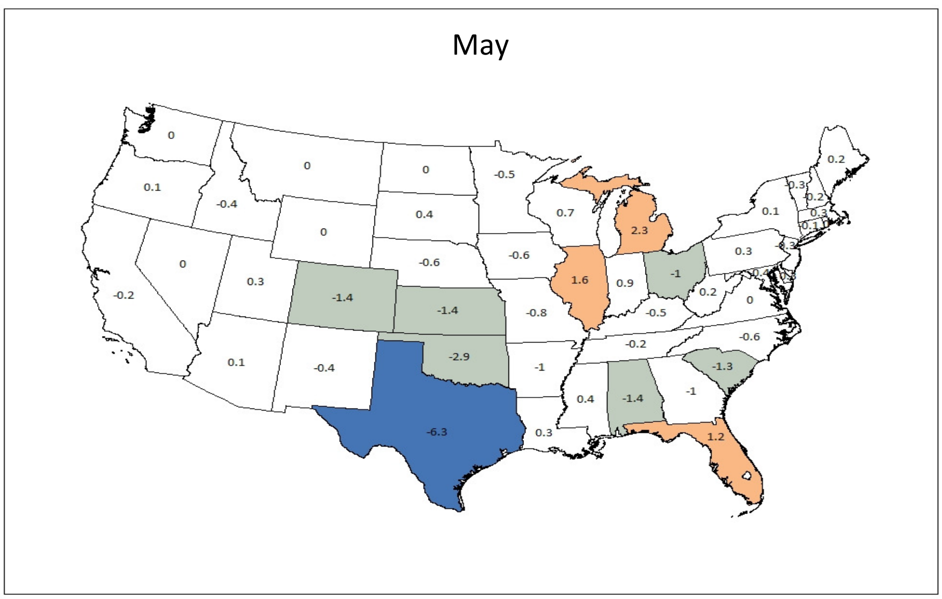


**Figure A.1 (continued) –** CCSM3 monthly model error in terms of F2+ tornado days per decade and per month. Continued on the next page.

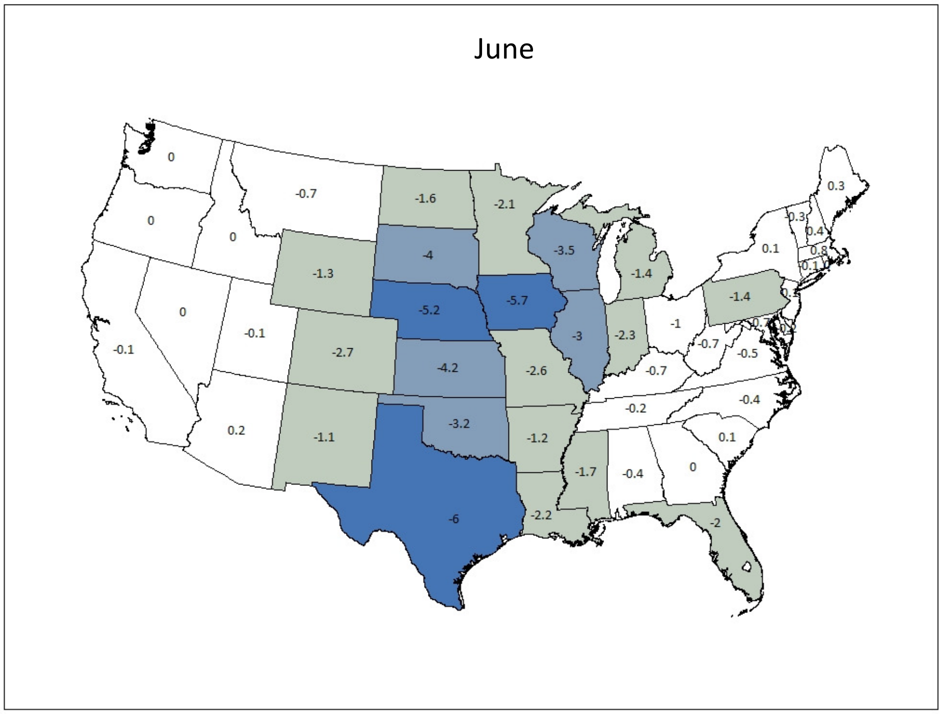


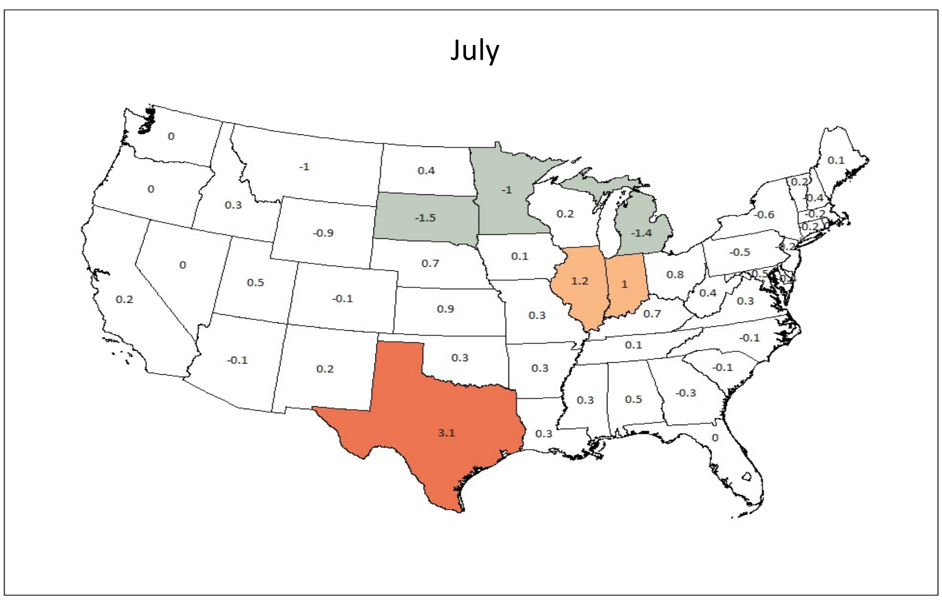


**Figure A.1 (continued) –** CCSM3 monthly model error in terms of F2+ tornado days per decade and per month. Continued on the next page.

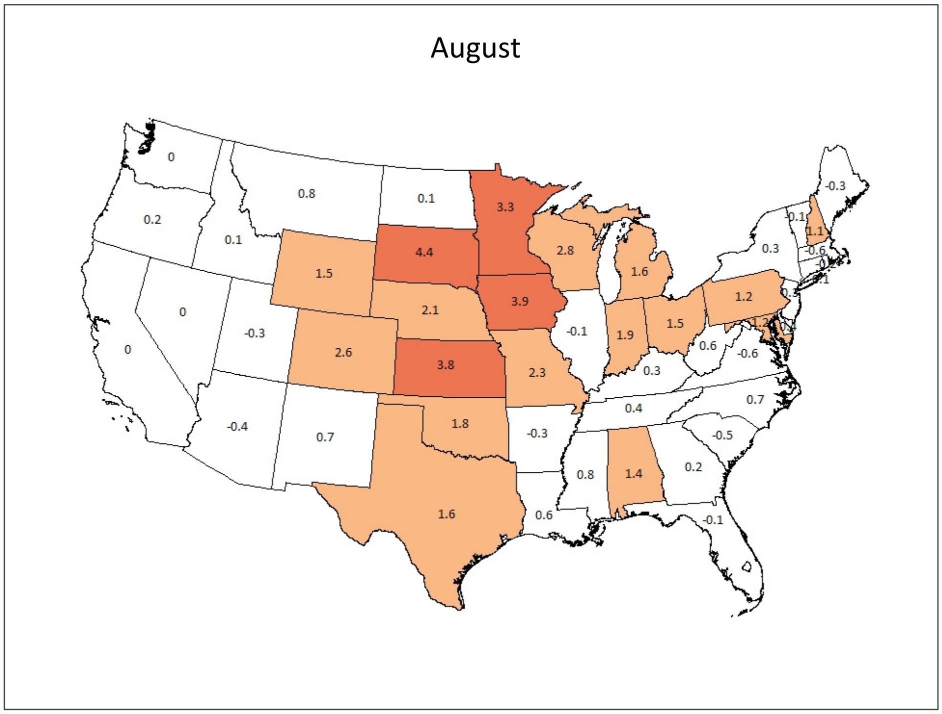


**Figure A.1 (continued)** – CCSM3 monthly model error in terms of F2+ tornado days per decade and per month.

## *A.2 – CGCM3 Monthly Model Error*

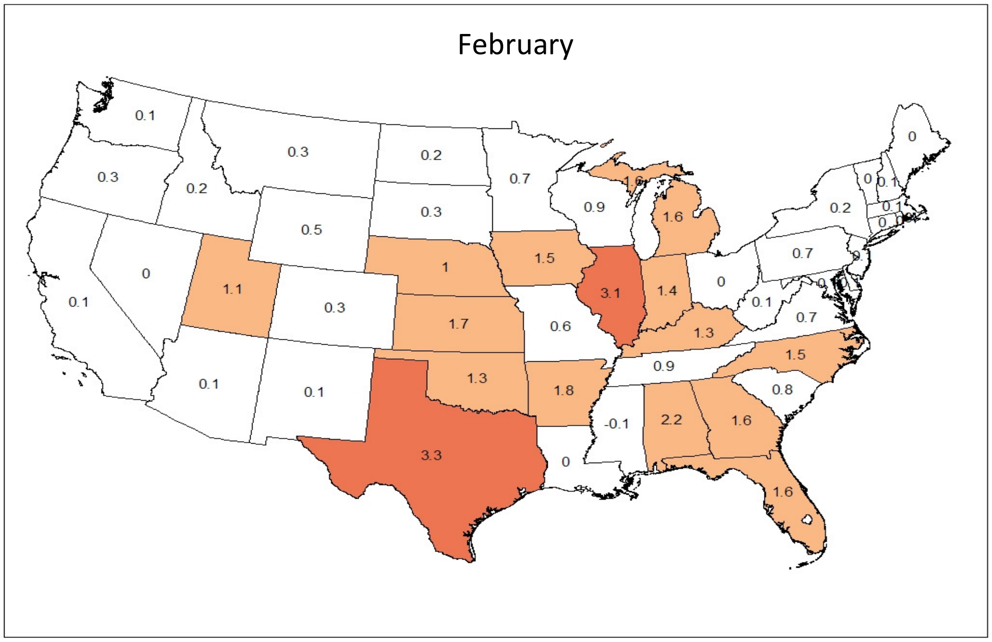


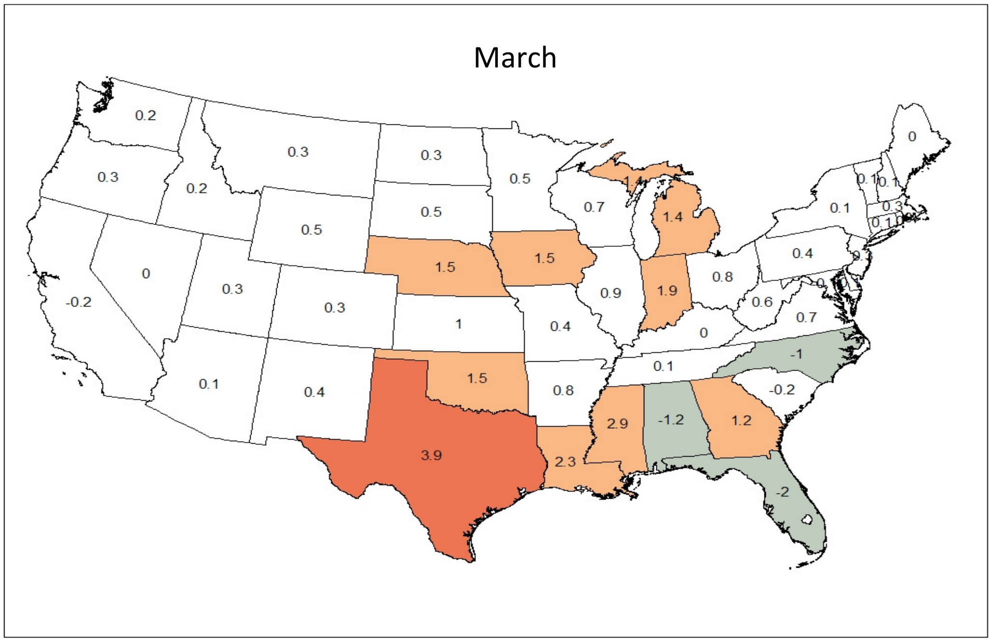


**Figure A.2 –** CGCM3 monthly model error in terms of F2+ tornado days per decade and per month. Continued on the next page.

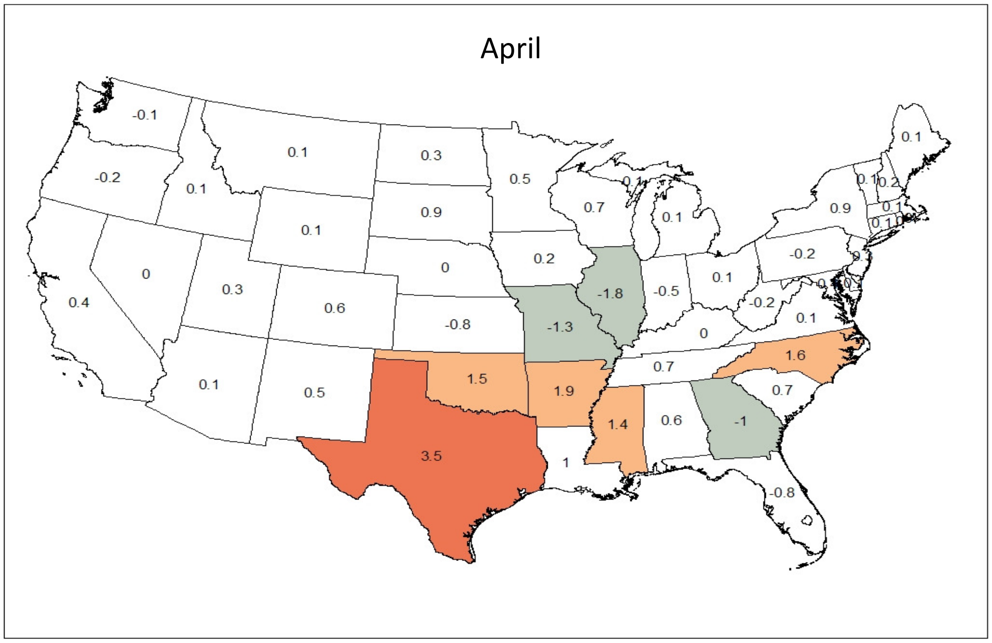


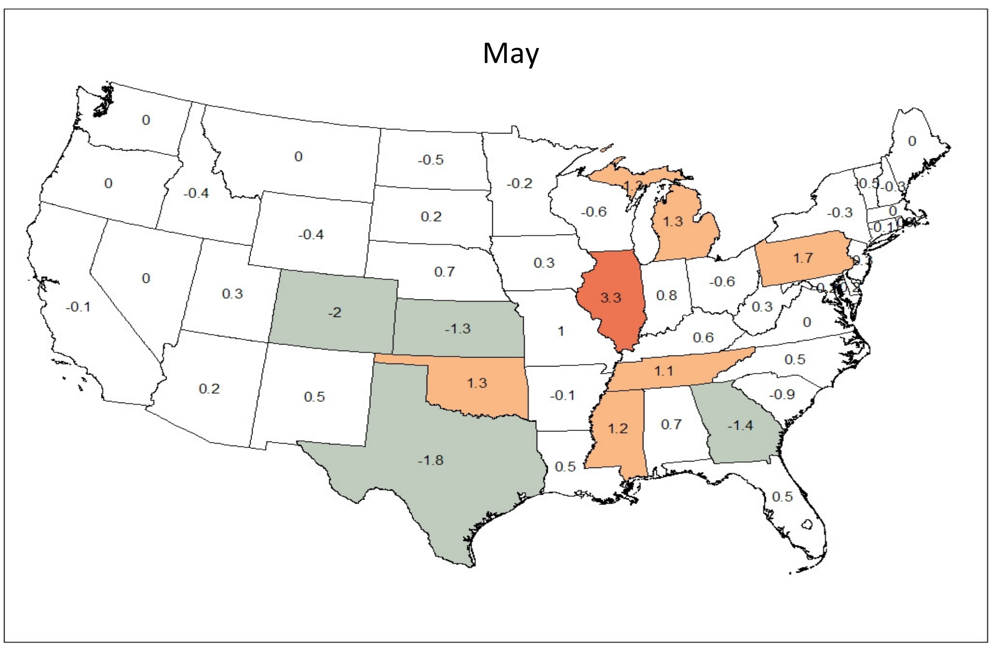


**Figure A.2 (continued) –** CGCM3 monthly model error in terms of F2+ tornado days per decade and per month. Continued on the next page.

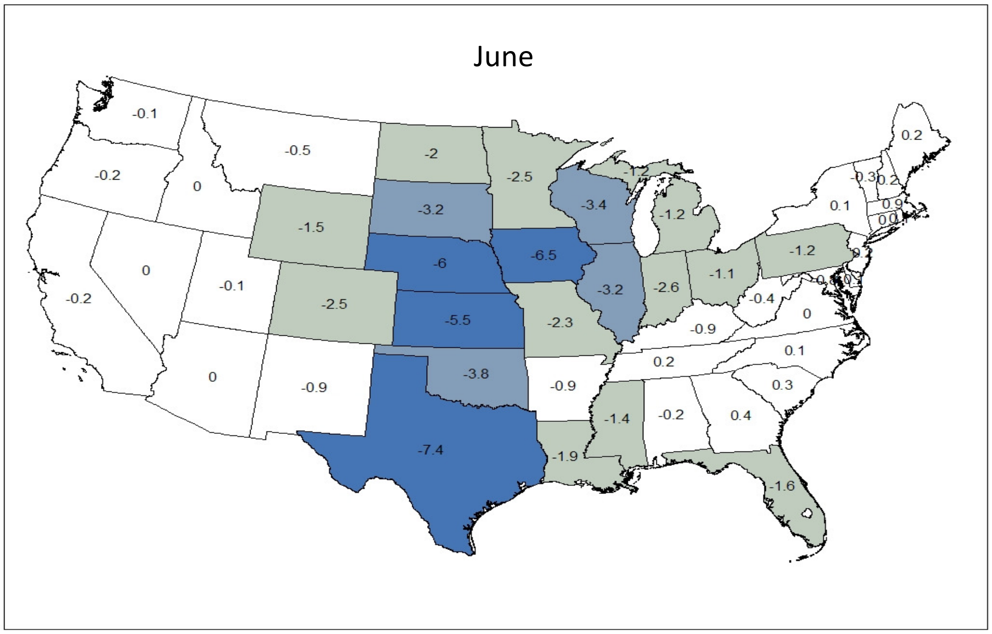


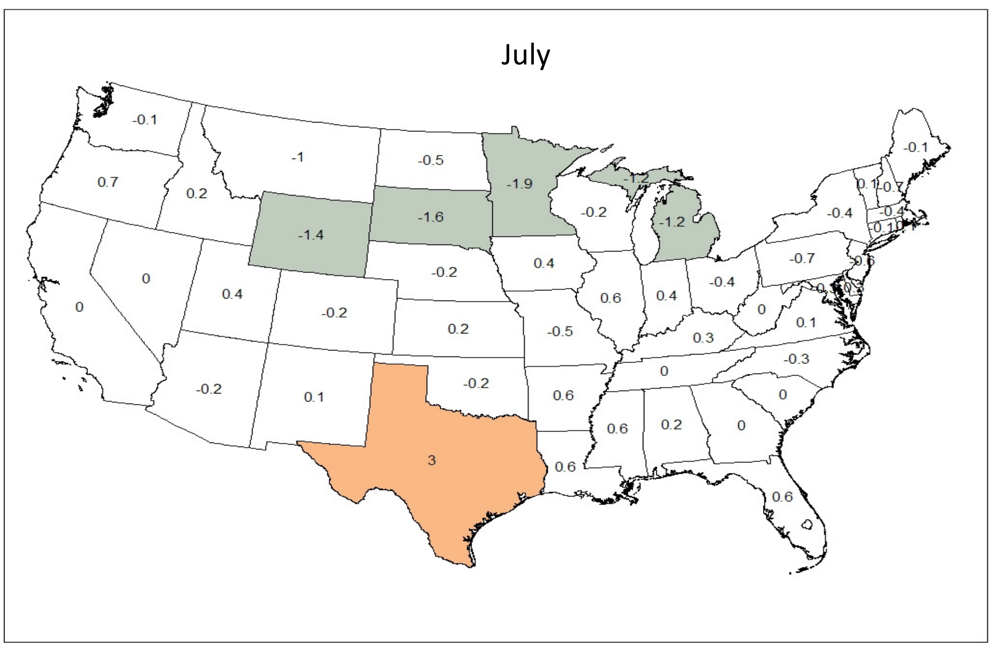


**Figure A.2 (continued) –** CGCM3 monthly model error in terms of F2+ tornado days per decade and per month. Continued on the next page.

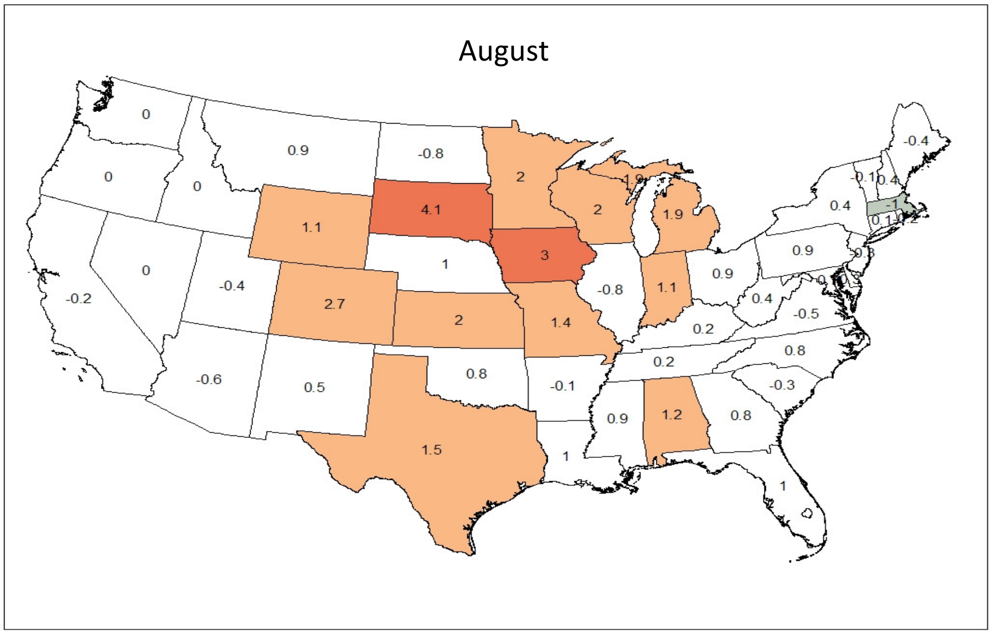


**Figure A.2 (continued) –** CGCM3 monthly model error in terms of F2+ tornado days per decade and per month.

# APPENDIX B

The maps and graphs in Appendix B represent the synoptic circulation patterns at the 500z, 700z and 850t levels of the atmosphere for the CGCM3 global climate model. The contours on the maps of 500z are at 60m intervals, 700z at 30m intervals, and 850t at 2°C intervals. The bar graphs represent the monthly frequency with which the patterns occurred in the GCM20c portion of the results and in the 2090s in the A2 and B1 scenarios. Note the change in the vertical axis with patterns that occur more than 50% of the time in any month. The associated tornado activity is in terms of the percentage point difference between actual tornado days and expected tornado days (as explained in section 4.2.1) represented in the legend below – which can be used with all maps in Appendix B.

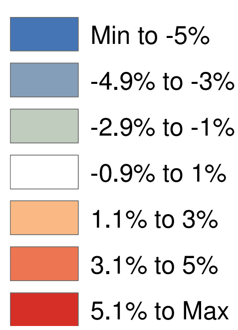

## *B.1 – 500z Patterns and Frequency*

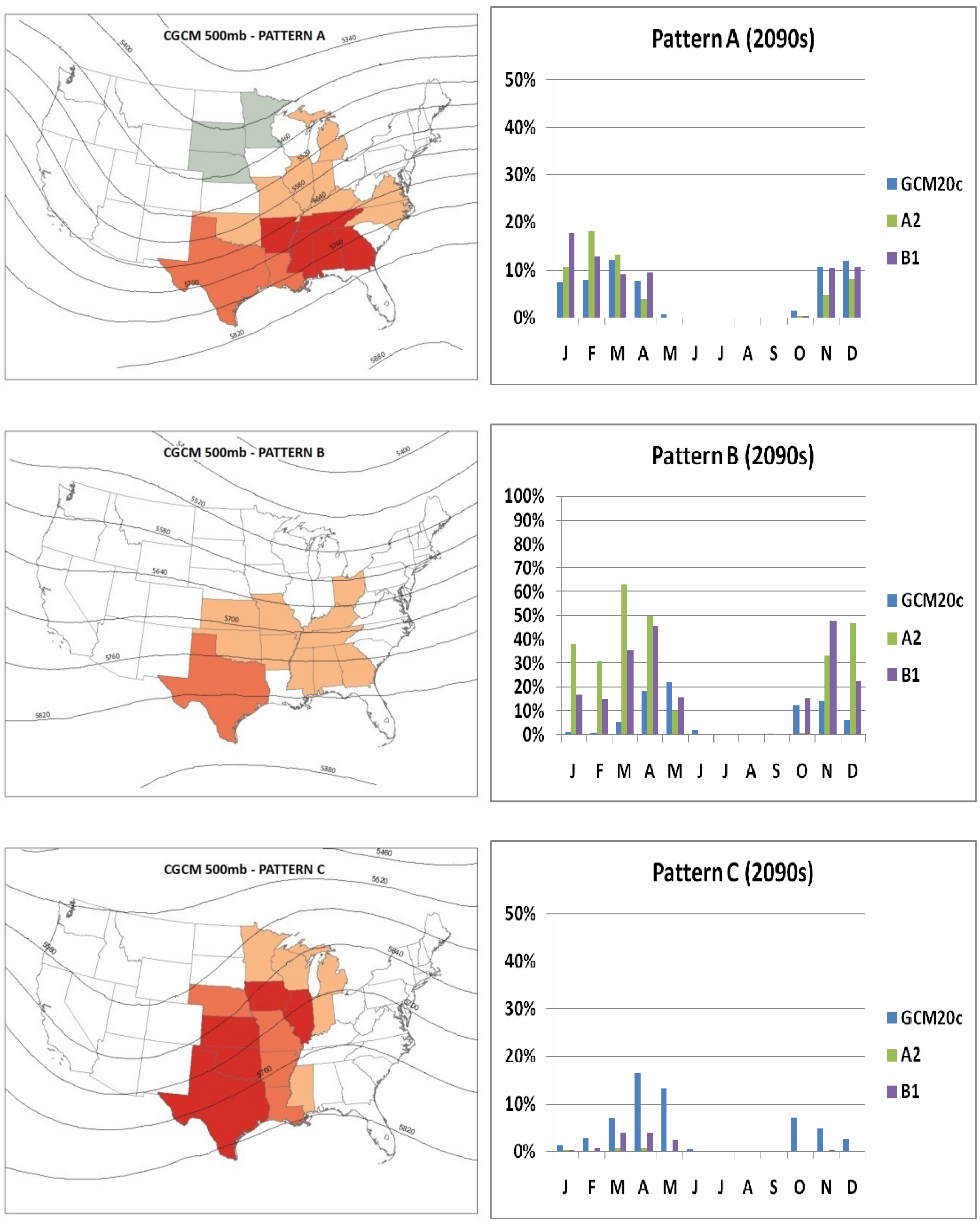


**Figure B.1** – The 15 atmospheric circulation patterns for CGCM3 at the 500z level, and their tornado association (left); and the frequency per month of these patterns in the GCM20c portion of the results and the 2090s under the A2 and B1 scenarios (right). Continued on the next page.

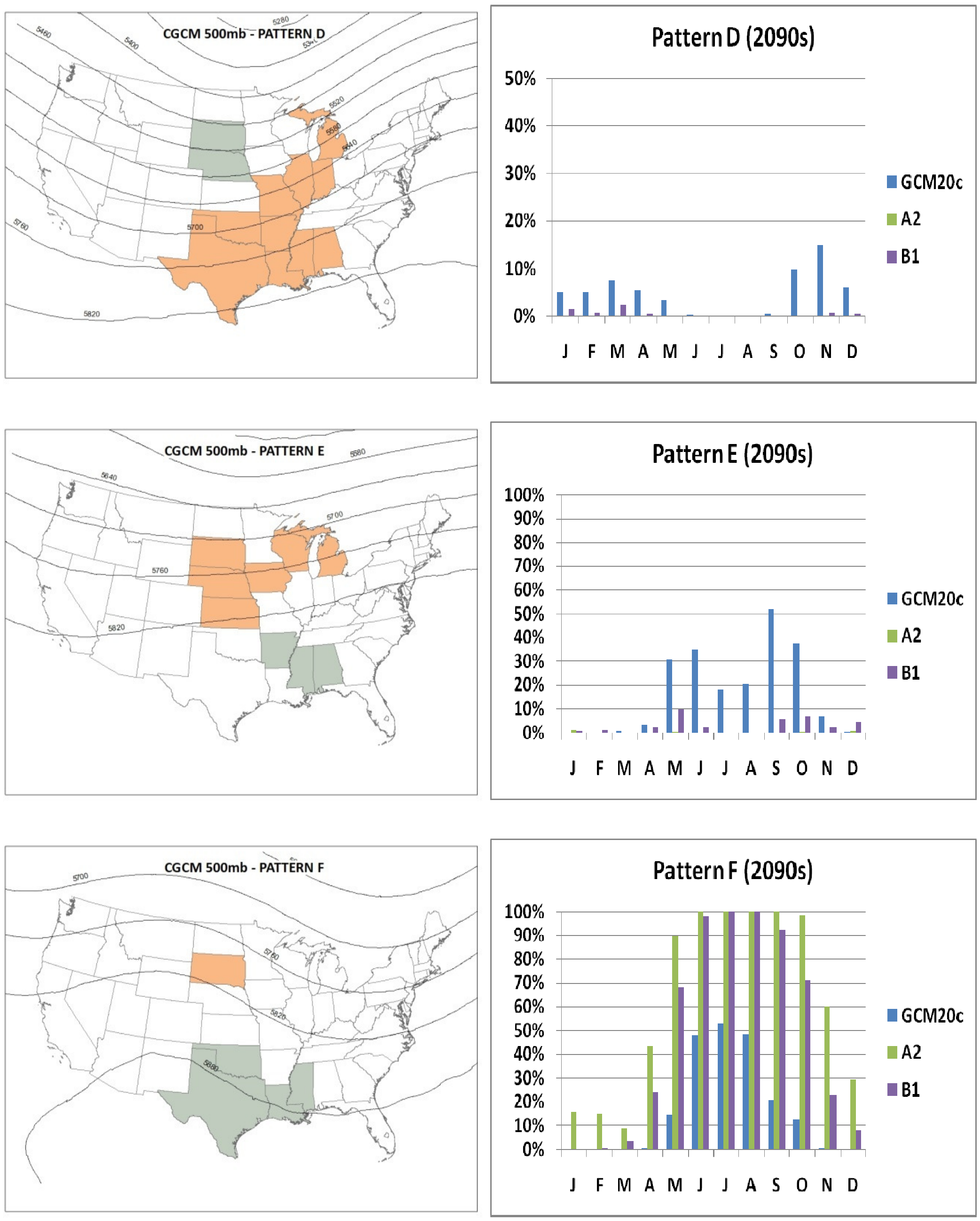


**Figure B.1 (continued)** – The 15 atmospheric circulation patterns for CGCM3 at the 500z level, and their tornado association (left); and the frequency per month of these patterns in the GCM20c portion of the results and the 2090s under the A2 and B1 scenarios (right). Continued on the next page.

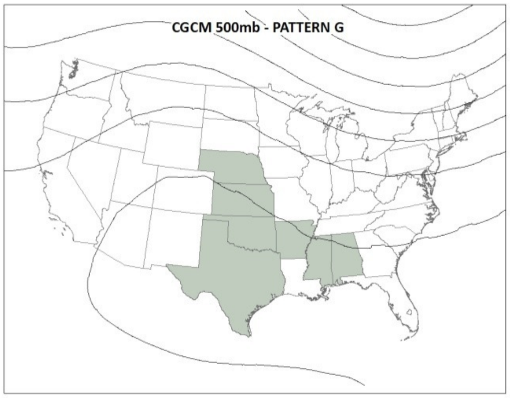


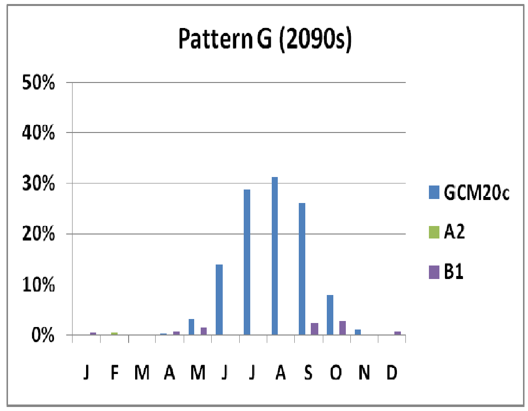


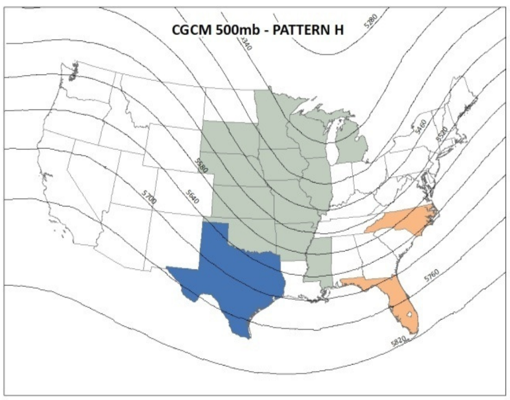


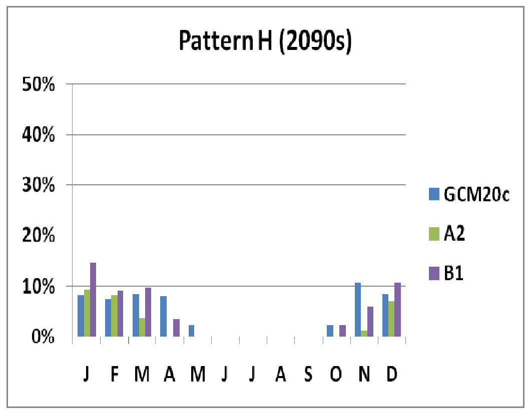


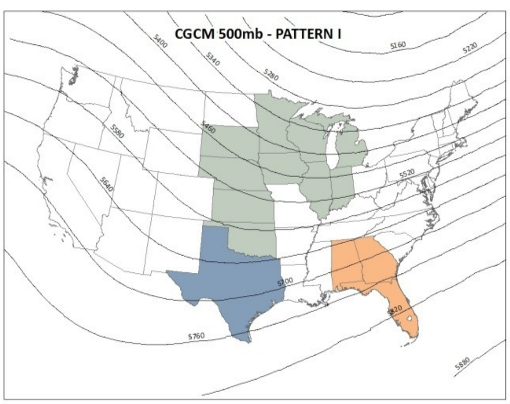


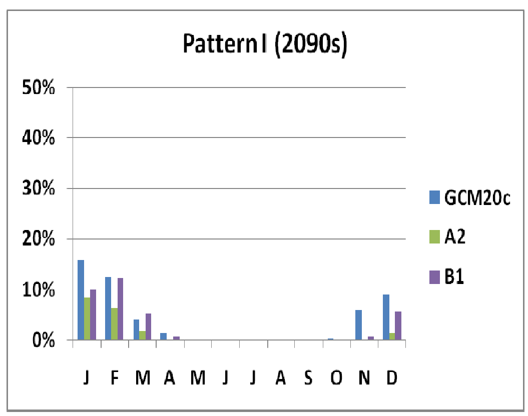


**Figure B.1 (continued)** – The 15 atmospheric circulation patterns for CGCM3 at the 500z level, and their tornado association (left); and the frequency per month of these patterns in the GCM20c portion of the results and the 2090s under the A2 and B1 scenarios (right). Continued on the next page.

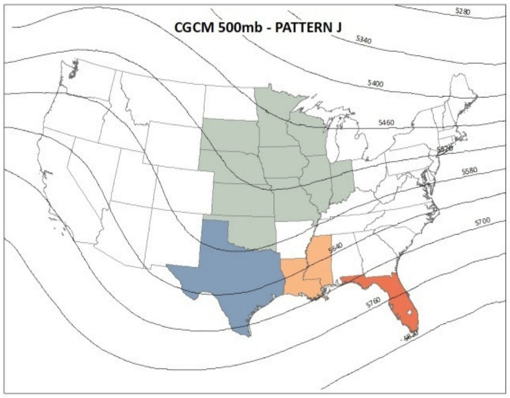


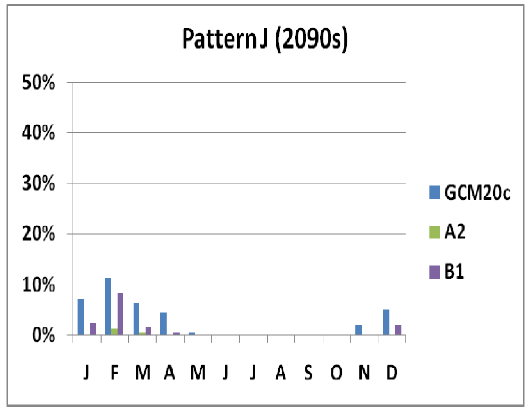


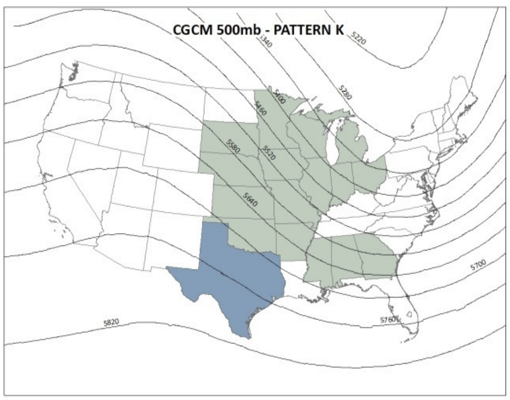


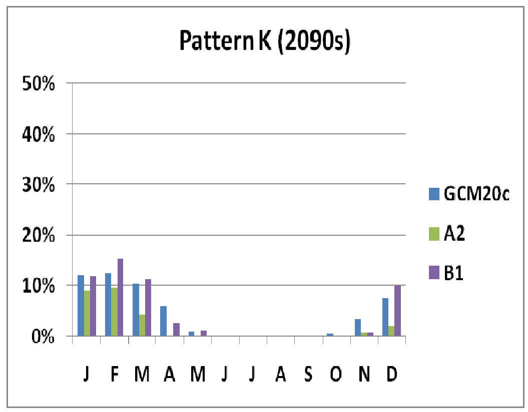


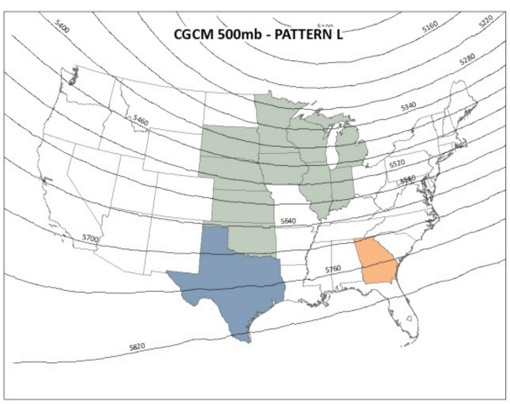


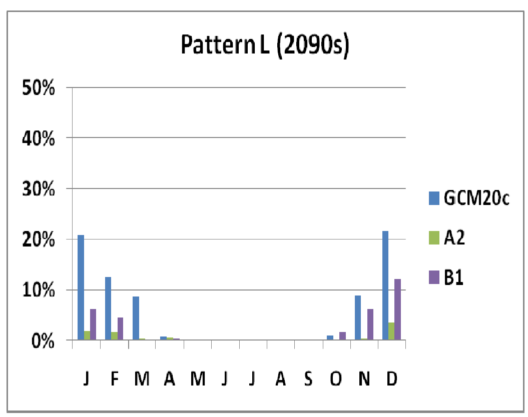


**Figure B.1 (continued)** – The 15 atmospheric circulation patterns for CGCM3 at the 500z level, and their tornado association (left); and the frequency per month of these patterns in the GCM20c portion of the results and the 2090s under the A2 and B1 scenarios (right). Continued on the next page.

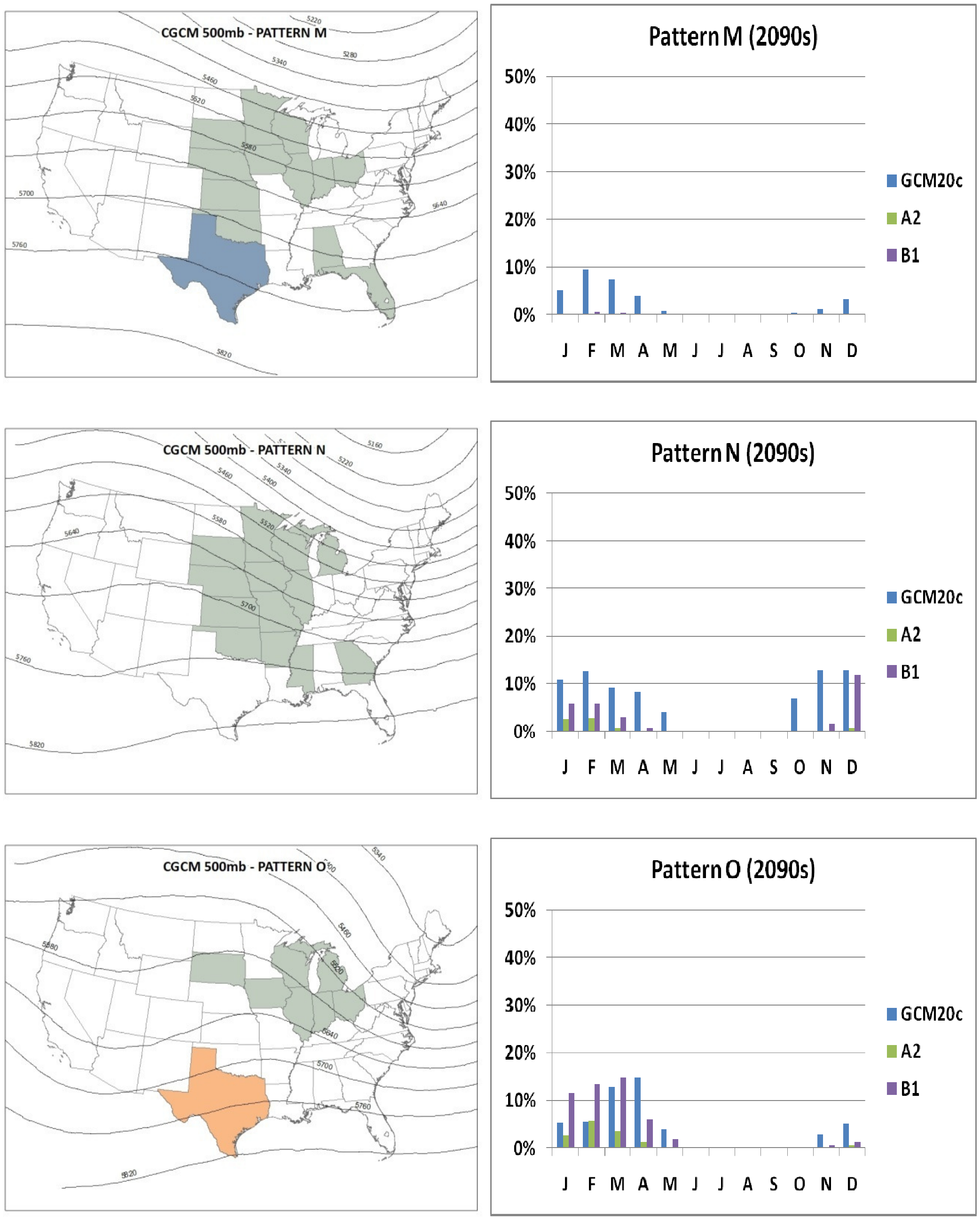


**Figure B.1 (continued)** – The 15 atmospheric circulation patterns for CGCM3 at the 500z level, and their tornado association (left); and the frequency per month of these patterns in the GCM20c portion of the results and the 2090s under the A2 and B1 scenarios (right).

*B.2 – 700z Patterns and Frequency*

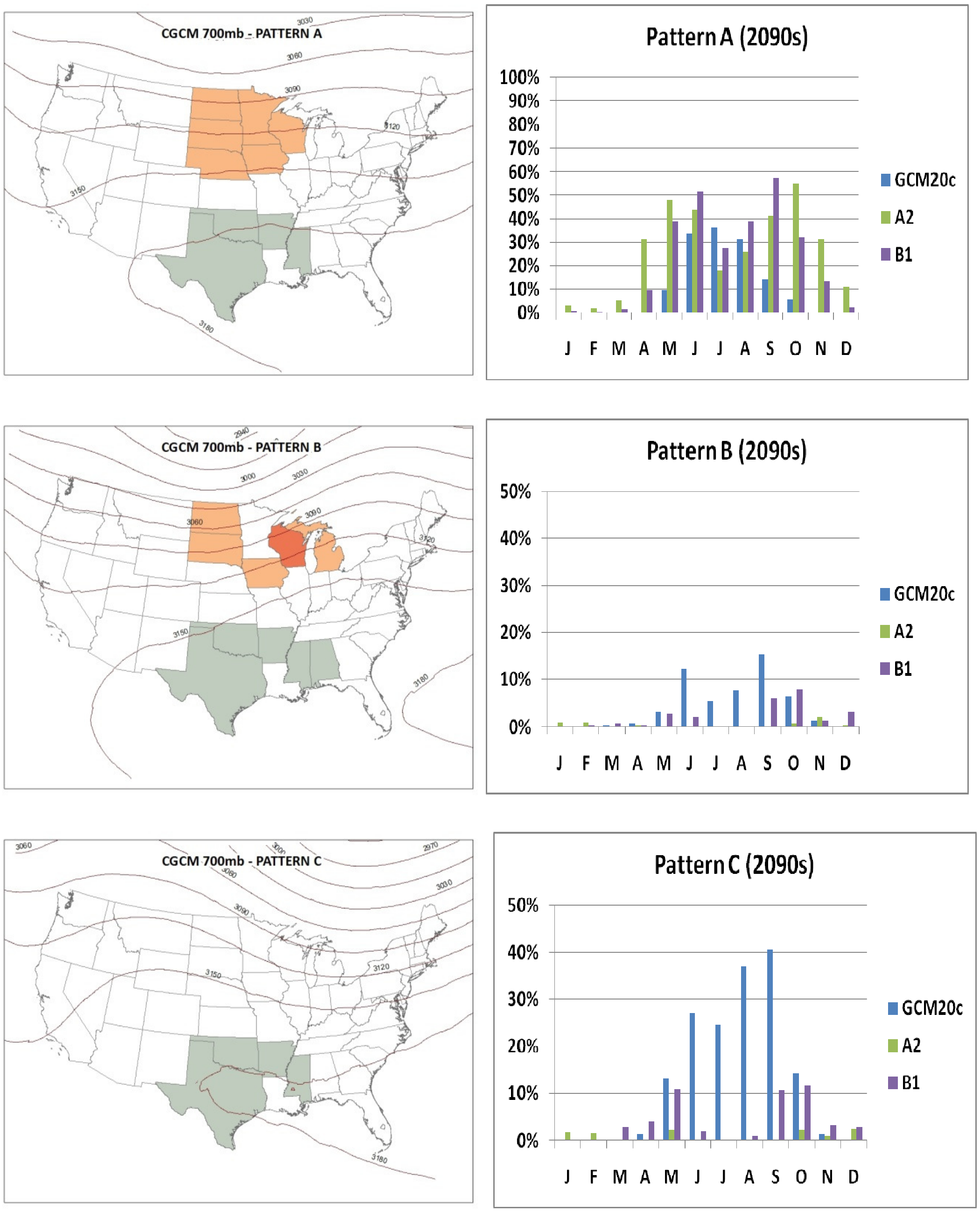


**Figure B.2** – The 15 atmospheric circulation patterns for CGCM3 at the 700z level, and their tornado association (left); and the frequency per month of these patterns in the GCM20c portion of the results and the 2090s under the A2 and B1 scenarios (right). Continued on the next page.

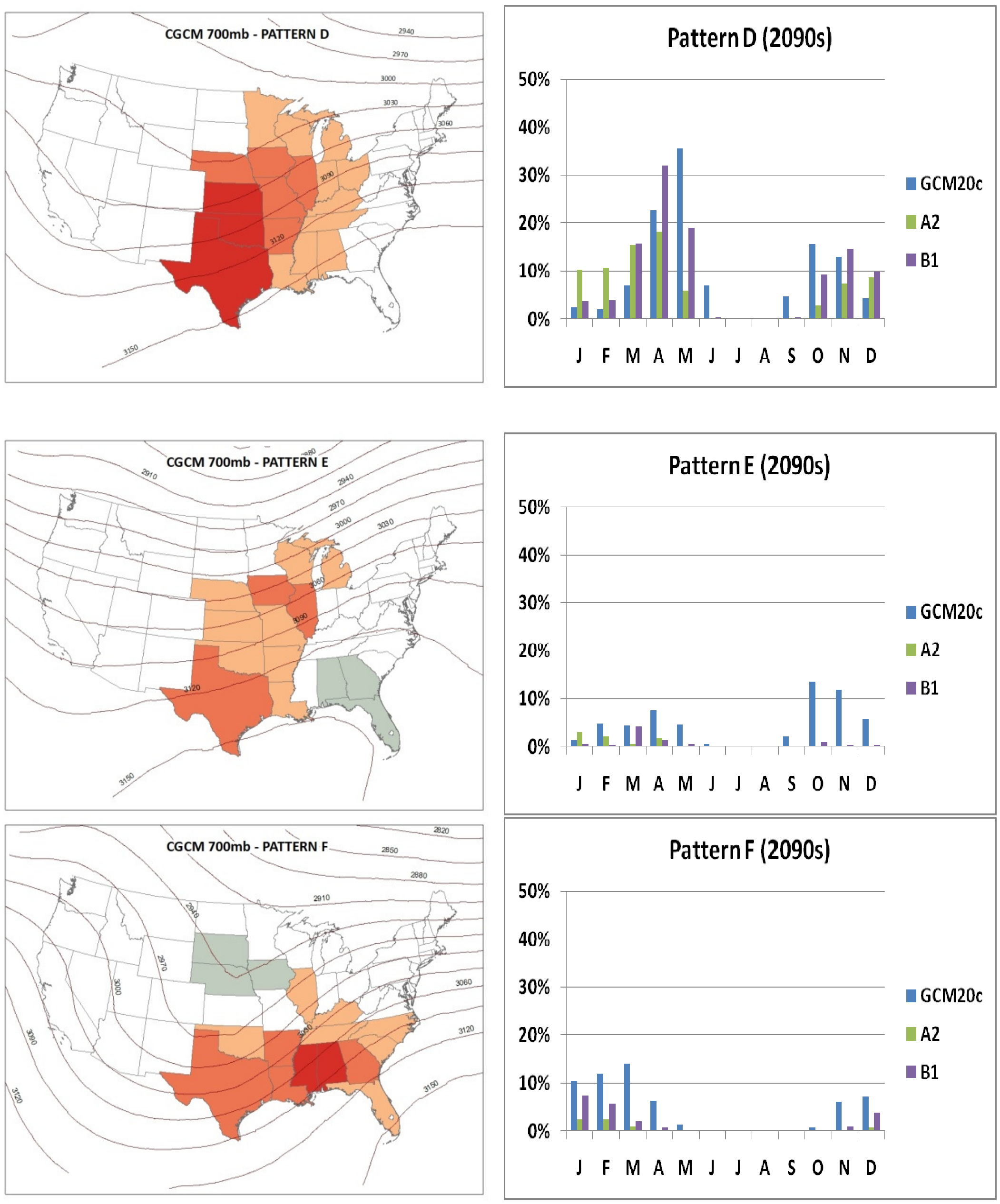


**Figure B.2 (continued)** – The 15 atmospheric circulation patterns for CGCM3 at the 700z level, and their tornado association (left); and the frequency per month of these patterns in the GCM20c portion of the results and the 2090s under the A2 and B1 scenarios (right). Continued on the next page.

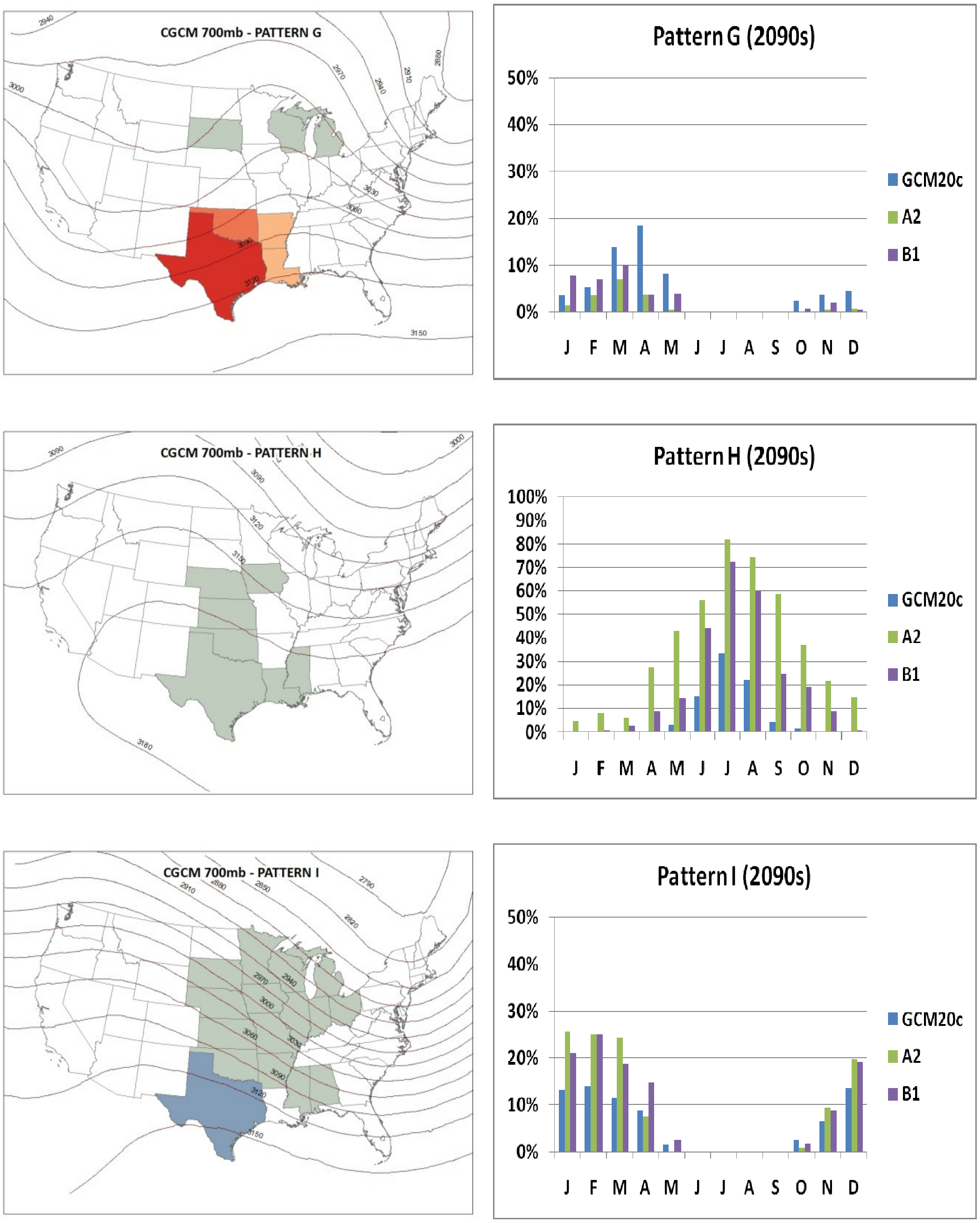


**Figure B.2 (continued)** – The 15 atmospheric circulation patterns for CGCM3 at the 700z level, and their tornado association (left); and the frequency per month of these patterns in the GCM20c portion of the results and the 2090s under the A2 and B1 scenarios (right). Continued on the next page.

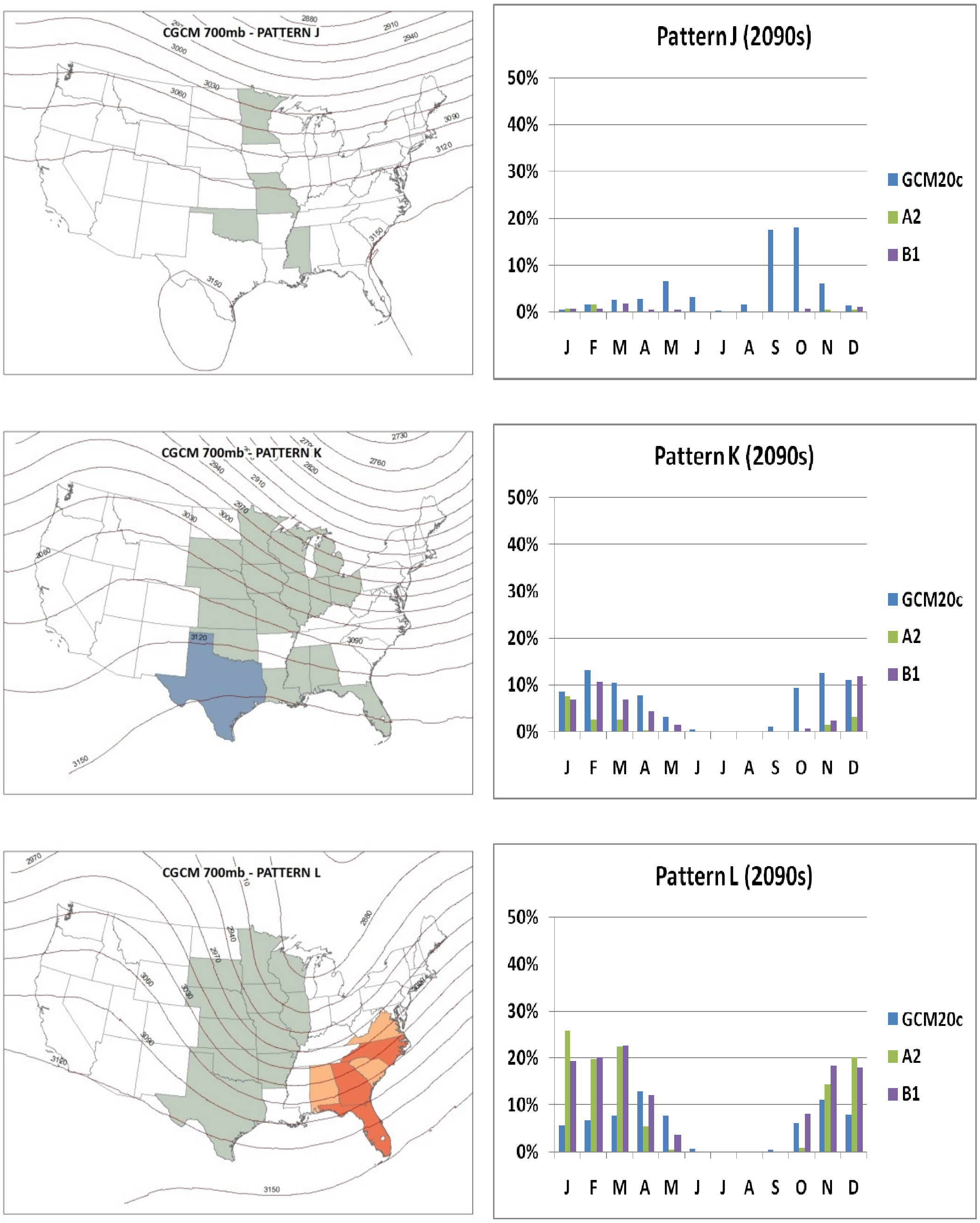


**Figure B.2 (continued)** – The 15 atmospheric circulation patterns for CGCM3 at the 700z level, and their tornado association (left); and the frequency per month of these patterns in the GCM20c portion of the results and the 2090s under the A2 and B1 scenarios (right). Continued on the next page.

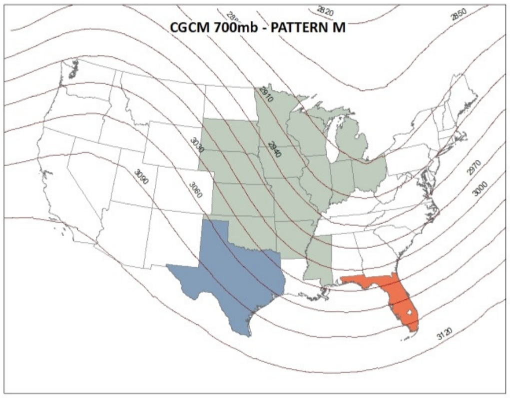


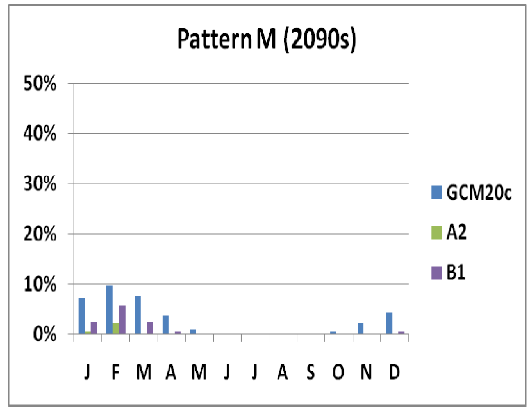


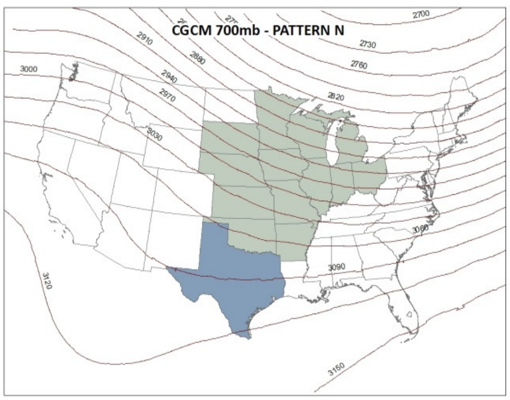


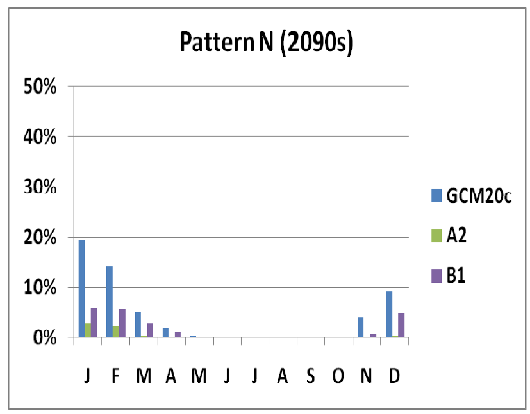


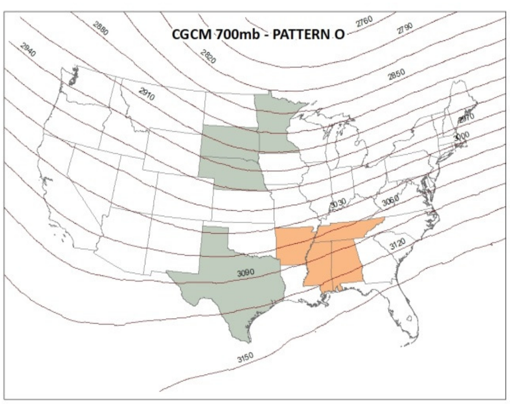


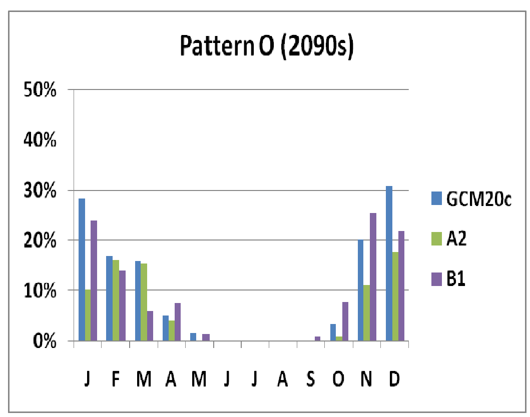


**Figure B.2 (continued)** – The 15 atmospheric circulation patterns for CGCM3 at the 700z level, and their tornado association (left); and the frequency per month of these patterns in the GCM20c portion of the results and the 2090s under the A2 and B1 scenarios (right).

## *B.3 – 850t Patterns and Frequency*

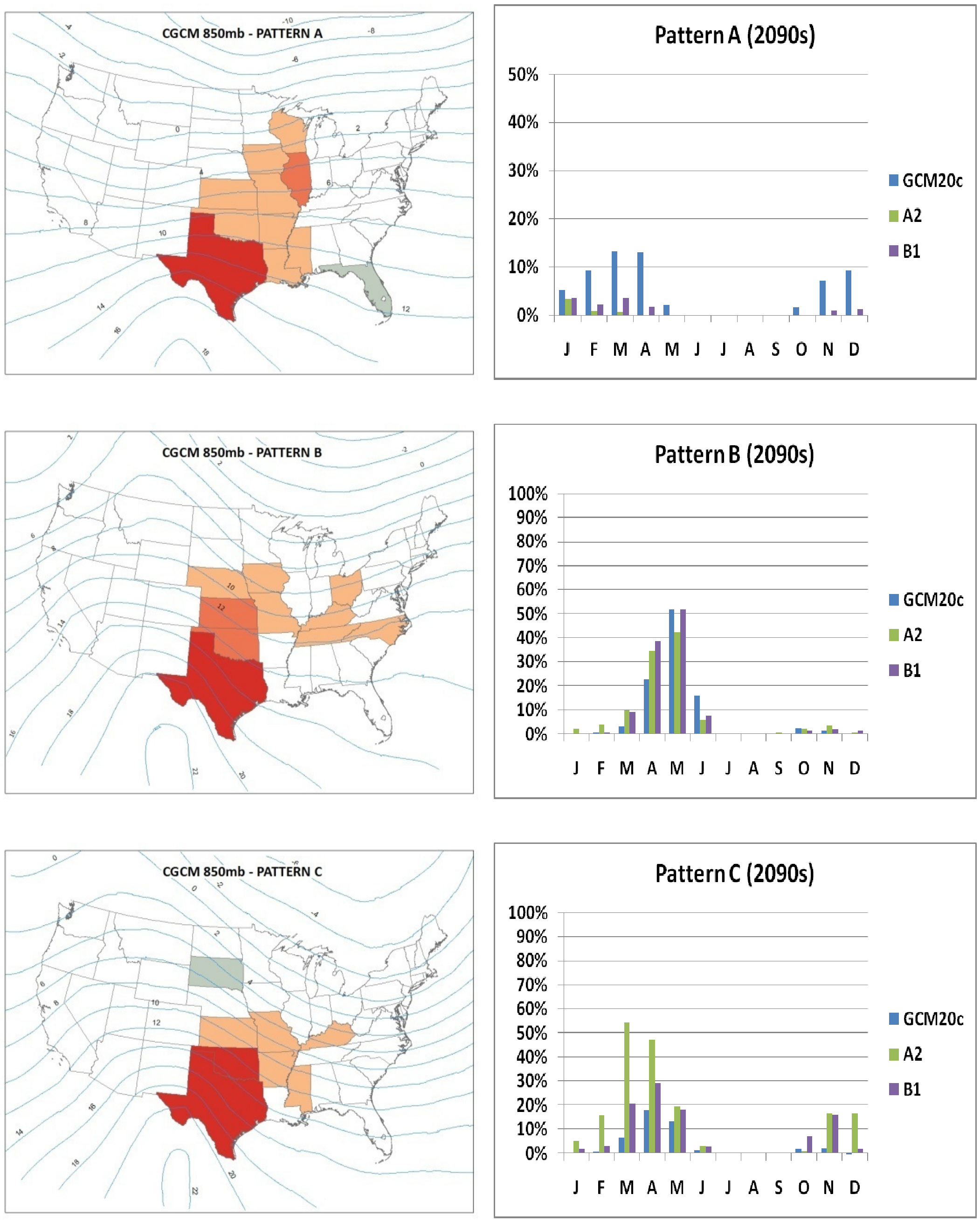


**Figure B.3** – The 15 atmospheric circulation patterns for CGCM3 at the 850t level, and their tornado association (left); and the frequency per month of these patterns in the GCM20c portion of the results and the 2090s under the A2 and B1 scenarios (right). Continued on the next page.

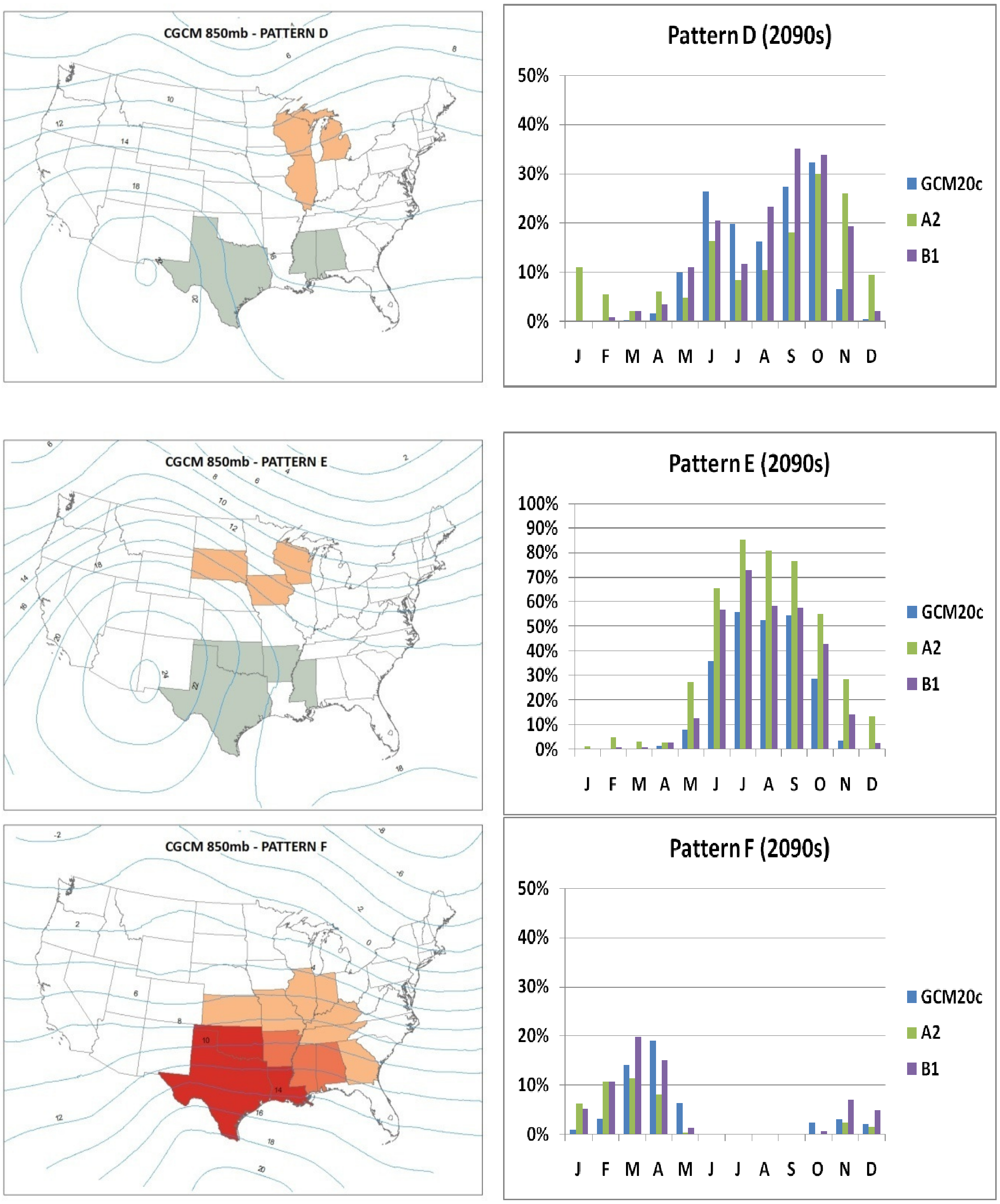


**Figure B.3 (continued)** – The 15 atmospheric circulation patterns for CGCM3 at the 850t level, and their tornado association (left); and the frequency per month of these patterns in the GCM20c portion of the results and the 2090s under the A2 and B1 scenarios (right). Continued on the next page.

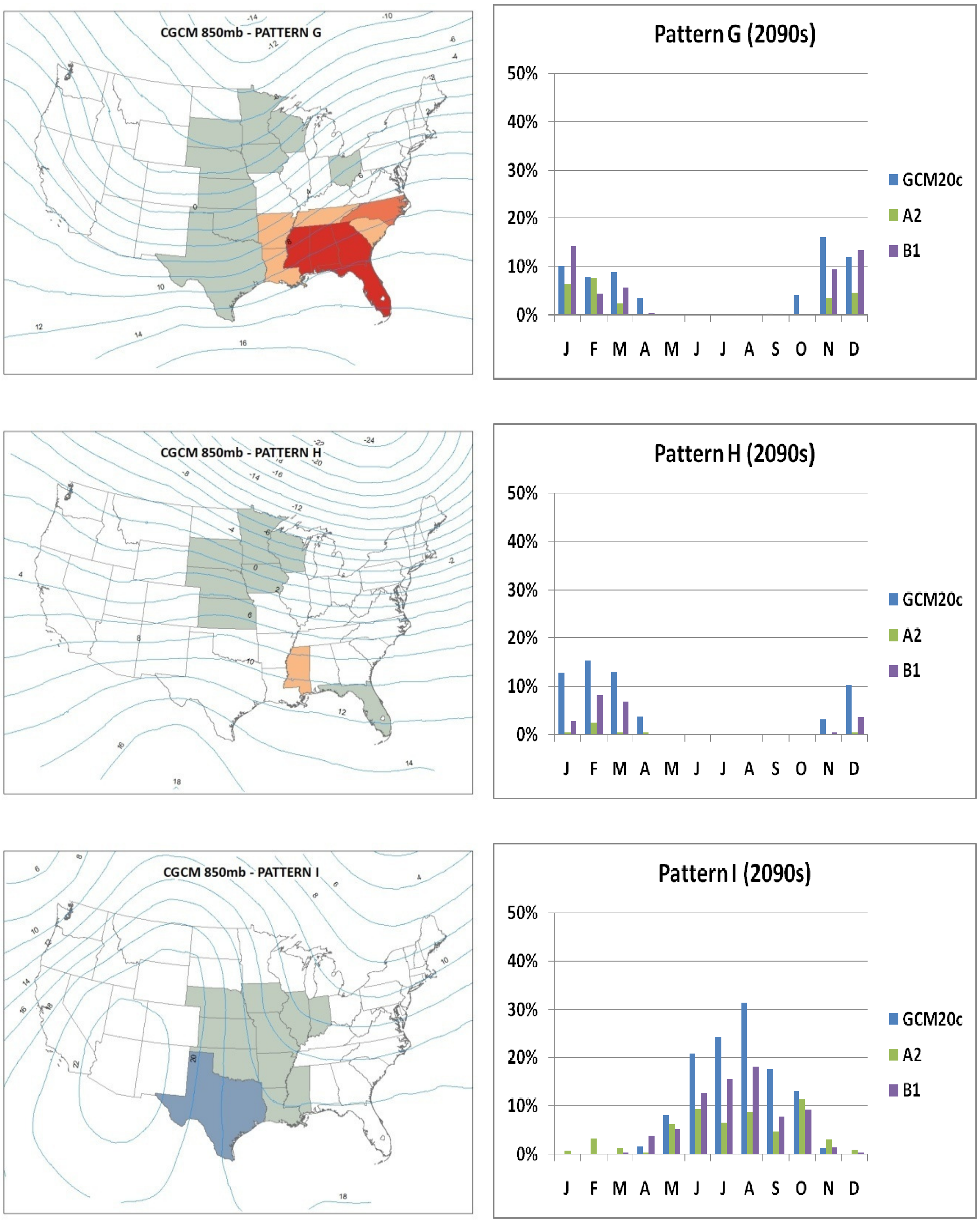


**Figure B.3 (continued)** – The 15 atmospheric circulation patterns for CGCM3 at the 850t level, and their tornado association (left); and the frequency per month of these patterns in the GCM20c portion of the results and the 2090s under the A2 and B1 scenarios (right). Continued on the next page.

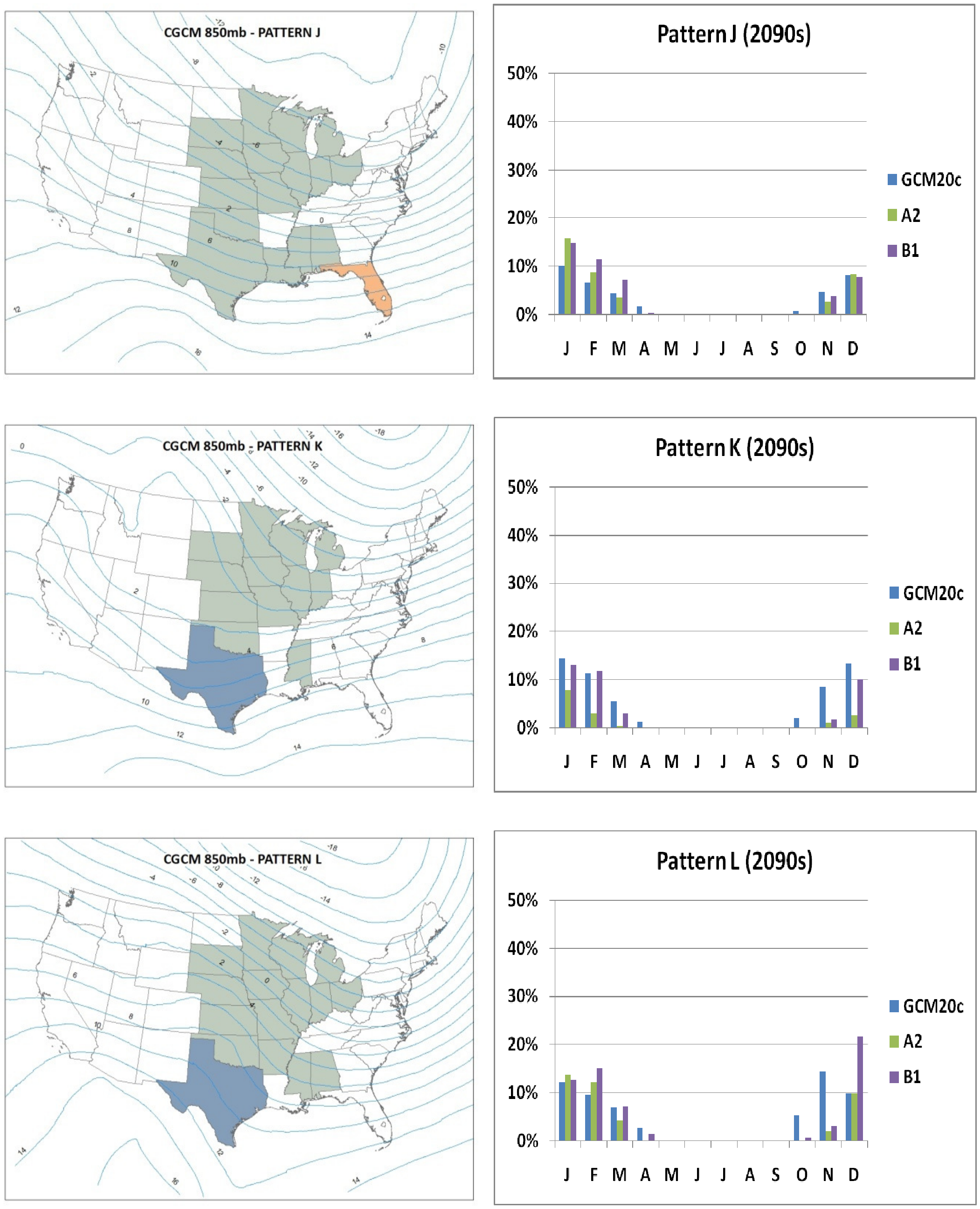


**Figure B.3 (continued)** – The 15 atmospheric circulation patterns for CGCM3 at the 850t level, and their tornado association (left); and the frequency per month of these patterns in the GCM20c portion of the results and the 2090s under the A2 and B1 scenarios (right). Continued on the next page.

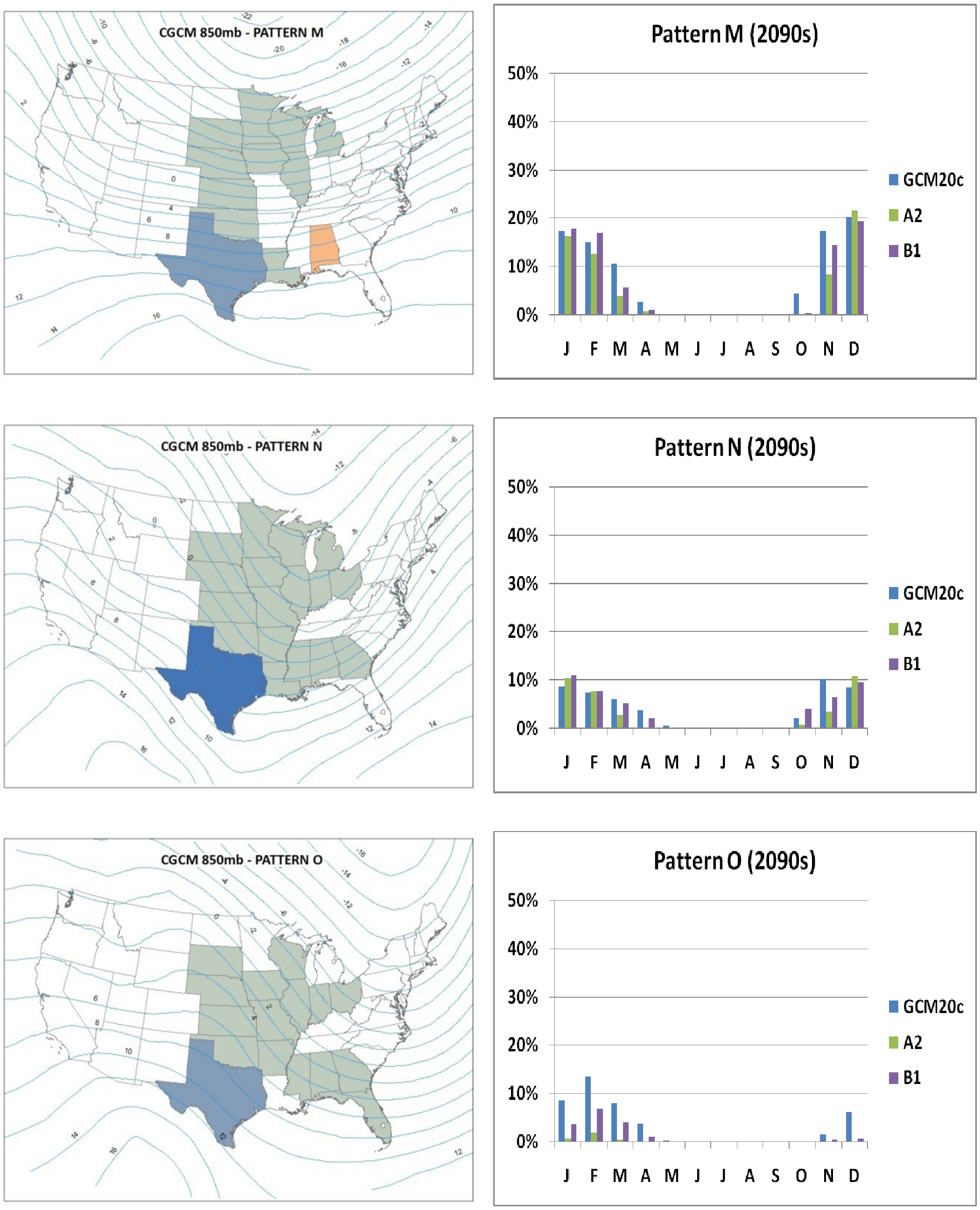


**Figure B.3 (continued)** – The 15 atmospheric circulation patterns for CGCM3 at the 850t level, and their tornado association (left); and the frequency per month of these patterns in the GCM20c portion of the results and the 2090s under the A2 and B1 scenarios (right).

# APPENDIX C

As mentioned in section 4.3, due to the method used, the atmospehric circulation patterns created in the 20th Century could be considered identical in shape to the patterns representing the future of each GCM. The tables in Appendix C are provided as evidence and are representing the similarities between the future patterns and the 20th Century patterns created with the CCSM3 global climate model. The top table on each page is a matrix of the pearson correlation coefficients between the GCM20c patterns (rows) and the GCM-Future patterns columns. The bottom table on each page is a matrix of the mean absolue error (MAE) between each of the GCM20c patterns and the GCM-Future. MAE values for 500z and 700z patterns are in terms of meters, while the MAE of the 850t patterns are in °C. The green boxes denote the correct corresponding pattern.

**Table C.1** – The Pearson correlation coeffecients (top) and the Mean Absolute Error (MAE; bottom) between the GCM20c and the GCM-Future portions of the CCSM3 – A1FI – 500mb geopotential heights. MAE in terms of meters.

| PEARSON | FUTURE-A | FUTURE-B | FUTURE-C | FUTURE-D | FUTURE-E | FUTURE-F | FUTURE-G | FUTURE-H | FUTURE-I | FUTURE-J | FUTURE-K | FUTURE-L | FUTURE-M | FUTURE-N | FUTURE-O |
|---|---|---|---|---|---|---|---|---|---|---|---|---|---|---|---|
| GCM20C-A | 0.9981 | 0.8892 | 0.9292 | 0.9587 | 0.9677 | 0.8855 | 0.9166 | 0.9365 | 0.8055 | 0.8557 | 0.7636 | 0.8032 | 0.7491 | 0.7776 | 0.9077 |
| GCM20C-B | 0.8784 | 0.9961 | 0.9016 | 0.8431 | 0.9267 | 0.9562 | 0.9202 | 0.9194 | 0.9444 | 0.8444 | 0.9353 | 0.8979 | 0.9044 | 0.9061 | 0.8722 |
| GCM20C-C | 0.9357 | 0.8974 | 0.9988 | 0.9185 | 0.9275 | 0.9502 | 0.9291 | 0.9656 | 0.8346 | 0.9403 | 0.8589 | 0.8385 | 0.8824 | 0.8320 | 0.8739 |
| GCM20C-D | 0.9687 | 0.8530 | 0.9362 | 0.9992 | 0.9442 | 0.9062 | 0.9648 | 0.9583 | 0.8374 | 0.8988 | 0.8273 | 0.8776 | 0.7828 | 0.8278 | 0.9660 |
| GCM20C-E | 0.9854 | 0.9343 | 0.9533 | 0.9472 | 0.9969 | 0.9431 | 0.9503 | 0.9702 | 0.8805 | 0.9242 | 0.8414 | 0.8452 | 0.8586 | 0.8706 | 0.9215 |
| GCM20C-F | 0.9064 | 0.9544 | 0.9421 | 0.9005 | 0.9490 | 0.9975 | 0.9555 | 0.9468 | 0.9139 | 0.9222 | 0.9247 | 0.9121 | 0.9260 | 0.9217 | 0.9165 |
| GCM20C-G | 0.9009 | 0.8999 | 0.9269 | 0.9535 | 0.9286 | 0.9563 | 0.9962 | 0.9717 | 0.9444 | 0.9337 | 0.9545 | 0.9596 | 0.9022 | 0.9408 | 0.9694 |
| GCM20C-H | 0.9406 | 0.9278 | 0.9750 | 0.9488 | 0.9622 | 0.9641 | 0.9853 | 0.9983 | 0.9325 | 0.9620 | 0.9326 | 0.9166 | 0.9255 | 0.9242 | 0.9410 |
| GCM20C-I | 0.7858 | 0.9108 | 0.8152 | 0.8161 | 0.8740 | 0.9068 | 0.9303 | 0.8991 | 0.9972 | 0.8621 | 0.9761 | 0.9291 | 0.9298 | 0.9814 | 0.8850 |
| GCM20C-J | 0.8779 | 0.8454 | 0.9364 | 0.8990 | 0.9234 | 0.9445 | 0.9489 | 0.9593 | 0.8901 | 0.9987 | 0.8904 | 0.8537 | 0.9422 | 0.9294 | 0.8896 |
| GCM20C-K | 0.7574 | 0.8963 | 0.8351 | 0.8111 | 0.8368 | 0.9225 | 0.9283 | 0.8935 | 0.9712 | 0.8601 | 0.9980 | 0.9591 | 0.9385 | 0.9624 | 0.8823 |
| GCM20C-L | 0.8083 | 0.8920 | 0.8433 | 0.8743 | 0.8618 | 0.9194 | 0.9480 | 0.9026 | 0.9415 | 0.8384 | 0.9715 | 0.9972 | 0.8813 | 0.9305 | 0.9429 |
| GCM20C-M | 0.7572 | 0.8767 | 0.8736 | 0.7744 | 0.8480 | 0.9329 | 0.8985 | 0.9022 | 0.9370 | 0.9299 | 0.9613 | 0.8812 | 0.9953 | 0.9614 | 0.8183 |
| GCM20C-N | 0.7915 | 0.8821 | 0.8238 | 0.8244 | 0.8895 | 0.9260 | 0.9331 | 0.9007 | 0.9730 | 0.9108 | 0.9520 | 0.9105 | 0.9517 | 0.9969 | 0.8875 |
| GCM20C-O | 0.9184 | 0.8890 | 0.9115 | 0.9744 | 0.9372 | 0.9367 | 0.9892 | 0.9607 | 0.9153 | 0.9021 | 0.9192 | 0.9644 | 0.8541 | 0.9093 | 0.9961 |

| MAE | FUTURE-A | FUTURE-B | FUTURE-C | FUTURE-D | FUTURE-E | FUTURE-F | FUTURE-G | FUTURE-H | FUTURE-I | FUTURE-J | FUTURE-K | FUTURE-L | FUTURE-M | FUTURE-N | FUTURE-O |
|---|---|---|---|---|---|---|---|---|---|---|---|---|---|---|---|
| GCM20C-A | 15.9834 | 85.4501 | 115.7246 | 116.1641 | 70.6353 | 92.5150 | 101.0755 | 115.4212 | 133.6543 | 121.6377 | 158.5911 | 157.4310 | 139.9293 | 125.2649 | 187.7881 |
| GCM20C-B | 84.5242 | 35.1683 | 126.8050 | 134.3044 | 79.5579 | 66.1184 | 101.6043 | 123.9108 | 92.0042 | 125.9046 | 109.5585 | 140.3721 | 96.6164 | 88.4985 | 187.5956 |
| GCM20C-C | 93.6505 | 107.8099 | 36.2674 | 178.6807 | 138.0284 | 83.1313 | 84.2998 | 67.6922 | 126.8785 | 77.9373 | 122.4485 | 206.6498 | 107.1785 | 126.0757 | 247.7499 |
| GCM20C-D | 104.7335 | 143.0098 | 184.8260 | 26.1797 | 67.6477 | 145.4747 | 154.1995 | 179.6007 | 182.2341 | 168.8342 | 195.6584 | 81.2033 | 180.2363 | 163.8043 | 100.8674 |
| GCM20C-E | 74.6202 | 103.2715 | 159.1490 | 65.1467 | 24.8521 | 113.4802 | 135.4390 | 155.7870 | 152.4780 | 142.3003 | 173.7641 | 100.8725 | 145.5461 | 133.6170 | 127.2429 |
| GCM20C-F | 74.4484 | 50.2210 | 99.8516 | 145.5692 | 89.6079 | 20.0136 | 77.2521 | 102.9043 | 89.5443 | 90.9032 | 102.5116 | 160.6159 | 76.8944 | 71.0117 | 206.6118 |
| GCM20C-G | 100.6391 | 102.0657 | 96.1800 | 161.6679 | 127.8199 | 76.5846 | 28.4757 | 68.1240 | 79.4474 | 82.2571 | 74.8876 | 177.9457 | 97.4246 | 82.8016 | 227.8711 |
| GCM20C-H | 92.2787 | 103.0804 | 79.3111 | 157.9750 | 121.3627 | 86.6699 | 55.8016 | 55.3892 | 98.2414 | 75.0500 | 96.9511 | 179.5789 | 98.6688 | 102.7899 | 224.7224 |
| GCM20C-I | 127.7200 | 89.1951 | 142.4868 | 171.8217 | 126.3584 | 90.7573 | 83.9572 | 113.2229 | 43.2726 | 114.3648 | 65.2325 | 169.4634 | 81.4419 | 54.4706 | 222.1021 |
| GCM20C-J | 107.2971 | 117.7097 | 90.5936 | 170.3861 | 127.5967 | 80.2050 | 71.8533 | 76.9319 | 103.9891 | 25.0616 | 109.0427 | 193.0094 | 76.9095 | 86.1651 | 234.4352 |
| GCM20C-K | 153.5054 | 114.2643 | 140.0527 | 193.4563 | 157.4610 | 102.2781 | 89.8140 | 115.4352 | 70.8847 | 122.4016 | 36.7276 | 184.9422 | 88.9181 | 83.5585 | 242.9630 |
| GCM20C-L | 148.8119 | 147.8458 | 213.0324 | 73.9852 | 96.0064 | 155.6060 | 170.3176 | 202.3653 | 176.5581 | 191.2208 | 180.5883 | 32.9145 | 175.2245 | 158.6848 | 93.1459 |
| GCM20C-M | 135.1605 | 103.0885 | 127.4315 | 170.7781 | 126.9214 | 84.2670 | 103.3707 | 117.1247 | 89.1135 | 89.4957 | 81.8539 | 167.7550 | 48.6200 | 72.0699 | 218.7893 |
| GCM20C-N | 116.3768 | 85.8637 | 133.9872 | 168.9064 | 116.0087 | 69.1927 | 80.9209 | 112.2220 | 54.7526 | 90.4897 | 82.1236 | 172.9864 | 61.0237 | 20.1520 | 221.9294 |
| GCM20C-O | 212.8702 | 230.9186 | 290.0031 | 94.5008 | 153.1188 | 240.7185 | 257.0598 | 283.7290 | 269.2209 | 266.6524 | 278.6793 | 78.3206 | 262.2626 | 248.3761 | 33.7251 |

**Table C.2** – The Pearson correlation coeffecients (top) and the Mean Absolute Error (MAE; bottom) between the GCM20c and the GCM-Future portions of the CCSM3 – A2 – 500mb geopotential heights. MAE in terms of meters.

| PEARSON | FUTURE-A | FUTURE-B | FUTURE-C | FUTURE-D | FUTURE-E | FUTURE-F | FUTURE-G | FUTURE-H | FUTURE-I | FUTURE-J | FUTURE-K | FUTURE-L | FUTURE-M | FUTURE-N | FUTURE-O |
|---|---|---|---|---|---|---|---|---|---|---|---|---|---|---|---|
| GCM20C-A | 0.9991 | 0.8928 | 0.9431 | 0.9658 | 0.9696 | 0.8996 | 0.9283 | 0.9474 | 0.8166 | 0.8752 | 0.7806 | 0.8130 | 0.7682 | 0.7920 | 0.9130 |
| GCM20C-B | 0.8826 | 0.9972 | 0.9033 | 0.8444 | 0.9295 | 0.9554 | 0.9189 | 0.9199 | 0.9409 | 0.8430 | 0.9312 | 0.8967 | 0.9017 | 0.9024 | 0.8725 |
| GCM20C-C | 0.9323 | 0.8987 | 0.9984 | 0.9171 | 0.9264 | 0.9525 | 0.9313 | 0.9666 | 0.8401 | 0.9428 | 0.8658 | 0.8437 | 0.8886 | 0.8381 | 0.8747 |
| GCM20C-D | 0.9700 | 0.8502 | 0.9239 | 0.9982 | 0.9457 | 0.8982 | 0.9598 | 0.9507 | 0.8317 | 0.8865 | 0.8152 | 0.8722 | 0.7679 | 0.8208 | 0.9669 |
| GCM20C-E | 0.9851 | 0.9320 | 0.9509 | 0.9435 | 0.9969 | 0.9390 | 0.9451 | 0.9672 | 0.8743 | 0.9212 | 0.8334 | 0.8382 | 0.8545 | 0.8647 | 0.9174 |
| GCM20C-F | 0.9003 | 0.9475 | 0.9456 | 0.8960 | 0.9440 | 0.9990 | 0.9541 | 0.9473 | 0.9106 | 0.9320 | 0.9241 | 0.9029 | 0.9324 | 0.9212 | 0.9085 |
| GCM20C-G | 0.9135 | 0.9093 | 0.9277 | 0.9591 | 0.9405 | 0.9604 | 0.9981 | 0.9729 | 0.9442 | 0.9316 | 0.9472 | 0.9553 | 0.8964 | 0.9392 | 0.9740 |
| GCM20C-H | 0.9474 | 0.9279 | 0.9773 | 0.9520 | 0.9660 | 0.9621 | 0.9839 | 0.9992 | 0.9270 | 0.9607 | 0.9250 | 0.9117 | 0.9195 | 0.9179 | 0.9412 |
| GCM20C-I | 0.7826 | 0.9116 | 0.8132 | 0.8116 | 0.8719 | 0.9057 | 0.9276 | 0.8968 | 0.9971 | 0.8593 | 0.9765 | 0.9283 | 0.9305 | 0.9809 | 0.8815 |
| GCM20C-J | 0.8833 | 0.8430 | 0.9382 | 0.9026 | 0.9256 | 0.9437 | 0.9477 | 0.9589 | 0.8829 | 0.9987 | 0.8824 | 0.8494 | 0.9362 | 0.9233 | 0.8899 |
| GCM20C-K | 0.7643 | 0.8999 | 0.8405 | 0.8161 | 0.8433 | 0.9260 | 0.9317 | 0.8985 | 0.9730 | 0.8656 | 0.9986 | 0.9607 | 0.9418 | 0.9650 | 0.8860 |
| GCM20C-L | 0.8098 | 0.8949 | 0.8381 | 0.8739 | 0.8653 | 0.9172 | 0.9486 | 0.9021 | 0.9462 | 0.8356 | 0.9707 | 0.9963 | 0.8792 | 0.9334 | 0.9444 |
| GCM20C-M | 0.7694 | 0.8837 | 0.8805 | 0.7827 | 0.8602 | 0.9396 | 0.9037 | 0.9086 | 0.9386 | 0.9370 | 0.9591 | 0.8807 | 0.9975 | 0.9639 | 0.8250 |
| GCM20C-N | 0.7406 | 0.8593 | 0.7932 | 0.7860 | 0.8464 | 0.9053 | 0.9103 | 0.8724 | 0.9689 | 0.8858 | 0.9614 | 0.9148 | 0.9516 | 0.9943 | 0.8619 |
| GCM20C-O | 0.9165 | 0.8806 | 0.9066 | 0.9759 | 0.9323 | 0.9300 | 0.9861 | 0.9561 | 0.9074 | 0.8957 | 0.9120 | 0.9624 | 0.8430 | 0.9013 | 0.9970 |

| MAE | FUTURE-A | FUTURE-B | FUTURE-C | FUTURE-D | FUTURE-E | FUTURE-F | FUTURE-G | FUTURE-H | FUTURE-I | FUTURE-J | FUTURE-K | FUTURE-L | FUTURE-M | FUTURE-N | FUTURE-O |
|---|---|---|---|---|---|---|---|---|---|---|---|---|---|---|---|
| GCM20C-A | 13.7066 | 83.9363 | 111.0897 | 114.4904 | 69.5446 | 87.6099 | 96.8029 | 111.7633 | 130.6314 | 115.5716 | 154.2537 | 155.7403 | 135.1178 | 121.4249 | 187.0115 |
| GCM20C-B | 82.5403 | 28.1074 | 121.9941 | 139.8324 | 83.1894 | 62.0695 | 98.4884 | 119.7185 | 88.4823 | 123.4189 | 106.9231 | 146.9488 | 93.8078 | 86.2014 | 194.1908 |
| GCM20C-C | 92.3358 | 104.8401 | 38.2393 | 176.0507 | 135.1065 | 79.6168 | 82.2678 | 67.6898 | 123.6848 | 75.6464 | 119.0325 | 203.0677 | 103.1187 | 122.1474 | 244.7764 |
| GCM20C-D | 107.7372 | 146.3143 | 190.2839 | 24.9278 | 69.3502 | 150.0128 | 158.5056 | 184.3022 | 186.0860 | 174.1631 | 200.5261 | 80.9181 | 185.3103 | 167.7817 | 97.7510 |
| GCM20C-E | 72.5778 | 101.5989 | 158.0052 | 67.6359 | 22.4841 | 112.1843 | 135.0835 | 155.0002 | 151.8503 | 141.3624 | 173.8259 | 103.3270 | 144.4945 | 132.7281 | 129.3881 |
| GCM20C-F | 76.6355 | 54.2644 | 98.8273 | 145.2140 | 90.1227 | 19.1143 | 77.9306 | 102.8076 | 91.2547 | 87.1077 | 102.8618 | 160.7272 | 74.6033 | 71.8392 | 206.1557 |
| GCM20C-G | 94.1174 | 96.1418 | 94.0447 | 161.2138 | 124.2436 | 71.3358 | 22.0384 | 66.1956 | 76.9421 | 81.7592 | 78.3414 | 179.3105 | 97.5080 | 80.5384 | 228.1864 |
| GCM20C-H | 89.6172 | 102.3327 | 73.9343 | 161.0190 | 122.7928 | 86.0177 | 53.8625 | 49.5005 | 98.4307 | 73.4487 | 98.7469 | 184.1056 | 99.5056 | 103.7583 | 228.6924 |
| GCM20C-I | 126.9796 | 86.5783 | 141.8712 | 172.3571 | 125.7423 | 88.8468 | 84.4770 | 113.5862 | 40.8573 | 114.2643 | 64.5394 | 169.8462 | 79.2361 | 51.7621 | 222.5959 |
| GCM20C-J | 104.3153 | 117.9929 | 91.6504 | 166.2184 | 124.2289 | 80.7660 | 73.7165 | 79.3383 | 107.9584 | 28.6190 | 113.6947 | 190.0627 | 80.9627 | 89.2107 | 230.6025 |
| GCM20C-K | 149.6813 | 109.9140 | 134.9277 | 193.9768 | 155.7335 | 97.0744 | 85.0457 | 110.4711 | 64.6435 | 117.4293 | 29.8873 | 186.9087 | 83.2693 | 77.7702 | 244.7841 |
| GCM20C-L | 147.3572 | 145.9799 | 212.7002 | 73.9117 | 94.1665 | 154.5633 | 168.9787 | 201.3122 | 174.4155 | 190.5443 | 179.5172 | 34.0051 | 174.2711 | 156.7967 | 93.7082 |
| GCM20C-M | 129.7032 | 97.2453 | 122.0581 | 170.5571 | 123.6419 | 77.0481 | 98.7096 | 112.2979 | 84.5108 | 83.2054 | 80.6581 | 169.7397 | 40.6705 | 65.8838 | 220.1336 |
| GCM20C-N | 126.9878 | 92.3226 | 145.4772 | 167.1348 | 118.6278 | 78.4242 | 93.2869 | 125.4036 | 62.1392 | 102.5290 | 81.3463 | 164.3847 | 63.8951 | 28.4457 | 215.8139 |
| GCM20C-O | 210.7872 | 229.0879 | 288.6860 | 91.8886 | 150.9106 | 238.9104 | 255.7205 | 282.6836 | 267.8481 | 265.4050 | 277.6993 | 76.2838 | 260.9726 | 246.6795 | 29.2220 |

**Table C.3** – The Pearson correlation coeffecients (top) and the Mean Absolute Error (MAE; bottom) between the GCM20c and the GCM-Future portions of the CCSM3 – B1 – 500mb geopotential heights. MAE in terms of meters.

| PEARSON | FUTURE-A | FUTURE-B | FUTURE-C | FUTURE-D | FUTURE-E | FUTURE-F | FUTURE-G | FUTURE-H | FUTURE-I | FUTURE-J | FUTURE-K | FUTURE-L | FUTURE-M | FUTURE-N | FUTURE-O |
|---|---|---|---|---|---|---|---|---|---|---|---|---|---|---|---|
| GCM20C-A | 0.9987 | 0.8965 | 0.9351 | 0.9610 | 0.9709 | 0.8945 | 0.9231 | 0.9421 | 0.8152 | 0.8633 | 0.7755 | 0.8114 | 0.7610 | 0.7879 | 0.9115 |
| GCM20C-B | 0.9009 | 0.9986 | 0.9175 | 0.8585 | 0.9411 | 0.9581 | 0.9236 | 0.9300 | 0.9340 | 0.8519 | 0.9228 | 0.8922 | 0.8983 | 0.8954 | 0.8783 |
| GCM20C-C | 0.9329 | 0.9005 | 0.9985 | 0.9194 | 0.9277 | 0.9543 | 0.9340 | 0.9679 | 0.8433 | 0.9433 | 0.8692 | 0.8480 | 0.8899 | 0.8412 | 0.8787 |
| GCM20C-D | 0.9693 | 0.8480 | 0.9284 | 0.9984 | 0.9458 | 0.9010 | 0.9619 | 0.9542 | 0.8334 | 0.8958 | 0.8180 | 0.8709 | 0.7753 | 0.8248 | 0.9654 |
| GCM20C-E | 0.9860 | 0.9301 | 0.9494 | 0.9484 | 0.9973 | 0.9376 | 0.9474 | 0.9677 | 0.8744 | 0.9192 | 0.8338 | 0.8434 | 0.8508 | 0.8645 | 0.9242 |
| GCM20C-F | 0.9028 | 0.9442 | 0.9505 | 0.8986 | 0.9406 | 0.9987 | 0.9524 | 0.9465 | 0.9030 | 0.9310 | 0.9198 | 0.9002 | 0.9273 | 0.9139 | 0.9060 |
| GCM20C-G | 0.9167 | 0.9012 | 0.9277 | 0.9645 | 0.9412 | 0.9566 | 0.9983 | 0.9734 | 0.9382 | 0.9343 | 0.9397 | 0.9517 | 0.8904 | 0.9352 | 0.9768 |
| GCM20C-H | 0.9551 | 0.9260 | 0.9769 | 0.9582 | 0.9707 | 0.9582 | 0.9837 | 0.9998 | 0.9213 | 0.9578 | 0.9159 | 0.9083 | 0.9098 | 0.9110 | 0.9453 |
| GCM20C-I | 0.8062 | 0.9212 | 0.8253 | 0.8304 | 0.8908 | 0.9115 | 0.9374 | 0.9094 | 0.9987 | 0.8664 | 0.9720 | 0.9301 | 0.9270 | 0.9800 | 0.8956 |
| GCM20C-J | 0.8817 | 0.8415 | 0.9398 | 0.9005 | 0.9238 | 0.9416 | 0.9457 | 0.9593 | 0.8815 | 0.9993 | 0.8818 | 0.8465 | 0.9370 | 0.9210 | 0.8869 |
| GCM20C-K | 0.7842 | 0.9081 | 0.8568 | 0.8342 | 0.8578 | 0.9342 | 0.9425 | 0.9123 | 0.9752 | 0.8761 | 0.9995 | 0.9649 | 0.9431 | 0.9656 | 0.8987 |
| GCM20C-L | 0.8117 | 0.8924 | 0.8425 | 0.8772 | 0.8655 | 0.9181 | 0.9498 | 0.9045 | 0.9434 | 0.8395 | 0.9703 | 0.9976 | 0.8800 | 0.9319 | 0.9461 |
| GCM20C-M | 0.7795 | 0.8825 | 0.8919 | 0.7919 | 0.8660 | 0.9426 | 0.9065 | 0.9153 | 0.9323 | 0.9454 | 0.9544 | 0.8788 | 0.9975 | 0.9594 | 0.8290 |
| GCM20C-N | 0.7484 | 0.8547 | 0.8128 | 0.7991 | 0.8480 | 0.9119 | 0.9193 | 0.8856 | 0.9674 | 0.9055 | 0.9654 | 0.9128 | 0.9588 | 0.9939 | 0.8652 |
| GCM20C-O | 0.9123 | 0.8719 | 0.9011 | 0.9757 | 0.9275 | 0.9237 | 0.9833 | 0.9521 | 0.9016 | 0.8918 | 0.9066 | 0.9608 | 0.8359 | 0.8964 | 0.9979 |

| MAE | FUTURE-A | FUTURE-B | FUTURE-C | FUTURE-D | FUTURE-E | FUTURE-F | FUTURE-G | FUTURE-H | FUTURE-I | FUTURE-J | FUTURE-K | FUTURE-L | FUTURE-M | FUTURE-N | FUTURE-O |
|---|---|---|---|---|---|---|---|---|---|---|---|---|---|---|---|
| GCM20C-A | 12.6087 | 81.7543 | 112.4725 | 117.4654 | 70.4670 | 88.1392 | 97.6908 | 112.4367 | 129.8741 | 118.3181 | 154.6540 | 157.6993 | 135.9436 | 121.4797 | 189.1365 |
| GCM20C-B | 75.1953 | 19.2264 | 114.1885 | 142.4580 | 83.4192 | 56.3565 | 94.4503 | 113.7748 | 87.2652 | 118.4038 | 107.4449 | 153.1075 | 91.7443 | 84.9867 | 199.2477 |
| GCM20C-C | 97.5886 | 107.8070 | 28.9224 | 185.1319 | 143.0818 | 81.3033 | 80.7899 | 62.7838 | 122.5212 | 75.0925 | 116.8407 | 211.8154 | 103.4515 | 122.9241 | 254.2258 |
| GCM20C-D | 106.6243 | 145.4936 | 188.3413 | 25.0908 | 68.2241 | 148.2680 | 156.9245 | 182.5257 | 184.6841 | 171.3141 | 199.0252 | 81.5737 | 183.0497 | 165.9522 | 98.8584 |
| GCM20C-E | 71.4146 | 100.0459 | 158.5630 | 66.4100 | 17.0223 | 110.8546 | 134.8045 | 155.7531 | 150.8290 | 141.7233 | 173.3759 | 101.9939 | 143.9094 | 130.9243 | 128.5045 |
| GCM20C-F | 75.5063 | 56.2360 | 97.6178 | 143.3728 | 89.8554 | 21.2624 | 79.0955 | 103.6150 | 94.6899 | 87.9270 | 104.8982 | 159.6124 | 77.4032 | 75.3963 | 204.8568 |
| GCM20C-G | 97.0839 | 103.4305 | 94.2958 | 164.2022 | 128.9527 | 77.6648 | 22.0759 | 64.2727 | 82.3165 | 81.4938 | 82.9879 | 183.7237 | 102.7615 | 86.2493 | 231.8233 |
| GCM20C-H | 90.1581 | 102.9581 | 61.2160 | 174.8243 | 132.6182 | 84.8560 | 45.6564 | 29.6832 | 94.6227 | 69.0189 | 97.3058 | 199.5932 | 99.5218 | 103.1799 | 244.1525 |
| GCM20C-I | 120.2520 | 81.1770 | 135.0937 | 173.8981 | 124.4270 | 83.9559 | 77.0937 | 105.6736 | 31.7880 | 109.5037 | 64.4761 | 174.9853 | 77.8875 | 47.9370 | 226.7266 |
| GCM20C-J | 104.0878 | 117.0976 | 89.3686 | 167.5755 | 124.7820 | 79.9400 | 73.8421 | 78.0244 | 106.9920 | 24.9062 | 112.9560 | 191.4894 | 78.8395 | 88.4170 | 232.0633 |
| GCM20C-K | 146.3458 | 108.5250 | 127.3459 | 195.7656 | 156.6765 | 94.4648 | 78.1167 | 102.0814 | 61.6756 | 112.7931 | 23.3557 | 191.4704 | 82.4695 | 77.8807 | 248.8140 |
| GCM20C-L | 150.8625 | 151.2167 | 217.7134 | 70.4914 | 95.6174 | 159.8747 | 175.5781 | 207.3965 | 181.3821 | 195.2887 | 186.8892 | 25.5593 | 179.6653 | 162.8037 | 85.7886 |
| GCM20C-M | 128.0311 | 95.7725 | 110.2864 | 180.4416 | 130.4041 | 70.5775 | 92.6972 | 102.7249 | 79.4285 | 72.2816 | 75.5924 | 183.0492 | 25.8044 | 61.3968 | 233.1248 |
| GCM20C-N | 125.7025 | 94.2916 | 139.6531 | 166.2277 | 119.3382 | 76.1008 | 89.0949 | 120.3486 | 62.3895 | 94.5516 | 78.3897 | 165.6462 | 59.5673 | 28.7501 | 216.6070 |
| GCM20C-O | 202.8372 | 220.8326 | 281.9984 | 83.7508 | 142.0873 | 230.7506 | 249.0502 | 276.5258 | 260.4546 | 258.4492 | 271.2951 | 68.6419 | 253.3480 | 238.4658 | 16.9131 |

**Table C.4** – The Pearson correlation coeffecients (top) and the Mean Absolute Error (MAE; bottom) between the GCM20c and the GCM-Future portions of the CCSM3 – A1FI – 700mb geopotential heights. MAE in terms of meters.

| PEARSON | FUTURE-A | FUTURE-B | FUTURE-C | FUTURE-D | FUTURE-E | FUTURE-F | FUTURE-G | FUTURE-H | FUTURE-I | FUTURE-J | FUTURE-K | FUTURE-L | FUTURE-M | FUTURE-N | FUTURE-O |
|---|---|---|---|---|---|---|---|---|---|---|---|---|---|---|---|
| GCM20C-A | 0.9994 | 0.9714 | 0.9355 | 0.9079 | 0.9657 | 0.9597 | 0.9036 | 0.8879 | 0.8098 | 0.8240 | 0.9187 | 0.9838 | 0.8829 | 0.8999 | 0.8845 |
| GCM20C-B | 0.9589 | 0.9985 | 0.8937 | 0.8405 | 0.9569 | 0.9023 | 0.8924 | 0.8448 | 0.8556 | 0.8708 | 0.9464 | 0.9236 | 0.8902 | 0.9631 | 0.9475 |
| GCM20C-C | 0.9072 | 0.8885 | 0.9962 | 0.8400 | 0.8451 | 0.8329 | 0.9278 | 0.8683 | 0.8173 | 0.7907 | 0.8820 | 0.9553 | 0.7659 | 0.8375 | 0.7848 |
| GCM20C-D | 0.9129 | 0.8518 | 0.8835 | 0.9989 | 0.8603 | 0.9059 | 0.7486 | 0.7418 | 0.7503 | 0.6069 | 0.7484 | 0.8984 | 0.7977 | 0.7139 | 0.6661 |
| GCM20C-E | 0.9752 | 0.9776 | 0.8836 | 0.8578 | 0.9966 | 0.9580 | 0.8884 | 0.8464 | 0.8082 | 0.8333 | 0.9302 | 0.9385 | 0.8737 | 0.9408 | 0.9350 |
| GCM20C-F | 0.9640 | 0.9070 | 0.8634 | 0.9036 | 0.9541 | 0.9986 | 0.8278 | 0.8067 | 0.6714 | 0.6818 | 0.8202 | 0.9275 | 0.7825 | 0.8035 | 0.8127 |
| GCM20C-G | 0.8607 | 0.8724 | 0.8993 | 0.6845 | 0.8337 | 0.7709 | 0.9959 | 0.9395 | 0.8724 | 0.9237 | 0.9460 | 0.8979 | 0.8416 | 0.8898 | 0.8949 |
| GCM20C-H | 0.8737 | 0.8441 | 0.8715 | 0.7052 | 0.8131 | 0.7722 | 0.9662 | 0.9968 | 0.8308 | 0.9107 | 0.8983 | 0.9109 | 0.8815 | 0.8358 | 0.8432 |
| GCM20C-I | 0.7923 | 0.8493 | 0.8207 | 0.7185 | 0.7832 | 0.6647 | 0.8774 | 0.8145 | 0.9986 | 0.9141 | 0.9240 | 0.8084 | 0.9216 | 0.8772 | 0.8476 |
| GCM20C-J | 0.8021 | 0.8587 | 0.7811 | 0.5832 | 0.7895 | 0.6643 | 0.9155 | 0.8819 | 0.9117 | 0.9991 | 0.9614 | 0.8173 | 0.9077 | 0.9175 | 0.9281 |
| GCM20C-K | 0.8876 | 0.9348 | 0.8705 | 0.7059 | 0.8876 | 0.7921 | 0.9479 | 0.8713 | 0.9192 | 0.9661 | 0.9983 | 0.8913 | 0.8990 | 0.9618 | 0.9638 |
| GCM20C-L | 0.9699 | 0.9363 | 0.9727 | 0.8586 | 0.9180 | 0.9011 | 0.9518 | 0.9267 | 0.8352 | 0.8608 | 0.9346 | 0.9950 | 0.8639 | 0.8879 | 0.8630 |
| GCM20C-M | 0.8600 | 0.8766 | 0.7677 | 0.7637 | 0.8441 | 0.7611 | 0.8529 | 0.8617 | 0.9367 | 0.9163 | 0.9161 | 0.8395 | 0.9974 | 0.8677 | 0.8758 |
| GCM20C-N | 0.8769 | 0.9557 | 0.8369 | 0.6903 | 0.9022 | 0.7817 | 0.9028 | 0.8312 | 0.8993 | 0.9493 | 0.9770 | 0.8573 | 0.8834 | 0.9953 | 0.9823 |
| GCM20C-O | 0.8620 | 0.9268 | 0.7728 | 0.6359 | 0.8982 | 0.7993 | 0.9019 | 0.8360 | 0.8365 | 0.9370 | 0.9619 | 0.8266 | 0.8674 | 0.9643 | 0.9970 |

| MAE | FUTURE-A | FUTURE-B | FUTURE-C | FUTURE-D | FUTURE-E | FUTURE-F | FUTURE-G | FUTURE-H | FUTURE-I | FUTURE-J | FUTURE-K | FUTURE-L | FUTURE-M | FUTURE-N | FUTURE-O |
|---|---|---|---|---|---|---|---|---|---|---|---|---|---|---|---|
| GCM20C-A | 23.9966 | 51.0617 | 55.4738 | 59.2914 | 101.3941 | 59.2504 | 72.9658 | 67.0621 | 80.0513 | 92.1267 | 73.6912 | 82.7213 | 72.4563 | 85.6221 | 64.4922 |
| GCM20C-B | 72.8735 | 12.4815 | 76.8847 | 53.9960 | 58.3734 | 36.8816 | 96.0529 | 87.0572 | 77.3579 | 108.2216 | 101.7844 | 130.7500 | 87.8466 | 37.0655 | 32.2718 |
| GCM20C-C | 55.3304 | 54.7260 | 25.6029 | 57.1784 | 106.2982 | 72.0046 | 60.2550 | 62.0030 | 65.8769 | 94.1872 | 79.3559 | 89.0590 | 81.5974 | 87.5449 | 75.1439 |
| GCM20C-D | 69.9165 | 44.5750 | 68.5300 | 17.2498 | 77.3974 | 41.4543 | 100.8874 | 89.7199 | 79.6907 | 126.8161 | 113.7656 | 122.3675 | 88.0206 | 73.4206 | 74.8954 |
| GCM20C-E | 134.7426 | 84.7596 | 140.9560 | 108.0894 | 20.5968 | 68.1227 | 160.4864 | 147.4823 | 142.1434 | 168.8946 | 165.9522 | 193.2769 | 152.8647 | 47.3523 | 80.3568 |
| GCM20C-F | 73.5266 | 44.3924 | 86.8748 | 55.2576 | 56.5623 | 9.9261 | 108.3080 | 97.2578 | 102.8909 | 131.0284 | 118.2431 | 132.6215 | 105.1477 | 58.0260 | 57.7930 |
| GCM20C-G | 65.1658 | 76.9382 | 51.2831 | 90.2064 | 132.3014 | 99.8512 | 20.4820 | 40.3396 | 57.8291 | 57.6296 | 50.9574 | 81.9561 | 65.5358 | 107.5916 | 79.5123 |
| GCM20C-H | 61.5891 | 70.1119 | 58.9311 | 81.9647 | 118.6860 | 88.0013 | 45.5933 | 21.9115 | 66.2259 | 66.9471 | 70.7529 | 89.1720 | 61.5234 | 97.7538 | 74.7690 |
| GCM20C-I | 76.5430 | 66.2222 | 62.5331 | 74.0688 | 121.1655 | 96.8543 | 62.0756 | 66.5700 | 12.2021 | 67.4498 | 65.5410 | 105.5059 | 46.9418 | 95.4643 | 75.1630 |
| GCM20C-J | 87.3652 | 93.4112 | 92.1609 | 119.2602 | 142.3024 | 121.7724 | 67.3863 | 72.2794 | 72.2791 | 25.0180 | 48.6894 | 105.1485 | 68.7966 | 112.5626 | 81.7373 |
| GCM20C-K | 66.4441 | 86.4515 | 73.2224 | 106.6782 | 142.3170 | 112.3773 | 52.7467 | 71.8252 | 67.7477 | 39.7477 | 19.4302 | 82.0243 | 66.6996 | 114.3657 | 80.8523 |
| GCM20C-L | 44.2682 | 95.8387 | 53.0676 | 96.2423 | 151.1706 | 110.1758 | 52.7436 | 62.2204 | 87.7022 | 77.5067 | 53.8967 | 36.4832 | 77.5825 | 131.3129 | 105.6900 |
| GCM20C-M | 64.6955 | 70.5423 | 77.6561 | 78.2093 | 123.0573 | 94.1820 | 69.9264 | 62.1809 | 45.6233 | 62.6384 | 63.4346 | 98.9917 | 24.2295 | 100.9519 | 74.8372 |
| GCM20C-N | 106.1636 | 52.4478 | 109.8163 | 90.9427 | 42.2635 | 60.8878 | 123.4171 | 114.7367 | 103.1767 | 124.4878 | 124.3110 | 161.9368 | 116.9633 | 13.5357 | 39.1320 |
| GCM20C-O | 82.7387 | 45.3992 | 94.5469 | 88.2377 | 73.5143 | 62.5094 | 94.5757 | 90.3933 | 86.0829 | 93.5324 | 91.9305 | 136.0070 | 92.1003 | 46.6073 | 12.1597 |

**Table C.5** – The Pearson correlation coeffecients (top) and the Mean Absolute Error (MAE; bottom) between the GCM20c and the GCM-Future portions of the CCSM3 – A2 – 700mb geopotential heights. MAE in terms of meters.

| PEARSON | FUTURE-A | FUTURE-B | FUTURE-C | FUTURE-D | FUTURE-E | FUTURE-F | FUTURE-G | FUTURE-H | FUTURE-I | FUTURE-J | FUTURE-K | FUTURE-L | FUTURE-M | FUTURE-N | FUTURE-O |
|---|---|---|---|---|---|---|---|---|---|---|---|---|---|---|---|
| GCM20C-A | 0.9994 | 0.9707 | 0.9360 | 0.9096 | 0.9655 | 0.9596 | 0.9024 | 0.8870 | 0.8102 | 0.8224 | 0.9178 | 0.9840 | 0.8828 | 0.8989 | 0.8826 |
| GCM20C-B | 0.9618 | 0.9980 | 0.8955 | 0.8350 | 0.9594 | 0.9082 | 0.9024 | 0.8537 | 0.8521 | 0.8759 | 0.9519 | 0.9275 | 0.8891 | 0.9636 | 0.9537 |
| GCM20C-C | 0.9072 | 0.8906 | 0.9952 | 0.8323 | 0.8453 | 0.8282 | 0.9345 | 0.8760 | 0.8254 | 0.8042 | 0.8899 | 0.9560 | 0.7738 | 0.8446 | 0.7934 |
| GCM20C-D | 0.9092 | 0.8506 | 0.8835 | 0.9988 | 0.8569 | 0.9006 | 0.7443 | 0.7352 | 0.7507 | 0.6023 | 0.7449 | 0.8948 | 0.7927 | 0.7130 | 0.6622 |
| GCM20C-E | 0.9739 | 0.9745 | 0.8796 | 0.8584 | 0.9975 | 0.9619 | 0.8813 | 0.8391 | 0.7967 | 0.8221 | 0.9229 | 0.9356 | 0.8651 | 0.9358 | 0.9300 |
| GCM20C-F | 0.9578 | 0.8966 | 0.8490 | 0.9068 | 0.9494 | 0.9986 | 0.8064 | 0.7918 | 0.6516 | 0.6573 | 0.7993 | 0.9167 | 0.7710 | 0.7879 | 0.7958 |
| GCM20C-G | 0.8931 | 0.8828 | 0.9246 | 0.7403 | 0.8584 | 0.8174 | 0.9979 | 0.9534 | 0.8575 | 0.8939 | 0.9343 | 0.9276 | 0.8429 | 0.8785 | 0.8798 |
| GCM20C-H | 0.8702 | 0.8363 | 0.8704 | 0.7029 | 0.8081 | 0.7714 | 0.9647 | 0.9975 | 0.8208 | 0.9012 | 0.8900 | 0.9089 | 0.8724 | 0.8265 | 0.8343 |
| GCM20C-I | 0.7764 | 0.8400 | 0.8060 | 0.7015 | 0.7685 | 0.6444 | 0.8635 | 0.7978 | 0.9980 | 0.9131 | 0.9191 | 0.7921 | 0.9159 | 0.8724 | 0.8423 |
| GCM20C-J | 0.8104 | 0.8670 | 0.7846 | 0.5932 | 0.7995 | 0.6749 | 0.9176 | 0.8859 | 0.9139 | 0.9996 | 0.9639 | 0.8224 | 0.9135 | 0.9239 | 0.9341 |
| GCM20C-K | 0.8954 | 0.9411 | 0.8752 | 0.7168 | 0.8956 | 0.8013 | 0.9495 | 0.8759 | 0.9209 | 0.9653 | 0.9992 | 0.8974 | 0.9044 | 0.9655 | 0.9662 |
| GCM20C-L | 0.9729 | 0.9356 | 0.9734 | 0.8680 | 0.9198 | 0.9064 | 0.9463 | 0.9243 | 0.8301 | 0.8515 | 0.9282 | 0.9970 | 0.8625 | 0.8829 | 0.8562 |
| GCM20C-M | 0.8532 | 0.8682 | 0.7617 | 0.7606 | 0.8366 | 0.7530 | 0.8480 | 0.8623 | 0.9354 | 0.9128 | 0.9085 | 0.8340 | 0.9978 | 0.8595 | 0.8667 |
| GCM20C-N | 0.8807 | 0.9581 | 0.8318 | 0.6955 | 0.9094 | 0.7901 | 0.8975 | 0.8273 | 0.8955 | 0.9449 | 0.9756 | 0.8568 | 0.8858 | 0.9961 | 0.9847 |
| GCM20C-O | 0.8583 | 0.9310 | 0.7559 | 0.6446 | 0.8994 | 0.7943 | 0.8783 | 0.8148 | 0.8445 | 0.9307 | 0.9553 | 0.8137 | 0.8794 | 0.9669 | 0.9960 |

| MAE | FUTURE-A | FUTURE-B | FUTURE-C | FUTURE-D | FUTURE-E | FUTURE-F | FUTURE-G | FUTURE-H | FUTURE-I | FUTURE-J | FUTURE-K | FUTURE-L | FUTURE-M | FUTURE-N | FUTURE-O |
|---|---|---|---|---|---|---|---|---|---|---|---|---|---|---|---|
| GCM20C-A | 20.8624 | 52.5711 | 53.8005 | 59.3256 | 104.1199 | 61.4659 | 71.2444 | 65.8273 | 79.0244 | 91.0307 | 71.9110 | 79.7883 | 70.8468 | 88.1182 | 66.4787 |
| GCM20C-B | 69.5601 | 11.9431 | 74.9811 | 54.7575 | 60.7755 | 36.7082 | 92.9854 | 84.5529 | 76.6470 | 105.3367 | 98.2531 | 127.6058 | 86.1329 | 39.1098 | 29.7492 |
| GCM20C-C | 54.9262 | 55.3374 | 24.7822 | 58.8173 | 107.6605 | 73.6382 | 57.8748 | 60.0104 | 64.3585 | 91.4652 | 77.0644 | 87.7177 | 80.0348 | 88.2130 | 74.8781 |
| GCM20C-D | 66.8186 | 46.3255 | 65.1171 | 13.7461 | 82.7689 | 45.4823 | 98.4352 | 88.1325 | 77.6194 | 125.2613 | 111.1897 | 118.1394 | 85.5864 | 77.6546 | 77.2359 |
| GCM20C-E | 133.0926 | 82.6860 | 139.0832 | 105.8046 | 17.7485 | 65.7663 | 158.8355 | 145.8363 | 140.4320 | 167.7987 | 164.6522 | 191.7347 | 151.2230 | 45.8323 | 78.9332 |
| GCM20C-F | 75.6211 | 47.2679 | 89.8840 | 56.3581 | 56.2064 | 11.0969 | 111.7919 | 100.1440 | 105.9665 | 134.5058 | 121.6233 | 134.9393 | 107.6421 | 59.6518 | 60.7546 |
| GCM20C-G | 57.2475 | 74.3679 | 43.8561 | 82.6253 | 129.9517 | 94.1457 | 19.2619 | 34.9741 | 59.3799 | 66.0581 | 55.2635 | 75.8465 | 64.5160 | 107.4801 | 80.7585 |
| GCM20C-H | 62.2890 | 71.4828 | 58.8442 | 82.3175 | 119.7105 | 88.6045 | 45.2880 | 20.5753 | 67.5181 | 68.8439 | 72.2085 | 88.9698 | 62.9134 | 99.2285 | 76.5826 |
| GCM20C-I | 79.0682 | 65.8560 | 65.2064 | 75.0938 | 119.8351 | 97.0651 | 65.5803 | 69.6639 | 14.1706 | 68.4866 | 67.5659 | 108.9695 | 49.1747 | 93.7819 | 74.2032 |
| GCM20C-J | 84.3122 | 91.2753 | 89.5683 | 116.6081 | 141.7094 | 120.0250 | 64.4517 | 69.2796 | 69.3612 | 22.0377 | 45.7971 | 102.4480 | 64.9606 | 111.9420 | 80.4643 |
| GCM20C-K | 63.0573 | 84.1308 | 69.9830 | 103.4612 | 141.3508 | 110.3812 | 49.6949 | 68.6622 | 64.6786 | 39.1679 | 16.5392 | 79.2648 | 62.9689 | 113.5185 | 79.8633 |
| GCM20C-L | 43.8843 | 97.2020 | 52.9695 | 95.8395 | 152.9481 | 111.1818 | 53.9098 | 62.8389 | 88.4700 | 79.8007 | 55.9030 | 32.7851 | 77.5617 | 133.4794 | 108.0934 |
| GCM20C-M | 65.6859 | 69.3287 | 76.6688 | 75.9704 | 121.9071 | 93.1499 | 69.7474 | 60.6468 | 43.2744 | 64.2776 | 65.9256 | 100.2177 | 22.5689 | 100.0669 | 74.8621 |
| GCM20C-N | 105.8731 | 51.8318 | 110.0895 | 90.1348 | 40.8557 | 59.5637 | 123.8333 | 114.9684 | 103.2978 | 125.1258 | 124.6872 | 162.1029 | 116.7150 | 12.3680 | 38.7190 |
| GCM20C-O | 83.1267 | 43.5853 | 95.9075 | 86.4762 | 72.7864 | 62.4421 | 97.2717 | 92.6265 | 84.4966 | 94.6201 | 93.0895 | 137.4566 | 90.1698 | 45.4849 | 11.9494 |

**Table C.6** – The Pearson correlation coeffecients (top) and the Mean Absolute Error (MAE; bottom) between the GCM20c and the GCM-Future portions of the CCSM3 – B1 – 700mb geopotential heights. MAE in terms of meters.

| PEARSON | FUTURE-A | FUTURE-B | FUTURE-C | FUTURE-D | FUTURE-E | FUTURE-F | FUTURE-G | FUTURE-H | FUTURE-I | FUTURE-J | FUTURE-K | FUTURE-L | FUTURE-M | FUTURE-N | FUTURE-O |
|---|---|---|---|---|---|---|---|---|---|---|---|---|---|---|---|
| GCM20C-A | 0.9996 | 0.9696 | 0.9341 | 0.9125 | 0.9670 | 0.9618 | 0.8976 | 0.8838 | 0.8056 | 0.8164 | 0.9132 | 0.9831 | 0.8804 | 0.8967 | 0.8792 |
| GCM20C-B | 0.9681 | 0.9983 | 0.9004 | 0.8485 | 0.9633 | 0.9196 | 0.8974 | 0.8529 | 0.8398 | 0.8617 | 0.9431 | 0.9335 | 0.8835 | 0.9562 | 0.9441 |
| GCM20C-C | 0.9129 | 0.8948 | 0.9972 | 0.8444 | 0.8520 | 0.8367 | 0.9314 | 0.8743 | 0.8256 | 0.7988 | 0.8881 | 0.9593 | 0.7769 | 0.8452 | 0.7925 |
| GCM20C-D | 0.9110 | 0.8521 | 0.8794 | 0.9996 | 0.8639 | 0.9068 | 0.7404 | 0.7326 | 0.7453 | 0.5983 | 0.7428 | 0.8936 | 0.7913 | 0.7157 | 0.6651 |
| GCM20C-E | 0.9722 | 0.9676 | 0.8758 | 0.8611 | 0.9989 | 0.9660 | 0.8742 | 0.8340 | 0.7858 | 0.8096 | 0.9138 | 0.9338 | 0.8579 | 0.9275 | 0.9211 |
| GCM20C-F | 0.9573 | 0.8942 | 0.8477 | 0.9101 | 0.9478 | 0.9980 | 0.8045 | 0.7930 | 0.6522 | 0.6542 | 0.7957 | 0.9159 | 0.7731 | 0.7839 | 0.7916 |
| GCM20C-G | 0.8609 | 0.8666 | 0.9046 | 0.6826 | 0.8306 | 0.7752 | 0.9958 | 0.9389 | 0.8536 | 0.9122 | 0.9386 | 0.9017 | 0.8243 | 0.8803 | 0.8855 |
| GCM20C-H | 0.8826 | 0.8442 | 0.8773 | 0.7180 | 0.8225 | 0.7902 | 0.9653 | 0.9986 | 0.8158 | 0.8963 | 0.8920 | 0.9190 | 0.8736 | 0.8301 | 0.8375 |
| GCM20C-I | 0.7930 | 0.8509 | 0.8288 | 0.7116 | 0.7779 | 0.6578 | 0.8805 | 0.8191 | 0.9976 | 0.9227 | 0.9285 | 0.8141 | 0.9186 | 0.8807 | 0.8477 |
| GCM20C-J | 0.8205 | 0.8719 | 0.7943 | 0.6007 | 0.8085 | 0.6877 | 0.9242 | 0.8942 | 0.9090 | 0.9997 | 0.9672 | 0.8337 | 0.9126 | 0.9268 | 0.9368 |
| GCM20C-K | 0.8967 | 0.9419 | 0.8785 | 0.7213 | 0.8968 | 0.8031 | 0.9470 | 0.8715 | 0.9206 | 0.9623 | 0.9991 | 0.8993 | 0.9021 | 0.9652 | 0.9638 |
| GCM20C-L | 0.9770 | 0.9373 | 0.9731 | 0.8765 | 0.9251 | 0.9148 | 0.9435 | 0.9234 | 0.8265 | 0.8445 | 0.9248 | 0.9984 | 0.8629 | 0.8812 | 0.8549 |
| GCM20C-M | 0.8691 | 0.8775 | 0.7720 | 0.7741 | 0.8522 | 0.7741 | 0.8544 | 0.8705 | 0.9292 | 0.9113 | 0.9132 | 0.8483 | 0.9989 | 0.8649 | 0.8731 |
| GCM20C-N | 0.8815 | 0.9582 | 0.8327 | 0.6912 | 0.9133 | 0.7942 | 0.8968 | 0.8261 | 0.8839 | 0.9403 | 0.9730 | 0.8578 | 0.8757 | 0.9981 | 0.9856 |
| GCM20C-O | 0.8674 | 0.9333 | 0.7746 | 0.6458 | 0.9023 | 0.8042 | 0.8974 | 0.8329 | 0.8395 | 0.9365 | 0.9630 | 0.8298 | 0.8738 | 0.9672 | 0.9980 |

| MAE | FUTURE-A | FUTURE-B | FUTURE-C | FUTURE-D | FUTURE-E | FUTURE-F | FUTURE-G | FUTURE-H | FUTURE-I | FUTURE-J | FUTURE-K | FUTURE-L | FUTURE-M | FUTURE-N | FUTURE-O |
|---|---|---|---|---|---|---|---|---|---|---|---|---|---|---|---|
| GCM20C-A | 12.1394 | 56.9966 | 50.4064 | 60.2327 | 111.4675 | 67.3660 | 67.1530 | 63.0189 | 77.2948 | 88.7314 | 67.9523 | 72.1950 | 67.0881 | 94.9988 | 71.9535 |
| GCM20C-B | 68.5172 | 10.1148 | 73.5641 | 51.9233 | 61.1431 | 34.7032 | 92.7588 | 83.8605 | 76.7317 | 106.5784 | 99.0601 | 126.6694 | 85.8819 | 40.9295 | 32.7002 |
| GCM20C-C | 51.9332 | 60.1125 | 15.6074 | 59.7191 | 115.4517 | 79.1359 | 52.7813 | 57.3599 | 62.1949 | 89.3721 | 73.1753 | 80.2426 | 76.6326 | 95.8162 | 80.4522 |
| GCM20C-D | 65.8790 | 45.7979 | 63.9352 | 9.7734 | 84.1919 | 45.8867 | 97.0375 | 86.7884 | 76.1037 | 124.3528 | 110.1945 | 117.0154 | 83.8922 | 78.5784 | 77.1637 |
| GCM20C-E | 127.9583 | 76.5466 | 133.1872 | 99.1771 | 9.9143 | 59.5030 | 153.2663 | 140.1759 | 134.4940 | 163.3554 | 159.9715 | 186.6402 | 145.5122 | 41.2198 | 74.3988 |
| GCM20C-F | 74.0041 | 46.2914 | 88.1704 | 54.0472 | 57.7453 | 10.5175 | 110.1649 | 98.2898 | 104.1870 | 133.4056 | 120.4555 | 133.3031 | 105.6423 | 60.5754 | 60.8699 |
| GCM20C-G | 65.1905 | 77.9690 | 50.3467 | 90.8741 | 132.6341 | 99.6691 | 20.7647 | 40.8387 | 61.8455 | 60.7575 | 53.1629 | 81.0156 | 69.2538 | 108.4983 | 80.9303 |
| GCM20C-H | 59.0287 | 73.1347 | 55.8502 | 81.5967 | 123.6195 | 90.1217 | 40.8430 | 14.1158 | 66.8172 | 67.9395 | 69.4374 | 83.3235 | 60.2181 | 103.3524 | 79.6798 |
| GCM20C-I | 76.5602 | 67.2691 | 60.5286 | 75.0482 | 123.4845 | 98.7455 | 60.3697 | 65.1823 | 10.2484 | 65.4334 | 64.2239 | 103.6511 | 46.5826 | 97.3664 | 77.0053 |
| GCM20C-J | 82.7874 | 94.7462 | 87.7334 | 118.0033 | 147.4618 | 123.2933 | 59.9062 | 66.5926 | 69.9207 | 13.9804 | 40.3524 | 96.2817 | 63.4307 | 117.9623 | 85.6942 |
| GCM20C-K | 65.3790 | 89.4476 | 72.4209 | 107.5098 | 146.7506 | 115.3126 | 52.0230 | 72.3684 | 68.3946 | 40.3673 | 13.7890 | 77.1637 | 65.9194 | 119.0429 | 85.6011 |
| GCM20C-L | 50.1901 | 106.3999 | 58.7174 | 102.4552 | 163.7695 | 120.5316 | 56.4790 | 67.4274 | 93.1879 | 83.3273 | 58.2966 | 20.3276 | 80.2090 | 144.2975 | 117.9127 |
| GCM20C-M | 62.5730 | 72.8943 | 75.0009 | 77.3006 | 127.4811 | 96.1599 | 66.3199 | 58.1359 | 44.2978 | 62.3365 | 62.0828 | 94.1173 | 15.6066 | 105.8271 | 79.2687 |
| GCM20C-N | 107.4096 | 51.8654 | 110.6996 | 89.5865 | 37.2724 | 58.1902 | 125.2107 | 115.9011 | 104.7006 | 127.8308 | 127.3489 | 163.8411 | 118.5364 | 8.2007 | 40.4587 |
| GCM20C-O | 82.0055 | 42.1466 | 93.5534 | 85.4747 | 71.2681 | 60.0780 | 95.1209 | 90.3500 | 84.7831 | 94.4552 | 92.6999 | 136.0827 | 90.9755 | 44.1111 | 9.0178 |

**Table C.7** – The Pearson correlation coeffecients (top) and the Mean Absolute Error (MAE; bottom) between the GCM20c and the GCM-Future portions of the CCSM3 – A1FI – 850mb temperatures. MAE in terms of °C.

| PEARSON | FUTURE-A | FUTURE-B | FUTURE-C | FUTURE-D | FUTURE-E | FUTURE-F | FUTURE-G | FUTURE-H | FUTURE-I | FUTURE-J | FUTURE-K | FUTURE-L | FUTURE-M | FUTURE-N | FUTURE-O |
|---|---|---|---|---|---|---|---|---|---|---|---|---|---|---|---|
| GCM20C-A | 0.9950 | 0.9542 | 0.9166 | 0.8645 | 0.7846 | 0.8133 | 0.8762 | 0.9436 | 0.9417 | 0.8982 | 0.8579 | 0.8696 | 0.8279 | 0.9042 | 0.7977 |
| GCM20C-B | 0.9591 | 0.9939 | 0.9060 | 0.9466 | 0.8827 | 0.9010 | 0.9630 | 0.8761 | 0.9630 | 0.9541 | 0.9293 | 0.8951 | 0.8778 | 0.9144 | 0.8869 |
| GCM20C-C | 0.8933 | 0.8658 | 0.9923 | 0.7832 | 0.7990 | 0.7084 | 0.8475 | 0.8394 | 0.8642 | 0.8046 | 0.7314 | 0.6960 | 0.6682 | 0.7124 | 0.6529 |
| GCM20C-D | 0.8903 | 0.9410 | 0.8118 | 0.9946 | 0.8737 | 0.9479 | 0.9406 | 0.7838 | 0.9613 | 0.9440 | 0.9378 | 0.9139 | 0.8597 | 0.9343 | 0.8902 |
| GCM20C-E | 0.8083 | 0.8519 | 0.8340 | 0.8770 | 0.9979 | 0.9296 | 0.9456 | 0.6022 | 0.8768 | 0.9503 | 0.8727 | 0.7327 | 0.8057 | 0.7683 | 0.8794 |
| GCM20C-F | 0.8342 | 0.8775 | 0.7351 | 0.9322 | 0.9234 | 0.9963 | 0.9324 | 0.6702 | 0.9087 | 0.9561 | 0.9132 | 0.8409 | 0.8750 | 0.8896 | 0.9500 |
| GCM20C-G | 0.8847 | 0.9418 | 0.8773 | 0.9438 | 0.9563 | 0.9473 | 0.9959 | 0.7509 | 0.9372 | 0.9566 | 0.8867 | 0.8024 | 0.8185 | 0.8407 | 0.8836 |
| GCM20C-H | 0.8956 | 0.8408 | 0.8163 | 0.7018 | 0.5170 | 0.5906 | 0.6938 | 0.9860 | 0.7932 | 0.6756 | 0.6569 | 0.7519 | 0.6526 | 0.7742 | 0.5847 |
| GCM20C-I | 0.9543 | 0.9487 | 0.8855 | 0.9435 | 0.8457 | 0.8991 | 0.9187 | 0.8692 | 0.9944 | 0.9383 | 0.9097 | 0.9231 | 0.8582 | 0.9461 | 0.8477 |
| GCM20C-J | 0.9226 | 0.9414 | 0.8478 | 0.9379 | 0.9477 | 0.9538 | 0.9537 | 0.7572 | 0.9562 | 0.9983 | 0.9582 | 0.8832 | 0.9048 | 0.9167 | 0.9330 |
| GCM20C-K | 0.8783 | 0.9159 | 0.7490 | 0.9147 | 0.8387 | 0.8991 | 0.8645 | 0.7441 | 0.9144 | 0.9471 | 0.9961 | 0.9646 | 0.9671 | 0.9557 | 0.9481 |
| GCM20C-L | 0.8597 | 0.8735 | 0.6847 | 0.8636 | 0.6682 | 0.8003 | 0.7607 | 0.8097 | 0.8868 | 0.8434 | 0.9253 | 0.9936 | 0.9217 | 0.9687 | 0.8516 |
| GCM20C-M | 0.8341 | 0.8607 | 0.6746 | 0.8193 | 0.7662 | 0.8438 | 0.7867 | 0.7166 | 0.8456 | 0.8913 | 0.9613 | 0.9480 | 0.9956 | 0.9285 | 0.9530 |
| GCM20C-N | 0.9227 | 0.9167 | 0.7433 | 0.9093 | 0.7467 | 0.8763 | 0.8323 | 0.8482 | 0.9405 | 0.9079 | 0.9382 | 0.9827 | 0.9229 | 0.9972 | 0.8872 |
| GCM20C-O | 0.8221 | 0.8747 | 0.6840 | 0.8728 | 0.8648 | 0.9388 | 0.8697 | 0.6691 | 0.8619 | 0.9372 | 0.9582 | 0.8931 | 0.9672 | 0.9071 | 0.9978 |

| MAE | FUTURE-A | FUTURE-B | FUTURE-C | FUTURE-D | FUTURE-E | FUTURE-F | FUTURE-G | FUTURE-H | FUTURE-I | FUTURE-J | FUTURE-K | FUTURE-L | FUTURE-M | FUTURE-N | FUTURE-O |
|---|---|---|---|---|---|---|---|---|---|---|---|---|---|---|---|
| GCM20C-A | 2.6902 | 5.5637 | 3.4175 | 11.0573 | 13.8156 | 13.1473 | 9.0760 | 2.6941 | 11.5095 | 16.0888 | 14.7913 | 13.5226 | 12.9810 | 13.1680 | 13.2953 |
| GCM20C-B | 2.8703 | 1.2849 | 4.8505 | 6.4686 | 9.3178 | 8.6302 | 4.4319 | 5.5833 | 7.1385 | 11.6360 | 10.2471 | 9.3017 | 8.7368 | 9.0373 | 8.8154 |
| GCM20C-C | 4.9110 | 7.1274 | 2.3880 | 12.3503 | 14.8422 | 14.5201 | 10.1706 | 3.5026 | 12.9902 | 17.8554 | 16.4494 | 15.1874 | 14.6122 | 15.1673 | 14.8460 |
| GCM20C-D | 7.6898 | 5.0655 | 9.4438 | 1.3655 | 5.9269 | 3.9981 | 3.0142 | 10.2661 | 3.0082 | 7.6561 | 5.9223 | 5.0435 | 5.4224 | 4.8760 | 5.1075 |
| GCM20C-E | 10.6226 | 8.3689 | 11.9101 | 5.4145 | 1.3752 | 4.2668 | 5.0518 | 13.6194 | 5.2425 | 5.4708 | 6.0162 | 7.6247 | 6.4777 | 7.2917 | 5.2362 |
| GCM20C-F | 9.7957 | 7.3634 | 11.5619 | 3.4000 | 4.2429 | 1.3440 | 4.3412 | 12.5289 | 3.8247 | 5.9853 | 5.0944 | 5.3904 | 4.6820 | 4.8523 | 3.1252 |
| GCM20C-G | 6.6024 | 4.0018 | 7.9498 | 3.5744 | 5.5018 | 5.0078 | 0.8774 | 9.2797 | 4.3492 | 8.5044 | 7.5799 | 7.2420 | 6.6345 | 7.0249 | 5.9925 |
| GCM20C-H | 6.1542 | 8.6685 | 5.1888 | 14.1144 | 17.2847 | 16.3685 | 12.2320 | 3.2108 | 14.7333 | 19.7189 | 18.1401 | 16.4979 | 16.1117 | 16.3643 | 16.5118 |
| GCM20C-I | 7.8064 | 5.5913 | 9.7535 | 2.9254 | 6.0599 | 4.5430 | 3.8109 | 10.5223 | 1.5337 | 7.1729 | 5.8646 | 4.5234 | 5.2248 | 4.2081 | 5.5024 |
| GCM20C-J | 11.9029 | 9.6899 | 14.0724 | 6.1017 | 4.1977 | 4.7861 | 7.0497 | 15.0928 | 5.0872 | 2.0218 | 3.9284 | 6.1981 | 5.7099 | 5.1166 | 5.0023 |
| GCM20C-K | 10.2992 | 7.8961 | 12.4687 | 4.6293 | 6.0116 | 4.6620 | 6.2469 | 13.1346 | 4.3386 | 5.3941 | 2.4406 | 3.3167 | 2.8458 | 3.2158 | 3.4183 |
| GCM20C-L | 9.7640 | 7.5212 | 11.8951 | 4.6485 | 8.1381 | 5.7491 | 6.6190 | 12.0727 | 4.2314 | 7.8139 | 4.7735 | 1.8984 | 3.6975 | 2.9079 | 5.1241 |
| GCM20C-M | 9.2620 | 7.0547 | 11.3399 | 5.3580 | 7.1241 | 5.4210 | 6.1151 | 11.8191 | 5.1049 | 7.4494 | 4.5325 | 3.8776 | 1.8327 | 4.2961 | 3.3611 |
| GCM20C-N | 9.0229 | 6.9799 | 11.5549 | 4.3089 | 7.5088 | 5.0830 | 6.0129 | 11.6914 | 3.5334 | 6.8603 | 4.8282 | 3.0880 | 4.1022 | 1.9318 | 4.8980 |
| GCM20C-O | 9.9429 | 7.4958 | 11.9195 | 4.7565 | 5.4654 | 3.5461 | 5.4564 | 12.6513 | 4.9134 | 6.2004 | 4.1475 | 4.7587 | 2.6626 | 4.5546 | 1.3267 |

**Table C.8** – The Pearson correlation coeffecients (top) and the Mean Absolute Error (MAE; bottom) between the GCM20c and the GCM-Future portions of the CCSM3 – A2 – 850mb temperatures. MAE in terms of °C.

| PEARSON | FUTURE-A | FUTURE-B | FUTURE-C | FUTURE-D | FUTURE-E | FUTURE-F | FUTURE-G | FUTURE-H | FUTURE-I | FUTURE-J | FUTURE-K | FUTURE-L | FUTURE-M | FUTURE-N | FUTURE-O |
|---|---|---|---|---|---|---|---|---|---|---|---|---|---|---|---|
| GCM20C-A | 0.9990 | 0.9613 | 0.9183 | 0.8803 | 0.8042 | 0.8360 | 0.8933 | 0.9397 | 0.9549 | 0.9129 | 0.8684 | 0.8781 | 0.8386 | 0.9159 | 0.8142 |
| GCM20C-B | 0.9568 | 0.9957 | 0.9045 | 0.9543 | 0.8894 | 0.9097 | 0.9700 | 0.8733 | 0.9680 | 0.9574 | 0.9323 | 0.8990 | 0.8811 | 0.9183 | 0.8923 |
| GCM20C-C | 0.9000 | 0.8777 | 0.9987 | 0.8070 | 0.8254 | 0.7386 | 0.8707 | 0.8384 | 0.8839 | 0.8250 | 0.7491 | 0.7117 | 0.6857 | 0.7300 | 0.6764 |
| GCM20C-D | 0.8785 | 0.9351 | 0.8023 | 0.9977 | 0.8854 | 0.9586 | 0.9471 | 0.7652 | 0.9592 | 0.9463 | 0.9365 | 0.9075 | 0.8587 | 0.9295 | 0.8961 |
| GCM20C-E | 0.8045 | 0.8508 | 0.8284 | 0.8836 | 0.9995 | 0.9360 | 0.9483 | 0.5971 | 0.8811 | 0.9512 | 0.8743 | 0.7373 | 0.8064 | 0.7732 | 0.8812 |
| GCM20C-F | 0.8249 | 0.8725 | 0.7291 | 0.9356 | 0.9247 | 0.9987 | 0.9337 | 0.6599 | 0.9089 | 0.9528 | 0.9100 | 0.8393 | 0.8702 | 0.8871 | 0.9473 |
| GCM20C-G | 0.8697 | 0.9306 | 0.8690 | 0.9396 | 0.9680 | 0.9515 | 0.9961 | 0.7255 | 0.9323 | 0.9576 | 0.8860 | 0.7946 | 0.8190 | 0.8317 | 0.8875 |
| GCM20C-H | 0.9083 | 0.8569 | 0.8294 | 0.7254 | 0.5432 | 0.6186 | 0.7185 | 0.9933 | 0.8157 | 0.6973 | 0.6745 | 0.7684 | 0.6697 | 0.7930 | 0.6062 |
| GCM20C-I | 0.9496 | 0.9465 | 0.8816 | 0.9492 | 0.8565 | 0.9110 | 0.9272 | 0.8588 | 0.9981 | 0.9420 | 0.9080 | 0.9203 | 0.8572 | 0.9464 | 0.8523 |
| GCM20C-J | 0.9167 | 0.9388 | 0.8430 | 0.9424 | 0.9526 | 0.9607 | 0.9567 | 0.7499 | 0.9580 | 0.9995 | 0.9591 | 0.8841 | 0.9058 | 0.9175 | 0.9365 |
| GCM20C-K | 0.8733 | 0.9153 | 0.7513 | 0.9199 | 0.8572 | 0.9105 | 0.8753 | 0.7315 | 0.9170 | 0.9548 | 0.9993 | 0.9599 | 0.9693 | 0.9521 | 0.9557 |
| GCM20C-L | 0.8602 | 0.8801 | 0.6952 | 0.8759 | 0.6868 | 0.8148 | 0.7773 | 0.8069 | 0.8970 | 0.8520 | 0.9314 | 0.9966 | 0.9272 | 0.9707 | 0.8616 |
| GCM20C-M | 0.8277 | 0.8608 | 0.6719 | 0.8274 | 0.7793 | 0.8572 | 0.7974 | 0.7071 | 0.8494 | 0.8959 | 0.9632 | 0.9474 | 0.9985 | 0.9286 | 0.9617 |
| GCM20C-N | 0.9180 | 0.9154 | 0.7400 | 0.9146 | 0.7549 | 0.8850 | 0.8373 | 0.8405 | 0.9429 | 0.9113 | 0.9416 | 0.9849 | 0.9273 | 0.9990 | 0.8939 |
| GCM20C-O | 0.8146 | 0.8712 | 0.6845 | 0.8746 | 0.8762 | 0.9440 | 0.8755 | 0.6564 | 0.8615 | 0.9390 | 0.9572 | 0.8869 | 0.9652 | 0.9007 | 0.9995 |

| MAE | FUTURE-A | FUTURE-B | FUTURE-C | FUTURE-D | FUTURE-E | FUTURE-F | FUTURE-G | FUTURE-H | FUTURE-I | FUTURE-J | FUTURE-K | FUTURE-L | FUTURE-M | FUTURE-N | FUTURE-O |
|---|---|---|---|---|---|---|---|---|---|---|---|---|---|---|---|
| GCM20C-A | 2.0290 | 4.9497 | 3.1623 | 10.4228 | 13.1964 | 12.4931 | 8.4283 | 2.6643 | 10.8746 | 15.4966 | 14.2054 | 12.9291 | 12.3897 | 12.5669 | 12.6805 |
| GCM20C-B | 3.0002 | 1.0216 | 4.9113 | 6.2099 | 9.1165 | 8.3885 | 4.1518 | 5.6789 | 6.9177 | 11.4882 | 10.0733 | 9.0989 | 8.5461 | 8.8564 | 8.6098 |
| GCM20C-C | 4.5726 | 6.7035 | 1.8691 | 11.8753 | 14.3789 | 14.0327 | 9.6903 | 3.3319 | 12.5319 | 17.4331 | 16.0176 | 14.7482 | 14.1739 | 14.7371 | 14.3886 |
| GCM20C-D | 8.0638 | 5.4031 | 9.7645 | 0.9371 | 5.5949 | 3.5588 | 3.0019 | 10.6316 | 2.8779 | 7.4047 | 5.7064 | 4.9192 | 5.2863 | 4.7720 | 4.8442 |
| GCM20C-E | 10.5843 | 8.2975 | 11.8612 | 5.1918 | 1.1967 | 4.0169 | 4.9000 | 13.5630 | 5.0617 | 5.4835 | 5.9360 | 7.4673 | 6.3783 | 7.1485 | 5.1188 |
| GCM20C-F | 9.8030 | 7.3457 | 11.5137 | 3.2570 | 4.2407 | 1.1822 | 4.2529 | 12.5007 | 3.7769 | 6.1312 | 5.1789 | 5.3744 | 4.7376 | 4.9052 | 3.1997 |
| GCM20C-G | 6.9734 | 4.3877 | 8.2647 | 3.5384 | 5.0715 | 4.7434 | 0.9106 | 9.6671 | 4.2711 | 8.2351 | 7.3887 | 7.1939 | 6.5081 | 6.9850 | 5.7805 |
| GCM20C-H | 5.7531 | 8.2434 | 4.7699 | 13.6719 | 16.8512 | 15.9188 | 11.7833 | 2.7450 | 14.2993 | 19.3182 | 17.7358 | 16.0849 | 15.7000 | 15.9574 | 16.0869 |
| GCM20C-I | 7.8080 | 5.5564 | 9.6928 | 2.6967 | 5.9040 | 4.2985 | 3.5715 | 10.5032 | 1.3334 | 7.2212 | 5.9229 | 4.5369 | 5.2008 | 4.2552 | 5.4017 |
| GCM20C-J | 11.8620 | 9.6266 | 14.0072 | 5.9471 | 3.9946 | 4.5587 | 6.9198 | 15.0401 | 4.9740 | 2.0010 | 3.8724 | 6.1320 | 5.6328 | 5.0508 | 4.8612 |
| GCM20C-K | 10.6739 | 8.2178 | 12.7791 | 4.6386 | 5.6193 | 4.3752 | 6.3123 | 13.5205 | 4.3207 | 4.9761 | 1.8997 | 3.2975 | 2.7180 | 3.2487 | 3.1315 |
| GCM20C-L | 9.5926 | 7.2682 | 11.6080 | 4.2492 | 7.8281 | 5.4167 | 6.2111 | 11.8765 | 3.9170 | 7.8344 | 4.7835 | 1.8311 | 3.5510 | 3.0483 | 4.9008 |
| GCM20C-M | 9.5660 | 7.2668 | 11.5727 | 5.1750 | 6.8257 | 5.0422 | 6.0433 | 12.1053 | 4.9370 | 7.2195 | 4.2550 | 3.6259 | 1.3405 | 4.1464 | 2.9250 |
| GCM20C-N | 9.1777 | 7.0730 | 11.6471 | 4.1197 | 7.3050 | 4.7965 | 5.9323 | 11.8308 | 3.3592 | 6.7225 | 4.6241 | 2.8060 | 3.8782 | 1.6739 | 4.6551 |
| GCM20C-O | 10.0829 | 7.6017 | 11.9902 | 4.7001 | 5.2110 | 3.3380 | 5.4032 | 12.7853 | 4.8772 | 6.1143 | 4.0882 | 4.7831 | 2.6555 | 4.6431 | 1.0588 |

**Table C.9** – The Pearson correlation coeffecients (top) and the Mean Absolute Error (MAE; bottom) between the GCM20c and the GCM-Future portions of the CCSM3 – B1 – 850mb temperatures. MAE in terms of °C.

| PEARSON | FUTURE-A | FUTURE-B | FUTURE-C | FUTURE-D | FUTURE-E | FUTURE-F | FUTURE-G | FUTURE-H | FUTURE-I | FUTURE-J | FUTURE-K | FUTURE-L | FUTURE-M | FUTURE-N | FUTURE-O |
|---|---|---|---|---|---|---|---|---|---|---|---|---|---|---|---|
| GCM20C-A | 0.9994 | 0.9613 | 0.9145 | 0.8781 | 0.8049 | 0.8360 | 0.8912 | 0.9374 | 0.9519 | 0.9153 | 0.8725 | 0.8788 | 0.8434 | 0.9171 | 0.8187 |
| GCM20C-B | 0.9598 | 0.9976 | 0.9042 | 0.9495 | 0.8795 | 0.9013 | 0.9657 | 0.8827 | 0.9629 | 0.9517 | 0.9278 | 0.8967 | 0.8781 | 0.9165 | 0.8871 |
| GCM20C-C | 0.9006 | 0.8800 | 0.9992 | 0.8112 | 0.8291 | 0.7425 | 0.8736 | 0.8383 | 0.8846 | 0.8275 | 0.7527 | 0.7136 | 0.6888 | 0.7320 | 0.6807 |
| GCM20C-D | 0.8832 | 0.9383 | 0.8138 | 0.9990 | 0.8886 | 0.9561 | 0.9516 | 0.7719 | 0.9611 | 0.9459 | 0.9315 | 0.9015 | 0.8512 | 0.9250 | 0.8890 |
| GCM20C-E | 0.8073 | 0.8506 | 0.8321 | 0.8825 | 0.9998 | 0.9350 | 0.9474 | 0.6004 | 0.8824 | 0.9517 | 0.8738 | 0.7376 | 0.8067 | 0.7737 | 0.8799 |
| GCM20C-F | 0.8285 | 0.8742 | 0.7283 | 0.9358 | 0.9244 | 0.9987 | 0.9321 | 0.6624 | 0.9107 | 0.9562 | 0.9154 | 0.8456 | 0.8768 | 0.8927 | 0.9505 |
| GCM20C-G | 0.8763 | 0.9355 | 0.8779 | 0.9423 | 0.9638 | 0.9478 | 0.9976 | 0.7398 | 0.9357 | 0.9549 | 0.8821 | 0.7952 | 0.8144 | 0.8328 | 0.8808 |
| GCM20C-H | 0.9230 | 0.8787 | 0.8362 | 0.7543 | 0.5720 | 0.6520 | 0.7442 | 0.9976 | 0.8363 | 0.7260 | 0.7067 | 0.7946 | 0.7012 | 0.8193 | 0.6423 |
| GCM20C-I | 0.9498 | 0.9472 | 0.8838 | 0.9523 | 0.8651 | 0.9157 | 0.9315 | 0.8548 | 0.9990 | 0.9471 | 0.9109 | 0.9183 | 0.8582 | 0.9454 | 0.8554 |
| GCM20C-J | 0.9190 | 0.9394 | 0.8420 | 0.9429 | 0.9509 | 0.9624 | 0.9568 | 0.7532 | 0.9597 | 0.9997 | 0.9585 | 0.8863 | 0.9073 | 0.9210 | 0.9375 |
| GCM20C-K | 0.8779 | 0.9184 | 0.7586 | 0.9205 | 0.8643 | 0.9131 | 0.8805 | 0.7342 | 0.9188 | 0.9588 | 0.9996 | 0.9572 | 0.9703 | 0.9510 | 0.9575 |
| GCM20C-L | 0.8644 | 0.8829 | 0.6942 | 0.8774 | 0.6988 | 0.8239 | 0.7821 | 0.8022 | 0.8980 | 0.8632 | 0.9408 | 0.9982 | 0.9378 | 0.9754 | 0.8738 |
| GCM20C-M | 0.8376 | 0.8652 | 0.6823 | 0.8305 | 0.7864 | 0.8617 | 0.8027 | 0.7146 | 0.8557 | 0.9024 | 0.9645 | 0.9477 | 0.9994 | 0.9322 | 0.9626 |
| GCM20C-N | 0.9187 | 0.9183 | 0.7394 | 0.9179 | 0.7639 | 0.8928 | 0.8443 | 0.8366 | 0.9436 | 0.9174 | 0.9456 | 0.9842 | 0.9321 | 0.9998 | 0.9021 |
| GCM20C-O | 0.8164 | 0.8720 | 0.6840 | 0.8740 | 0.8753 | 0.9448 | 0.8762 | 0.6586 | 0.8620 | 0.9394 | 0.9561 | 0.8866 | 0.9651 | 0.9019 | 0.9996 |

| MAE | FUTURE-A | FUTURE-B | FUTURE-C | FUTURE-D | FUTURE-E | FUTURE-F | FUTURE-G | FUTURE-H | FUTURE-I | FUTURE-J | FUTURE-K | FUTURE-L | FUTURE-M | FUTURE-N | FUTURE-O |
|---|---|---|---|---|---|---|---|---|---|---|---|---|---|---|---|
| GCM20C-A | 1.4703 | 4.4433 | 3.0857 | 9.9191 | 12.7142 | 11.9844 | 7.9381 | 2.7416 | 10.3628 | 15.0048 | 13.6830 | 12.4053 | 11.8604 | 12.0566 | 12.1593 |
| GCM20C-B | 3.0806 | 0.6668 | 4.9903 | 6.0179 | 9.0227 | 8.2341 | 3.9807 | 5.7167 | 6.7412 | 11.3861 | 9.9158 | 8.8878 | 8.3591 | 8.6829 | 8.4462 |
| GCM20C-C | 4.1388 | 6.1330 | 1.1935 | 11.2487 | 13.7770 | 13.4163 | 9.0715 | 3.1921 | 11.9088 | 16.8510 | 15.4136 | 14.1361 | 13.5756 | 14.1504 | 13.7895 |
| GCM20C-D | 8.2161 | 5.5440 | 9.8800 | 0.6209 | 5.4566 | 3.4558 | 2.9943 | 10.7753 | 2.7102 | 7.3029 | 5.6451 | 4.8560 | 5.2914 | 4.7473 | 4.8493 |
| GCM20C-E | 10.9398 | 8.6464 | 12.2332 | 5.3385 | 0.7751 | 3.9942 | 5.2150 | 13.9225 | 5.0949 | 5.1876 | 5.7895 | 7.4186 | 6.3681 | 7.1088 | 5.1144 |
| GCM20C-F | 10.3155 | 7.8539 | 12.0797 | 3.5300 | 4.0929 | 0.7980 | 4.7395 | 13.0484 | 3.8508 | 5.6300 | 4.7925 | 5.2133 | 4.6085 | 4.6849 | 2.9932 |
| GCM20C-G | 6.9378 | 4.3324 | 8.2299 | 3.4413 | 5.1292 | 4.7615 | 0.7467 | 9.6086 | 4.1747 | 8.2627 | 7.4062 | 7.1423 | 6.5256 | 6.9443 | 5.8375 |
| GCM20C-H | 4.7346 | 7.1557 | 3.9979 | 12.5703 | 15.8178 | 14.8278 | 10.7147 | 1.6138 | 13.1995 | 18.2516 | 16.6401 | 14.9729 | 14.6062 | 14.8549 | 14.9961 |
| GCM20C-I | 8.2582 | 5.9923 | 10.1568 | 2.6759 | 5.5973 | 4.0360 | 3.7990 | 10.9902 | 0.8695 | 6.7486 | 5.5693 | 4.3385 | 5.0701 | 3.9867 | 5.2260 |
| GCM20C-J | 12.3117 | 10.0529 | 14.4581 | 6.1694 | 4.1413 | 4.6047 | 7.2732 | 15.4716 | 5.1252 | 1.4609 | 3.7773 | 6.0942 | 5.6913 | 5.0246 | 4.9284 |
| GCM20C-K | 11.1167 | 8.6396 | 13.1981 | 4.8269 | 5.4665 | 4.3096 | 6.5664 | 13.9690 | 4.4000 | 4.5898 | 1.3429 | 3.2436 | 2.7095 | 3.2468 | 3.0786 |
| GCM20C-L | 10.1035 | 7.7695 | 12.1751 | 4.4685 | 7.6901 | 5.2942 | 6.5381 | 12.4616 | 4.0040 | 7.3719 | 4.2551 | 1.2445 | 3.2301 | 2.6093 | 4.6537 |
| GCM20C-M | 9.6761 | 7.3830 | 11.6898 | 5.1240 | 6.6701 | 4.8896 | 6.0485 | 12.2450 | 4.7974 | 7.0108 | 4.0800 | 3.4759 | 1.0690 | 3.9857 | 2.7985 |
| GCM20C-N | 9.8027 | 7.6376 | 12.2588 | 4.2790 | 7.1231 | 4.5815 | 6.2345 | 12.4810 | 3.4217 | 6.2122 | 4.1444 | 2.4845 | 3.6783 | 0.9739 | 4.4012 |
| GCM20C-O | 10.4242 | 7.9283 | 12.3406 | 4.8076 | 5.1559 | 3.2201 | 5.6297 | 13.1294 | 4.8934 | 5.8697 | 3.8625 | 4.6665 | 2.5620 | 4.5271 | 0.6758 |

# APPENDIX D

The figures presented in Appendix D all represent the CCSM3 global climate model. The first set of figures are the bar graphs that show the future monthly frequency of both the 2050s (on the left) and the 2090s (on the right) of the patterns denoted as 'tornado unfavorable' at each level. These graphs are divided into three sections, one for each level of the atmosphere. There are nine tornado unfavorable patterns at the 500z level, and eight patterns at both the 700z level and the 850t level. Note the change in the vertical axis of the patterns that occur more than 50% of the time in any month.

The second set of graphics are tables that present the future frequency of every CCSM3 pattern on a decade by decade basis (from the NNR portion of the study, through the GCM20c time period, and into the future decades as well). The main difference between these tables and the afmorementioned bar graphs is that no monthly delineation is made. The tables in section two are seperated by level and by future emissions scenario.

*<u>D.1 – Monthly Frequency of Tornado Unfavorable Patterns</u>*

*<u>D.1.1 – Tornado Unfavorable 500z Patterns: Monthly Frequency</u>*

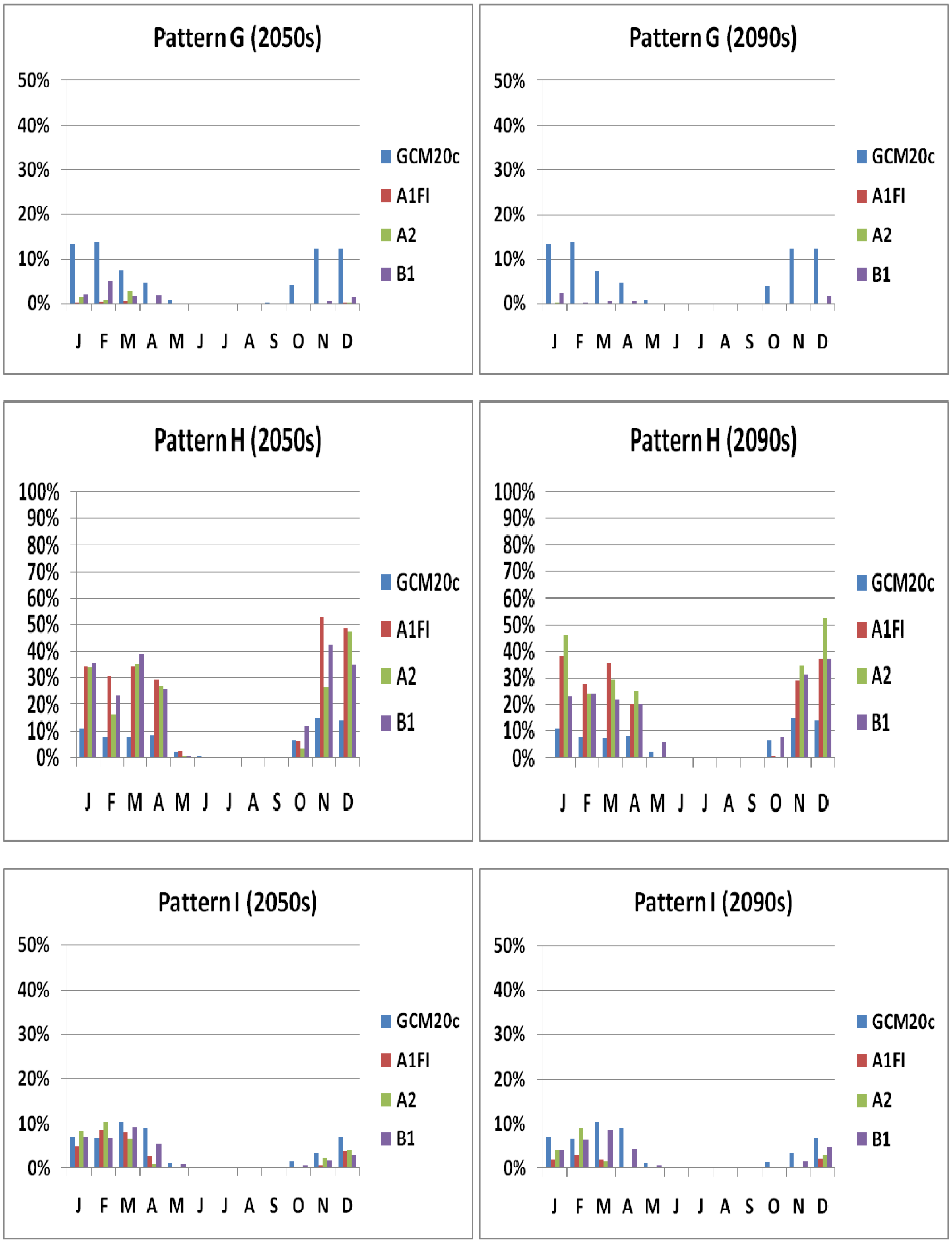


**Figure D.1** – The GCM20c and GCM-Future monthly percent frequency of the tornado unfavorable 500z synoptic patterns in the 2050s (left) and the 2090s (right) for CCSM3. Note the change in the vertical axis with patterns that occur more often than 50% of the time in any month. Continued on the next page.

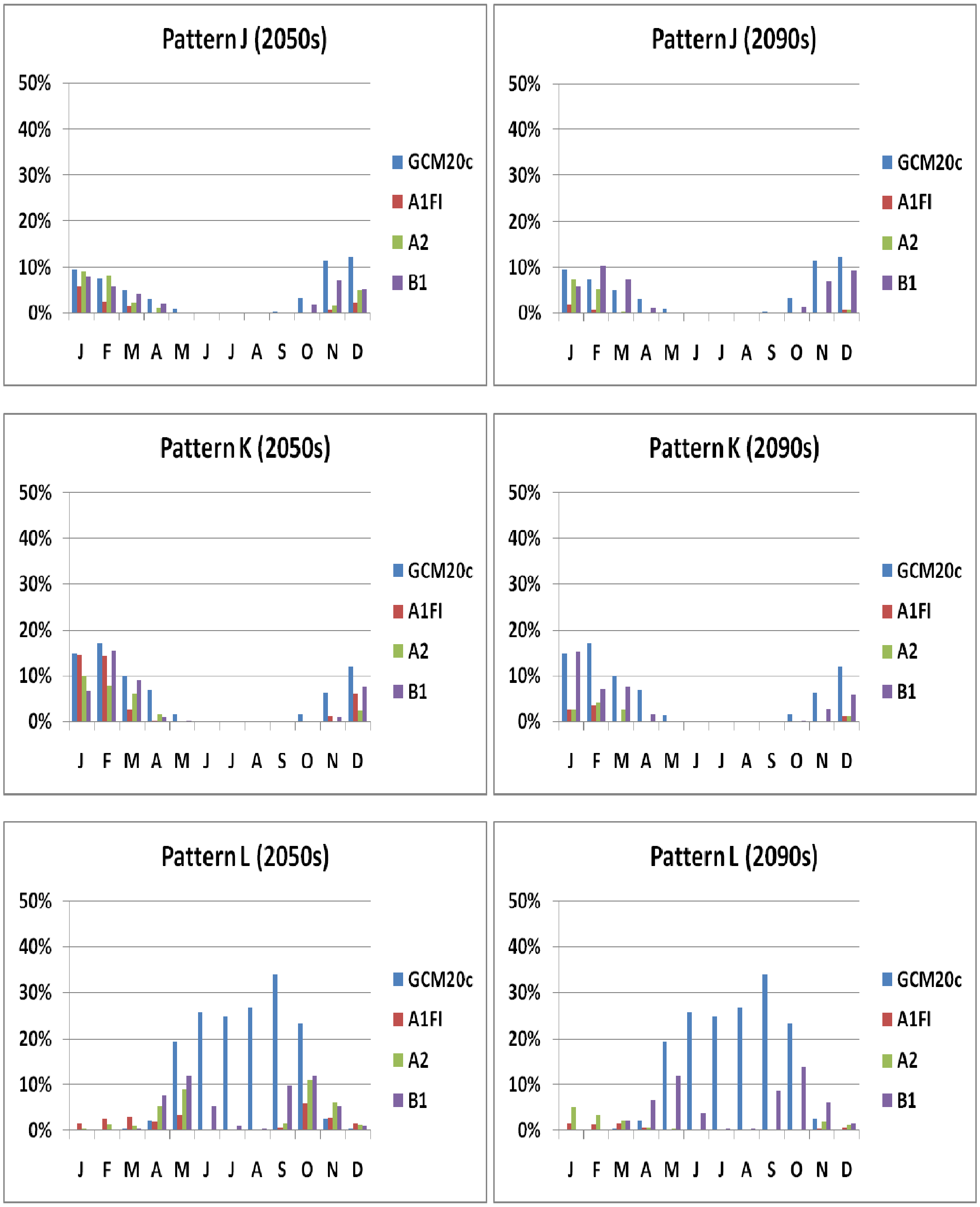


**Figure D.1 (continued)** – The GCM20c and GCM-Future monthly percent frequency of the tornado unfavorable 500z synoptic patterns in the 2050s (left) and the 2090s (right) for CCSM3. Note the change in the vertical axis with patterns that occur more often than 50% of the time in any month. Continued on the next page.

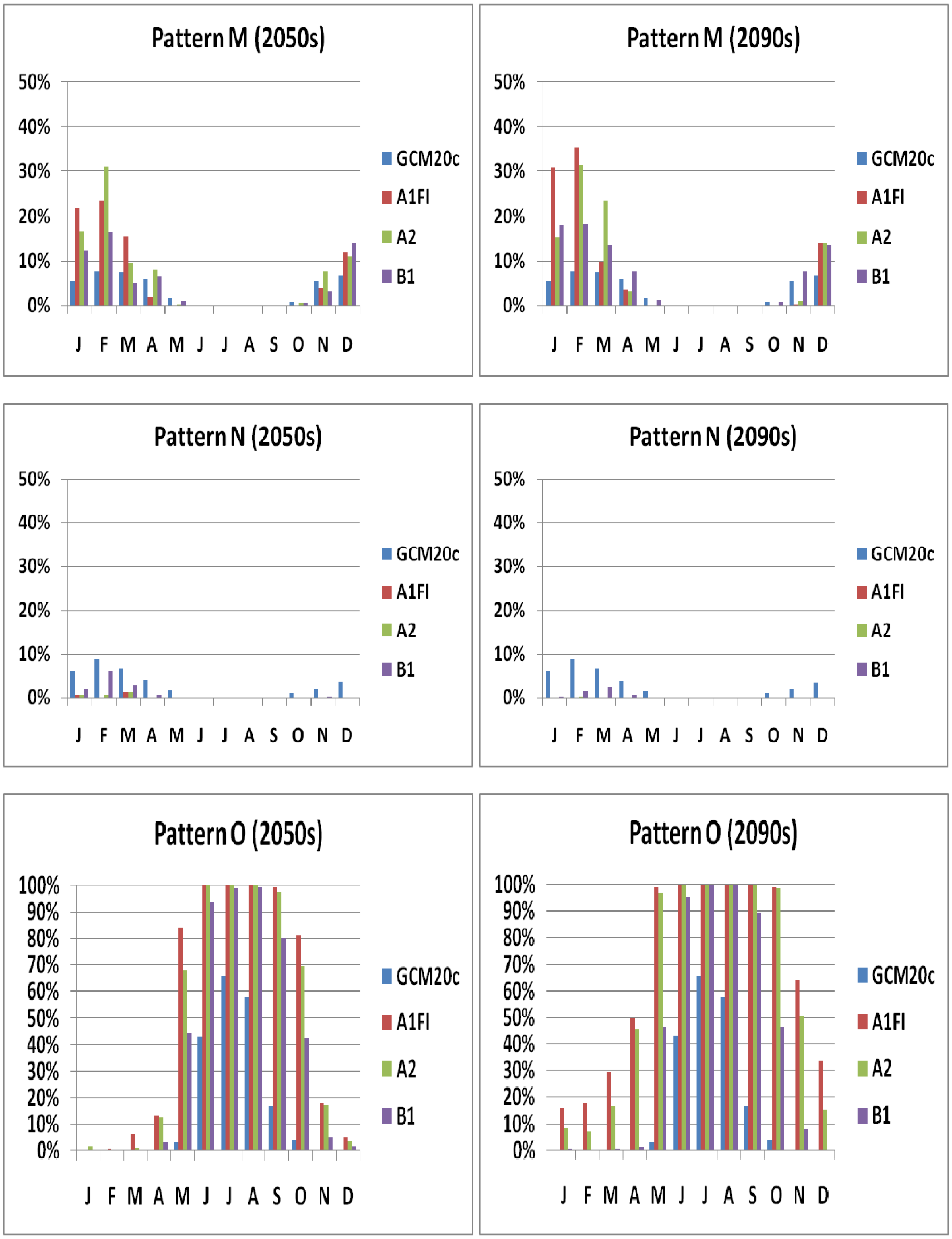


**Figure D.1 (continued)** – The GCM20c and GCM-Future monthly percent frequency of the tornado unfavorable 500z synoptic patterns in the 2050s (left) and the 2090s (right) for CCSM3. Note the change in the vertical axis with patterns that occur more often than 50% of the time in any month.

*D.1.2 – Tornado Unfavorable 700z Patterns: Monthly Frequency*

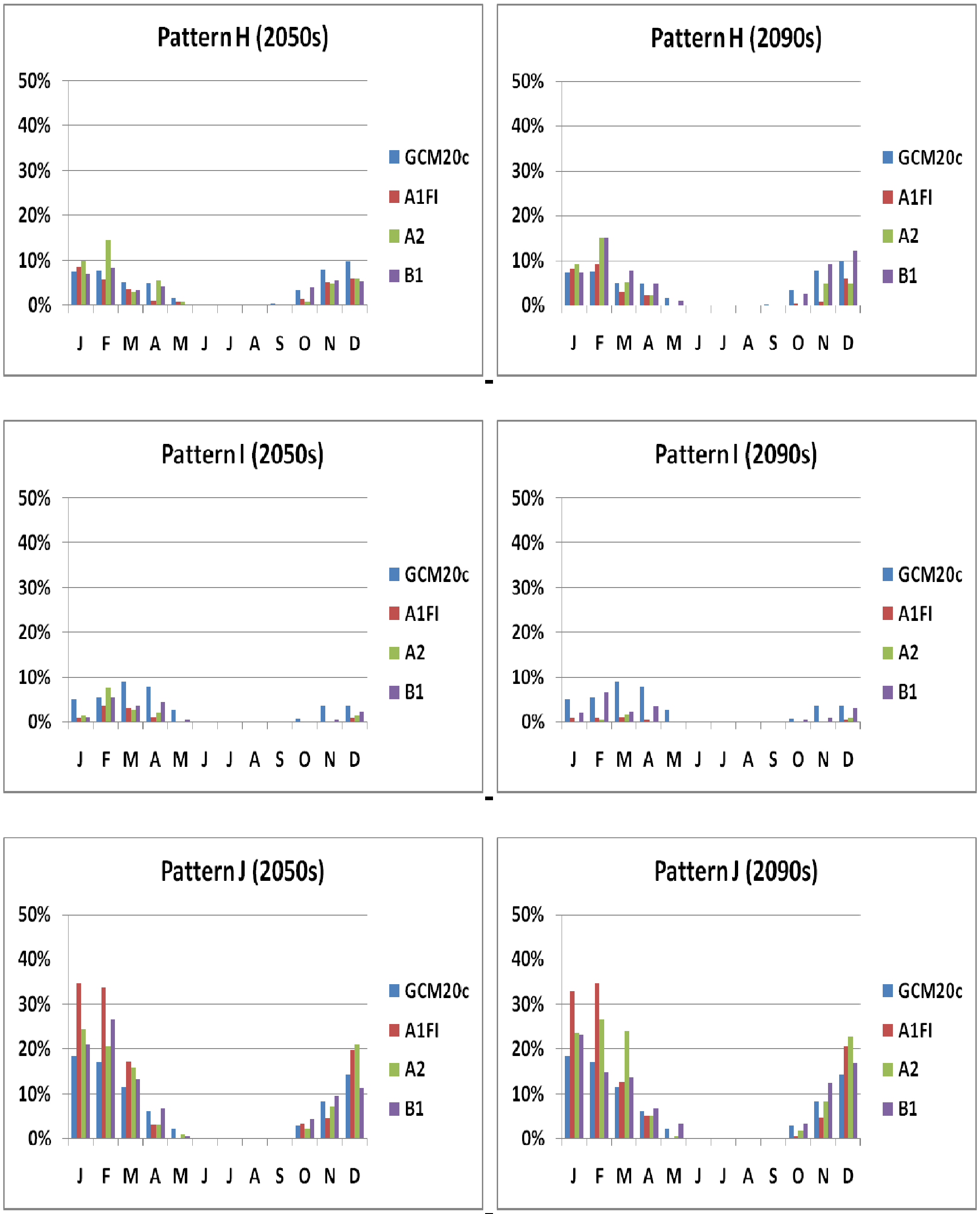


**Figure D.2** – The GCM20c and GCM-Future monthly percent frequency of the tornado unfavorable 700z synoptic patterns in the 2050s (left) and the 2090s (right) for CCSM3. Note the change in the vertical axis with patterns that occur more often than 50% of the time in any month. Continued on the next page.

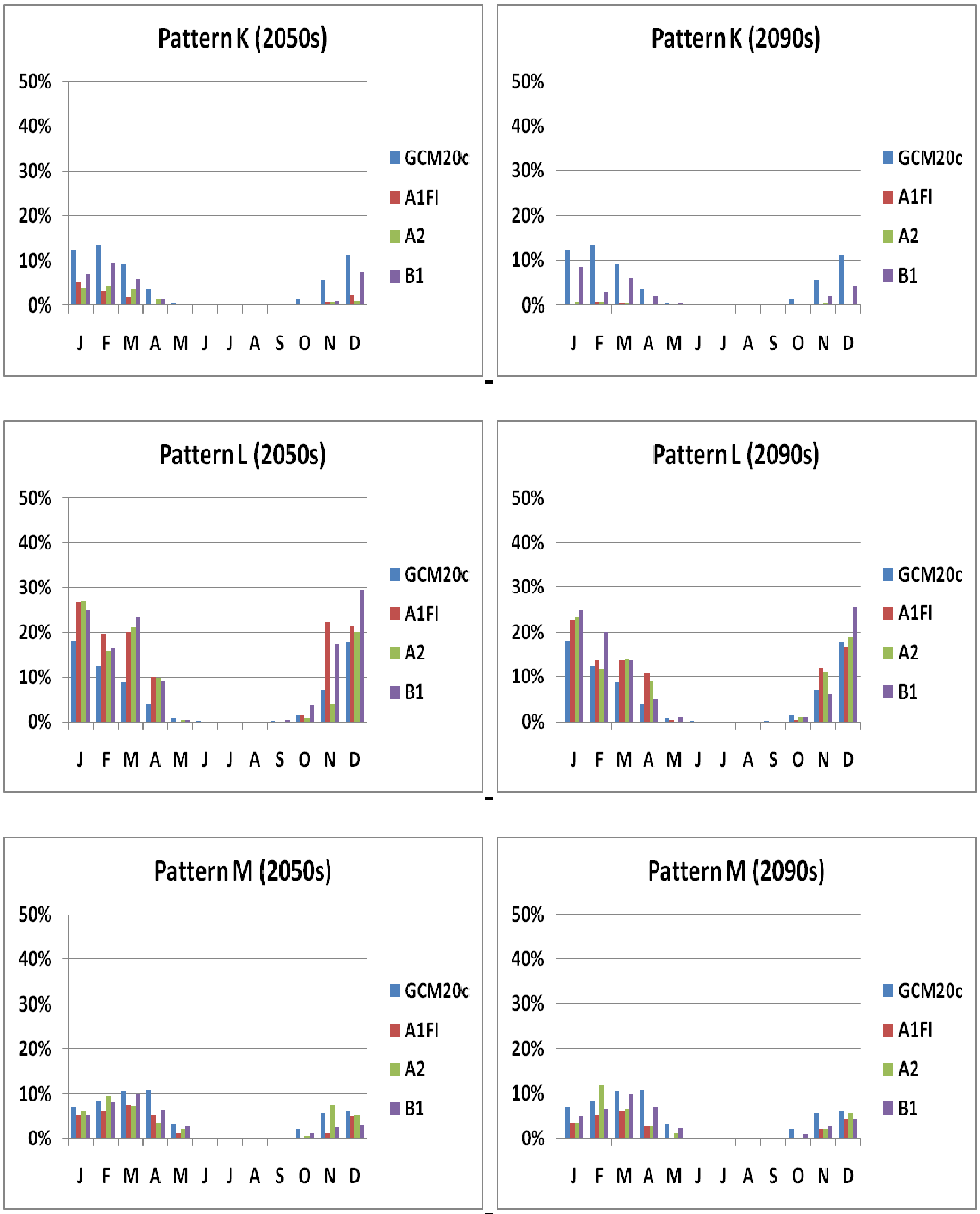


**Figure D.2 (continued)** – The GCM20c and GCM-Future monthly percent frequency of the tornado unfavorable 700z synoptic patterns in the 2050s (left) and the 2090s (right) for CCSM3. Note the change in the vertical axis with patterns that occur more often than 50% of the time in any month. Continued on the next page.

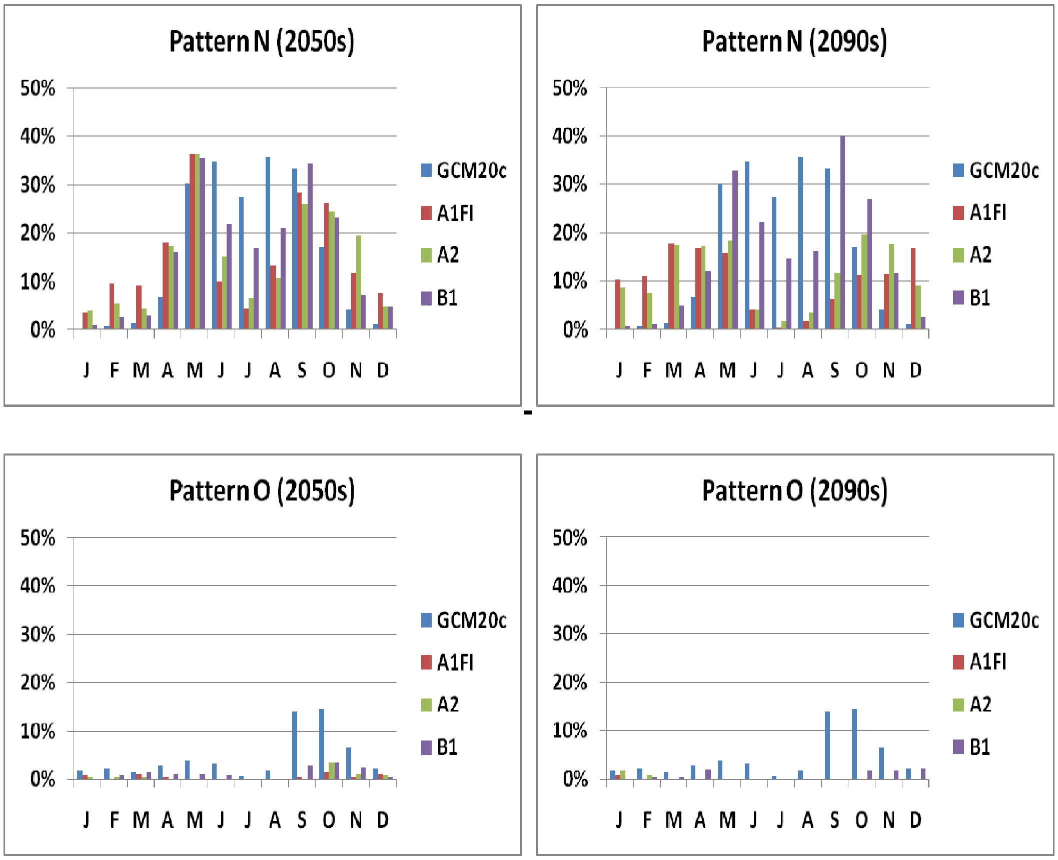


**Figure D.2 (continued)** – The GCM20c and GCM-Future monthly percent frequency of the tornado unfavorable 700z synoptic patterns in the 2050s (left) and the 2090s (right) for CCSM3. Note the change in the vertical axis with patterns that occur more often than 50% of the time in any month.

*D.1.3 – Tornado Unfavorable 850t Patterns: Monthly Frequency*

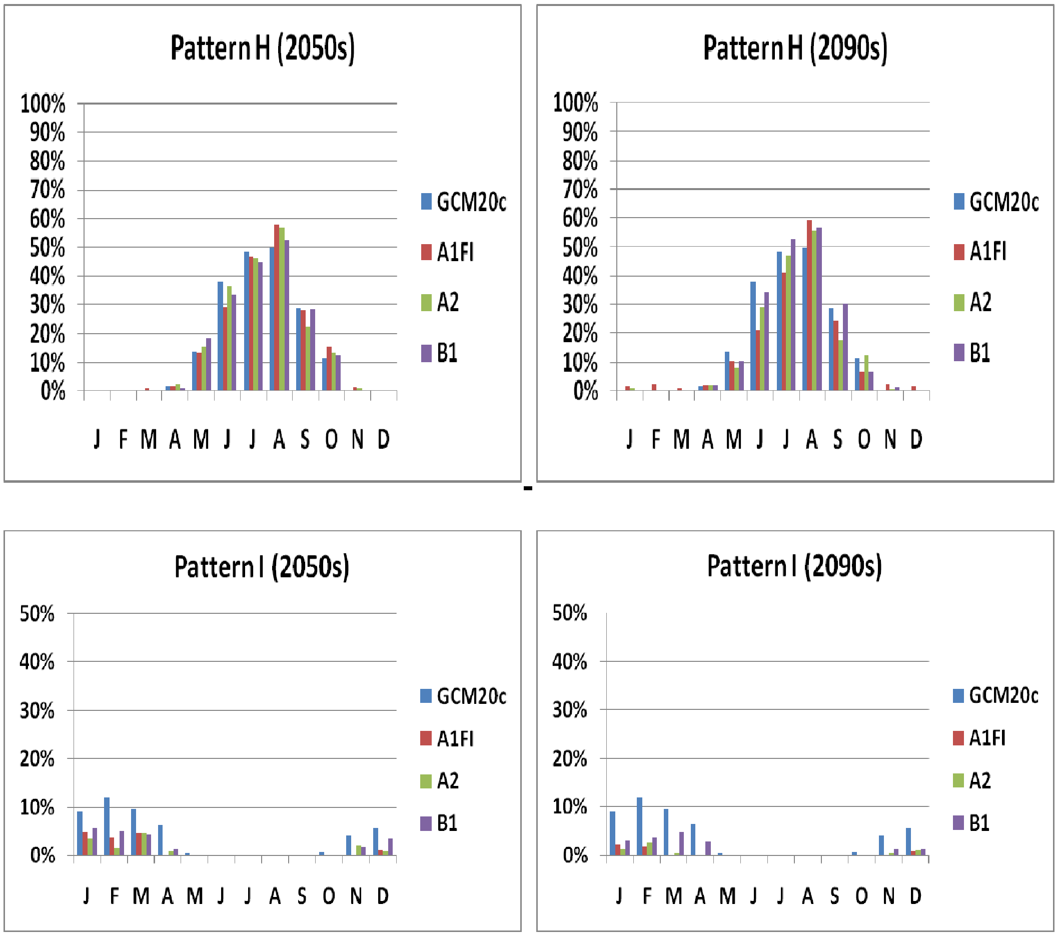


**Figure D.3** – The GCM20c and GCM-Future monthly percent frequency of the tornado unfavorable 850t synoptic patterns in the 2050s (left) and the 2090s (right) for CCSM3. Note the change in the vertical axis with patterns that occur more often than 50% of the time in any month. Continued on the next page.

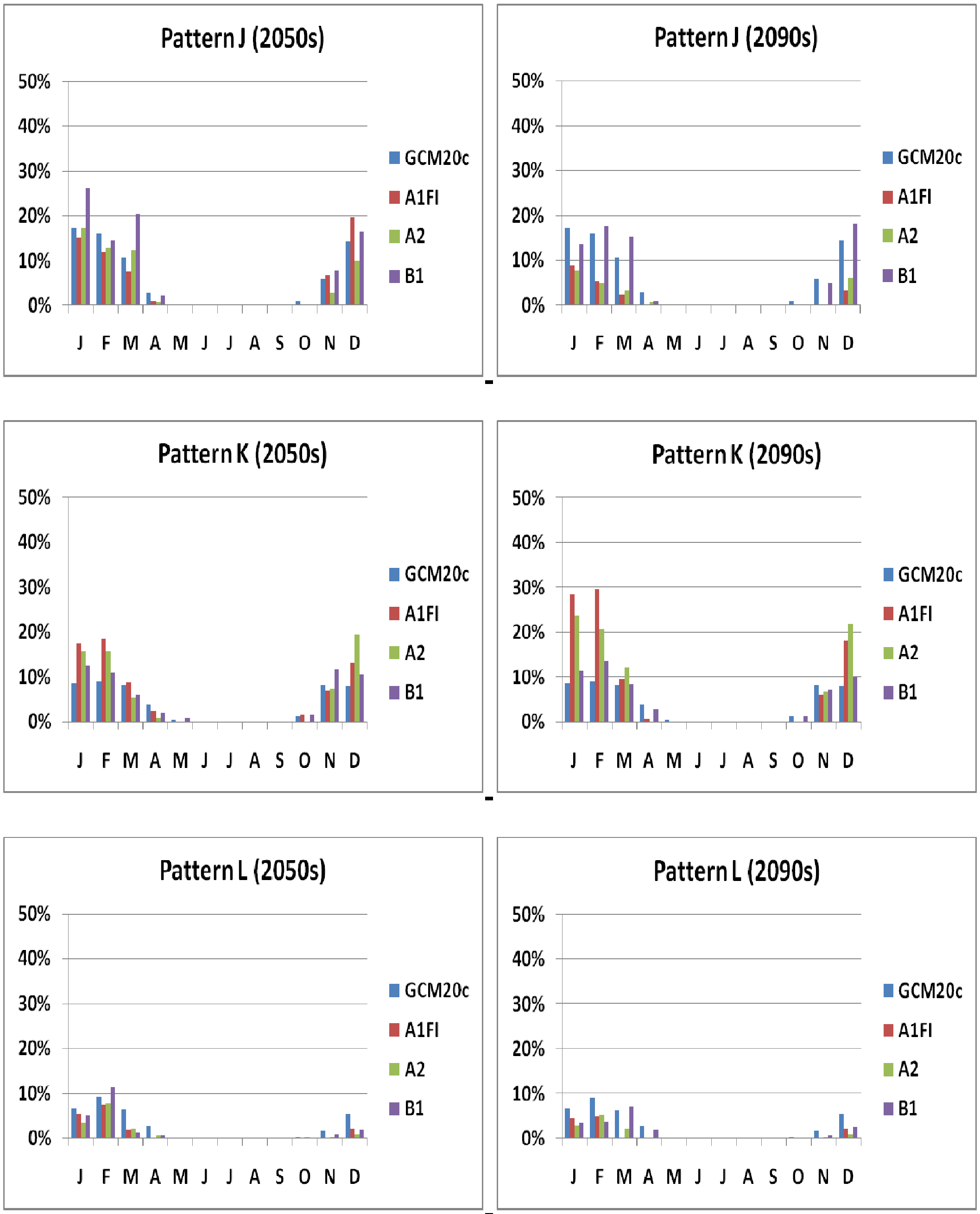


**Figure D.3 (continued)** – The GCM20c and GCM-Future monthly percent frequency of the tornado unfavorable 850t synoptic patterns in the 2050s (left) and the 2090s (right) for CCSM3. Note the change in the vertical axis with patterns that occur more often than 50% of the time in any month. Continued on the next page.

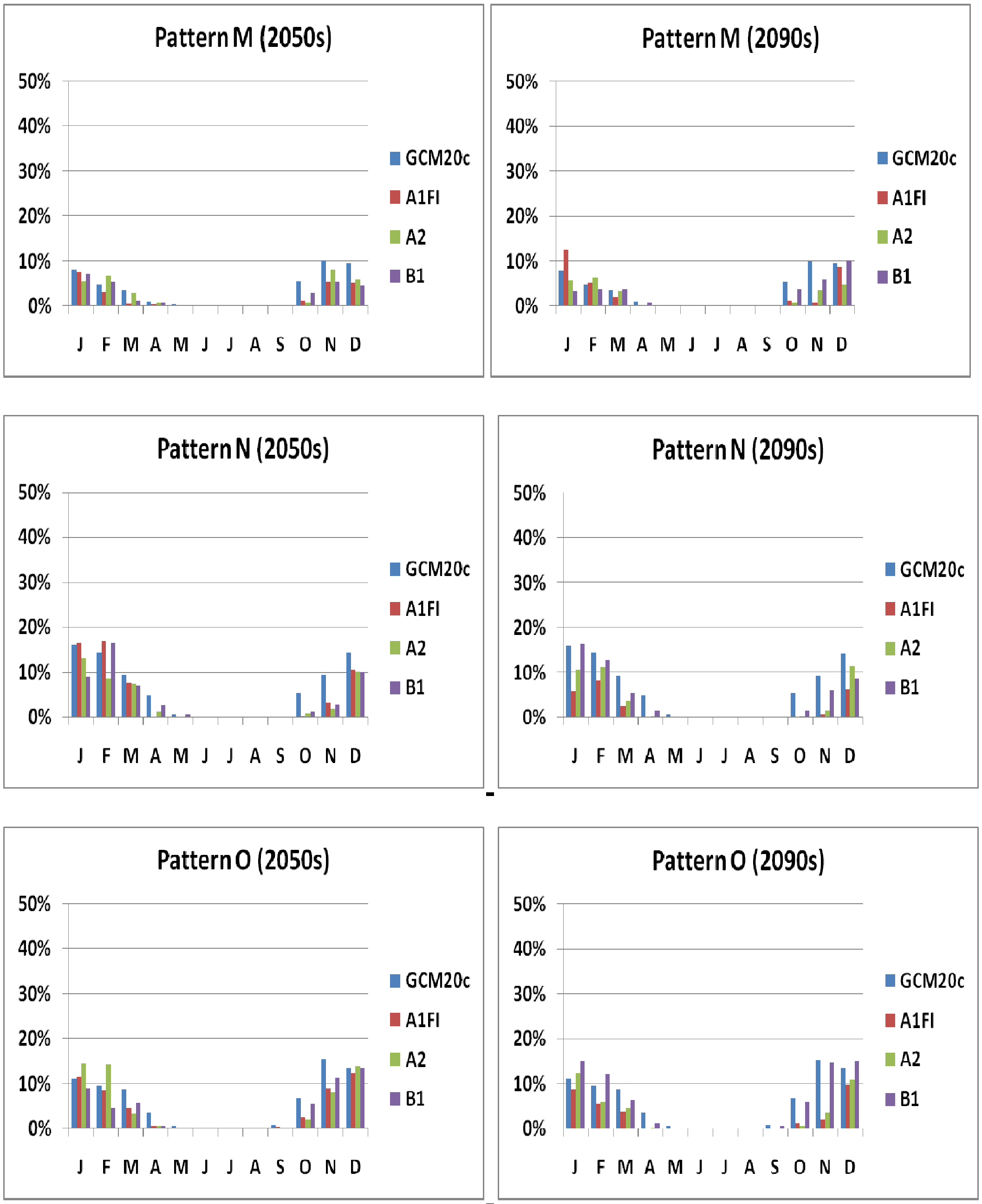


**Figure D.3 (continued)** – The GCM20c and GCM-Future monthly percent frequency of the tornado unfavorable 850t synoptic patterns in the 2050s (left) and the 2090s (right) for CCSM3. Note the change in the vertical axis with patterns that occur more often than 50% of the time in any month.

## *D.2 – Mean Frequency per Decade of CCSM3 Patterns*

### 500mb Geopotential Height Patterns – A2

**Table D.1** – The mean frequency per decade of the 15 patterns at the 500z level for the NNR, GCM20c and GCM-Future portion of the CCSM3 – A1FI results.

| | NNR | | | | GCM 20th Century | | | | GCM Future | | | | | | | | | |
|---|---|---|---|---|---|---|---|---|---|---|---|---|---|---|---|---|---|---|
| | **1960s** | **1970s** | **1980s** | **1990s** | **1960s** | **1970s** | **1980s** | **1990s** | **2000s** | **2010s** | **2020s** | **2030s** | **2040s** | **2050s** | **2060s** | **2070s** | **2080s** | **2090s** |
| **A** | 8.3% | 6.9% | 6.0% | 6.2% | 7.1% | 6.8% | 5.6% | 4.4% | 3.8% | 3.0% | 2.4% | 1.5% | 0.9% | 0.3% | 0.0% | 0.0% | 0.0% | 0.0% |
| **B** | 3.6% | 4.4% | 4.2% | 3.9% | 3.4% | 3.0% | 3.8% | 3.6% | 3.2% | 4.0% | 2.6% | 2.8% | 2.6% | 2.2% | 2.2% | 1.8% | 1.6% | 1.0% |
| **C** | 5.7% | 6.6% | 6.2% | 5.5% | 5.7% | 6.4% | 5.5% | 4.3% | 7.0% | 4.7% | 5.6% | 3.5% | 5.1% | 2.4% | 2.4% | 0.8% | 1.5% | 0.4% |
| **D** | 15.2% | 16.0% | 12.1% | 12.7% | 17.1% | 15.7% | 13.0% | 11.2% | 8.9% | 8.2% | 5.2% | 3.6% | 2.1% | 0.9% | 0.5% | 0.1% | 0.1% | 0.0% |
| **E** | 4.1% | 5.3% | 6.9% | 6.1% | 5.0% | 5.1% | 5.2% | 6.8% | 7.5% | 8.8% | 8.0% | 7.7% | 9.9% | 8.0% | 7.7% | 8.1% | 7.1% | 5.4% |
| **F** | 5.3% | 3.8% | 3.8% | 3.9% | 4.0% | 4.5% | 4.0% | 4.1% | 1.6% | 2.3% | 1.6% | 0.4% | 0.5% | 0.1% | 0.1% | 0.1% | 0.0% | 0.0% |
| **G** | 5.7% | 5.9% | 4.2% | 3.8% | 5.7% | 5.9% | 6.2% | 5.0% | 2.4% | 1.9% | 1.3% | 0.7% | 0.1% | 0.1% | 0.1% | 0.0% | 0.0% | 0.0% |
| **H** | 3.9% | 4.8% | 6.6% | 7.0% | 6.5% | 6.0% | 5.9% | 5.4% | 13.2% | 10.7% | 14.5% | 16.7% | 18.0% | 19.7% | 19.7% | 17.4% | 16.5% | 15.7% |
| **I** | 4.4% | 4.3% | 3.7% | 3.4% | 3.6% | 3.3% | 4.1% | 4.3% | 3.2% | 3.8% | 3.3% | 3.8% | 3.0% | 2.4% | 1.1% | 1.6% | 1.3% | 0.8% |
| **J** | 4.6% | 5.1% | 4.4% | 5.0% | 4.4% | 4.9% | 4.5% | 3.8% | 4.2% | 3.7% | 2.9% | 2.0% | 2.1% | 1.0% | 0.5% | 0.5% | 0.4% | 0.3% |
| **K** | 4.5% | 4.3% | 5.3% | 4.8% | 6.1% | 5.2% | 4.6% | 7.3% | 3.6% | 4.3% | 4.2% | 3.9% | 3.0% | 3.2% | 2.7% | 1.1% | 0.6% | 0.6% |
| **L** | 14.3% | 13.7% | 11.9% | 10.2% | 13.3% | 13.5% | 13.8% | 12.9% | 9.4% | 7.4% | 6.1% | 5.7% | 2.1% | 1.9% | 1.6% | 0.9% | 1.0% | 0.5% |
| **M** | 3.3% | 3.5% | 3.0% | 3.8% | 2.0% | 3.0% | 4.1% | 4.5% | 4.2% | 5.5% | 5.2% | 5.9% | 5.2% | 6.5% | 7.3% | 7.8% | 7.9% | 7.7% |
| **N** | 3.3% | 2.1% | 2.9% | 2.2% | 2.5% | 2.4% | 3.5% | 2.7% | 0.9% | 0.9% | 0.4% | 0.5% | 0.2% | 0.2% | 0.0% | 0.1% | 0.1% | 0.0% |
| **O** | 14.0% | 13.3% | 18.8% | 21.4% | 13.6% | 14.2% | 16.3% | 19.8% | 26.8% | 30.9% | 36.8% | 41.4% | 45.1% | 51.0% | 54.2% | 59.7% | 62.0% | 67.6% |

## 500mb Geopotential Height Patterns – A2

**Table D.2** – The mean frequency per decade of the 15 patterns at the 500z level for the NNR, GCM20c and GCM-Future portion of the CCSM3 – A2 results.

| | NNR | | | | GCM 20th Century | | | | GCM Future | | | | | | | | | |
|---|---|---|---|---|---|---|---|---|---|---|---|---|---|---|---|---|---|---|
| | **1960s** | **1970s** | **1980s** | **1990s** | **1960s** | **1970s** | **1980s** | **1990s** | **2000s** | **2010s** | **2020s** | **2030s** | **2040s** | **2050s** | **2060s** | **2070s** | **2080s** | **2090s** |
| **A** | 8.3% | 6.9% | 6.0% | 6.2% | 7.1% | 6.8% | 5.6% | 4.4% | 3.6% | 2.7% | 2.9% | 1.6% | 1.3% | 0.5% | 0.2% | 0.2% | 0.3% | 0.0% |
| **B** | 3.6% | 4.4% | 4.2% | 3.9% | 3.4% | 3.0% | 3.8% | 3.6% | 2.9% | 3.8% | 3.8% | 3.1% | 4.4% | 3.4% | 1.9% | 2.0% | 2.0% | 1.8% |
| **C** | 5.7% | 6.6% | 6.2% | 5.5% | 5.7% | 6.4% | 5.5% | 4.3% | 6.8% | 4.7% | 5.3% | 5.0% | 3.8% | 2.9% | 3.6% | 2.3% | 1.6% | 0.7% |
| **D** | 15.2% | 16.0% | 12.1% | 12.7% | 17.1% | 15.7% | 13.0% | 11.2% | 9.1% | 6.7% | 6.5% | 5.6% | 3.4% | 2.5% | 1.3% | 1.0% | 0.3% | 0.1% |
| **E** | 4.1% | 5.3% | 6.9% | 6.1% | 5.0% | 5.1% | 5.2% | 6.8% | 6.5% | 8.1% | 10.0% | 8.7% | 8.3% | 8.8% | 5.8% | 7.8% | 7.1% | 6.0% |
| **F** | 5.3% | 3.8% | 3.8% | 3.9% | 4.0% | 4.5% | 4.0% | 4.1% | 3.0% | 1.6% | 1.2% | 0.9% | 0.5% | 0.4% | 0.0% | 0.1% | 0.1% | 0.0% |
| **G** | 5.7% | 5.9% | 4.2% | 3.8% | 5.7% | 5.9% | 6.2% | 5.0% | 2.8% | 1.6% | 1.5% | 1.4% | 0.5% | 0.4% | 0.0% | 0.0% | 0.1% | 0.0% |
| **H** | 3.9% | 4.8% | 6.6% | 7.0% | 6.5% | 6.0% | 5.9% | 5.4% | 9.6% | 11.1% | 10.8% | 13.3% | 17.4% | 15.8% | 23.4% | 21.8% | 21.5% | 17.6% |
| **I** | 4.4% | 4.3% | 3.7% | 3.4% | 3.6% | 3.3% | 4.1% | 4.3% | 3.7% | 3.8% | 4.3% | 3.2% | 3.3% | 2.7% | 2.1% | 2.1% | 1.3% | 1.4% |
| **J** | 4.6% | 5.1% | 4.4% | 5.0% | 4.4% | 4.9% | 4.5% | 3.8% | 4.4% | 3.8% | 3.5% | 2.4% | 2.5% | 2.2% | 1.4% | 1.4% | 0.5% | 1.1% |
| **K** | 4.5% | 4.3% | 5.3% | 4.8% | 6.1% | 5.2% | 4.6% | 7.3% | 5.6% | 5.0% | 3.6% | 4.7% | 3.4% | 2.3% | 1.5% | 1.6% | 1.2% | 0.9% |
| **L** | 14.3% | 13.7% | 11.9% | 10.2% | 13.3% | 13.5% | 13.8% | 12.9% | 9.0% | 9.5% | 7.2% | 4.8% | 3.8% | 3.1% | 2.3% | 1.5% | 1.6% | 1.2% |
| **M** | 3.3% | 3.5% | 3.0% | 3.8% | 2.0% | 3.0% | 4.1% | 4.5% | 3.9% | 5.2% | 4.9% | 5.2% | 4.9% | 6.9% | 5.9% | 6.9% | 5.9% | 7.2% |
| **N** | 3.3% | 2.1% | 2.9% | 2.2% | 2.5% | 2.4% | 3.5% | 2.7% | 1.7% | 1.6% | 1.0% | 0.7% | 0.2% | 0.2% | 0.0% | 0.0% | 0.0% | 0.0% |
| **O** | 14.0% | 13.3% | 18.8% | 21.4% | 13.6% | 14.2% | 16.3% | 19.8% | 27.3% | 31.0% | 33.5% | 39.3% | 42.3% | 47.9% | 50.6% | 51.3% | 56.7% | 61.9% |

## 500mb Geopotential Height Patterns – B1

**Table D.3** – The mean frequency per decade of the 15 patterns at the 500z level for the NNR, GCM20c and GCM-Future portion of the CCSM3 – B1 results.

| | NNR | | | | GCM 20th Century | | | | GCM Future | | | | | | | | | |
|---|---|---|---|---|---|---|---|---|---|---|---|---|---|---|---|---|---|---|
| | **1960s** | **1970s** | **1980s** | **1990s** | **1960s** | **1970s** | **1980s** | **1990s** | **2000s** | **2010s** | **2020s** | **2030s** | **2040s** | **2050s** | **2060s** | **2070s** | **2080s** | **2090s** |
| **A** | 8.3% | 6.9% | 6.0% | 6.2% | 7.1% | 6.8% | 5.6% | 4.4% | 3.2% | 3.6% | 2.8% | 2.8% | 1.9% | 2.1% | 1.5% | 2.0% | 1.2% | 1.5% |
| **B** | 3.6% | 4.4% | 4.2% | 3.9% | 3.4% | 3.0% | 3.8% | 3.6% | 4.1% | 2.8% | 3.0% | 3.6% | 2.5% | 3.4% | 2.8% | 4.8% | 2.9% | 3.8% |
| **C** | 5.7% | 6.6% | 6.2% | 5.5% | 5.7% | 6.4% | 5.5% | 4.3% | 7.0% | 6.5% | 6.0% | 6.2% | 5.4% | 5.3% | 5.0% | 4.4% | 5.4% | 5.3% |
| **D** | 15.2% | 16.0% | 12.1% | 12.7% | 17.1% | 15.7% | 13.0% | 11.2% | 8.7% | 6.7% | 7.1% | 7.0% | 5.5% | 3.2% | 3.8% | 4.1% | 3.6% | 2.6% |
| **E** | 4.1% | 5.3% | 6.9% | 6.1% | 5.0% | 5.1% | 5.2% | 6.8% | 6.8% | 8.2% | 7.5% | 6.8% | 8.2% | 8.0% | 8.8% | 9.3% | 7.4% | 9.3% |
| **F** | 5.3% | 3.8% | 3.8% | 3.9% | 4.0% | 4.5% | 4.0% | 4.1% | 1.7% | 1.7% | 1.0% | 0.9% | 0.8% | 0.8% | 1.1% | 1.0% | 0.6% | 0.8% |
| **G** | 5.7% | 5.9% | 4.2% | 3.8% | 5.7% | 5.9% | 6.2% | 5.0% | 2.6% | 2.1% | 1.1% | 1.4% | 1.0% | 1.0% | 0.7% | 0.4% | 0.7% | 0.5% |
| **H** | 3.9% | 4.8% | 6.6% | 7.0% | 6.5% | 6.0% | 5.9% | 5.4% | 11.7% | 10.7% | 15.1% | 13.5% | 14.3% | 17.7% | 15.6% | 13.2% | 15.7% | 14.2% |
| **I** | 4.4% | 4.3% | 3.7% | 3.4% | 3.6% | 3.3% | 4.1% | 4.3% | 3.4% | 3.2% | 2.5% | 3.0% | 3.0% | 2.8% | 2.7% | 2.4% | 2.8% | 2.6% |
| **J** | 4.6% | 5.1% | 4.4% | 5.0% | 4.4% | 4.9% | 4.5% | 3.8% | 3.6% | 3.2% | 3.7% | 3.4% | 3.7% | 2.8% | 3.3% | 3.2% | 2.2% | 3.5% |
| **K** | 4.5% | 4.3% | 5.3% | 4.8% | 6.1% | 5.2% | 4.6% | 7.3% | 4.7% | 5.2% | 4.7% | 3.9% | 4.7% | 3.4% | 4.0% | 3.4% | 3.7% | 3.4% |
| **L** | 14.3% | 13.7% | 11.9% | 10.2% | 13.3% | 13.5% | 13.8% | 12.9% | 10.3% | 8.8% | 6.9% | 6.6% | 6.0% | 4.5% | 4.2% | 4.6% | 5.5% | 4.6% |
| **M** | 3.3% | 3.5% | 3.0% | 3.8% | 2.0% | 3.0% | 4.1% | 4.5% | 4.1% | 3.9% | 3.9% | 6.0% | 4.5% | 4.9% | 5.4% | 5.5% | 6.7% | 6.7% |
| **N** | 3.3% | 2.1% | 2.9% | 2.2% | 2.5% | 2.4% | 3.5% | 2.7% | 1.1% | 1.6% | 1.0% | 0.9% | 0.5% | 1.0% | 0.5% | 0.7% | 0.4% | 0.4% |
| **O** | 14.0% | 13.3% | 18.8% | 21.4% | 13.6% | 14.2% | 16.3% | 19.8% | 27.0% | 31.9% | 33.7% | 34.0% | 38.0% | 39.3% | 40.7% | 40.8% | 41.2% | 40.8% |

## 700mb Geopotential Height Patterns – A1FI

**Table D.4** – The mean frequency per decade of the 15 patterns at the 700z level for the NNR, GCM20c and GCM-Future portion of the CCSM3 – A1FI results.

| | NNR | | | | GCM 20th Century | | | | GCM Future | | | | | | | | | |
|---|---|---|---|---|---|---|---|---|---|---|---|---|---|---|---|---|---|---|
| | **1960s** | **1970s** | **1980s** | **1990s** | **1960s** | **1970s** | **1980s** | **1990s** | **2000s** | **2010s** | **2020s** | **2030s** | **2040s** | **2050s** | **2060s** | **2070s** | **2080s** | **2090s** |
| **A** | 6.3% | 5.3% | 7.5% | 8.7% | 7.4% | 5.9% | 7.1% | 4.9% | 8.9% | 9.1% | 9.7% | 9.6% | 9.5% | 9.4% | 9.5% | 9.3% | 8.5% | 6.8% |
| **B** | 6.3% | 6.4% | 5.6% | 5.8% | 5.4% | 4.1% | 4.7% | 3.4% | 2.6% | 2.4% | 2.2% | 1.6% | 1.0% | 0.5% | 0.6% | 0.2% | 0.1% | 0.0% |
| **C** | 6.0% | 8.3% | 6.6% | 7.2% | 8.5% | 9.6% | 8.1% | 7.1% | 7.8% | 8.0% | 7.5% | 6.0% | 6.7% | 5.0% | 5.3% | 4.7% | 3.8% | 2.6% |
| **D** | 5.6% | 4.9% | 4.9% | 5.2% | 5.0% | 4.4% | 4.5% | 4.3% | 4.9% | 4.7% | 4.2% | 3.8% | 3.8% | 2.4% | 2.6% | 2.2% | 2.2% | 1.6% |
| **E** | 14.9% | 16.9% | 19.0% | 21.2% | 16.1% | 16.4% | 17.3% | 18.9% | 22.4% | 24.7% | 28.5% | 31.0% | 34.5% | 39.7% | 44.1% | 48.9% | 51.2% | 57.3% |
| **F** | 7.2% | 6.5% | 4.2% | 5.0% | 7.8% | 8.3% | 6.1% | 7.1% | 4.7% | 4.4% | 3.3% | 2.4% | 2.0% | 1.2% | 0.5% | 0.6% | 0.3% | 0.2% |
| **G** | 2.7% | 2.6% | 2.2% | 2.2% | 2.2% | 3.2% | 2.5% | 2.5% | 0.8% | 1.5% | 1.1% | 0.4% | 0.4% | 0.2% | 0.2% | 0.4% | 0.1% | 0.0% |
| **H** | 4.4% | 4.4% | 4.9% | 4.0% | 3.3% | 4.0% | 4.2% | 4.3% | 4.3% | 4.5% | 3.1% | 3.0% | 3.2% | 2.6% | 2.6% | 3.6% | 3.2% | 2.4% |
| **I** | 4.7% | 4.1% | 3.9% | 3.4% | 2.6% | 2.6% | 3.5% | 3.6% | 1.8% | 2.4% | 1.0% | 1.0% | 0.7% | 0.7% | 0.5% | 0.7% | 0.3% | 0.2% |
| **J** | 5.1% | 5.0% | 6.5% | 5.5% | 6.8% | 5.5% | 6.9% | 7.6% | 7.1% | 7.1% | 7.8% | 9.1% | 8.4% | 9.5% | 8.8% | 7.7% | 8.7% | 9.1% |
| **K** | 5.1% | 6.5% | 4.9% | 5.0% | 4.8% | 5.1% | 4.0% | 5.1% | 3.1% | 2.7% | 2.5% | 1.9% | 1.3% | 1.1% | 1.0% | 0.2% | 0.4% | 0.1% |
| **L** | 5.0% | 5.6% | 6.1% | 5.4% | 6.3% | 6.3% | 6.1% | 4.6% | 10.4% | 6.5% | 7.6% | 8.1% | 10.6% | 10.1% | 9.0% | 6.6% | 8.2% | 7.5% |
| **M** | 6.1% | 4.4% | 5.1% | 4.2% | 3.6% | 4.3% | 4.5% | 5.3% | 2.9% | 4.0% | 3.0% | 3.5% | 3.2% | 2.5% | 1.8% | 2.7% | 1.9% | 1.9% |
| **N** | 14.6% | 14.3% | 15.7% | 13.6% | 16.5% | 15.9% | 15.8% | 16.1% | 16.5% | 15.3% | 16.5% | 17.5% | 14.2% | 14.8% | 13.2% | 12.0% | 11.2% | 10.3% |
| **O** | 6.0% | 4.6% | 3.0% | 3.8% | 3.8% | 4.4% | 4.7% | 5.2% | 1.9% | 2.7% | 1.8% | 1.2% | 0.5% | 0.4% | 0.4% | 0.1% | 0.0% | 0.1% |

## 700mb Geopotential Height Patterns – A2

**Table D.5** – The mean frequency per decade of the 15 patterns at the 700z level for the NNR, GCM20c and GCM-Future portion of the CCSM3 – A2 results.

| | NNR | | | | GCM 20th Century | | | | GCM Future | | | | | | | | | |
|---|---|---|---|---|---|---|---|---|---|---|---|---|---|---|---|---|---|---|
| | **1960s** | **1970s** | **1980s** | **1990s** | **1960s** | **1970s** | **1980s** | **1990s** | **2000s** | **2010s** | **2020s** | **2030s** | **2040s** | **2050s** | **2060s** | **2070s** | **2080s** | **2090s** |
| **A** | 6.3% | 5.3% | 7.5% | 8.7% | 7.4% | 5.9% | 7.1% | 4.9% | 7.4% | 6.8% | 8.2% | 9.3% | 9.7% | 9.0% | 10.9% | 9.6% | 9.1% | 7.3% |
| **B** | 6.3% | 6.4% | 5.6% | 5.8% | 5.4% | 4.1% | 4.7% | 3.4% | 2.3% | 2.2% | 2.4% | 2.0% | 1.2% | 0.9% | 0.3% | 0.3% | 0.3% | 0.1% |
| **C** | 6.0% | 8.3% | 6.6% | 7.2% | 8.5% | 9.6% | 8.1% | 7.1% | 8.2% | 7.5% | 7.1% | 7.0% | 7.4% | 6.6% | 5.8% | 5.7% | 5.7% | 4.5% |
| **D** | 5.6% | 4.9% | 4.9% | 5.2% | 5.0% | 4.4% | 4.5% | 4.3% | 3.9% | 4.6% | 5.0% | 3.6% | 3.9% | 3.2% | 2.4% | 2.8% | 2.8% | 2.2% |
| **E** | 14.9% | 16.9% | 19.0% | 21.2% | 16.1% | 16.4% | 17.3% | 18.9% | 24.2% | 24.5% | 25.9% | 30.6% | 32.8% | 37.8% | 39.3% | 41.8% | 46.3% | 51.0% |
| **F** | 7.2% | 6.5% | 4.2% | 5.0% | 7.8% | 8.3% | 6.1% | 7.1% | 4.6% | 4.2% | 4.3% | 3.5% | 2.3% | 2.0% | 1.3% | 1.2% | 0.3% | 0.1% |
| **G** | 2.7% | 2.6% | 2.2% | 2.2% | 2.2% | 3.2% | 2.5% | 2.5% | 1.7% | 1.2% | 1.0% | 0.3% | 0.4% | 0.3% | 0.1% | 0.1% | 0.1% | 0.1% |
| **H** | 4.4% | 4.4% | 4.9% | 4.0% | 3.3% | 4.0% | 4.2% | 4.3% | 3.8% | 4.1% | 4.2% | 4.1% | 3.4% | 3.6% | 2.7% | 3.2% | 2.5% | 3.3% |
| **I** | 4.7% | 4.1% | 3.9% | 3.4% | 2.6% | 2.6% | 3.5% | 3.6% | 2.0% | 2.3% | 1.6% | 1.6% | 1.6% | 1.2% | 0.5% | 0.5% | 0.4% | 0.2% |
| **J** | 5.1% | 5.0% | 6.5% | 5.5% | 6.8% | 5.5% | 6.9% | 7.6% | 7.5% | 7.7% | 7.7% | 7.6% | 7.9% | 7.8% | 7.5% | 8.8% | 6.5% | 9.2% |
| **K** | 5.1% | 6.5% | 4.9% | 5.0% | 4.8% | 5.1% | 4.0% | 5.1% | 4.2% | 3.1% | 2.6% | 2.7% | 1.8% | 1.2% | 0.9% | 0.4% | 0.6% | 0.2% |
| **L** | 5.0% | 5.6% | 6.1% | 5.4% | 6.3% | 6.3% | 6.1% | 4.6% | 7.3% | 7.4% | 7.4% | 7.0% | 7.9% | 8.2% | 12.7% | 11.1% | 10.7% | 7.4% |
| **M** | 6.1% | 4.4% | 5.1% | 4.2% | 3.6% | 4.3% | 4.5% | 5.3% | 3.9% | 4.2% | 4.1% | 3.3% | 3.5% | 3.3% | 2.4% | 2.4% | 1.5% | 2.7% |
| **N** | 14.6% | 14.3% | 15.7% | 13.6% | 16.5% | 15.9% | 15.8% | 16.1% | 16.0% | 17.8% | 16.8% | 16.0% | 15.4% | 14.4% | 13.0% | 12.1% | 13.0% | 11.4% |
| **O** | 6.0% | 4.6% | 3.0% | 3.8% | 3.8% | 4.4% | 4.7% | 5.2% | 2.8% | 2.3% | 1.6% | 1.4% | 0.8% | 0.5% | 0.3% | 0.1% | 0.2% | 0.2% |

## 700mb Geopotential Height Patterns – B1

**Table D.6** – The mean frequency per decade of the 15 patterns at the 700z level for the NNR, GCM20c and GCM-Future portion of the CCSM3 – B1 results.

| | NNR | | | | GCM 20th Century | | | | GCM Future | | | | | | | | | |
|---|---|---|---|---|---|---|---|---|---|---|---|---|---|---|---|---|---|---|
| | **1960s** | **1970s** | **1980s** | **1990s** | **1960s** | **1970s** | **1980s** | **1990s** | **2000s** | **2010s** | **2020s** | **2030s** | **2040s** | **2050s** | **2060s** | **2070s** | **2080s** | **2090s** |
| **A** | 6.3% | 5.3% | 7.5% | 8.7% | 7.4% | 5.9% | 7.1% | 4.9% | 8.8% | 7.1% | 10.1% | 8.6% | 8.9% | 8.9% | 8.9% | 7.4% | 8.5% | 8.4% |
| **B** | 6.3% | 6.4% | 5.6% | 5.8% | 5.4% | 4.1% | 4.7% | 3.4% | 2.3% | 2.3% | 2.5% | 2.5% | 2.0% | 1.7% | 1.5% | 1.9% | 1.3% | 1.3% |
| **C** | 6.0% | 8.3% | 6.6% | 7.2% | 8.5% | 9.6% | 8.1% | 7.1% | 8.2% | 8.2% | 7.3% | 8.5% | 6.8% | 7.7% | 8.0% | 8.4% | 6.2% | 8.8% |
| **D** | 5.6% | 4.9% | 4.9% | 5.2% | 5.0% | 4.4% | 4.5% | 4.3% | 4.3% | 4.1% | 4.4% | 4.4% | 4.9% | 4.5% | 3.6% | 5.5% | 3.8% | 3.7% |
| **E** | 14.9% | 16.9% | 19.0% | 21.2% | 16.1% | 16.4% | 17.3% | 18.9% | 22.6% | 26.1% | 27.1% | 27.0% | 30.8% | 29.7% | 31.9% | 32.1% | 31.5% | 31.0% |
| **F** | 7.2% | 6.5% | 4.2% | 5.0% | 7.8% | 8.3% | 6.1% | 7.1% | 5.0% | 5.1% | 3.9% | 3.8% | 3.2% | 2.1% | 3.2% | 2.8% | 3.0% | 2.3% |
| **G** | 2.7% | 2.6% | 2.2% | 2.2% | 2.2% | 3.2% | 2.5% | 2.5% | 1.6% | 1.0% | 1.0% | 0.9% | 0.7% | 0.6% | 0.9% | 1.0% | 0.8% | 0.7% |
| **H** | 4.4% | 4.4% | 4.9% | 4.0% | 3.3% | 4.0% | 4.2% | 4.3% | 3.7% | 3.5% | 3.3% | 3.8% | 3.2% | 3.0% | 3.8% | 4.1% | 3.5% | 4.8% |
| **I** | 4.7% | 4.1% | 3.9% | 3.4% | 2.6% | 2.6% | 3.5% | 3.6% | 1.7% | 2.0% | 1.1% | 1.9% | 1.2% | 1.4% | 1.3% | 1.9% | 1.3% | 1.5% |
| **J** | 5.1% | 5.0% | 6.5% | 5.5% | 6.8% | 5.5% | 6.9% | 7.6% | 6.5% | 7.5% | 6.5% | 6.9% | 7.3% | 7.6% | 7.1% | 6.7% | 7.8% | 7.8% |
| **K** | 5.1% | 6.5% | 4.9% | 5.0% | 4.8% | 5.1% | 4.0% | 5.1% | 4.8% | 2.5% | 2.6% | 3.0% | 3.2% | 2.6% | 2.7% | 2.1% | 2.5% | 2.2% |
| **L** | 5.0% | 5.6% | 6.1% | 5.4% | 6.3% | 6.3% | 6.1% | 4.6% | 7.4% | 7.9% | 10.2% | 8.2% | 7.9% | 10.4% | 8.7% | 7.8% | 9.9% | 8.0% |
| **M** | 6.1% | 4.4% | 5.1% | 4.2% | 3.6% | 4.3% | 4.5% | 5.3% | 3.2% | 3.9% | 2.9% | 3.2% | 3.6% | 3.1% | 3.4% | 3.0% | 3.0% | 3.1% |
| **N** | 14.6% | 14.3% | 15.7% | 13.6% | 16.5% | 15.9% | 15.8% | 16.1% | 17.6% | 16.6% | 15.8% | 15.2% | 14.7% | 15.6% | 13.9% | 14.5% | 16.0% | 15.5% |
| **O** | 6.0% | 4.6% | 3.0% | 3.8% | 3.8% | 4.4% | 4.7% | 5.2% | 2.4% | 2.1% | 1.3% | 2.2% | 1.6% | 1.1% | 1.0% | 0.9% | 0.8% | 0.7% |

## 850mb Temperature Patterns – A1FI

**Table D.7** – The mean frequency per decade of the 15 patterns at the 850t level for the NNR, GCM20c and GCM-Future portion of the CCSM3 – A1FI results.

| | NNR | | | | GCM 20th Century | | | | GCM Future | | | | | | | | | |
|---|---|---|---|---|---|---|---|---|---|---|---|---|---|---|---|---|---|---|
| | 1960s | 1970s | 1980s | 1990s | 1960s | 1970s | 1980s | 1990s | 2000s | 2010s | 2020s | 2030s | 2040s | 2050s | 2060s | 2070s | 2080s | 2090s |
| A | 5.6% | 5.6% | 7.2% | 7.4% | 8.6% | 6.7% | 7.9% | 8.2% | 7.9% | 11.2% | 8.9% | 12.7% | 11.6% | 14.3% | 13.8% | 18.4% | 18.5% | 18.9% |
| B | 7.9% | 7.6% | 8.2% | 9.4% | 7.8% | 8.5% | 8.4% | 8.7% | 12.7% | 14.5% | 13.1% | 15.8% | 17.7% | 19.8% | 21.5% | 25.7% | 25.5% | 27.3% |
| C | 15.3% | 16.0% | 14.9% | 16.1% | 16.8% | 16.3% | 15.2% | 16.2% | 15.6% | 13.8% | 16.7% | 14.7% | 15.2% | 14.4% | 15.9% | 15.4% | 13.9% | 16.1% |
| D | 5.1% | 5.7% | 6.6% | 6.1% | 5.0% | 4.9% | 5.8% | 5.9% | 4.4% | 5.1% | 4.3% | 4.6% | 4.4% | 4.4% | 3.8% | 5.3% | 3.8% | 3.6% |
| E | 3.6% | 4.1% | 4.7% | 3.9% | 6.5% | 6.0% | 5.2% | 3.9% | 5.3% | 4.5% | 4.4% | 3.5% | 3.8% | 3.3% | 2.8% | 1.9% | 2.5% | 1.4% |
| F | 4.9% | 5.6% | 5.1% | 5.4% | 3.9% | 4.9% | 4.4% | 2.9% | 2.3% | 2.5% | 2.0% | 1.2% | 1.8% | 1.0% | 1.4% | 0.6% | 0.3% | 0.2% |
| G | 4.2% | 4.8% | 4.2% | 4.3% | 5.6% | 5.5% | 4.9% | 4.3% | 5.6% | 4.6% | 5.0% | 4.7% | 3.9% | 2.4% | 2.4% | 2.0% | 1.9% | 0.5% |
| H | 19.2% | 18.9% | 18.8% | 16.9% | 15.1% | 16.0% | 16.2% | 16.8% | 16.5% | 14.9% | 17.0% | 16.0% | 16.1% | 16.4% | 16.4% | 12.1% | 14.4% | 14.4% |
| I | 6.9% | 5.1% | 4.3% | 4.5% | 4.2% | 4.0% | 3.5% | 3.9% | 2.2% | 2.4% | 2.9% | 2.0% | 1.6% | 1.2% | 0.5% | 0.4% | 0.7% | 0.4% |
| J | 4.7% | 6.6% | 5.1% | 6.3% | 6.2% | 5.8% | 5.4% | 5.2% | 8.7% | 5.8% | 6.2% | 6.3% | 6.0% | 5.1% | 4.4% | 2.2% | 2.1% | 1.6% |
| K | 5.1% | 5.1% | 4.2% | 4.1% | 3.5% | 3.2% | 4.4% | 4.4% | 3.9% | 5.0% | 4.5% | 4.5% | 4.4% | 5.7% | 5.7% | 6.6% | 6.9% | 7.6% |
| L | 3.8% | 2.4% | 2.9% | 1.6% | 2.4% | 2.7% | 3.0% | 2.9% | 1.8% | 2.7% | 1.3% | 2.2% | 1.3% | 1.4% | 0.9% | 0.5% | 1.0% | 1.0% |
| M | 3.9% | 2.9% | 2.5% | 2.9% | 3.0% | 3.1% | 3.8% | 4.3% | 3.0% | 3.4% | 2.8% | 2.4% | 2.5% | 1.9% | 1.9% | 2.0% | 2.6% | 2.6% |
| N | 4.8% | 4.1% | 5.5% | 4.7% | 6.0% | 5.7% | 6.2% | 6.9% | 5.0% | 4.3% | 5.6% | 5.5% | 5.1% | 4.5% | 3.8% | 2.9% | 2.5% | 1.9% |
| O | 4.7% | 5.6% | 5.8% | 6.3% | 5.4% | 6.7% | 5.7% | 5.6% | 4.9% | 5.4% | 5.4% | 3.9% | 4.8% | 4.1% | 4.7% | 3.8% | 3.4% | 2.6% |

## 850mb Temperature Patterns – A2

**Table D.8** – The mean frequency per decade of the 15 patterns at the 850t level for the NNR, GCM20c and GCM-Future portion of the CCSM3 – A2 results.

| | NNR | | | | GCM 20th Century | | | | GCM Future | | | | | | | | | |
|---|---|---|---|---|---|---|---|---|---|---|---|---|---|---|---|---|---|---|
| | **1960s** | **1970s** | **1980s** | **1990s** | **1960s** | **1970s** | **1980s** | **1990s** | **2000s** | **2010s** | **2020s** | **2030s** | **2040s** | **2050s** | **2060s** | **2070s** | **2080s** | **2090s** |
| **A** | 5.6% | 5.6% | 7.2% | 7.4% | 8.6% | 6.7% | 7.9% | 8.2% | 9.5% | 11.4% | 10.8% | 10.0% | 11.1% | 11.8% | 15.8% | 15.3% | 15.1% | 17.5% |
| **B** | 7.9% | 7.6% | 8.2% | 9.4% | 7.8% | 8.5% | 8.4% | 8.7% | 7.9% | 9.5% | 11.3% | 12.2% | 14.5% | 15.7% | 16.0% | 18.9% | 19.2% | 22.6% |
| **C** | 15.3% | 16.0% | 14.9% | 16.1% | 16.8% | 16.3% | 15.2% | 16.2% | 17.1% | 14.9% | 16.4% | 17.5% | 15.4% | 17.3% | 15.5% | 15.6% | 15.8% | 16.8% |
| **D** | 5.1% | 5.7% | 6.6% | 6.1% | 5.0% | 4.9% | 5.8% | 5.9% | 5.1% | 5.6% | 5.9% | 5.6% | 6.7% | 6.6% | 4.7% | 4.8% | 6.4% | 5.2% |
| **E** | 3.6% | 4.1% | 4.7% | 3.9% | 6.5% | 6.0% | 5.2% | 3.9% | 5.4% | 5.0% | 4.5% | 4.8% | 4.3% | 3.8% | 4.8% | 4.0% | 3.9% | 1.9% |
| **F** | 4.9% | 5.6% | 5.1% | 5.4% | 3.9% | 4.9% | 4.4% | 2.9% | 3.6% | 2.3% | 2.5% | 2.4% | 2.2% | 1.6% | 1.2% | 1.1% | 1.0% | 0.7% |
| **G** | 4.2% | 4.8% | 4.2% | 4.3% | 5.6% | 5.5% | 4.9% | 4.3% | 5.1% | 4.5% | 4.1% | 4.6% | 5.4% | 3.6% | 3.2% | 3.0% | 2.5% | 1.7% |
| **H** | 19.2% | 18.9% | 18.8% | 16.9% | 15.1% | 16.0% | 16.2% | 16.8% | 16.0% | 16.6% | 15.0% | 16.0% | 15.9% | 16.4% | 15.4% | 14.3% | 17.1% | 14.7% |
| **I** | 6.9% | 5.1% | 4.3% | 4.5% | 4.2% | 4.0% | 3.5% | 3.9% | 3.0% | 1.9% | 2.9% | 2.1% | 2.0% | 1.0% | 0.8% | 0.9% | 0.8% | 0.4% |
| **J** | 4.7% | 6.6% | 5.1% | 6.3% | 6.2% | 5.8% | 5.4% | 5.2% | 4.9% | 5.4% | 5.1% | 5.9% | 5.2% | 4.6% | 7.2% | 5.9% | 4.4% | 1.9% |
| **K** | 5.1% | 5.1% | 4.2% | 4.1% | 3.5% | 3.2% | 4.4% | 4.4% | 3.4% | 4.5% | 5.2% | 3.9% | 3.8% | 5.3% | 5.2% | 5.5% | 4.9% | 7.1% |
| **L** | 3.8% | 2.4% | 2.9% | 1.6% | 2.4% | 2.7% | 3.0% | 2.9% | 2.7% | 2.4% | 2.1% | 2.3% | 2.0% | 1.3% | 1.1% | 1.5% | 0.7% | 1.0% |
| **M** | 3.9% | 2.9% | 2.5% | 2.9% | 3.0% | 3.1% | 3.8% | 4.3% | 3.3% | 3.2% | 3.3% | 2.7% | 2.2% | 2.6% | 1.8% | 2.1% | 2.2% | 2.1% |
| **N** | 4.8% | 4.1% | 5.5% | 4.7% | 6.0% | 5.7% | 6.2% | 6.9% | 6.7% | 6.4% | 5.1% | 5.4% | 4.0% | 3.6% | 2.8% | 3.1% | 2.3% | 3.3% |
| **O** | 4.7% | 5.6% | 5.8% | 6.3% | 5.4% | 6.7% | 5.7% | 5.6% | 6.3% | 6.4% | 5.7% | 4.6% | 5.3% | 4.7% | 4.5% | 3.9% | 3.6% | 3.2% |

## 850mb Temperature Patterns – B1

**Table D.9** – The mean frequency per decade of the 15 patterns at the 850t level for the NNR, GCM20c and GCM-Future portion of the CCSM3 – B1 results.

| | NNR | | | | GCM 20th Century | | | | GCM Future | | | | | | | | | |
|---|---|---|---|---|---|---|---|---|---|---|---|---|---|---|---|---|---|---|
| | **1960s** | **1970s** | **1980s** | **1990s** | **1960s** | **1970s** | **1980s** | **1990s** | **2000s** | **2010s** | **2020s** | **2030s** | **2040s** | **2050s** | **2060s** | **2070s** | **2080s** | **2090s** |
| **A** | 5.6% | 5.6% | 7.2% | 7.4% | 8.6% | 6.7% | 7.9% | 8.2% | 9.8% | 10.9% | 10.2% | 11.6% | 10.5% | 10.7% | 10.2% | 11.9% | 13.0% | 10.6% |
| **B** | 7.9% | 7.6% | 8.2% | 9.4% | 7.8% | 8.5% | 8.4% | 8.7% | 10.6% | 12.0% | 9.3% | 10.1% | 11.5% | 14.1% | 12.8% | 12.2% | 12.5% | 13.0% |
| **C** | 15.3% | 16.0% | 14.9% | 16.1% | 16.8% | 16.3% | 15.2% | 16.2% | 16.3% | 15.9% | 17.6% | 17.0% | 17.8% | 15.4% | 17.9% | 16.2% | 16.2% | 15.7% |
| **D** | 5.1% | 5.7% | 6.6% | 6.1% | 5.0% | 4.9% | 5.8% | 5.9% | 5.8% | 4.4% | 5.6% | 6.1% | 4.2% | 5.7% | 4.8% | 7.5% | 6.3% | 6.2% |
| **E** | 3.6% | 4.1% | 4.7% | 3.9% | 6.5% | 6.0% | 5.2% | 3.9% | 4.6% | 4.9% | 5.8% | 5.6% | 6.1% | 5.5% | 5.2% | 4.0% | 5.0% | 5.0% |
| **F** | 4.9% | 5.6% | 5.1% | 5.4% | 3.9% | 4.9% | 4.4% | 2.9% | 4.1% | 3.7% | 2.7% | 2.7% | 2.7% | 2.7% | 3.4% | 3.3% | 2.5% | 2.7% |
| **G** | 4.2% | 4.8% | 4.2% | 4.3% | 5.6% | 5.5% | 4.9% | 4.3% | 4.8% | 3.5% | 4.7% | 4.3% | 5.2% | 3.8% | 4.8% | 5.5% | 5.0% | 4.2% |
| **H** | 19.2% | 18.9% | 18.8% | 16.9% | 15.1% | 16.0% | 16.2% | 16.8% | 16.2% | 15.7% | 16.4% | 15.5% | 15.8% | 16.1% | 15.9% | 15.7% | 14.0% | 16.2% |
| **I** | 6.9% | 5.1% | 4.3% | 4.5% | 4.2% | 4.0% | 3.5% | 3.9% | 3.1% | 2.5% | 2.4% | 2.3% | 2.5% | 1.7% | 1.8% | 1.1% | 1.3% | 1.4% |
| **J** | 4.7% | 6.6% | 5.1% | 6.3% | 6.2% | 5.8% | 5.4% | 5.2% | 6.1% | 6.3% | 7.3% | 6.4% | 6.4% | 7.2% | 6.1% | 4.4% | 5.3% | 5.8% |
| **K** | 5.1% | 5.1% | 4.2% | 4.1% | 3.5% | 3.2% | 4.4% | 4.4% | 2.9% | 4.3% | 3.2% | 3.7% | 3.4% | 4.7% | 3.9% | 4.1% | 5.4% | 4.5% |
| **L** | 3.8% | 2.4% | 2.9% | 1.6% | 2.4% | 2.7% | 3.0% | 2.9% | 1.8% | 1.8% | 1.8% | 1.1% | 1.7% | 1.7% | 1.3% | 1.1% | 1.2% | 1.6% |
| **M** | 3.9% | 2.9% | 2.5% | 2.9% | 3.0% | 3.1% | 3.8% | 4.3% | 3.2% | 3.0% | 2.4% | 3.0% | 2.7% | 2.3% | 2.6% | 2.9% | 2.5% | 2.7% |
| **N** | 4.8% | 4.1% | 5.5% | 4.7% | 6.0% | 5.7% | 6.2% | 6.9% | 5.3% | 5.6% | 4.7% | 4.9% | 4.5% | 4.1% | 4.0% | 4.8% | 4.6% | 4.4% |
| **O** | 4.7% | 5.6% | 5.8% | 6.3% | 5.4% | 6.7% | 5.7% | 5.6% | 5.4% | 5.4% | 5.9% | 5.9% | 5.0% | 4.2% | 5.1% | 5.3% | 5.3% | 5.9% |